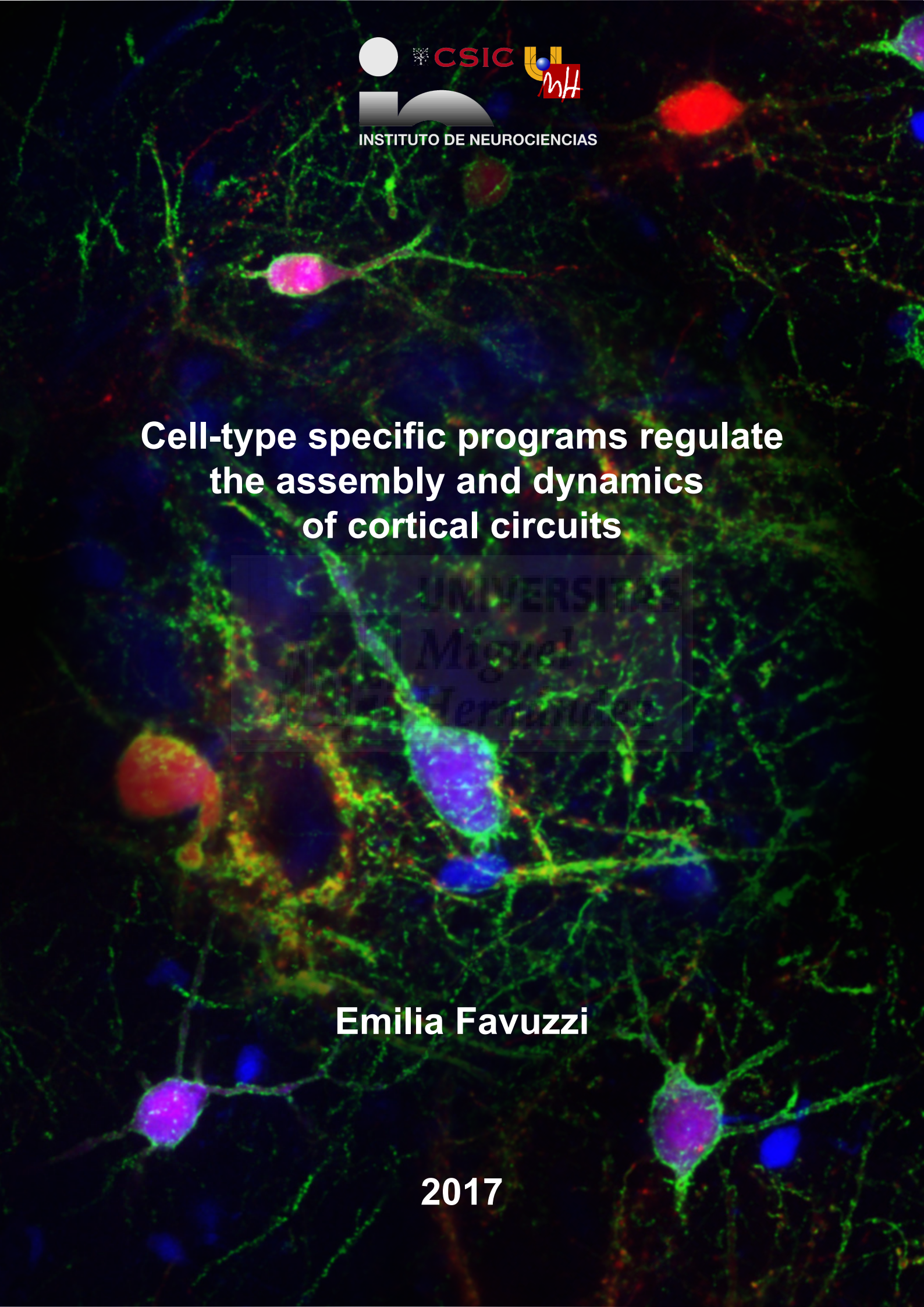

Cell-type specific programs regulate the assembly and dynamics of cortical circuits

Emilia Favuzzi

2017

Cell-type specific programs regulate the assembly and dynamics of cortical circuits

Emilia Favuzzi

Director: Beatriz Rico Gozalo

Instituto de Neurociencias CSIC-UMH 2017

UNIVERSITAS
Miguel
Hernández

Half of the work presented in this thesis
was performed at King's College London, UK

UNIVERSITAS
Miguel
Hernández

INSTITUTO DE NEUROCIENCIAS

Consejo Superior de Investigaciones Científicas
Universidad Miguel Hernández
Instituto de Neurociencias

Prof. Salvador Martínez
Director

Prof. Salvador Martínez Pérez, Director del Instituto de Neurociencias, centro mixto de la Universidad Miguel Hernández, UMH y la Agencia Estatal Consejo Superior de Investigaciones Científicas, CSIC,

CERTIFICA :

Que la Tesis Doctoral titulada: *"Cell-type specific programs regulate the assembly and dynamics of cortical circuits"* ha sido realizada por D.ª Emilia Favuzzi (Pasaporte: YA1667628), bajo la dirección de la Dra. Beatriz Rico Gozalo, y da su conformidad para que sea presentada a la Comisión de Doctorado de la Universidad Miguel Hernández.

Para que así conste a los efectos oportunos, firma el presente certificado en San Juan de Alicante, a 29 de junio de 2017

Salvador Martínez
Director

direccion.in@umh.es
direccion.in@csic.es
www.ina.umh.es

Tel : +34 965 919220 (s)
+ 34 965 919221 (d)
Fax: +34 965 919561

Av Ramón y Cajal s/n
Campus de San Juan
03550 SAN JUAN DE ALICANTE– ESPAÑA

UNIVERSITAS
Miguel
Hernández

ACKNOWLEDGEMENTS

UNIVERSITAS
Miguel
Hernández

The brain is worth the billions of years of evolution that produced it. It is arguably the only entity that simultaneously has the highest diversity, wiring precision and complexity of anything on earth. As such, it is simply breathtaking. Working on it is a privilege and an honor and I sincerely want to thank all the people that so generously helped me to give my little contribution to the common endeavor of trying to understand its underpinnings.

Special mention goes to my enthusiastic supervisor, **Beatriz Rico**; one simply could not wish for a better mentor. My Ph.D. has been an amazing experience and I thank Beatriz wholeheartedly for her constant tremendous support, for her patience, for giving me intellectual freedom in my research —which undoubtedly fostered my growth as a scientist— and for the so many wonderful opportunities she gave me over this six-year journey of doctoral research.

I would not be writing this page today, had it not been for the 'support network' around me. First and foremost, I wish to thank the three fellow lab mates and collaborators that worked with me on both projects, Rubén, André and Patri.

Saying that **Rubén** is an extremely reliable and generous source of practical knowledge would be an understatement. He is the mind behind pretty much all molecular engineering used in this thesis, most prominently the conditional constructs employed for the cell-autonomous manipulations in both projects (and which are probably second in greatness only to his 'croquetas'). Rubén also deserves credit for the Clbn4 data mentioned in this thesis. It has been a true pleasure to co-lead the Synapdomain project with Rubén and, in my daily work, I have gained so much from our constant scientific exchange. Moreover —and perhaps more importantly—, I have been blessed not only with a wonderful collaborator but also with a lasting friend.

Every physiology result described in this thesis was performed, with great enthusiasm, by **Andre**. I was fortunate to have the chance to work with Andre in the Brevican project and I greatly benefited from his scientific curiosity, keen scientific insight, and vast physiology knowledge. I truly enjoyed our inspirational scientific discussions and gained a lot from Andre's insightful comments and ideas. I also appreciate his generosity in sharing the Lgi2 data mentioned in this thesis.

I owe a debt of gratitude to **Patri** who —with dedicated and tireless attitude— has been an invaluable cheerful help in a countless number of experiments. Just to mention some: going far beyond the call of duty, she was a great companion in otherwise exhausting FACS experiments over weekends and holidays. She also was 'the hands' behind all constructs and viruses used in this thesis. And yet she provided something much greater, a true and dearest friendship. I have fond memories of our time together both inside and outside the lab over the past years. I will take them with me after the Ph.D. and hang on them as much as I can.

Throughout my Ph.D., I also greatly benefited from the close proximity to and constant interaction with **Oscar Marín** (and his laboratory). Oscar's insightful feedback on my research has been critical for its progress and also greatly stimulated my personal scientific growth. He has taught me, both consciously and unconsciously, how good science is done and I am thankful for the excellent example he has provided as a successful scientist.

A special thanks goes to **Nancy**, who kept the lab running smoothly in London and who I had the pleasure and the fortune to work with in the last year. I have immensely benefited from her excellent technical assistance, especially during the intense revision of the Brevican paper. Without her incomparable keenness and commitment, both the first submission and the resubmission of the paper would have been much delayed. I owe her a lot.

Nowadays science is increasingly collaborative. During my Ph.D., I was fortunate to have the chance to build and participate in collaborations with researchers outside our lab that fundamentally facilitated the progress of the Brevican project.

I am indebted to **Christian Winterflood**, who deserves the credit for the success of the STORM experiments. His knack for solving seemingly unsolvable practical difficulties and his ability to understand our scientific questions despite having (initially) no idea of what an interneuron was, allowed us to accomplish an endeavor that when we started to work together appeared truly impossible: studying the (co)localization of individual molecules with nanometer resolution at a specific type of synapse in a subset of rare interneurons from a given hippocampal region in brain sections. To work with Christian has been a true pleasure and a privilege.

I am also very grateful to **Joris de Wit**, who —together with Jeff Savas— did the Ecto-Fc-MS experiment. I met Joris at the Gordon Conference only one year ago, his excitement and scientific curiosity are at the root of the proteomic screening performed in record time and shown in the appendix of this thesis.

I would also like to thank **Cathy Fernandes**, who trained me in the Morris Water Maze and who made available her equipment at Denmark Hill, without which the behavioral experiments I performed for the Brevican project would not have been possible.

All (past and present) members of the Rico and Marín labs have contributed immensely to my personal and professional time both in Alicante and at King's. The group has been a source of friendships as well as good advice and collaboration.

I am grateful to **Alberto**, who I will never thank enough for finishing —with uncommon dedication— the mEPSCs/mIPSCs experiment we needed to resubmit the Brevican paper.

I was very lucky to have the chance to supervise and mentor outstanding MSc and Ph.D./rotation students who tirelessly and with much enthusiasm tackled difficult projects over the course of several months and contributed to the data included in this thesis. I would like to thank **Alastair**, not only for his excellent work on potassium channels in the context of the Brevican project but also for his fundamental help in improving and further automatizing the analysis scripts in ImageJ, for which I am truly indebted to him. **Victoria**, who enthusiastically worked on the very first chandelier injections and sh*Fgf13* experiments. **Sophie**, for performing the final cloning of the *shBcan* and for her help with the mixed cultures showed in the appendix of this thesis.

I also wish to thank **David**, who performed and shared with me the PCA, cluster analysis, as well as the list of 'top 20 specific genes' included in the thesis.

I am indebted to **Isabel**, for handing me over her deep knowledge on synapse analysis and confocal imaging, for being a caring and mentoring companion at my first conference, and because, together with **Jorge**, she patiently provided lots of advice on behavior; without Isabel's and Jorge's long-distance help, it would have undoubtedly been much more difficult to perform those experiments.

I also would like to thank **Antonio**, for his fundamental help with the Imaris/MATLAB analysis, for kindly offering me his *in situ* hybridization *Hapln1* plasmid and for the discussions we had over the years.

I am also grateful to the most recent addition to the team, **Maddalena**, not only because she will certainly manage to get the chandelier functional data but also for spoiling us with her tasty cakes.

I am grateful to **Cristina**, not only because she has always been willing to help in the lab but also for accepting to evaluate this thesis and for her insightful comments and suggestions; **Catarina**, who excellently thought me how to do primary cultures; **Clémence**, for our constant and prolific discussions about perineuronal nets and the theoretical and technical aspects of our projects; **Ana**, for kindly providing the sections with electroporated brains I used to check Brevican expression in pyramidal cells and for explaining me the FACS protocol. **Diana**, for keeping the lab in Alicante well organized and stocked with general supplies as well as for brilliantly taking care of all of us; **Aida**, whose friendship I very much enjoyed outside the lab and who very generously perfused (together with Diana) a lot of mice from the maternal separation that I had to leave in Alicante when we moved to London.

Giorgia who, apart from being a good friend, has been a generous source of information and aid both at the beginning (from the *in situ* to the tamoxifen injection protocols) and at the end of my Ph.D. (tirelessly answering all my questions about the thesis).

Alfredo, for our stimulating scientific discussions and for being such a dear friend outside the lab too.

Trini, because the smooth running of both labs in Alicante was much more a testament to her efforts than anyone else's. Saying that Trini was always ready to help would be an understatement. One simply could not wish for a better lab manager (which is also a curse, as it seems I will forever miss her).

I am grateful to **Virtu** for her fundamental help with the 'bureaucratic issues' of submitting the thesis from London, I am truly in her debt. I would be remiss if I did not thank Virtu also for providing much-needed assistance with administrative tasks in Alicante.

I would like to thank the other various past and present members of the Rico and Marín labs with whom I had the opportunity to work with or alongside of: **Martijn, Gabriele, Nathalie, Asha, Nasrath, Anna, Veronique, Kinga, Amanda, Ignasi, Fong, Monika, Lynette, Varun, Sandra, Charlotte, Sunny, Verona, Ricardo, Nines, Malik, Adrián, Carol, Juan Antonio,** and **Caroline**. They provided a friendly and cooperative atmosphere at work (and many of them have been —and will be— dear friends outside the lab too), stimulating scientific discussions, as well as useful feedback and suggestions on my work.

I also wish to thank many other people who at both King's College and the Institute of Neuroscience contributed in some way to the work described in this thesis.

Very special thanks go to **Ian Andrew**, for outstandingly and flawlessly taking care of our mouse colonies in London (despite the tons of mice, plugs, and breedings I had) and for always quickly and patiently replying to my 'mouse questions', even in the middle of the night or on weekends. I owe Ian a debt also for providing English language advice on several sentences while writing this thesis.

The care our mice received in Alicante was equally exceptional. I am thankful to M. Jesus Molina and all the people in the 'Animalario'. In particular, I was fortunate to have the chance to work with **Patricia Muñoz** (who also performed some tamoxifen injections for me over the Christmas holidays), **Sandra Gonzalez** and **Veronica Jimenez**. Their driven, thorough, excellent support truly made my own work easier and I miss the pleasant long-lasting chats I had with the three of them.

The FACS of chandelier cells has been probably the most intense and tiring experience of my Ph.D. and it would have been much more difficult without **Antonio Caler**'s assistance. His optimisms, willingness to help and to overcome the technical difficulties was key for the success of the arduous effort of isolating and collecting chandelier cells.

Antonio also deserves credit for helping with the genotyping of my (many) mice in Alicante, as **Alina** and **Matt** have to be thanked for the genotyping service in London.

I also wish to thank the Genomic and Bioinformatic Units of the **Centre for Genomic Regulation in Barcelona** (CRG) for performing the RNA-seq experiments and the bioinformatic analysis, respectively. I am particularly grateful to Jean François Tily and Luca Cozzuto for hosting me at the CRG to participate in the very first analysis of the RNA-seq data.

Over my Ph.D., I also greatly benefited from our lab meetings with **Nuria Flames**'s lab. I gained a lot from Nuria's ideas and always useful comments on my work. For instance, it was Nuria who, during one of my lab meetings, suggested to do the screening at two stages in order to better pick up synaptic genes —an idea that, in retrospect, was undeniably excellent and critically instrumental in the success of the project. I also wish to thank Nuria for finding the time to read and evaluate this thesis, I truly appreciate it.

I also would like to acknowledge all the people that kindly shared mice and reagents; without their generosity, many of the experiments included in this thesis would not have existed. **Reinhard Fässler** for *Bcan*$^{-/-}$ mice, **Renato Frischknecht** for Brevican antibodies, **Elke Fuchs**, **Anne Herb** and **Hannah Monyer** for *PV-Cre;GluA1*$^{F/F}$ brains, **Silvia Arber** for *PV-Cre* mice. Conversely, I sincerely hope that one day Xu Zhang, Hailin Zhang, Chuan Wang, who did not want to distribute their published *Fgf13* conditional knock-out mice (Wang et al., 2017; Wu et al., 2012a) will also understand the importance of sharing and collaboration in science (Fishell, 2013).

I am truly grateful to **Laura Mantoan** who openhandedly shared with me the epilepsy tissue she obtained from the London Neurodegenerative Diseases Brain Bank and Brains for Dementia Research, which —together with their donors— I also thank.

Moreover, I gratefully acknowledge the funding sources that made my Ph.D. work possible. I was initially funded by JAE-Pre fellowship (CSIC) and, afterward, by King's College London funds.

A final —but by no means least— thank-you goes to the people that provided emotional support, regardless of whether this meant sharing the joys and sorrows of the doctoral life or providing distraction and escapism.

My **lifelong friends from Molfetta**, especially Vale P, Mariella, Corrado, Vale B and Cinzia, for their understanding and support as well as for providing the requisite breaks from science.

Marian, the only person who over these years actually experienced and truly shared all the screams and hurray, the manic laughing and crying, the moments of frustration as well as those of accomplishment and profound happiness, the adrenaline rushes, the intellectual galvanization, the marvellous sense of agony and awe that characterized my (as many other) Ph.D.; I will never thank her enough for her almost unbelievable support and understanding.

Finally, I wish to thank **my parents** for their unyielding and unconditional encouragement and because the individual I am today —and will always be— is fundamentally the result of what they are.

UNIVERSITAS Miguel Hernández

UNIVERSITAS Miguel Hernández

INDEX

UNIVERSITAS
Miguel
Hernández

ABSTRACT

UNIVERSITAS
Miguel
Hernández

The exquisite repertoire of animal behaviors relies on the precise assembly and fine-tuning of synaptic connections amongst different neuronal subtypes. Wiring specificity implies both cell and synaptic diversity, which, in turn, are determined by tightly regulated developmental cell-specific gene programs. By virtue of the remarkable diversity of types and connectivity patterns, inhibitory neurons are particularly well suited to perform functionally relevant circuit-specific roles and critically shape cortical function. Consistently, GABAergic dysfunction has been implicated in several neurological and psychiatric disorders. While some progress has been made towards understanding the molecular and structural components that broadly distinguish inhibitory synapses and their assembly, the molecular mechanisms underlying interneuron subtype-specific connectivity are largely unknown. In the first part of this work we combined cell sorting approaches and high-throughput RNA-sequencing techniques to investigate interneuron subtype-specific transcriptome dynamics across early developmental stages. The resulting transcriptome profile revealed the existence of highly selective cell-type specific programs in developing cortical interneurons. We then coupled the gene expression longitudinal profiles with loss-of-function experiments using a systematic virus-mediated gene knockdown strategy. These experiments showed that the identified cell-specific molecular signatures support interneuron early wiring and underlie the specification of different patterns of connectivity.

Understanding the relationship between behavior and inhibitory circuit function (as well as dysfunction) entails uncovering not only the hardwired organizing principles but also the specific logic of inhibitory circuit dynamics. Activity-dependent neuronal plasticity is a fundamental mechanism through which the nervous system adapts to sensory experience. Several lines of evidence suggest that parvalbumin (PV+) interneurons are essential in this process, but the molecular mechanisms underlying the influence of experience on interneuron plasticity remain poorly understood. Perineuronal nets (PNN) enwrapping PV+ cells are long-standing candidates for playing such a role, yet their precise contribution has remained elusive. In the second part of the thesis, we show that the PNN protein Brevican is a critical regulator of interneuron plasticity. We find that Brevican simultaneously controls cellular and synaptic forms of plasticity in PV+ interneurons by regulating the localization of potassium channels and AMPA receptors, respectively. By modulating Brevican levels, experience introduces precise molecular and cellular modifications in PV+ cells that are required for learning and memory. These findings uncover a molecular program through which a PNN protein facilitates appropriate behavioral responses to experience by dynamically gating PV+ interneuron function.

Resumen (Spanish)

El extraordinario repertorio de comportamientos animales se basa en el preciso ensamblaje y refinamiento de conexiones sinápticas entre diferentes subtipos neuronales. Dicha especificidad, implica tanto la diversidad celular como la sináptica que, a su vez, están determinadas por programas de genes específicamente expresados en dichas células y estrictamente regulados durante el desarrollo. En virtud de la notable diversidad de tipos y patrones de conectividad, las neuronas inhibidoras son particularmente adecuadas para desempeñar papeles específicos y funcionalmente relevantes en los circuitos neuronales y, por lo tanto, configuran de forma crítica la función cortical. De acuerdo con esto, la disfunción GABAérgica está implicada en varios trastornos neurológicos y psiquiátricos. Aunque se han hecho algunos progresos hacia la comprensión de los componentes moleculares y estructurales que distinguen ampliamente las sinapsis inhibitorias y su ensamblaje, los mecanismos moleculares subyacentes a la conectividad específica de los subtipos de interneuronas son en gran parte desconocidos. En la primera parte de este trabajo se combinaron técnicas de “FACS sorting” de células y “RNA-sequencing” para investigar los cambios dinámicos en el transcriptoma de subtipos específicos de interneuronas durante etapas tempranas del desarrollo. El perfil transcripcional de dichas interneuronas reveló la existencia de programas moleculares altamente selectivos para cada tipo de interneurona cortical durante el desarrollo. A continuación, se complementaron los perfiles de expresión génica con experimentos de pérdida de función utilizando un sistema de virus y la estrategia de “protein knockdown”. Estos experimentos mostraron que, durante el desarrollo de las conexiones sinápticas, diferentes interneuronas presentan “improntas moleculares” específicas que determinan los patrones de conectividad.

Comprender la relación entre el comportamiento y la función (así como la disfunción) de los circuitos inhibitorios implica descubrir no sólo los principios de organización sino también la lógica específica de la dinámica de dichos circuitos. La plasticidad neuronal dependiente de la actividad es un mecanismo fundamental a través del cual el sistema nervioso se adapta a la experiencia sensorial. Varias líneas de investigacion sugieren que las interneuronas que expresan parvalbúmina (PV+) son esenciales en este proceso, pero los mecanismos moleculares subyacentes a la influencia de la experiencia en la plasticidad de las interneuronas siguen siendo poco conocidos. Las redes perineuronales (PNN) que envuelven las células PV+ vienen siendo las candidatas para desempeñar ese papel, pero su contribución precisa ha permanecido difícil de aclarar. En la segunda parte de la tesis, mostramos que la proteína PNN Brevican regula críticamente la plasticidad interneuronal. Encontramos que Brevican controla simultáneamente las formas celulares y sinápticas de plasticidad en interneuronas PV+ regulando, respectivamente, la localización de canales de potasio y de receptores AMPA. Al modular los niveles de Brevican, la experiencia introduce modificaciones moleculares y celulares precisas en células PV + que son necesarias para el aprendizaje y la memoria. Estos descubrimientos revelan un programa molecular a través del cual una proteína PNN facilita respuestas conductuales apropiadas a la experiencia mediante la activación dinámica de la función de interneuronas PV+.

Table of abbreviations

5HT3AR	5-hydroxytryptamine receptor 3A
8-oxo-dG	8-oxo-7,8-dihydro-20-deoxyguanine
AAV	Adeno-Associated Virus
AIS	Axon Initial Segment
AMPA	α-amino-3-hydroxy-5-methyl-4-isoxazolepropionic acid
AMPARs	AMPA receptors
AnkG	Ankyrin G
CAMs	Cell Adhesion Molecules
CCK	Cholecystokinin
CGE	CGE caudal ganglionic eminence
ChC	Chandelier Cell
CS	Chondroitin Sulfate
CSPGs	Chondroitin Sulfate Proteoglycans
DG	Dentate Gyrus
E/I	Excitatory/Inhibitory
ECM	Extracellular Matrix
Ecto-Fc MS	Ecto-Fc Mass Spectrometry
ENO	Early Network Oscillation
FACS	Fluorescence-Activated Cell Sorting
fAHP	Fast After-Hyperpolarization
FGF	Fibroblast Growth Factor
FHFs	Fibroblast Growth Factor Homologous Factors
FLRT	Fibronectin Leucine-Rich Repeat Transmembrane
FPKM	Fragments Per Kilobase Of Exon Per Million Fragments Mapped
FS	Fast-Spiking
GABA	Gamma-Aminobutyric Acid
GDP	Giant Depolarizing Potentials
GEF	Guanine Nucleotide Exchange Factor
GFAP	Glial Fibrillary Acidic Protein
GFP	Green Fluorescence Protein
GO	Gene Ontology
GPCRs	G protein-coupled receptors
GPI	glycosylphophatidyl
GSEA	Gene Set Enrichment Analysis
Ig-CAMs	Ig-like Cell Adhesion Molecules
IHC	Immunohistochemistry
IP	Immunoprecipitation
ISH	In Situ Hybridization
KEGG	Kyoto Encyclopedia Of Genes And Genomes
LGE	Lateral Ganglionic Eminence

LRR	Leucine Rich Repeat
LTP	Long-Term Potentiation
MAGUKs	Membrane-Associated Guanylate Kinases
MAPs	Microtubule Associated Proteins
mEPSCs	Miniature Excitatory Postsynaptic Currents
mEPSCs	miniature Excitatory Postsynaptic Currents
MGE	Medial Ganglionic Eminence
mIPSCs	miniature Inhibitory Postsynaptic Currents
MS	Maternal Separation
MS/MS	Tandem Mass Spectrometry
MWM	Morris Water Maze
NGLs	Netrin-G Ligands
NLS	Nuclear Localization Signal
NMDA	N-Methyl-D-aspartate
NMDARs	NMDA receptors
P	Postnatal day
PCA	Principal Component Analysis
PFC	Prefrontal Cortex
PNN	Perineuronal Nets
POA	Preoptic Area
PSA	Polysialic Acid
PV	Parvalbumin
qPCR	quantitative PCR
RELN	Reelin
RGC	Retinal Ganglion Cell
RNA-seq	RNA sequencing
ROS	Reactive Oxygen Species
sEPSCs	spontaneous Excitatory Postsynaptic Currents
shRNA	short-hairpin RNA
SSC	Somatosensory Cortex
SST	Somatostatin
TCA	Tricarboxylic Acid
VGSCs	Voltage-Gated Sodium Channels

UNIVERSITAS Miguel Hernández

GENERAL INTRODUCTION

UNIVERSITAS
Miguel
Hernández

"Wooing, wedding, and repenting, is as a Scotch jig,
a measure, and a cinque pace:
the first suit is hot and hasty, like a Scotch jig, and full as fantastical;
the wedding, mannerly-modest, as a measure, full of state and ancientry;
and then comes repentance and, with his bad legs,
falls into the cinque pace faster and faster,
till he sink into his grave.

— William Shakespeare, Much Ado About Nothing, Act II, Scene I[1]

The courtship-like process of neural circuit formation is no less of a multifaceted dance than the one of Shakespeare's words[1]. The beauty and sophistication that characterizes this process is truly astonishing and even more so if one considers its outcome, us.

The exquisite repertoire of animal behaviors relies on the precise assembly and fine-tuning of synaptic connections amongst different neuronal subtypes. From both an evolutionary and a developmental perspective, brain wiring reaches an exceptional level of complexity in the cerebral cortex. Cortical circuits, honed over hundreds of million years of evolution, contain a richly interconnected array of diverse cell types, whose patterns of connectivity underlie the cortex's extraordinary computational prowess (Harris and Shepherd, 2015; Rakic, 2009).

Understanding how elaborate molecular and cellular interactions give rise to functional cortical networks during brain development is a major endeavor in neuroscience. Such understanding is critical not only to answer philosophically challenging questions about the underpinnings of cognition and emotion but also because defects in the formation and adaptation of neuronal circuits lie at the root of some of the most severe and hitherto untreatable human disorders such as autism or schizophrenia (Marín, 2016; Paz and Huguenard, 2015).

1. Actors on the stage: cell diversity and organization of cortical circuits

From a historical perspective, both Ramón y Cajal's uncanny sense of the functional implication of his work and the riveting pioneering experiments of Hubel and Wiesel have inspired generations of neuroscientists to explore how the anatomy of the brain gives rise to its function (Llinás, 2003; Wurtz, 2009).

The most obvious anatomical feature of the cerebral cortex is arguably its organization in different layers. Although some cortical areas, such as the hippocampus and the pyriform cortex, have only rudimentary lamination, most of the cortex, termed "isocortex" or "neocortex", has six more or less well-defined layers (Pandya et al., 2015). The cortex's ability to process and integrate information relies on intricate networks of excitatory and inhibitory neurons —the main cellular elements of the individual circuits— within and between these layers, as well as across different cortical areas (Harris and Mrsic-Flogel, 2013).

Cellular elements of cortical circuits

The excitatory glutamatergic neurons —termed pyramidal or principal cells— numerically provide the largest proportion (80%) of cortical cells, and fall into multiple classes distributed across and within cortical layers (Greig et al., 2013). Principal cells respond selectively to specific features of sensory stimuli and through long-range projections

[1] For non-English readers: here Shakespeare compares the three phases of a relationship to three different types of dance.

transmit information both between different cortical regions and to other areas of the brain (Harris and Mrsic-Flogel, 2013).

Inhibitory gamma-aminobutyric acid (GABA)ergic interneurons, despite representing the minority of cells (20%), comprise an extremely diverse population of cells —with different embryonic origin, birth, postsynaptic targets, circuit integration and function— that make mostly local connections (DeFelipe et al., 2013). Interneurons shape various forms of collective activity and primarily contribute to local assemblies, where they provide inhibitory inputs that modulate the responses of pyramidal neurons, thereby controlling information flow (Cossart, 2011; Isaacson and Scanziani, 2011; Kepecs and Fishell, 2014; Le Magueresse and Monyer, 2013; Somogyi and Klausberger, 2005; Tremblay et al., 2016).

Although these different types of neurons hold “cortical citizenship”, they are all born elsewhere. Quoting the famous neuroscientist Paško Rakić, “what interests me, in particular, is something that most people do not realize, none of the cortical neurons are generated in the cortex” (Zhou). In fact, pyramidal cells are generated in the ventricular zone of the dorsal telencephalon. During embryonic development, they migrate radially and populate the future multilayered cortex in an 'inside-out' manner and with specific temporal patterns (Greig et al., 2013; Hayashi et al., 2015; Molyneaux et al., 2007; Nadarajah and Parnavelas, 2002)[2].

Cortical GABAergic interneurons, instead, originate in proliferative territories of the embryonic ventral telencephalon. With a precise temporal sequence, the embryonic medial (MGE) and caudal (CGE) ganglionic eminences and, secondarily, the preoptic area (POA) give rise to cortical interneurons, with a small contribution from the lateral ganglionic eminence (LGE). Afterward, during late embryogenesis, interneurons migrate tangentially towards all regions of the cortex where they disperse radially to integrate within the nascent laminar layers (Danglot et al., 2006; Gelman and Marín, 2010; Wonders and Anderson, 2006).

Cortical interneuron diversity

Cortical GABAergic interneurons exhibit such a uniquely high diversity that repeated communal efforts had to be made by the scientific community to support a consensus classification for data sharing (DeFelipe et al., 2013; Petilla Interneuron Nomenclature Group et al., 2008). Yet, the cortex contains only three major families of interneurons (Rudy et al., 2011), each of which divides into multiple subclasses (Figure 1), characterized by distinct morphologies, molecular markers, synaptic specificity and electrophysiological properties (Somogyi and Klausberger, 2005; Tremblay et al., 2016).

If we adopt a neurochemical classification criterion, we can broadly distinguish interneurons that express the calcium-binding protein parvalbumin (PV+), the neuropeptides somatostatin (SST+) and the serotonin (5-hydroxytryptamine) receptor 3A (5HT3AR+). Together, neurons expressing at least one of these markers account for almost all interneurons within the cortex (Rudy et al., 2011).

---

[2] These reviews focus mostly on the generation and diversity of pyramidal cells in the mouse cortex, which are more pertinent to this thesis. However, important differences have been observed on this matter across evolution. Because evolution of the neocortex in mammals is considered to be a key advance that enabled higher cognitive function, a large amount of research focused on the development and evolution of the human neocortex. Although such topic is out of the scope of this thesis, in addition to Rakic, 2009 present in the main bibliography, we provide here two supplementary references for readers interested in further insights.

Lui, J.H., Hansen, D.V. and Kriegstein, A.R. 2011. Development and evolution of the human neocortex. *Cell* 146(1), pp. 18–36.

Taverna, E., Götz, M. and Huttner, W.B. 2014. The cell biology of neurogenesis: toward an understanding of the development and evolution of the neocortex. *Annual Review of Cell and Developmental Biology* 30, pp. 465–502.

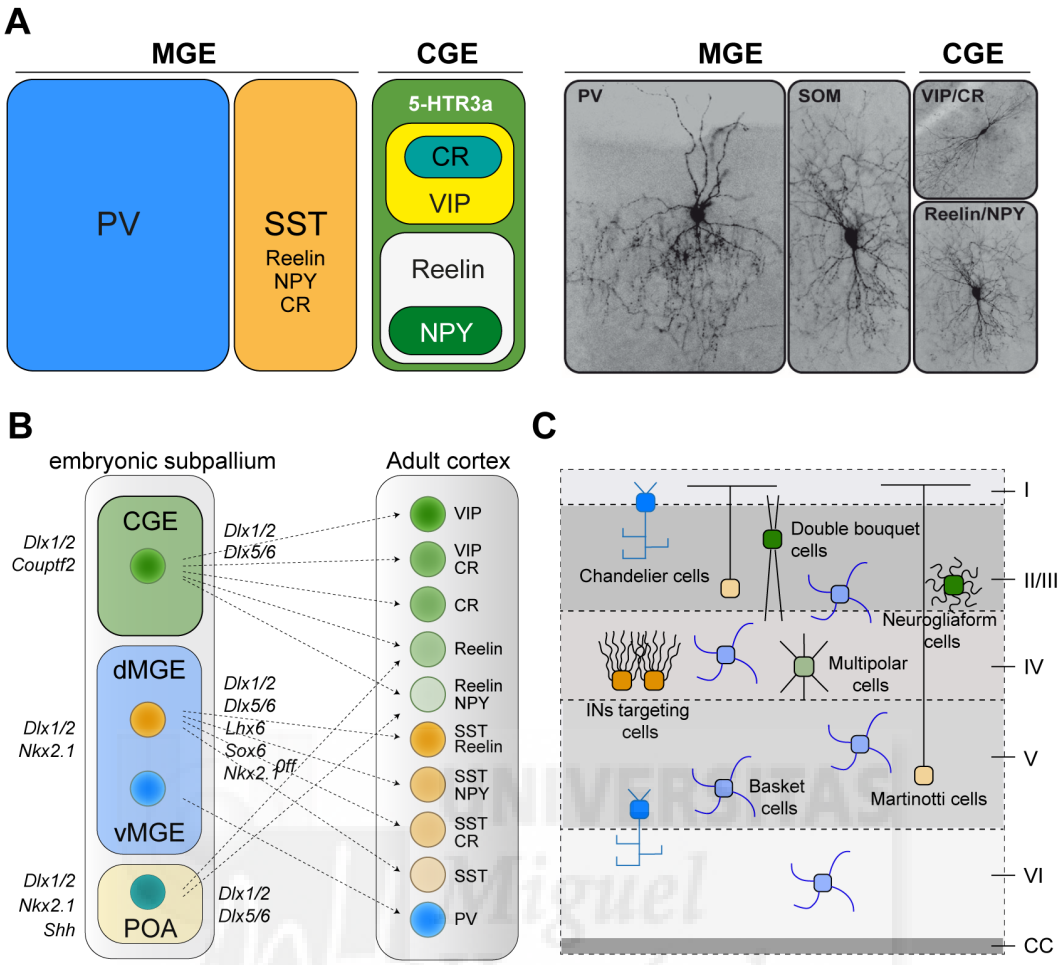

Figure 1. Classification and molecular specification of cortical inhibitory interneuron subtypes.
(A) Characterization of cortical interneuron subtypes according to the expression of neurochemical markers and morphology. Cortical GABAergic interneurons belong to three main non-overlapping groups. PV+ and SST+ interneurons originate embryonically in the medial ganglionic eminences whereas 5HTR3A+ interneurons derive from the CGE. Each of these classes comprehends different subtypes that are specified through a complex network of transcription factors.
(B) The main molecules involved in the developmental specification of different interneuron subtypes. C. Laminar distribution of the different interneuron subtypes in the adult cortex. Cc, corpus callosum; MGE, medial ganglionic eminence; CGE, caudal ganglionic eminence; POA, preoptic area; I-VI, cortical layers I to VI. Adapted from (Bartolini et al., 2013; Gelman and Marín, 2010).

PV+ interneurons are born in the ventral MGE and their firing is characterized by uniquely high frequency and temporal precision, a feature that earned them the name of 'fast-spiking (FS) cells' (Hu et al., 2014). PV+ cells play fundamental roles in basic circuit functions, including feedforward and feedback inhibition, stabilizing and shaping the activity of cortical networks, as well as establishing and maintaining fast cortical rhythms linked to cognitive function. In addition, PV+ interneurons regulate critical-period experience-dependent plasticity and are also involved in mediating complex network operations, such as expansion of dynamic activity range, pattern separation and gain modulation of sensory responses. Because of their essential functions, it is not surprising that PV+ interneuron dysfunction has been implicated in several neurological

and psychiatric disorders (Hu et al., 2014). Based on the pyramidal cell domain they target, PV+ interneurons can be further subdivided in the soma-targeting basket cells and axon initial segment (AIS)-targeting chandelier cells. **PV+ basket cells** constitute the most abundant and best-studied population of GABAergic cells within the cortex. As such, the general roles attributed above to PV+ fast-spiking interneurons can most likely be entirely ascribed to PV+ basket cells only (Hu et al., 2014). The fewer **PV+ chandelier cells** are much less studied, in part because of the lack of a specific marker to distinguish them from the much more abundant 'half-sister' PV+ basket cells (Inan and Anderson, 2014; Inan et al., 2013; Wang et al., 2016; Woodruff et al., 2010). Of note, relatively recent work described the existence of (possibly POA-derived) PV-chandelier cells in the mouse prefrontal cortex (Taniguchi et al., 2013). For these reasons and because of their disputed possible depolarizing effect on the membrane potential, chandelier cells have been —and continue to be— shrouded in mystery (Howard et al., 2005; Woodruff et al., 2009, 2010, 2011; Zhu et al., 2004). However, very recent work suggested an intriguing role for chandelier cells not only in directional inhibition between local pyramidal cell ensembles but also in shaping communication hierarchies between global networks (Lu et al., 2017).

SST+ interneurons, the second more abundant population of cortical interneurons, derive from the dorsal MGE and target dendrites. They comprise mostly, but not exclusively, Martinotti cells that make synapses onto the distal dendrites of principal cells, as well as inhibiting other interneurons (Cottam, 2009; McGarry et al., 2010; Pfeffer et al., 2013; Wang et al., 2004c; Xu et al., 2013). Consistent with their synaptic targeting, SST+ cells have been implicated in behavior-dependent control of dendritic integration, as well as in more general lateral inhibition (Adesnik et al., 2012; Gentet et al., 2012; Murayama et al., 2009).

5HT3AR+ interneurons are CGE-derived, account for only 30% of all cortical interneurons and are mainly located in superficial cortical layers. 5HT3AR+ cells comprise two prominent subgroups: interneurons that express the vasoactive intestinal peptide (VIP+) and those expressing the secreted signaling protein reelin (RELN+). Cortical **VIP+ interneurons** preferentially target SST+ cells and have an important role in disinhibition (Lee et al., 2013; Pfeffer et al., 2013). VIP+ interneurons are implicated in several important processes, including learning and visual processing (Ayzenshtat et al., 2016; Garcia-Junco-Clemente et al., 2017; Jackson et al., 2016; Letzkus et al., 2011; Muñoz et al., 2017; Pi et al., 2013). RELN+ interneurons are **neurogliaform cells**, which mediate slow GABA release by volume transmission and can affect both principal cells and other interneurons (Oláh et al., 2009; Overstreet-Wadiche and McBain, 2015; Palmer et al., 2012). Of note, as some SST+ cells also express reelin, RELN expression *per se* does not unequivocally identify neurogliaform cells but it does when combined with SST staining (RELN+SST−). Because of their unique properties, RELN+ interneurons are capable of governing many diverse processes from circuit development to sculpting the activity of large neuronal ensembles (Overstreet-Wadiche and McBain, 2015).

Of note, other less abundant interneurons subtypes which do not fall in the abovementioned main categories also play important roles in cortical processing. Perhaps most notable among these are the CGE-derived Cholecystokinin (CCK+) basket cells that have been shown to be involved in learning and spatial coding in the hippocampus (Armstrong and Soltesz, 2012; Basu et al., 2013; Del Pino et al., 2017).

Interneuron diversity and synapse specificity

Perhaps the most striking aspect emerging from this brief description of cortical interneurons is that their roles could not be more different, despite the use of the same neurotransmitter. Each class of interneuron modulates pyramidal cell function in a

unique manner. It is fascinating to contemplate how the connectivity patterns of different interneurons are perfectly suited to fulfill their specific functional roles in the circuits. In fact, it appears that the exquisite power each interneuron type can exert over cortical function is only possible because of their extremely diverse properties, most notably synaptic specificity.

In addition to having different intrinsic properties (which plays a crucial role), multiple types of inhibitory neurons —for example SST+, PV+ basket and chandelier cells— form synaptic inputs on distinct subcellular domains of pyramidal neurons (Figure 2). Since the location of a synaptic contact largely determines its influence on the postsynaptic cell, the inhibitory effects of these synapses are markedly different. Whereas perisomatic inhibition profoundly affects action potentials elicited in the postsynaptic cells, inhibitory synapses onto distal dendrites mostly dampen dendritic spikes (Miles et al., 1996). Such different inhibitory synaptic populations can also differ in their feedback responses to activation of the pyramidal cell: perisomatic synapses function immediately at the onset of action potentials, whereas inhibition later shifts to apical dendrites in response to the rate of action potentials (Pouille and Scanziani, 2004).

The prevalent view is that this elaborate organization of inputs greatly increases the overall computational power of cortical circuits (Buzsáki and Draguhn, 2004; Häusser et al., 2000; Pouille and Scanziani, 2001; Wang et al., 2004b). These considerations thus raise the question of how such specificity is generated during development and suggest that unveiling the fundamental mechanisms regulating inhibitory synapse specificity may be critical to understand how a functional network is assembled.

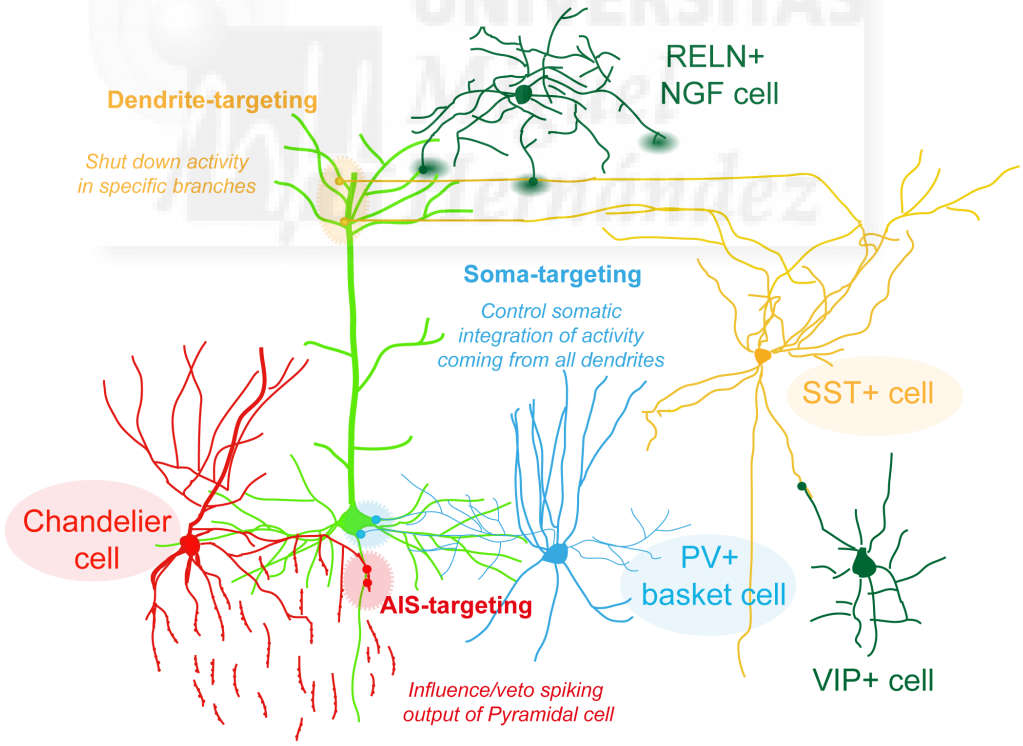

Figure 2. Chandelier, PV+ basket and SST+ cells form synaptic inputs on distinct subcellular domains of pyramidal neurons.
Different types of inhibitory neurons have different properties, different synaptic specificity and different roles. Because of their markedly different targeting profiles, three different MGE-derived interneuron subtypes —chandelier, PV+ basket and SST+ cells— best illustrate the exceptional diversity of the GABAergic circuits. Since the location of a synaptic contact largely determines its influence on the postsynaptic cell, the inhibitory effects of chandelier, PV+ basket and SST+ synapses are markedly different.

Shaping early networks to rule mature circuits[3]

A balanced interplay between the abovementioned different types of inhibitory neurons and excitatory pyramidal neurons is a prerequisite for normative brain function, as neuronal circuits can only operate effectively within certain bounds of excitation and inhibition (Isaacson and Scanziani, 2011; Vogels and Abbott, 2009). In fact, overstepping these boundaries can have drastic pathological consequences and lead to neurodevelopmental and neurological disorders, including autism, schizophrenia and epilepsy (Marín, 2016; Paz and Huguenard, 2015).

How the relative bounds of excitation and inhibition are established during development as well as maintained or shifted during experience-dependent plasticity has been and remains an exciting and fruitful topic of research (Froemke, 2015; Hensch and Fagiolini, 2005; Nelson and Valakh, 2015; Takesian and Hensch, 2013; Vogels and Abbott, 2009).

During brain development a plethora of turbulent events frames mature neural circuits: endogenous spontaneous rhythms give way to sensory-driven activity, GABA switches polarity, canonical circuits are formed, potentiated and refined, and eventually synapses elevate their threshold for plasticity, narrowing integration windows to become fast, precise reporters of spiking activity. Each of these processes is regulated by intrinsically determined genetic programs, which are tuned by neural activity in a bidirectional manner. What could quickly become a neural cacophony actually plays out as a beautifully orchestrated symphony; transcriptional programs regulate expression of ion channels, neurotransmitter receptors and transporters, restraining patterns of network activity and controlling the transition between them (Marques-Smith et al., 2016a). The intimate association of several such developmental processes —e.g. dendritic arbor elaboration and synapse formation— dictates the precise code for a coordinated and balanced development of neural circuits.

Pyramidal neurons receive inhibition in proportion to their afferent synaptic excitation levels, meaning excitatory/inhibitory (E/I) balances across cells are stable even though afferent excitation levels differ widely (Xue et al., 2014). In addition, with the ultimate purpose of maintaining stable and functional networks, any change in, for instance, inhibition, will be accompanied by proportional changes in excitation, a concept known as homeostatic plasticity (Takesian and Hensch, 2013; Turrigiano, 2012). In fact, it is well documented that neurons and networks are highly reactive to, and capable of compensating for, changes in their excitatory-inhibitory environment (Xue et al., 2014). Yet, a large amount of evidence also shows that some alterations in E/I balance are not compensated and can lead to lasting deficits in the adult (Figure 3) (Lippi et al., 2016; Marques-Smith et al., 2016a).

Interestingly, the prevalent view in the field is that, although development is a continuous process, there are particularly sensitive developmental windows in which modifications in network organization have a long-lasting impact over the lifespan (Marín, 2016). These sensitive periods are pivotal milestones for the assembly of neural circuits. Some such milestones are directly linked to the maturation of GABAergic interneurons and inhibitory circuits, including the switch from depolarizing to hyperpolarizing GABA (Ben-Ari, 2002), the generation of transient (early network oscillation, ENO; giant depolarizing potentials, GDP) and mature (θ, γ) oscillatory rhythms —considered a prerequisite for various cognitive processes—, as well as the critical period for ocular dominance plasticity (Marín, 2016). For example, early GABAergic activity is required for dendritic elaboration (Cancedda et al., 2007) and giant depolarizing potentials (GDPs) by synchronizing developing network activity play a

[3] This paragraph contains full extracts from:
Marques-Smith, A*., Favuzzi, E*., and Rico, B. (2016). Shaping Early Networks to Rule Mature Circuits: Little MiRs Go a Long Way. *Neuron* 92, 1154–1157. *co-first authors

central role in their construction (Allène et al., 2008). Consistently, increasing evidence is highlighting the crucial role of inhibition in shaping cortical activity (Isaacson and Scanziani, 2011). Unveiling how inhibitory and excitatory neurons connect during development —i.e. the assembly of neural circuits— as well as identifying the main regulators of such a complex process might, therefore, help to shed light on early potential therapeutic interventions to restore normal brain function in neurodevelopmental disorders (Marín, 2016).

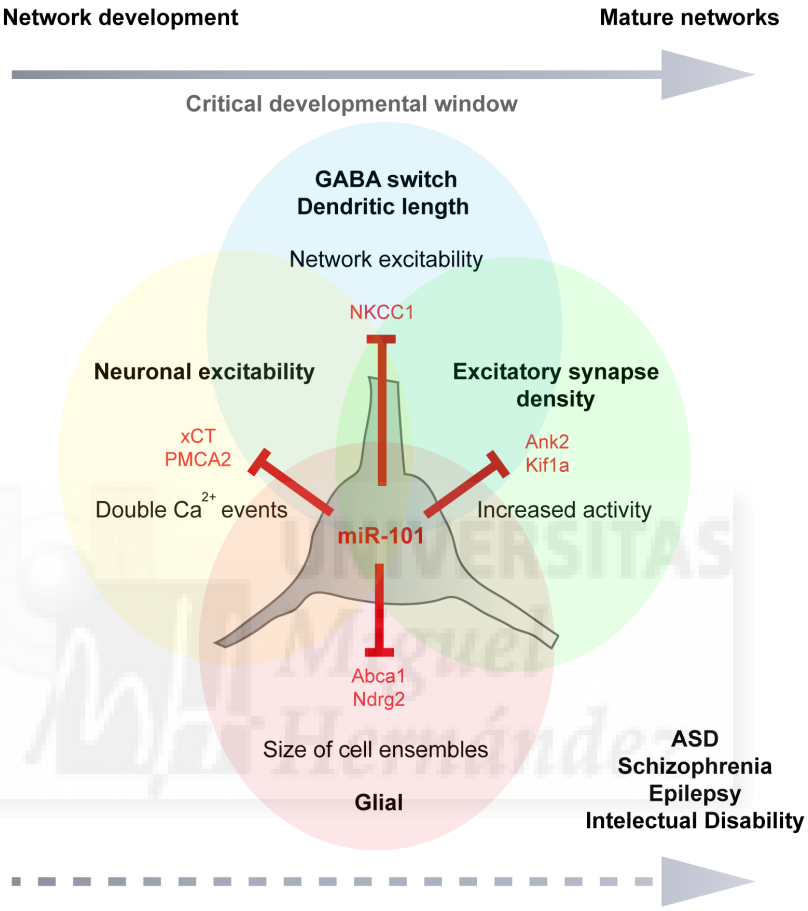

Figure 3. Alterations in E/I balance during particularly sensitive developmental windows are not compensated and can lead to lasting deficits in the adult.
Neurons and neural circuits are plastic and able to compensate for changes in the excitatory-inhibitory balance except during pivotal milestones for the assembly of neural circuits when alterations can have a long-lasting impact over the lifespan. Example of how miR-101 regulates the development of neural circuits during a particularly sensitive period and consequently shapes mature networks in the adult. Adapted from (Marques-Smith et al., 2016a).

Moreover, inhibition not only provides balance, it also ensures richness in the possible dynamic patterns of connectivity within networks of pyramidal neurons. In fact, neural circuits show exquisite fine-structure, with spatially proximal cells often participating in completely different microcircuits and subnetworks (Lee et al., 2014a, 2014c). As such, the study of the development of neural circuits cannot overlook cell-type rules of innervation. On the contrary, understanding brain function (and dysfunction) exactly requires knowledge on how the precision of its connections is established and organized. Wiring specificity implies both cell and synaptic diversity, which, in turn, are determined by tightly regulated developmental cell-specific gene programs that ultimately sculpt neuronal connectivity. By virtue of the remarkable diversity of

interneuron types and connectivity patterns, inhibitory circuits are particularly well suited to perform functionally relevant circuit-specific roles (Isaacson and Scanziani, 2011; Kepecs and Fishell, 2014). As such, it is surprising that the molecular mechanisms underlying interneuron subtype-specific connectivity are so poorly understood. With this in mind, we anticipate that gaining insights into how the elaborate organization of inhibitory connections is established will lead to an appreciation of how they critically contribute to cortical function.

In the next chapters of this introduction, we hope to accompany the reader on a journey through the sophisticated 'courtship-like' process of neural circuit formation, with a constant particular emphasis on wiring specificity. As we hope will become clear during the reading (and regardless of whether it is 'wiring' or 'synaptic'), specificity can be present only if and when diversity exists. Therefore, because they patently constitute two sides of the same coin, we will use the terms "specificity" and "diversity" interchangeably. With this introduction, we hope to provide a comprehensive framework of the different but coordinated cellular and molecular mechanisms that operate throughout development (which, often, also means throughout evolution) to accomplish the ultimate purpose of the brain's exceptional wiring specificity. In trying to do this, we will not exclusively confine the description to the mouse cortex; we will also include some relevant examples from other brain regions and, very occasionally, from invertebrate systems. The reader will probably notice a frequent lack of detailed information about inhibitory circuits. Although in the last years we have witnessed an enormous increase in our understanding of the development and function of interneurons and inhibitory circuits, such knowledge has undoubtedly lagged behind that of excitatory neurons. As a prelude to the results of this thesis, in the last chapter, we will zoom out from the molecular mechanisms and reexamine interneuron wiring specificity in the context of both the background provided and the circuit-specific roles of different interneuron types.

2. Circuit formation and synapse specificity: a long path towards stable relations

The most remarkable feature of the neural circuits is the precision of the synaptic circuitry. How does an axon find the right —among numerous available— partner to form a synapse that not only functions but also lasts for a long time? The cellular and molecular mechanisms underlying the formation of specific synaptic connections have long been investigated (Langley, 1895; Speidel, 1942; Sperry, 1963), demonstrating that it emerges through an exquisitely complex sequence of developmental processes. This includes the appropriate generation, fate determination and positioning of individual cell types, neurite extension and axon pathfinding, the creation of elaborated terminal arborizations, target innervation, up to mechanisms that control the cellular and subcellular specificity of synaptic connections, and then culminates with synaptic plasticity (Figure 4).

Similar in concept to Waddington's landscape model (Waddington, 1959), each step gradually restricts the number of potential synaptic partners and further sculpts neuronal connectivity. Regardless of its multiplicity, it is generally agreed that the development of neural circuits involves two broad sequential phases. First, mostly genetically determined processes lead to a transient and relatively nonspecific contact that is stabilized by molecular interactions. Afterward, a series of progressively more activity-dependent processes kicks in and ultimately shape brain circuits (Figure 4).

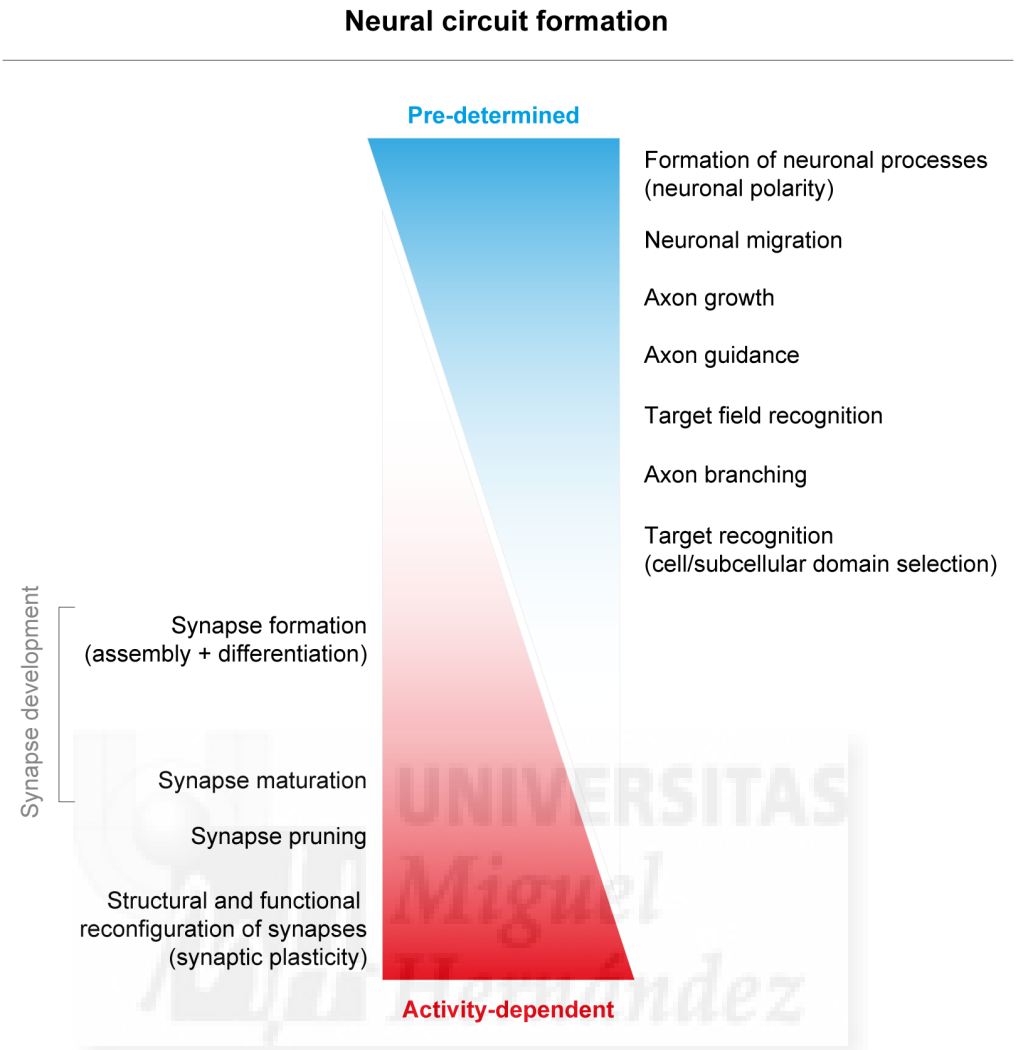

Figure 4. Sequence of developmental processes that lead to the formation of neural circuits.
The development of neural circuits involves a first sequence of mainly genetically determined events and, next, several progressively more activity-dependent processes. After fate determination, neurons acquire polarity and migrate. Afterward, they extend the axon that grows, guided by several cues, and ultimately finds its target field where it branches and contacts the postsynaptic cell. Subsequently, the contact is stabilized and the assembly and differentiation of a synapse occurs, followed by its maturation (collectively: synapse development). Those synapses that are not stabilized are eliminated by activity-dependent competitive processes. Each of these steps gradually restricts the number of potential synaptic partners and contributes to specifying neuronal connectivity. Newly formed neural circuits are plastic and are continuously remodeled upon changes in the environment (synaptic plasticity).

3. The importance of being Axon[4]: growth, guidance and branching

Before newly generated and specified neurons can differentiate and establish synaptic contacts, they migrate—up to thousands of cell diameters—and follow complex routes, changing direction at landmarks along the way (Marín et al., 2010). Being critical for the

[4] Title freely adapted from Oscar Wilde's 1895 "The Importance of Being Earnest", regarded by many as Oscar Wilde's masterpiece. Part satire, part comedy of manners, and part intellectual farce, "The Importance of Being Earnest" reveals the portrayal of marriage during the late Victorian era.

development of brain architecture, neuronal migration is the very first step of brain wiring. As such, migration (in particular tangential migration, as is the case of interneurons in the cerebral cortex) contributes to increasing the complexity of the cortical circuits (Marín et al., 2010).

Axon growth and guidance

Neuronal migration is tightly coupled to axon growth and guidance. In most instances, while cells are migrating towards their target, they emit a trailing process (Marín et al., 2010). In the last phases of migration and once differentiating neurons have reached their final position, the trailing process becomes the axon. Of note, in cortical interneurons the leading process branches and grows as part of the migratory cycle (Marín et al., 2010). An elongating axon has a unique cytoskeleton structure and is tipped at its leading edge with a highly motile and sensitive structure, the growth cone. While growth cones migrate through the environment toward their future synaptic targets, the axons extend rapidly and are steered by a wide range of guidance cues and intermediate guideposts (Goldberg, 2003; Lewis et al., 2013).

By the early 1990s, a burst of research on axon guidance led to the discovery of several conserved families of axon pathfinding molecules, providing the molecular basis for Sperry's pioneering chemoaffinity hypothesis (Sperry, 1963). Guidance cues regulating chemotaxis operate at close or large distances and can either attract or repel growth cones. Prominent among these molecules are the netrins, Slits, semaphorins, and ephrins (Dickson, 2002; Tessier-Lavigne and Goodman, 1996). In addition to extracellular molecules and their corresponding receptors, much has been learned about the complex intracellular effectors and signaling pathways that mediate the response of the axon to specific cues (Bashaw and Klein, 2010; Dent et al., 2011). Activation of specific signaling pathways can alter the directional response elicited by a particular cue (attraction versus repulsion). Moreover, signaling events that act locally to modulate cytoskeletal dynamics can also result in growth cone collapse or affect the rate of axon extension. Downstream effectors and regulators of axon growth include calcium and cyclic nucleotide signaling, Rho-family GTPases, kinase cascades and, finally, actin- and microtubule-associated proteins that regulate cytoskeletal dynamics (Bashaw and Klein, 2010; Dent et al., 2011; Lewis et al., 2013; Navarro and Rico, 2014). Of note, recent evidence underscored a role for synaptic proteins in axon growth and guidance. For instance, SNARE proteins have been shown to couple axon guidance to the membrane dynamics occurring at the growth cone (Barrecheguren et al., 2016; Cotrufo et al., 2011).

The establishment of proper circuit connectivity also requires that different neuronal populations respond selectively to guidance cues at particular times and at specific locations. Transcription factors act as master regulators of most cellular processes, and axon guidance is no exception. For instance, Satb2 and Ctip2 are two mutually repressive transcription factors that critically regulate whether neocortical pyramidal neurons form interhemispheric or corticofugal connections respectively (Alcamo et al., 2008; Chen et al., 2005). Another example is how the specific expression of the zinc-finger transcription factor ZIC2 guides the midline crossing choice made by retinal ganglion cell (RGC) axons at the level of the optic chiasm (García-Frigola et al., 2008; Herrera et al., 2003). Over the past decade, significant progress has been made in the identification of the transcription factors that coordinate the precise spatial, temporal and cell-type-specific expression of axon guidance molecules, showing that they critically contribute to specifying neural connectivity (Polleux et al., 2007; Santiago and Bashaw, 2014).

Target field recognition

Just before axonal branching takes place, axon terminals are further sorted into restricted target fields, such as appropriate layers or topographic locations (Figure 5).

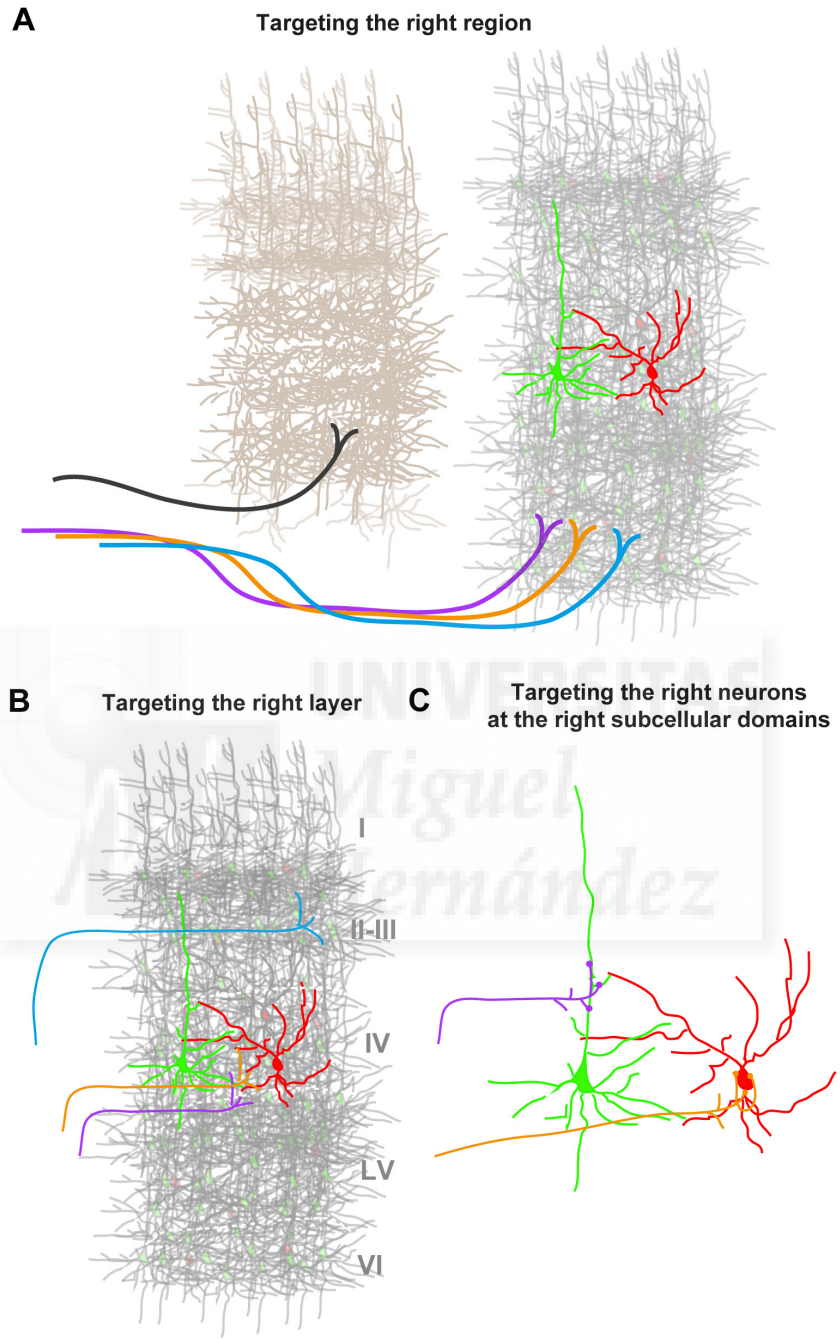

Figure 5. The coordination and summation several processes specifies neuronal connectivity.
(A) A neuron sends an unbranched axon over a long distance and targets a specific area (e.g. visual cortex).
(B) The axon invades the cortical layers, sending out small branches and terminating in a specific layer or in the right topographic zone (e.g. layer 4).
(C) The axon branches form synaptic contacts with specific postsynaptic targets within the neuropil (e.g. dendrites of pyramidal somata). Each of these individual processes plays a role in establishing a synaptic pattern although none of them uniquely accounts for synapse specificity.

This is well illustrated by how specifically thalamic axons of the visual system enter the cortex and extend collaterals in layer 6, then grow straight through layer 5, and terminate in layer 4 where they extensively branch and synapse with cortical neurons (Yamamoto et al., 1989). Another classic example is represented by SST-positive Martinotti cells, which are particularly abundant in neocortical layer V and possess ascending axons that arborize in layer I where they establish synapses onto the dendritic tufts of pyramidal neurons (Kawaguchi and Kubota, 1997; Wang et al., 2004c). Interestingly, the remaining Martinotti cells found throughout layers II-VI also exhibit exquisite target selectivity despite the multiplicity of cortical layers contacted (Wang et al., 2004c).

Although the molecular mechanisms that direct target field specificity are not fully understood, there is compelling evidence suggesting that they are not dissimilar from those mediating long-range axon guidance. Receptors on growth cones sense maps of soluble, membrane-bound, and matrix-associated ligands and navigate by altering their direction in response to them (Inoue and Sanes, 1997). In addition, axonal expression of hemophilic cell-adhesion molecules, such as cadherins or Ig-like cell adhesion molecules (Ig-CAMs), seems to promote layer-specific interactions with corresponding populations of neurons that express the same molecule (Poskanzer et al., 2003; Yamagata and Sanes, 2008; Yamagata et al., 2002).

Axon branching

Axons select appropriate target regions during pathfinding, but it is the last step of axon development —their extensive branching and the formation of elaborate terminal arbors— that is responsible for virtually all of the synaptic connections of a neuron. Each neuron generates a single axon but makes synaptic contacts with many target cells. As such, the formation of axon branches not only allows neurons to establish complex patterns of connectivity but also provides an additional mechanism for target selection. Given its importance in establishing neural circuits, it is surprising how little attention the mechanisms underlying axonal branching have received as compared to axon guidance.

Axon branches can arise through two distinct mechanisms (Gallo, 2011). In the neocortex, the emergence of protrusive filopodia and lamellipodia generates branches directly along the axon shaft (interstitial branching or axon sprouting). This mechanism increases axon coverage to define its “presynaptic territory”, and it is thought to contribute to increased network connectivity (Portera-Cailliau et al., 2005). In certain circumstances, cortical neurons can branch by splitting of the terminal growth cone (axon bifurcation). This second mechanism is linked to axon guidance and to the capacity of one single neuron and one single axon to reach two targets that are far apart (Gallo, 2011; Lewis et al., 2013).

Regardless of what type of protrusion gives rise to a branch, time-lapse imaging revealed that there is an inverse correlation between growth cone speed and branching extension and complexity (Lewis et al., 2013), suggesting that branches extend while axons stall or retract. Therefore, different types or concentrations of target-derived cues are likely to evoke either further growth or branching in developing axons. Consistent with this idea, classical families of axon guidance cues (netrins, Slits, semaphorins, and ephrins) —in addition to growth factors, neurotrophins and morphogens— have been shown to determine the correct position of branches or to shape the terminal arbors (Kalil and Dent, 2014). Further supporting the similarities and cross-talk between axon guidance and branching, some of the signaling pathways activated by extracellular cues during axon pathfinding (e.g. calcium signaling and Rho GTPases) also regulate the formation of branches (Kalil and Dent, 2014; Spillane and Gallo, 2014).

Of note, neuromodulators, such as serotonin, also play a critical role in axon refinement (as well as in axon growth and guidance) (Gaspar et al., 2003).

All of these pathways eventually converge on the ultimate effector of axon branching, the cytoskeleton. A coordinated reorganization of F-actin filaments and microtubules respectively initiates and sustains axon branching (Dent and Kalil, 2001). However, just like growth cone-mediated axon elongation, neither actin filaments nor microtubules act alone. For example, during the formation and stabilization of axon branches the properties of microtubules are regulated by diverse cellular factors, including microtubule-associated proteins (MAPs) which bind microtubules along their lengths and thus critically regulate cytoskeletal dynamics (Armijo-Weingart and Gallo, 2017).

4. An Ideal Husband, Act I[5]: post-synaptic target recognition

Within a target field, the widespread branching of an axon results in random and transient contacts with both neuropil and somas of countless different cells. However, axon terminals are endowed with exquisite ability to discriminate their correct synaptic targets among a dense array of potential partners (Figure 5).

Almost a hundred years ago Speidel saw this process during development of the innervation of the tadpole's tail fin: the ingrowing axons branched profusely before some terminals connected with skip or muscles. Subsequently, unwanted branches were eliminated by autotomy or withdrawal (Speidel, 1942). Post-synaptic target selection and synapse formation in the mammalian cerebral cortex is no different. While correct contacts are made on the basis of chance, permanent connections are formed as a result of chemoaffinity (Sperry, 1963).

Molecular mechanisms of target recognition

Several chemoaffinity-based recognition strategies exist —from invertebrates to the cerebral cortex in mammals— that cooperatively ensure correct matching of synaptic partners (Figure 6) (Christensen et al., 2013; Lu et al., 2009; Williams et al., 2010; Yogev and Shen, 2014).

Transmembrane cell adhesion molecules (CAMs), which mediate recognition of partner cells and tethering of their membranes, are uniquely suited for this role. Cell adhesion molecules, among which a prominent role is played by cadherins, serve both as permissive adhesion substrates and as recognition tags. As such, they have been shown to trigger transient, weak and relatively nonspecific as well as strong and more selective contacts between putative synaptic partners (Fannon and Colman, 1996; Shapiro et al., 2007; Takeichi, 2007). In addition to cadherins, distinct leucine-rich repeat (LRR) proteins are expressed in different cell types and can regulate input-specific target selection. For example, Netrin-Gs interact with members of the leucine-rich repeat (LRR) family of cell adhesion proteins called Netrin-G ligands (NGLs). Different Netrin-Gs are expressed on the surface of distinct axonal populations and determine dendritic clustering of their respective postsynaptic NGLs in a pathway-specific manner (Lin et al., 2003; de Wit and Ghosh, 2014).

Worth mentioning, as an alternative to the binary code of presence or absence of adhesion molecules, connectivity can be specified by generating gradients of expression levels of a given molecule. A **combination of qualitative (identity) and quantitative (levels) aspects** determines the type and strength of the resulting cell-cell interaction and hence adds greater complexity to the control of synaptic specificity (Hirano and Takeichi, 2012). This is how, in the fly olfactory system, a dorsolateral-to-ventromedial

[5] For readers interested in literature insights: Oscar Wilde's 1895 play "An Ideal Husband" concerns marriage. "An Ideal Husband" enfolds you in a dream world of Victorian London people, flirting and exchanging bons mots. With decadent irony, Wilde offers insights into the perils of idealization, and simultaneously reveals how human imperfections characterize personal relationships.

gradient of the transmembrane Semaphorin Sema-1a instructs projection neuron dendritic targeting in the antennal lobe (Komiyama et al., 2007).

Transmembrane molecules that mediate **contact-dependent repulsion**, such as Dscam in Drosophila or protocadherins in mammals (Hayashi and Takeichi, 2015) also play a role in directing synapse specificity. For example, repulsive interactions between similar Dscam isoforms ensures correct partner choice in tetrad synapses of the Drosophila lamina (Millard et al., 2010).

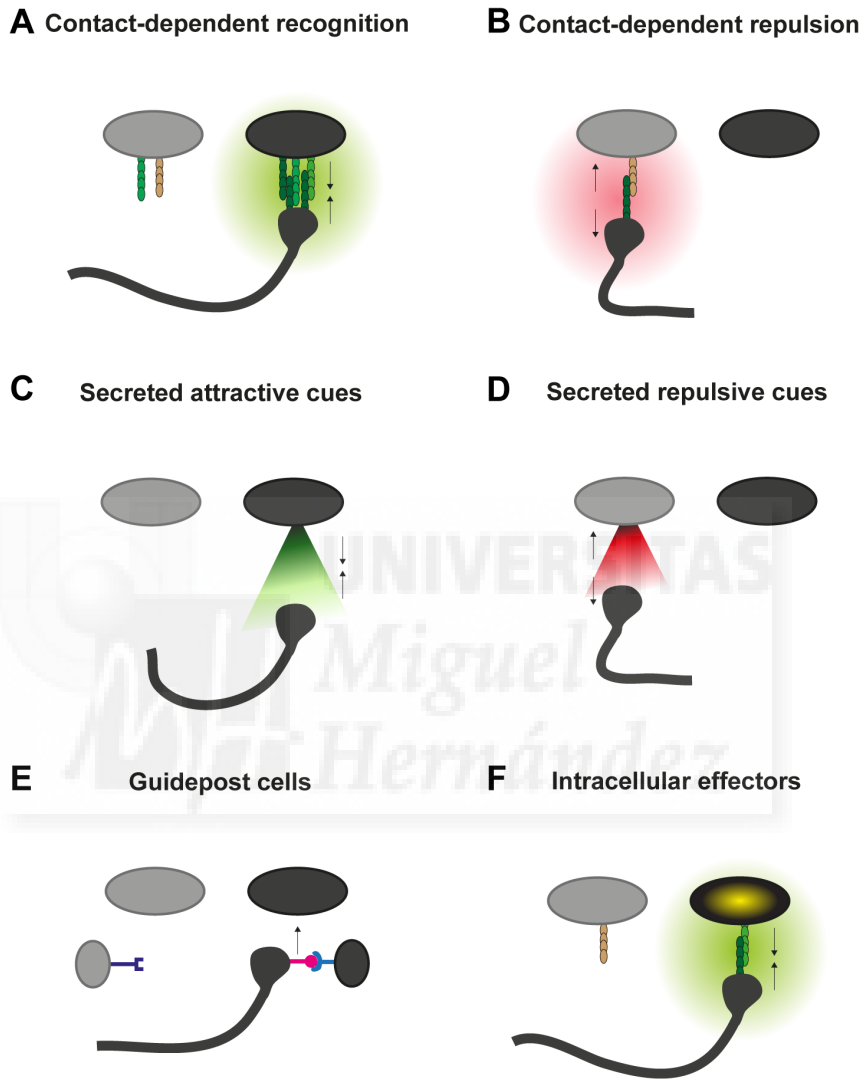

Figure 6. Several chemoaffinity-based recognition strategies cooperatively ensure correct matching of synaptic partners and synapse specificity.
Model mechanisms for synaptic specificity during development. Interactions with appropriate synaptic partners can be accomplished through (A) contact-dependent recognition (green) or (B) contact-dependent repulsion (red). Alternatively, attractive (C) or repulsive (D) secreted cues derived from target cells can guide the axons towards the appropriate target. (E) The formation of transient synapses with guidepost cells (squares) can provide a means of prepatterning synaptic structures before final target cells have arrived or matured in the target area. In some systems, guidepost cells are transient populations that are eliminated by cell death once the final wiring pattern has been accomplished. (F) Intracellular signals (e.g. calcium) contribute to marking the correct target recognition by activating intracellular pathways.

It is important to note that, in many cases, target cell recognition may be fairly considered a kind of short-range axon guidance (Sanes and Yamagata, 2009). As such,

secreted and transmembrane **guidance cues** may play a role not only *en route* to a target region but also within it, thus directly contributing to synaptic choices. Because of its topographic connections, the vertebrate retina is the structure that probably best illustrates how homophilic interactions among cell surface molecules generate sublaminar and hence synaptic specificity. In fact, in the retinotopic system, a map of axon position is converted into a map of synaptic connectivity without the need for positional labels on the target cells (Missaire and Hindges, 2015; Sanes and Yamagata, 2009; Yogev and Shen, 2014).

In addition, attractive and repulsive **secreted cues** have also been identified as mediators of target recognition. An example is the specific secretion of Sonic Hedgehog by postsynaptic deep-layer neocortical projection neurons which promotes synapse formation with callosal presynaptic terminals expressing the receptor Brother of CDO (Boc) (Harwell et al., 2012).

Furthermore, a number of inhibitory secreted molecules have been shown to be implicated in synapse specificity. In the *C. elegans* DA9 motorneuron, presynapse formation onto postsynaptic muscles is restricted to the dorsal axon by specific secretion of two diffusible molecules, Wnt homolog LIN-44 and UNC-6/Netrin from ventral cells (Klassen and Shen, 2007; Poon et al., 2008). However, probably the best example of repulsive secreted molecules that direct synapse specificity are Semaphorins which, in addition to their role in axon guidance, have been shown to inhibit inappropriate target selection in multiple systems and throughout evolution (Ding et al., 2011; Matsuoka et al., 2011a, 2011b; Mizumoto and Shen, 2013; Pecho-Vrieseling et al., 2009; Tran et al., 2009).

Importantly, the **extracellular matrix** provides an ideal substrate to bind and retain secreted specificity cues (Xiao et al., 2011; Yamagata and Sanes, 2005). This is well illustrated by how a basement membrane type IV Collagen retains Slit1a secreted by neurons in the zebrafish optic tectum (Xiao et al., 2011). This binding is critical for the assembly of lamina-specific connections, raising the possibility that similar mechanisms might also be in place during target recognition.

Moreover, positive and inhibitory diffusible cues may also be expressed by nontarget cells, such as **guidepost cells**. In the cerebellar cortex, the immunoglobulin-like protein Close Homologue of L1 (CHL1) directs the stellate cell axons to specific dendritic regions in Purkinje cells. Interestingly, CHL1 is not expressed in the target cell itself but in neighboring Bargmann glia that function as guidepost cells (Ango et al., 2008). Determination of target specificity by a signal from nearby guidepost cells has also been reported in C. elegans (Colón-Ramos et al., 2007).

Although many **intracellular effectors** undoubtedly still await discovery, a direct relationship between local calcium signals and target recognition has been shown, suggesting that differences in intracellular signaling also contribute to specifying connectivity (Lohmann and Bonhoeffer, 2008).

Once again, as for axon guidance, the ultimate level at which target recognition appears to be regulated is **transcription**. Seminal work on the mechanisms that control cellular target specificity in the spinal cord revealed how intrinsic transcriptional programs regulate the expression of specific surface molecules (Pecho-Vrieseling et al., 2009; Vrieseling and Arber, 2006).

Finally, it is worth mentioning two other aspects that can regulate the assembly of synapses and, in a broader sense, the selectivity inherent in their formation: **timing** and the use of **post-translational modifications**. Both aspects are well illustrated by the observation that polysialic acid (PSA), which is attached to the cell adhesion molecule NCAM, prevents precocious maturation of GABAergic synapses in the visual cortex of mammals and, thus, regulates the onset of ocular dominance plasticity (Di Cristo et al., 2007). This and other works (Deguchi et al., 2011; Imamura et al., 2011; Petrovic and

Hummel, 2008; Tripodi et al., 2011) provide some support to Jacobson's outdated 'timing hypothesis' (Jacobson, 1969) and suggests that, in some cases, timing of innervation can be used together with other recognition cues to determine synapse specificity.

Subcellular specificity

Because of the highly polarized structure of neurons, the subcellular location of synaptic inputs profoundly impacts the response of the postsynaptic cell and hence the function of neural circuits. In particular, the relative position of synapses along the axo-somato-dendritic axis critically and differentially affects the generation of action potentials. It is therefore not surprising that synapse formation mostly occurs with subcellular precision. But why 'wasting time and energy' targeting, for instance, the cell body of a given cell and, only after, a specific subcellular compartment when we could use a combinatorial molecular code to achieve both goals at the same time? It seems that evolution agrees with us. Although, for the sake of simplicity, in the examples above specificity was considered on a whole-cell targeting basis, clearly it often involved —and directly resulted in— subcellular specificity as well.

Moreover, many brain structures are divided in layers or laminae where specific subcellular domains of the target cell lay. As a result of the laminar organization of certain subcellular domains, some of the previously described target field recognition may also inherently determine subcellular specificity. In addition to the abovementioned example of how retinal axons are guided to and topographically organized within their target field, another paradigm can be found in the rodent hippocampus. In the *Cornu Ammonis* (CA) regions, the dendritic tree of pyramidal neurons branches specifically (and extensively) in the *strata radiatum* and *lacunosum-moleculare*. Consequently, for some dendritic inputs, the laminar distribution of the targeting axons also determines their subcellular localization (Frotscher et al., 1997; Sanes and Yamagata, 1999). Yet, how does a thalamic input in the CA1 region of the hippocampus select between pyramidal cell dendrites in the stratum lacunosum or the dendrites of at least ten different types of interneurons? This could be considered another example of cellular specificity possibly being determined at the same time (or after) the subcellular one.

Therefore, it is important to note that, although we have presented them as a separate sequence, all these selection processes are often overlapping both temporally and mechanistically. This concept is further supported by the similarity of cues and molecules that have been shown to determine subcellular specificity to the ones described in the previous examples (de Wit and Ghosh, 2016; Yogev and Shen, 2014), with once again the aforementioned cadherins playing a recurrent key role (Rebsam and Mason, 2011; de Wit and Ghosh, 2016). Remarkably, these choices can also be made later, at the level of assembling synapses [(Williams et al., 2011), see next chapter].

Nevertheless, at least some mechanisms of subcellular specificity seem to follow a precise temporal sequence and involve a restriction of a formerly determined cellular specificity. In the cerebellum, specialized inhibitory basket neurons synapse specifically onto the axon initial segment (AIS) of Purkinje neurons. During development, basket axons travel first to Purkinje somata and are then guided to the AIS where they eventually develop synapses (Ango et al., 2004). Some evidence suggests that this could be due to the ability of the membrane-associated adaptor protein Ankyrin-G to restrict expression of several cell adhesion molecules to the AIS, including the L1 cell adhesion molecule neurofascin. These molecules might then act as recognition signals and thus guide the axon to the AIS (Ango et al., 2004). With this being the only known instance so far of subcellular specificity arising from a restriction of cellular specificity and since the molecular mechanisms that establish subcellular domains are not fully understood (de Wit and Ghosh, 2016), the question remains as to how common this mechanism is in different neurons, regions and organisms.

In summary, two general principles can be inferred from the global picture drawn so far. First, both evolution and development bring recurrent molecular mechanisms (Figure 6) and sometimes even recurrent type of molecules, such as semaphorins or cadherins, back to achieve the common goal of synapse specificity. Second, synapse specificity can take many 'forms' (Figure 5), yet each of these individual processes plays a role in establishing a synaptic pattern but probably does not uniquely account for it. In the establishment of particular sets of connections, all these processes are anything but independent; their coordination and summation are critical to accomplishing the ultimate purpose of specifying connectivity.

5. An Ideal Husband, Act II: synapse formation and maturation

Once matching synaptic partners are in contact, they engage in some 'cell-to-cell serious talk' —bidirectional signaling mediated by signaling molecules— that ultimately leads to the assembly and differentiation of pre- and postsynaptic membrane specializations.

Forming a synapse

Synapses are specialized, highly asymmetric intercellular junctions through which neurons communicate. Forming a synapse requires the **first immature contact** to be followed by a coordinated **assembly** of components on either side of the synaptic cleft. On the presynaptic side, synapse **differentiation** begins with the formation of an 'active zone' where neurotransmitters are released into the synaptic cleft. On the postsynaptic side, receptors and signaling molecules are induced and localized, conferring the capacity to transduce the given signal into a postsynaptic response.

Which are the molecules that in the mammalian brain drive these structural and functional changes in developing synapses? With regard to this question, the 2000s were to synapse formation what the 1990s were to axon guidance: an exciting era in which several so-called 'synaptogenic molecules' were brought to light. Although cell adhesion molecules had long been known to hold synaptic membranes together, it was only relatively recently that heterophilic or homophilic interactions between some membrane-bound molecules were shown to have an instructive role and critically trigger synapse formation (Biederer et al., 2002; Linhoff et al., 2009; Scheiffele et al., 2000). Such molecules have a cohesive role in the initial establishment of a synaptic contact, thereby aligning pre- and postsynaptic specializations with each other. In addition, they also initiate trans-synaptic signaling events and, thus, function as key **synaptic organizers** (Siddiqui and Craig, 2011).

The best example of cell adhesion molecules with both adhesive and inducing function at synapses are **neuroligins and neurexins**. Interaction of neurexin with neuroligin results in bidirectional differentiation signals and recruitment of additional pre- and post-synaptic proteins, respectively (Scheiffele, 2003; Shen and Scheiffele, 2010; Siddiqui and Craig, 2011). Of note, neurexin-neuroligin adhesion complexes promote both excitatory and inhibitory synapse formation (Chih et al., 2005; Prange et al., 2004; Ullrich et al., 1995), although different variants seem to have a bias toward a specific class (Siddiqui and Craig, 2011). As a retrograde signal, the neurexin-neuroligin complex organizes the presynaptic compartment, inducing the accumulation of active zone components and synaptic vesicles as well as the release of neurotransmitters upon depolarization. The response triggered in the postsynaptic cell is equally profound: postsynaptic scaffolding molecules and neurotransmitter receptors are recruited to synaptic sites and, for excitatory synapses, dendritic spines are formed (Siddiqui and Craig, 2011).

The elegant experiment that led to the discovery of neuroligins and neurexins as potent inducers of synapse formation has become a 'classic' of neuroscience. In this assay, non-neuronal cells expressing a candidate synaptic cell adhesion molecule were co-cultured with neurons, and the formation of synapses by the neuron on the non-neuronal cell was examined (Scheiffele et al., 2000).

Assay systems that are similar to those used for the characterization of the neurexin-neuroligin complex led to the discovery of several other synaptogenic adhesion complexes, such as the cell adhesion molecule, SynCAM (Biederer et al., 2002) or members of the **leucine-rich repeat (LRR) family** of cell adhesion proteins (de Wit and Ghosh, 2014, 2016; de Wit et al., 2011).

LRR proteins, including LRR transmembrane neuronal proteins (LRRTMs), Slit- and Trk-like proteins (Slitrks) and Netrin-G ligands, are key organizers of excitatory and/or inhibitory synapses in the central nervous system (de Wit and Ghosh, 2014, 2016; de Wit et al., 2011). Cell surface proteins containing an extracellular LRR domain are generally localized to the postsynaptic membrane and interact with distinct presynaptic partners, including neurexins (de Wit et al., 2009).

Finally, in addition to neuroligins and specific LRR proteins, another structurally distinct ligand pair, the complex of **Cbln1**-GluRδ2, was also identified as the trans-synaptic binding partners for a specific neurexin isoform in the cerebellum (Matsuda et al., 2010; Uemura et al., 2010).

All synaptic organizers, like neuroligins or LRR proteins, have two fundamental properties: (1) ability to activate a trans-synaptic signaling cascade that stabilizes a first transient synaptic contact and (2) instructive ability to produce presynaptic terminals with a complete physiological complement, as shown by induction of presynaptic differentiation in co-culture assays (Shen and Scheiffele, 2010).

The resulting synapses are functional but immature. Subsequently, a combination of intrinsically determined genetic programs and activity-dependent processes mediates synapse maturation.

Synapse maturation

Immature excitatory and inhibitory synapses are constantly generated at a high rate in the developing brain. Many of such synapses are eliminated during circuit refinement, but a subset is selected for maturation and stabilized. The role of activity in driving the maturation of newly generated synapses is a long-standing, well-documented staple in developmental neuroscience (Katz and Shatz, 1996). It was only very recently, however, that solid evidence was provided for a comparable critical role of activity-independent genetically predetermined developmental programs in basic circuit connectivity (Sando et al., 2017; Sigler et al., 2017; Varoqueaux et al., 2002; Verhage et al., 2000).

The maturation of a synapse involves a morphological expansion of the synaptic junctional membrane that is intimately related to both an increased efficacy of presynaptic neurotransmitter release and a mature profile of postsynaptic receptors. Despite obvious fundamental differences in the maturation of excitatory versus inhibitory synapses associated with the release of different neurotransmitters and although much less is known about inhibitory compared to excitatory synapses, it appears that the basic organizing principles of synapse maturation hold true for both classes (Fossati et al., 2016; Fritschy et al., 2012; Huang and Scheiffele, 2008; McMahon and Díaz, 2011; Sassoè-Pognetto et al., 2011; Sheng and Kim, 2011; Siddiqui and Craig, 2011).

The maturation of a synapse involves both structural and functional changes and affects: (1) type and abundance of post-synaptic receptors, (2) scaffold proteins, (3) cytoskeleton structure, (4) presynaptic active zone, (5) presynaptic release and (6) subunit composition of post-synaptic receptors (Figure 7).

The first step in synapse maturation is the synaptic incorporation of clusters of AMPA (for excitatory synapses) and $GABA_A$ (for inhibitory synapses) receptors (Huang and Scheiffele, 2008; O'Brien et al., 1998). The importance of this step has been well studied for glutamatergic synapse maturation. Immature excitatory synapses are 'silent' (Graf et al., 2004) meaning that they contain only NMDA but lack AMPA receptors (Isaac et al., 1995; Liao et al., 1995). NMDA receptors (NMDARs) are largely non-conducting at resting membrane potentials but conduct at depolarized membrane potentials. Synaptic accumulation of AMPA receptors (AMPARs) and consequent AMPA receptor-mediated depolarization leads to the simultaneous activation of NMDA receptors and, thus, to the further potentiation of the synapse (Hanse et al., 2013). Of note, most regulators of synapse maturation play a role precisely in this first critical step, further underscoring its prominence [(Dalva et al., 2000; DeNardo et al., 2012; Kalashnikova et al., 2010; Kim et al., 2006; Ko et al., 2006; O'Brien et al., 1999; Siddiqui et al., 2013), see also Part II of the thesis]. Although less studied, regulation of $GABA_A$ receptor trafficking is thought to critically determine inhibitory synaptic strength in a relatively similar way (Luscher et al., 2011).

Synapse maturation also involves recruitment of scaffolding proteins, abundant and essential components of the postsynaptic specialization (Kim and Sheng, 2004). Scaffold proteins anchor both neurotransmitter receptors and adhesion molecules linking them with downstream signaling proteins. At the excitatory synapses, such scaffold proteins include the membrane-associated guanylate kinases (MAGUKs), among which prominent in synapse maturation is the role of PSD95 (Béïque et al., 2006; Ehrlich et al., 2007; El-Husseini et al., 2000; De Roo et al., 2008; Sala et al., 2001; Zheng et al., 2011). Likewise, the scaffold protein gephyrin and several gephyrin-associated proteins are recruited at the inhibitory synapses (Fritschy et al., 2008; Poulopoulos et al., 2009; Tyagarajan et al., 2011). Scaffold proteins also bind to and regulate the dynamics of the subsynaptic cytoskeleton, another structural element that undergoes profound remodeling on both sides of the maturing synapse. Postsynaptically, actin dynamics structurally support the generation of dendritic spines, the site of most excitatory synapses and some inhibitory synapses associated with them (Chiu et al., 2013; Ethell and Pasquale, 2005; Fukazawa et al., 2003; Hlushchenko et al., 2016). Presynaptically, the cytoskeletal structure supports the mature molecular organization of the active zone (Gundelfinger and Fejtova, 2012; Schoch and Gundelfinger, 2006). At both classes of synapses, this maturation results in stabilization of mobile vesicles pools (Fu et al., 2012; Toth et al., 2013), one of the most important determinants of the reliability of synaptic transmission (Südhof, 2013). Accordingly, such presynaptic changes lead to an increased release of neurotransmitter, which, in turn, further potentiates the synapse (Lauri et al., 2007).

Other functionally relevant changes required for synapse stabilization and to increase synapse strength are the switch in the synaptic NMDAR subunit composition from GluN2B- to GluN2A-containing NMDARs (Bellone and Nicoll, 2007; Sanz-Clemente et al., 2013) and a similar developmental change in $GABA_A$ receptor subunits (Galanopoulou, 2008; Ortinski et al., 2004). Of note, although excitatory synapse maturation on different types of GABAergic interneurons is also characterized by analogous developmental changes, they exhibit remarkable heterogeneity with regard to the type, composition or relative abundance of glutamate receptors (Matta et al., 2013).

Finally, in addition to the molecules listed above, multiple sets of proteins are recruited in a subtype-specific manner to the maturing pre- and postsynapse and regulate synapse development in specific neuronal cell types (Dunah et al., 2005; Fazzari et al., 2010; Li et al., 2007; Lovero et al., 2015; Pelkey et al., 2015).

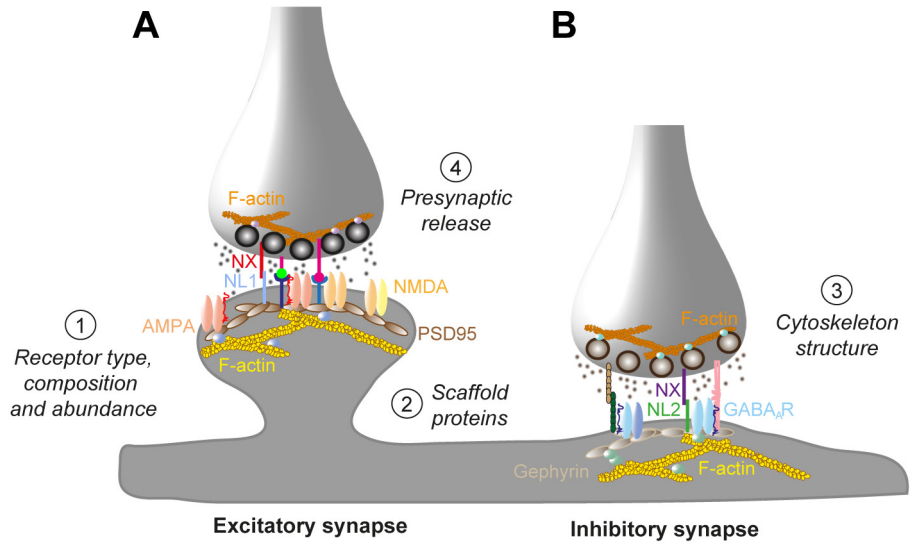

Figure 7. Structural and functional changes that lead to the maturation of a synapse. The basic organizing principles of synapse maturation are shared by both excitatory (A) and inhibitory (B) synapses and include modifications in (1) type, composition and abundance of post-synaptic receptors, (2) scaffold proteins, (3) pre- and postsynaptic cytoskeleton structure, (4) presynaptic active zone and consequent presynaptic release. Note that the numbers do not implicate a strict temporal order of such events. Several additional synapse-specific proteins are recruited in each of these steps and further contribute to the maturation of different types of synapses.

Processes driving synapse maturation

What causes this gigantic and elaborate synapse construction? The current view is that the initial molding is likely to result from bidirectional signals triggered by the very same adhesion systems that initiate synaptogenesis (Sigler et al., 2017). In turn, such genetically predetermined synaptic pathways promote recruitment of key synaptic components and regulators responsible for the subsequent transformation. For example, Neuroligin 2 interacts with gephyrin and recruits gephyrin-associated proteins to inhibitory postsynapses (Poulopoulos et al., 2009).

The cell-autonomous processes dictated by genetic programs are critically complemented by signaling via trophic factors and guidance cues, secreted by both neurons and glial cells (Christopherson et al., 2005; Clarke and Barres, 2013; Hall et al., 2000; Huang et al., 1999; Ledda et al., 2007; Ohba et al., 2005; Poo, 2001; Terauchi et al., 2010; Umemori et al., 2004). Moreover, both glutamate and GABA release play a critical role. Interestingly, GABA signaling —which, in developing neurons, is depolarizing and supports synchronous network activity (Ben-Ari, 2002) — appears to be critical for both excitatory and inhibitory synapse maturation (Chattopadhyaya et al., 2007; Fu et al., 2012; Hanse et al., 1997; Huupponen et al., 2013; Leinekugel et al., 1997; Owens and Kriegstein, 2002), underscoring the importance of a coordinated development of both systems to achieve a balanced and stable mature network (Marques-Smith et al., 2016a). As such, the developmental program independent of neurotransmitter signaling “lays out a carpet” of functional synapses onto which activity leaps and operates.

The increase in presynaptic neurotransmission allows a release-dependent further potentiation of nascent synapses (Katz and Shatz, 1996; Okabe et al., 1999; Philpot et al., 2001; Rao and Craig, 1997; Star et al., 2002). For example, correlated pre- and postsynaptic activity increases the synaptic incorporation of AMPARs (Durand et al., 1996; Liao et al., 1995). As sensory systems mature and sensory input increases,

activity-dependent changes in synapse number, structure and function take place. Those synapses that are not stabilized and fail to become potentiated are consequently targeted for elimination and phagocytosed by astrocytes and microglia (Bian et al., 2015; Chung et al., 2013; Clarke and Barres, 2013; Hall and Ghosh, 2008; Hanse et al., 2009; Kettenmann et al., 2013; Lee et al., 2014b; Mataga et al., 2004; Schafer and Stevens, 2010; Stevens et al., 2007; Wu et al., 2012b). This elimination process is driven by neuronal activity and serves as a way for neural activity to carve connectivity during the maturation of the synaptic circuit. Conversely, at potentiated synapses, neural activity induces entire transcriptional programs that further sculpt the final synaptic patterns (Chattopadhyaya et al., 2004; Chen et al., 2003; Flavell et al., 2006; Lin et al., 2008; Majdan and Shatz, 2006; West and Greenberg, 2011). It is however of primary importance to highlight that these "final synaptic patterns" are nothing more than a modeling clay whose shaping extends into the entire postnatal life and is regulated by experience (experience-dependent synaptic plasticity, see Part II of the thesis).

What does generate synapse diversity?

At which of the different stages of their development the synapses acquire the exceptional diversity that characterizes them and that ultimately determines the diversity of neural circuits distinctive of our brain?

An important consideration should be done in the context of wiring specificity and in relation to the synaptic organizers: molecules like neuroligins, SynCAM and the majority of LRR proteins are ubiquitously expressed. As such, it is hard to imagine how specificity would be generated if synapse development was triggered only by these molecules (Südhof, 2006). How could neurons end up with the staggering diversity of different types of inhibitory synapses? Or, more strictly, how could they even build inhibitory —and not only excitatory— synapses? Given the apparent promiscuity of initial synaptogenesis, it was postulated that other synaptic proteins might be more important for wiring specificity than these conventional —albeit essential— core building blocks mediating the early formation of synapses (Südhof, 2006).

Although not patently wrong, what this assumption did not take into account is the exceptional diversity of both isoforms (e.g. neurexins) and ligands (e.g. LRRTMs) that the aforementioned synaptic organizers can combine in a cell- or circuit-specific manner to achieve the ultimate goal of synaptic diversity and wiring specificity (Aoto et al., 2013; Chen et al., 2017; Levinson and El-Husseini, 2005; Traunmüller et al., 2016; de Wit and Ghosh, 2016). For example, Neuroligin 2 selectively induces GABAergic presynaptic differentiation (Chih et al., 2006) and pan-neurexin deletion produces dramatically diverse synaptic phenotypes at different types of synapses (Chen et al., 2017). It is nevertheless true that, in addition to ubiquitous synaptic organizers, synaptic proteins specifically expressed in distinct populations of neurons provide a further level of molecular diversity. As such, they are uniquely suited to exert a more fine-tuned control of synapse and circuit formation. In contrast to synaptic organizers, such synaptic regulators do not drive a near-complete program for pre- and postsynaptic differentiation but are essential to confer **cell type- and synapse type-specific identities** which, in turn, critically sculpt neuronal connectivity (Emes and Grant, 2012; de Wit and Ghosh, 2016).

If we adopt once again a historical perspective on neuroscience, we find ourselves in the present. Concomitant with the revolutionary advances in single-cell techniques that fostered a burst of interest in cell diversity (Harbom et al., 2016; Poulin et al., 2016; Shapiro et al., 2013; Wang and Navin, 2015), over the past 6 years we have witnessed a remarkable increase in our understanding of the cell-specific synaptic mechanisms that control wiring specificity, although undoubtedly many more still await discovery. A first process in which cell type-specific synaptic proteins can contribute to the remarkable

diversity of brain circuits is **synapse formation *sensu stricto***. The presence or absence of given proteins involved in synapse formation can dictate whether a transient contact is transformed in a synapse or not.

An excellent example of this selective synaptogenesis onto correct targets is how cadherin-9 (Cdh9) regulates synapse formation of dentate gyrus (DG) axons onto CA3 but not CA1 pyramidal neurons in the hippocampus (Williams et al., 2011). Remarkably, the permissive choice here is neither made at the level of axon targeting nor at the level of synapse elimination. DG axons do not grow preferentially toward CA3 cells —and, in fact, they contact dendrites of both DG and CA1 cells— but do preferentially innervate only CA3 neurons.

Other aspects of the later stages of synapse development are also regulated in a cell- or type-specific manner. For example, neuronal activity regulated pentraxin (NARP), Eph receptor tyrosine kinases and several LRR proteins specifically regulate excitatory **synapse differentiation and/or maturation** due to their ability to recruit key components of the excitatory synaptic machinery (e.g. AMPA receptors) to the postsynaptic density [(Dalva et al., 2000; DeNardo et al., 2012; Kalashnikova et al., 2010; Kim et al., 2006; Ko et al., 2006; O'Brien et al., 1999; Pelkey et al., 2015; Siddiqui et al., 2013), see also Part II of the thesis], or to the presynaptic terminal (Figure 8) (Takahashi et al., 2012; Toth et al., 2013).

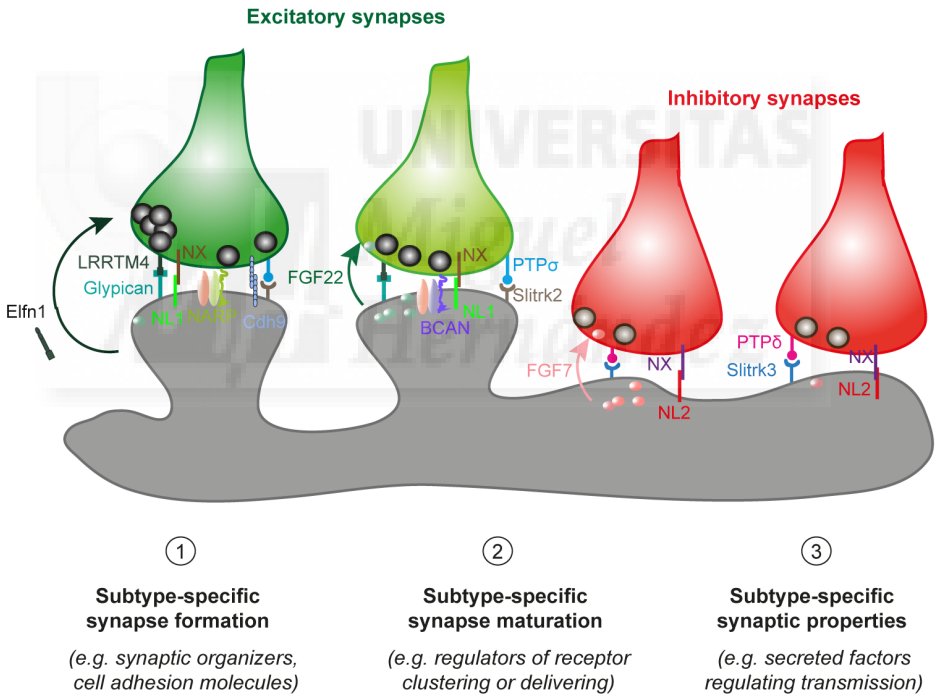

Figure 8. Examples of mechanisms driving synapse specificity.
Cell type- or subtype-specific synaptic organizers (e.g. Neuroligin 2) and adhesion molecules (e.g. Slitrk3, LRRTM4, Cdh9) involved in synapse formation are the first mechanism underlying synapse diversity (1). In addition, several proteins generate specificity at the level of synapse maturation (2). These proteins can act at the postsynaptic site and regulate the synaptic delivery or the composition of postsynaptic receptors (e.g. NARP). Mediators of subtype-specific synapse maturation can also act presynaptically (e.g. FGF22 is secreted from the postsynaptic cell and regulates excitatory synapse maturation whereas FGF7 is secreted from the same cell but regulates inhibitory synapse maturation). An additional level for generating synapse diversity and ultimately imparting specificity on synaptic connections is the regulation of synaptic properties (e.g. Elfn1 target-induced control of presynaptic release properties of some excitatory synapses but not others). Note that, apart from the ones shown in this schematic drawing, many other synapse subtype-specific proteins have been described for excitatory synapses. Conversely, the schematic is comprehensive of all molecules so far known to generate inhibitory synapse specificity.

Worth mentioning, all these studies revealed several proteins selectively regulating different aspects of excitatory synapse formation or function. Conversely, very little is known about the molecules mediating inhibitory synapse specificity (Takahashi et al., 2012). Compounding the issue, the identity of molecules involved in regulating synapse diversity within —the very diverse— class of **inhibitory synapses is still essentially unknown**.

Another process in which cell type-selective proteins impart specificity on synaptic connections is the determination of **synaptic properties**, both pre- and postsynaptically. In this context, the target-induced differences in presynaptic release properties depending on the expression of the LRR protein Elfn1 are particularly illustrative (Sylwestrak and Ghosh, 2012). In the CA1 region of the mouse hippocampus, pyramidal cell axons contact both somatostatin-positive (SST+) interneurons, which express Elfn1, and parvalbumin-positive (PV+) cells, that do not express this protein. As a result of Elfn1 function, the two classes of synapses made by the same axon have strikingly different functional characteristics: synapses made onto SST+ cells are strongly facilitating (low release probability), whereas synapses onto PV+ cells are depressing (high release probability).

Another example of regulation of synaptic specificity at the level of late synapse maturation is provided by the RNA-binding protein SLM2. SLM2 is essential for functional specification of glutamatergic synapses and drives an excitatory synapse-specific alternative splicing program that selectively controls glutamatergic transmission and plasticity (Traunmüller et al., 2016). The activity-dependent transcriptional regulation induced in the last phase of synapse maturation also exhibits a high degree of selectivity. The transcription factor Npas4 drives a transcriptional program that specifically regulates inhibitory synapse development (Lin et al., 2008). Remarkably, these studies identified **transcriptional and post-transcriptional events** as critical determinants of synapse specificity and, once again, showed how selective master regulators that globally influence protein expression ultimately contribute to the diversity of cortical circuits.

It is important to emphasize that the existence of cell-specific mechanisms responsible for the superb combination of specificity and diversity of neural circuits is not limited to synapse development or synaptic properties; they operate throughout development and, as such, characterize and influence all steps of brain wiring. Exactly like how molecular codes ensure the specificity of neuronal target selection before synapse formation (see previous chapter), **cell- or cell type-specific programs also function after synapse formation**, for example in circuit remodeling (van Versendaal et al., 2012; Vidal et al., 2016) and synaptic plasticity (Blackman et al., 2013; Bloodgood et al., 2013; Pelkey and McBain, 2008; Spiegel et al., 2014; Toth et al., 2013). Noteworthy, the very same proteins responsible for synaptic diversity during development can then be re-used in a cell-specific manner during experience-dependent plasticity [(Bloodgood et al., 2013; Lin et al., 2008; Spiegel et al., 2014; Sun and Lin, 2016), see also Part II of the thesis]. Nevertheless, —of all steps that lead to the formation of neural circuits— those involving the creation of synapse specificity are the ones with arguably the higher potential to, in turn, generate wiring specificity. From core synaptic organizers to transcription factors to proteins that regulate the clustering of transmitter receptors, they all orchestrate the masterpiece of synapse diversity: molecules with different molecular composition, structure and partners connect specific presynaptic and postsynaptic cells, control exactly where and when to form which type of synapses, and even which functional properties these synapses have. The only sour note, that may cause the reader to shudder, is the lack of knowledge of how the exceptional diversity of the inhibitory circuits is generated.

6. Subtype-specific connectivity and function of inhibitory GABAergic circuits

The variety of inhibitory GABAergic connections is arguably the quintessence of synapse diversity. While some progress has been made towards understanding the molecular and structural components that broadly distinguish inhibitory synapses and their assembly (Chih et al., 2005, 2006; Kuzirian and Paradis, 2011; Takahashi et al., 2012), the molecular mechanisms underlying interneuron subtype-specific connectivity are largely unknown.

Every complex system appears chaotic until organizing principles are revealed. As such, understanding how this elaborate organization of inputs is established will lead to an appreciation of how the computational power of single neurons is implemented at the circuit level to produce behavioral outcomes. The functional relevance of interneuron synapse diversity is demonstrated by the circuit-specific roles of precise interneuron types and by the impact such difference has on cortical computation (Isaacson and Scanziani, 2011; Kepecs and Fishell, 2014).

Apart from characteristically safeguarding brain networks against runaway excitation, individual interneuron types differentially normalize the activity of local excitatory networks. In particular, they potently influence the flow of information by providing (or not) feedforward and feedback inhibition, engage in disinhibitory circuits and thus increase activity, segregate pyramidal cell populations by imposing lateral inhibition and can also synchronize pyramidal cell assemblies. For example, PV+ axo-somatic and axo-axonic inhibitory inputs are strategically positioned to control the spiking output of principal cells. As such, they have been shown to modulate the gain of sensory responses (Kuhlman et al., 2013; Wilson et al., 2012; Xue et al., 2014; Yazaki-Sugiyama et al., 2009). In addition, and among other critical functions, PV+ basket cell synchronous firing coordinates the spiking of local subsets of pyramidal cells in the gamma frequency band, thus critically influencing the generation of network oscillations associated with cognitive processing (Cardin et al., 2009; Hu et al., 2014). Interneuron-targeting VIP+ cells, instead, characteristically provide a form of gain control by forming disinhibitory microcircuits (Lee et al., 2013; Pfeffer et al., 2013; Pi et al., 2013). Some SST+ interneurons are also specialized in disinhibiting local principal cells (Xu et al., 2013) or engage in recurrent inhibitory circuits (Kapfer et al., 2007). Owing to their broad spatial tuning, SST+ neurons in the visual cortex mediate layer-specific modulation of sensory responses (Adesnik and Scanziani, 2010). Interestingly, Martinotti cells, a subtype of SST+ interneurons which inhibit the dendrites of pyramidal cells in layer 1 of the cerebral cortex, can dampen activity in specific branches and control burst firing (Murayama et al., 2009).

Although the line traced when ascribing a specific function to a particular interneuron type is likely to be less clear-cut than what is currently assumed, it is undeniable that the individual features of different interneurons tailor them to fulfill some functions over others. Broadly speaking, these demarcating features comprise (1) where (on which cell and on which subcellular domain) they make synapses, (2) their spiking properties, (3) the specific circuits they engage in (how many cells, intralaminar versus translaminar connectivity, and so forth). Because most of these properties relate to their efferent connections, it is surprising that such an increased knowledge on the computational functions of interneurons was not accompanied by a parallel understanding of the molecular mechanisms underlying subtype-specific connectivity. How do different interneurons form connections with such a wide variety of synaptic partners? Based on what we have described in the previous chapters, this aspect — interneuron subtype synapse specificity— is likely to depend on selective developmental

genetic programs. Do different interneurons have completely distinct cohorts of molecular synaptic components? And, if so, how does this molecular diversity contribute to the encoding of synaptic diversity and wiring specificity? These are pressing questions that beg for further investigations in order to be able to understand how a functional network is assembled. In the first part of this thesis, we contribute to addressing these questions showing that cell-specific molecular signatures support interneuron early wiring and underlie the specification of different patterns of connectivity.

Understanding the relationship between behavior and inhibitory circuit function (as well as dysfunction) entails uncovering not only the hardwired organizing principles but also the specific logic of inhibitory circuit dynamics. For example, how do interneurons gate information flow in reference to definite behavioral events? How is this regulated in the context of wiring specificity? What are the underlying molecular mechanisms and how do they relate to the genetic programs that drive the assembly of the neural circuits? What is the role of activity and on which cell-specific properties does it act? How are interneuron subtypes selected and recruited to fire in response to a particular experience? Such operational responses largely depend on both afferent connectivity and intrinsic properties of neurons, which in turn are the result of both intrinsically determined genetic programs and activity-dependent processes (see also short introduction to part II of the thesis). In the second part of this thesis, we focus on a specific subtype of inhibitory neurons —PV+ basket cells— and provide insights into how cell-specific molecular programs can regulate the maturation of excitatory afferents onto PV+ interneurons during development but also dynamically gate their function in the adult, thereby facilitating appropriate behavioral responses to experience.

UNIVERSIDAD Miguel Hernández

UNIVERSITAS
Miguel
Hernández

OBJECTIVES

UNIVERSITAS
Miguel
Hernández

The general goal developed during the Ph.D. was to gain insights into both the hardwired organizing principles and the dynamics of cortical circuits.

In particular, the Thesis work aimed at elucidating how inhibitory circuit specificity is achieved during development and how interneurons and their networks respond to experience, with a focus on the underlying cell-specific mechanisms.

To this end, we established the following specific objectives:

1. To study interneuron subtype-specific transcriptional dynamics across early brain wiring and identify cell-specific molecular signatures.

2. To verify whether the identified cell-type selective genetic programs underlie the specification of interneuron early synaptic connectivity.

3. To investigate the dynamic interaction between specific molecular programs driving neural circuit formation and experience-dependent plasticity in interneurons.

UNIVERSITAS Miguel Hernández

UNIVERSITAS
Miguel
Hernández

Part I

Highly selective cell-type specific programs regulate inhibitory synapse specificity[1]

Manuscript in preparation[1]

UNIVERSITAS Miguel Hernández

---

[1] This part of the thesis is mostly my contribution to a wider body of data produced also by other members of the laboratory and that constitutes the following manuscript in preparation:

Favuzzi E*, Deogracias R*, Marques-Smith A, Maeso P, Exposito-Alonso D, Balia M, Hinojosa AJ. Rico B. Highly selective cell-type specific programs regulate inhibitory synapse specificity. * co-first authors

Although I have focused the "Results" and "Discussion" sections mostly on my contribution, to be able to give an overview of the broader significance of the work I have occasionally included a summary description of some results obtained by the other authors. For the sake of transparency, this is indicated in brackets next to such data.

UNIVERSITAS
Miguel
Hernández

RESULTS

UNIVERSITAS
Miguel
Hernández

To investigate the cell-specific mechanisms underlying inhibitory circuit specificity, we focused on three different MGE-derived interneuron subtypes: chandelier, PV+ basket and SST+ cells. Because of their markedly different targeting profiles, these three interneuron subtypes best illustrate the exceptional diversity of the GABAergic circuits (see Figure 2 in General Introduction).

In order to identify cell-specific molecular signatures that specify the different patterns of connectivity of chandelier, PV+ basket and SST+ cells, we decided to perform a gene expression longitudinal profile across developmental stages that are relevant for synapse formation.

1. Developmental analysis of different GABAergic synapses

Previous studies have characterized multiple classes of cortical GABAergic interneurons and their synaptic targets (Chattopadhyaya et al., 2004; DeFelipe and Fariñas, 1992; De Felipe et al., 1997; Fish et al., 2011; Inda et al., 2009; Kawaguchi and Kubota, 1997; Klausberger and Somogyi, 2008; Wang et al., 2004c; Xu and Callaway, 2009), but the precise development of the different subtypes of GABAergic inputs to pyramidal cells is not well understood. For example, it has been shown that a substantial number of GABAergic synapses are already formed at postnatal day (P) 4 in the mouse somatosensory cortex and that their number increases progressively from this stage to adulthood (De Felipe et al., 1997). However, it is unknown whether GABAergic synapses targeting different subcellular compartments develop at the same time or if they follow a similar pattern of development. As this detailed information was crucial for the efficient implementation of our screening approach, we studied the development of axo-axonic, somatic and dendritic presynaptic contacts made by chandelier, PV+ basket and somatostatin cells, respectively.

To study the temporal development of chandelier AIS-targeting synapses, we performed double immunohistochemistry for the high-affinity plasma membrane transporter GAT-1 —localized at the presynaptic terminals of GABAergic synapses—, and the axonal initial segment (AIS) scaffold protein Ankyrin G (AnkG) on the postsynaptic compartment. We analyzed the temporal development of chandelier inhibitory boutons in layer II-III of the mouse prefrontal cortex (PFC) (Figure 1A-C), where chandelier cells are more abundant (Taniguchi et al., 2013). Although synapse formation is a continuous process (Figure 1), quantification of the density of GAT-1 presynaptic puncta contacting the AIS of pyramidal cells revealed that the highest increase in chandelier bouton formation occurs between P10 and P12 (m= 0.21, Figure 1C).

Next, we explored the development of PV+ basket cell perisomatic contacts by counting the number of presynaptic boutons that surround the soma of pyramidal cells in layer II-III of the mouse somatosensory cortex (SSC) (Figure 1D-F). Using GAD67 —the GABA-synthesizing enzyme enriched in the PV+ presynaptic terminals— we could easily identify perisomatic synapses by their typical ring-like structure (Figure 1E). We found that the biggest difference in the number of presynaptic puncta contacting the soma of pyramidal neurons appears between P10 and P12 (m= 0.96, Figure 1F). It is important to mention, however, that a significant number of PV+ basket cell synaptic contacts are also made after P12 (m= 0.52, Figure 1F).

Finally, we studied the development of dendritic synapses over time. We quantified the density of GAD67 puncta in layer I of the mouse SSC (Figure 1G-H), where the majority of inhibitory synapses are made on the terminal tuft dendrites of pyramidal cells (Bloss et al., 2016). Although a large rise in the number of GAD67 boutons was

observed between P5 and P10, the increase observed between P10 and P12 was greater (*m*= 0.02, Figure 1I).

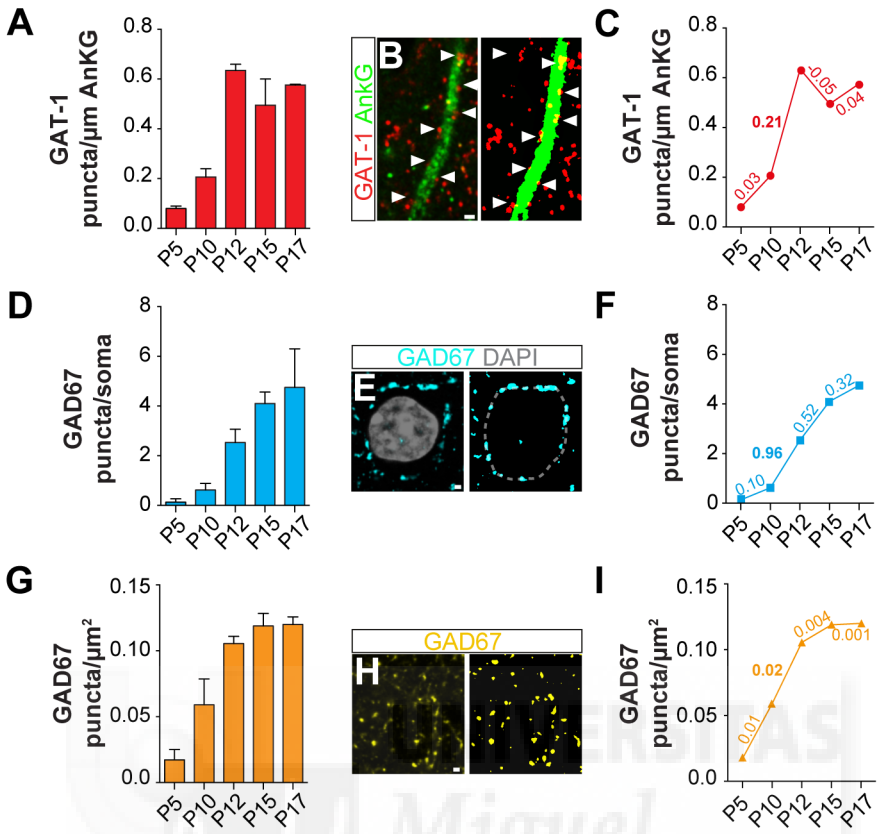

Figure 1. Early development of different types of inhibitory synapses over time.
(A) Density of GAT-1 presynaptic boutons contacting the postsynaptic axonal initial segment (AIS) scaffold protein Ankyrin G (AnkG) at different stages of early postnatal development in layer II-III of the mouse prefrontal cortex (n = 3 for each stage).
(B) Representative image showing GAT-1 boutons contacting the AIS (AnkG) at P15 and corresponding thresholded mask used for quantification. Scale bar equal 1 µm.
(C) Same as in (A), the numbers indicate the slope (*m*) of the line connecting two consecutive timepoints. Note that the highest increase in chandelier bouton formation occurs between P10 and P12 and is highlighted in bold (*m*= 0.21).
(D) Number of GAD67 presynaptic boutons forming ring-like structures around the soma of pyramidal neurons in layer II-III of the mouse somatosensory cortex at different stages of early postnatal development (n = 3 for each stage).
(E) Representative image showing GAD67 somatic boutons contacting a cell body at P15 and corresponding thresholded mask used for quantification. Scale bar equal 1 µm.
(F) Same as in (D), the numbers indicate the slope (*m*) of the line connecting two consecutive timepoints. Note that the highest increase in the number of presynaptic puncta contacting the soma of pyramidal neurons appears between P10 and P12 (*m*= 0.96).
(G) Density of GAD67 presynaptic boutons at different stages of early postnatal development in layer I of the mouse somatosensory cortex where the majority of dendritic inhibitory synapses are made by Martinotti cells on the terminal tuft dendrites of pyramidal cells (n = 3 for each stage).
(H) Representative image showing GAD67 puncta in layer I at P15 and corresponding thresholded mask used for quantification. Scale bar equal 1 µm.
(I) Same as in (G), the numbers indicate the slope (*m*) of the line connecting two consecutive timepoints. Note that the highest increase in the density of GAD67 presynaptic boutons in layer I appears between P10 and P12 (*m*= 0.02).
One-way ANOVA detected significant differences ($p<0.05$) among means over time for all three types of synapses (A, D and G). Because development is a continuous process and the number of

groups is particularly high, to avoid increasing the risk of making a Type II error, instead of performing *post hoc* tests corrected for multiple comparisons we instead used the slope (*m*) to identify the stages where synapse formation appears to be more intense.

These results revealed only small differences in the temporal development of GABAergic synapses targeting different subcellular compartments. For instance, dendritic synapses develop slightly earlier than perisomatic synapses (Figure 1D and 1G), which is consistent with their earlier birth (Miyoshi et al., 2007) and earlier functional maturation (Marques-Smith et al., 2016b; Tuncdemir et al., 2016). Despite these minor differences, the developmental analysis of domain-restricted GABAergic synapses allowed us to identify a common time window (P10-P12) when the highest increment in the density of inhibitory boutons contacting the different postsynaptic targets occurs.

2. Transgenic lines, brain regions and stages used for transcriptome profiling

mRNA levels are, in general, an excellent proxy for the presence of a protein and hence for the appearance of its biological effect (Vogel and Marcotte, 2012). However, several factors, including translation efficiency, influence the correlation between mRNA, protein abundances and biological effects. We reasoned that this correlation would increase if the mRNA measurements are shifted back in time by at least 48 hours. Genes that regulate the assembly of inhibitory synapses and trigger an increase in their density between P10 and P12 should, therefore, display a correspondent mRNA increase between P5 and P10. Indeed, previous studies showed a huge increase in *GAD* mRNA levels already between P4 and P7 in the mouse somatosensory cortex (Golshani et al., 1997). Consequently, to gather genes involved in the specific wiring of inhibitory circuits, we chose to isolate interneurons with different targeting profiles at P5 and P10 (Table 1).

To perform transcriptome profiling of different interneurons at the selected stages, we employed a combination of genetically modified mouse lines in which specific subpopulations of GABAergic neurons are fluorescently labeled (Table 1).

Mouse strain	Type of synapses	Cell	T1	T2	Brain region	Replicates
Nkx2.1CreERT2; Tomato	AIS-targeting	Chandelier cells	P8	P10	PFC, upper layers	3
G42	Soma-targeting	PV+ basket cells	P5	P10	PFC, lower layers	3
GIN	Dendrite-targeting	Martinotti cells	P5	P10	SSC, all layers	3
Nex-Cre;RCE	Glutamatergic synapses	Pyramidal cells	NA	P12	PFC, all layers	3
Nkx2.1Cre;RCE	General interneuron genes	Interneurons	P0	NA	PFC, all layers	3
PLP-GFP	General oligodendrocyte genes	Oligodendrocytes	NA	P10	PFC, upper layers	2

Table 1. Transgenic lines, brain regions and stages used for gene expression profiling.

Characterization of Nkx2.1-CreER mice to label AIS-targeting chandelier cells

A new generation of genetically modified mice in which *Cre* is expressed under the control of genes that are unique to some populations of interneurons allows the labeling of interneuron subtypes when crossed with reporter lines, such as RCE (green

fluorescent protein, GFP reporter) and Ai9 (red fluorescent protein, Tomato reporter) strains (Taniguchi et al., 2011, 2013).

Specifically, the *Nkx2.1CreERT2* driver labels a subpopulation of neurons that is enriched in chandelier cells [(Taniguchi et al., 2013), Figure 2A-2D]. *Nkx2.1CreERT2* transgenic mice are a knock-in mouse strain in which *CreERT2* (a tamoxifen-inducible form of Cre) is expressed under the control of *Nkx2.1* genetic locus (Taniguchi et al., 2011). Although the *Nkx2.1CreERT2* driver is the best available tool to label chandelier cells, it has some obvious disadvantages that critically challenged the feasibility of our screening approach. First, it also labels other cell types that express the *Nkx2.1* gene. This problem could be partially circumvented by focusing on cortical areas and/or layers enriched in chandelier cells, such as the upper layers of the PFC (Taniguchi et al., 2013). In addition to the lack of absolute specificity, because the labeling depends on tamoxifen-induced recombination, the *CreER*-induction does not label all chandelier cells but only a subpopulation (Taniguchi et al., 2013). Despite the enormous progress made in new generation sequencing techniques that permit to obtain high-quality transcriptome data with low input starting material, the total number of chandelier that we could isolate represented a serious difficulty.

In order to identify the best possible balance between the highest percentage of ChC/Tomato+ cells and the highest number of chandelier cells labeled, we used *Nkx2.1CreERT2;Ai9* mice and compared how the relative fraction and total number of chandelier cells in the upper layers of various cortical areas were affected by the use of different tamoxifen administration routes or by the stage of tamoxifen induction (Figure 2E and 2F). When we compared tamoxifen inductions by intraperitoneal, intragastric, subcutaneous injection and by oral gavage, we did not observe a significant difference in either the percentage or the density of chandelier cells labeled in several brain regions, suggesting that the administration route does not influence chandelier cell labeling.

Next, we analyzed the effect of different stages of inductions. Although embryonic inductions at E17.5 labeled more chandelier cells (Figure 2F), we also observed a higher number of Tomato+ basket cells (Figure 2E). On the contrary, early postnatal tamoxifen inductions at P2 yielded an overall smaller Tomato+ population (Figure 2F) that was, however, slightly but significantly more enriched in chandelier cells (Figure 2E). This advantage was completely lost if tamoxifen was injected at P5 when both a low percentage and a low density of chandelier cells were observed. Finally, consistent with previous studies (Taniguchi et al., 2013), a much higher number of labeled chandelier cells was consistently observed in the upper layers of the PFC when compared to other regions (Figure 2F).

It is important to mention that, because early postnatal tamoxifen inductions label the very last temporal cohort of chandelier cells, several of these cells are still migrating at P5 (Figure 2G and 2H). To avoid isolating migrating chandelier cells that would “contaminate” our transcriptome data with genes involved in chandelier cell migration rather than synapse formation, we decided to sort chandelier cells at P8 and P10, instead of P5 and P10 (Table 1). Altogether, these results showed that the best strategy to isolate chandelier cells for our screening was to carry out a microdissection of upper layers in the PFC of P8 and P10 *Nkx2.1CreERT2;Ai9* mice after early postnatal tamoxifen induction (Figure 2B).

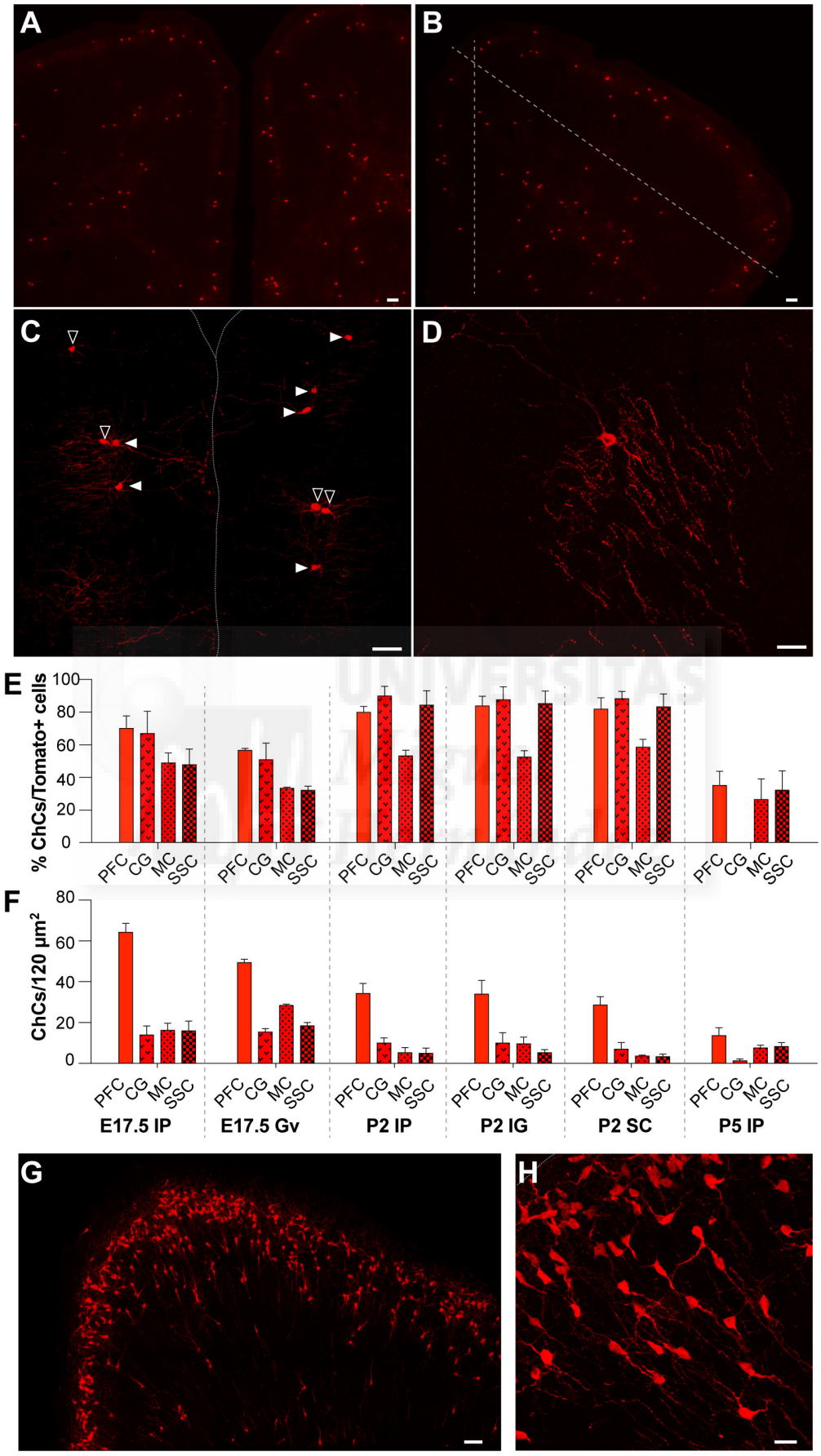

Figure 2. *Nkx2.1CreERT2* driver labels a subpopulation of neurons enriched in chandelier cells. *[Legend continues on next page]*

[Legend Figure 2 from the previous page]
(A-D) Representative images showing the high number and percentage of chandelier cells labeled in the upper layers of the prefrontal cortex of *Nkx2.1CreERT2;Ai9* mice upon *CreER* induction with tamoxifen. The dotted lines in (B) indicate how the upper layers were microdissected for transcriptome profiling. Scale bars equal 100 µm (A and B), 40 µm (C) and 20 µm (D).
(E and F) Percentage of ChC/Tomato+ cells (E) and density of chandelier cells labeled (F) in the upper layers of various cortical areas of *Nkx2.1CreERT2;Ai9* mice at P30 upon use of different tamoxifen administration routes or various stages of induction (n = 3 for all conditions). For the percentage of chandelier cells, two-way ANOVA showed the following significant differences: $p<0.001$ for 'stage/route' (raw effect) as well as for 'region' (column effect) factors; $p<0.05$ for interaction between stage/route and region. For the density of chandelier cells, two-way ANOVA showed the following significant differences: $p<0.001$ for 'stage/route' (raw effect) as well as for 'region' (column effect) factors; $p<0.001$ for interaction between stage/route and region. As the much higher number of chandelier cells in the prefrontal cortex was evident, *post hoc* Tukey's multiple comparisons test was performed only for the main raw effect (stage/route).
The observed significant differences in the percentage of labeled chandelier cells were: E17.5 IP vs. P2 IG p value=0.0461, E17.5 IP vs. P2 SC p value=0.0346, E17.5 IP vs. P5 IP p value <0.0001, E17.5 Gavage vs. P2 IP p value=0.0002, E17.5 Gavage vs. P2 IG p value=0.0002, E17.5 Gavage vs. P2 SC p value=0.0001, E17.5 Gavage vs. P5 IP p value=0.0378, P2 IP vs. P5 IP p value <0.0001, P2 IG vs. P5 IP p value <0.0001, P2 SC vs. P5 IP p value <0.0001. The observed significant differences in the density of labeled chandelier cells were: E17.5 IP vs. P2 IP, E17.5 IP vs. P2 IG, E17.5 IP vs. P2 SC, E17.5 IP vs. P5 IP, E17.5 Gavage vs. P2 IP, E17.5 Gavage vs. P2 IG, E17.5 Gavage vs. P2 SC, E17.5 Gavage vs. P5 IP and p value <0.0001 for all these comparisons.
(G and H) Low and high magnification images showing chandelier cells that are still migrating at P5 in *Nkx2.1CreERT2;Ai9* mice induced at P2 with tamoxifen. Scale bars equal 50 µm (G), 20 µm (H).

The Nkx2.1+ subpopulation labeled with this approach, although enriched in chandelier cells, is still contaminated by a small fraction of non-chandelier cells. Since knowing the identity of these cells was critical to ensure a correct interpretation of the chandelier cell transcriptome data, we crossed *Nkx2.1CreERT2* mice with the *Ai9* reporter line and colocalized Tomato+ cells with markers of dorsal and ventral MGE- as well as CGE- and POA- derived interneurons (Gelman and Marín, 2010) (Figures 3A-3H). At P30, although the majority of Tomato+ cells in the upper layers of the PFC were chandelier cells, both PV+ and PV-, we also found a 16% of PV+ basket cells (Figures 3A and 3C). The remaining 10% were mostly Reelin-expressing neurogliaform (RELN+SST-) interneurons derived from the preoptic area (POA) (Gelman and Marín, 2010) or GABAergic cells that did not colocalize with any of the markers that we used (Figures 3A-3H).

It is important to mention that at P10, when we cannot yet unequivocally recognize the unique chandelier axonal arbor, we also identified by morphology several Tomato+ putative glial cells (Figure 3B and 3I-3J). This was not surprising, as *Nkx2.1* is known to control the differentiation of MGE-derived cortical oligodendrocytes that are eliminated during postnatal life (Kessaris et al., 2006) and has more recently been shown to also regulate astrogliogenesis in the telencephalon (Minocha et al., 2017). Altogether, these results showed that the main cell types contaminating the Tomato+ subpopulation that we labeled with our strategy are PV+ basket, RELN+ and glial cells.

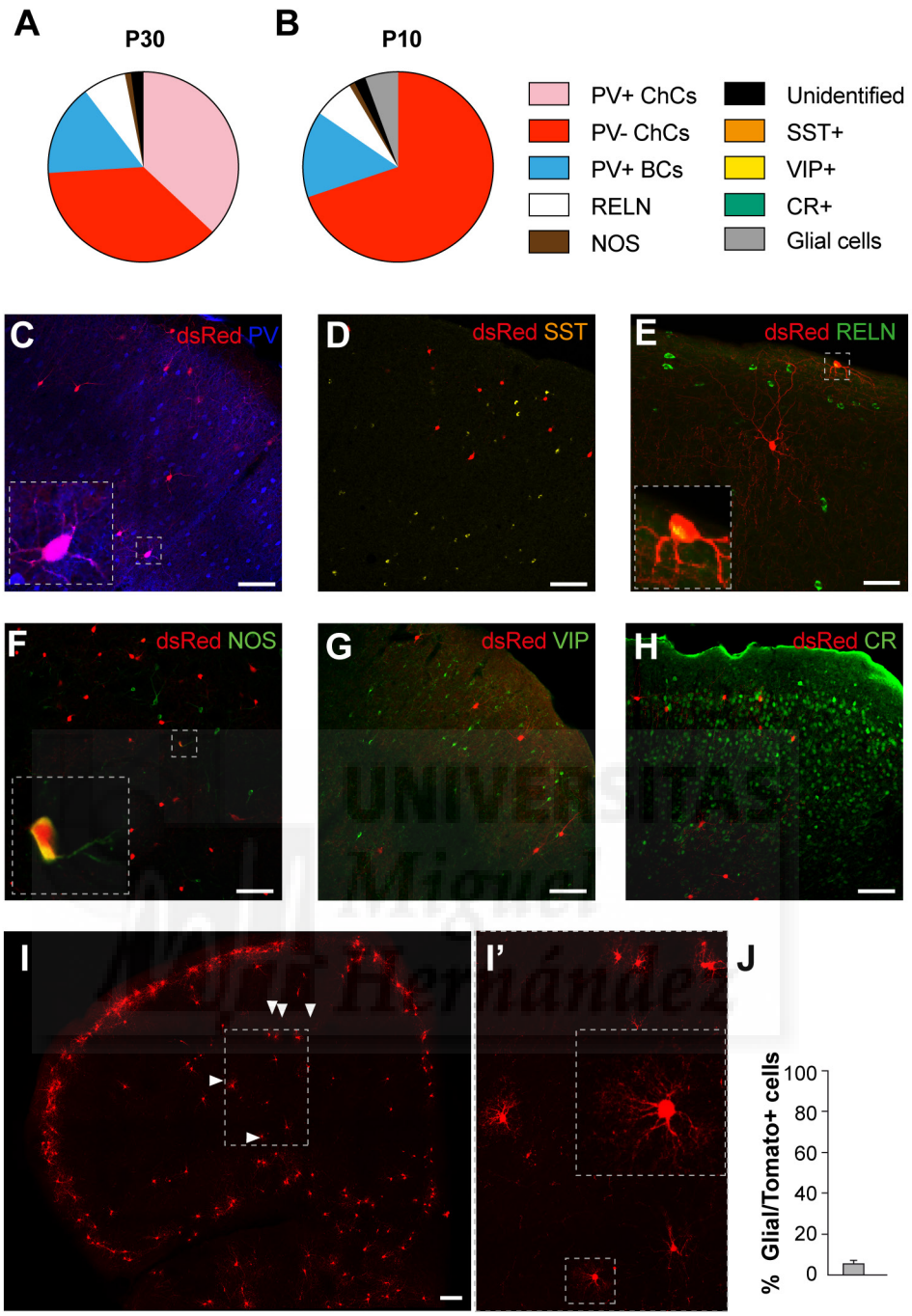

Figure 3. Identity of labeled cells in *Nkx2.1CreERT2;Ai9*.
(A and B) Pie graph showing that at both P10 and P30 the majority of Tomato+ cells labeled in the upper layers of the prefrontal cortex upon P2 tamoxifen *CreER* induction in *Nkx2.1CreERT2;Ai9* mice are chandelier cells (n = 3 mice per condition). Note that at P30 50% of these cells are PV+ and the other 50% are PV- whereas at P10 it is not possible to distinguish PV+ and PV- cells because the PV staining starts to be visible only after P12. The pie graphs also show that the main cell types contaminating the Tomato+ subpopulation are PV+ basket, RELN+ and (at P10) glial cells (n = 3 mice per condition).
(C-H) Representative images showing colocalization of Tomato+ cells with different cell markers. Scale bars equal 50 μm.
(I-J) Representative images and quantification of Tomato+ cells with glial morphology in the prefrontal cortex of P10 *Nkx2.1CreERT2;Ai9* mice (n = 3 mice). Scale bar equal 50 μm.

Transgenic lines to label soma- and dendrite-targeting interneurons

Transgenic lines that use broad GABAergic promoters, such as those regulating *Gad1* or *Gad2* are well-characterized mouse lines that have been successfully used to label different populations of interneurons (Chattopadhyaya et al., 2004; Oliva et al., 2000; Sugino et al., 2006; Xu and Callaway, 2009). Differences in the length of the *Gad1* fragment used and/or their genome insertion are enough to create different transgenic mouse strains in which only some classes of interneurons are labeled with the green fluorescent protein (GFP).

To label soma-targeting PV+ basket cells, we used the bacterial artificial chromosome (BAC) transgenic mouse line G42 (*Gad1-EGFP*, *G42Zjh/J*) (Figure 4A and 4B). In these mice, a BAC containing the mouse GAD67 gene (and 60 kb of upstream and downstream sequence) was modified by insertion of an Enhanced Green Fluorescent Protein (EGFP) cDNA and phosphoglycerate kinase polyadenylation sequence in the first coding exon at the translation initiation site of the GAD67 gene, which resulted in the labeling of PV+ interneurons (Chattopadhyaya et al., 2004).

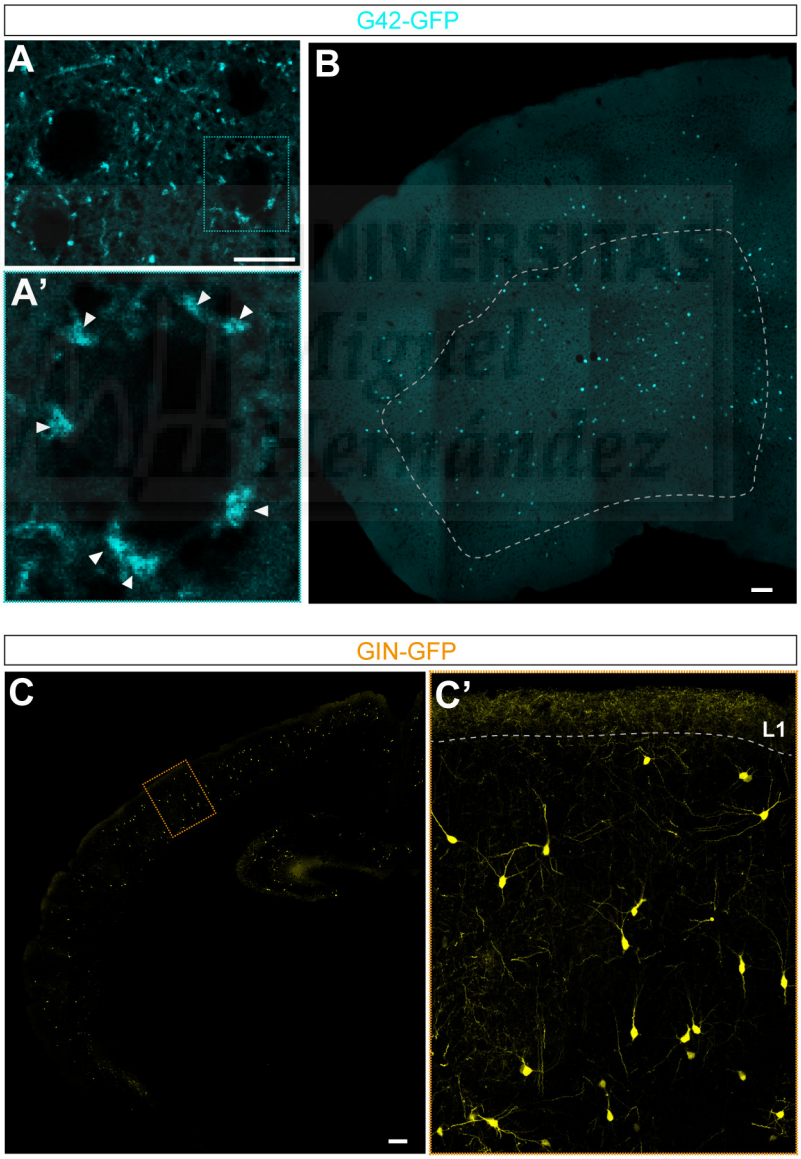

Figure 4. *G42* and *GIN* transgenic lines label PV+ basket and SST+ Martinotti cells. *[Legend continues on next page]*

[Legend Figure 4 from the previous page]
(A and B) Representative images showing PV+ basket cells labeled in the prefrontal cortex of *G42* mice at P30. (A) shows that GFP+ synaptic terminals are perisomatic and that no clear cartridge-like structures can be identified; (A') is a blow up from (A). The dotted line in (B) indicates how the lower layers were microdissected for transcriptome profiling. Scale bars equal 10 µm (A) and 100 µm (B).
(C) Representative images showing Martinotti cells labeled in the somatosensory cortex of *GIN* mice at P30. (C') is a blow up from (C). Note the high density of labeled axons in layer I where Martinotti cells typically branch and form synapses (C'). Scale bar equal 200 µm.

Although some GFP-expressing cells in these mice have been found to be chandelier cells (Xu and Callaway, 2009), it is likely to be a very small fraction of labeled cells as shown by the observation that GFP+ synaptic terminals are generally perisomatic and we could not detect any clear cartridge-like structure in G42 mice (Figure 4A). However, to avoid isolation of even just a small number of chandelier cells we decided to sort GFP+ cells only from lower layers (Figure 4B), where very few chandelier cells have been described (Taniguchi et al., 2013). The PFC is the only region that would allow us to isolate a high number of chandelier cells but, unavoidably, also some contaminating PV+ basket cells (Figures 2 and 3). As such, sorting PV+ basket cells from the PFC would guarantee a comparison between the transcriptome profile of PV+ basket and chandelier cells, while avoiding the variability that might be intrinsic to different cortical areas. Moreover, since no chandelier cell is labeled in the lower layers of the G42 PFC (Yang et al., 2013), this region has the additional advantage of restricting GFP expression exclusively to the PV+ basket cell population. Consequently, we decided to isolate PV+ basket cells from the lower layers of the PFC at P5 and P10 (isolation performed by P. Maeso, Figure 4B).

To label interneurons that make dendrite-targeting synapses, we used GIN transgenic mice, in which GFP expression is driven by a 2.8 kb fragment of the mouse *GAD67* promoter (Oliva et al., 2000). GFP-labeled cells in these mice are mostly distributed in superficial layers of the cortex and correspond predominantly to Martinotti cells (Oliva et al., 2000; Xu and Callaway, 2009). Martinotti cells are a subgroup of somatostatin cells and represent the most prominent distal dendrite-targeting interneurons in the cortex. As the GIN line had been well-characterized in the somatosensory cortex, we decided to isolate dendrite-targeting Martinotti cells from all layers of the somatosensory cortex at P5 and P10 (isolation performed by P. Maeso, Figure 4C).

Other mouse lines to label control populations

To obtain a list of genes that are specifically expressed by unique classes of interneurons during the period of synapse formation, we also carried out additional isolation and transcriptome profiling of other populations (Table 1). The aim was to discard "undesired" genes, such as genes whose expression changes because of the experimental manipulation (e.g. genes up-regulated by stress), genes that belong to "contaminating" cells (e.g. glial cells in the *Nkx2.1CreERT2* line), genes that are involved in early events (e.g. interneuron specification, migration) or genes that are involved in general processes of synapse formation (e.g. synaptic structural genes).

First, to 'subtract' those genes that are interneuron-specific to but that are not related to synapse formation, we used *Nkx2.1Cre;RCE* mice to isolate all MGE-derived interneurons from the PFC at an early stage of development (P0), when synaptic genes would still be inactive (work performed by P. Maeso). Next, with the aim of removing genes that are ubiquitously involved in synapse formation, we used *Nex-Cre;RCE* mice to isolate pyramidal cells from the PFC at P12 (work performed by P. Maeso), when glutamatergic synapse formation is particularly intense (Antonio Hinojosa, unpublished).

Finally, to eliminate genes that are expressed in contaminating glial cells we used the *PLP-GFP* transgenic line to isolate oligodendrocytes from the upper layers of the PFC at P10. The different mouse lines, brain regions and stages used for gene profiling are summarized in Table 1.

3. Transcriptional profiling of different interneuron subtypes across early developmental stages

As a first step toward identifying cell-specific molecules regulating synaptic specificity, we combined cell sorting approaches with high-throughput RNA-sequencing to purify the abovementioned cell populations at the selected postnatal stages and perform systematic whole-transcriptome analyses.

To isolate individual cells, we sectioned fresh brains from the corresponding transgenic mice (and across two developmental stages for chandelier, PV+ basket and Martinotti cells), microdissected the region of interest, generated single-cell suspensions (see Methods), isolated fluorescently labeled cells by fluorescence-activated cell sorting (FACS) and performed RNA sequencing (RNA-seq) (Figure 5).

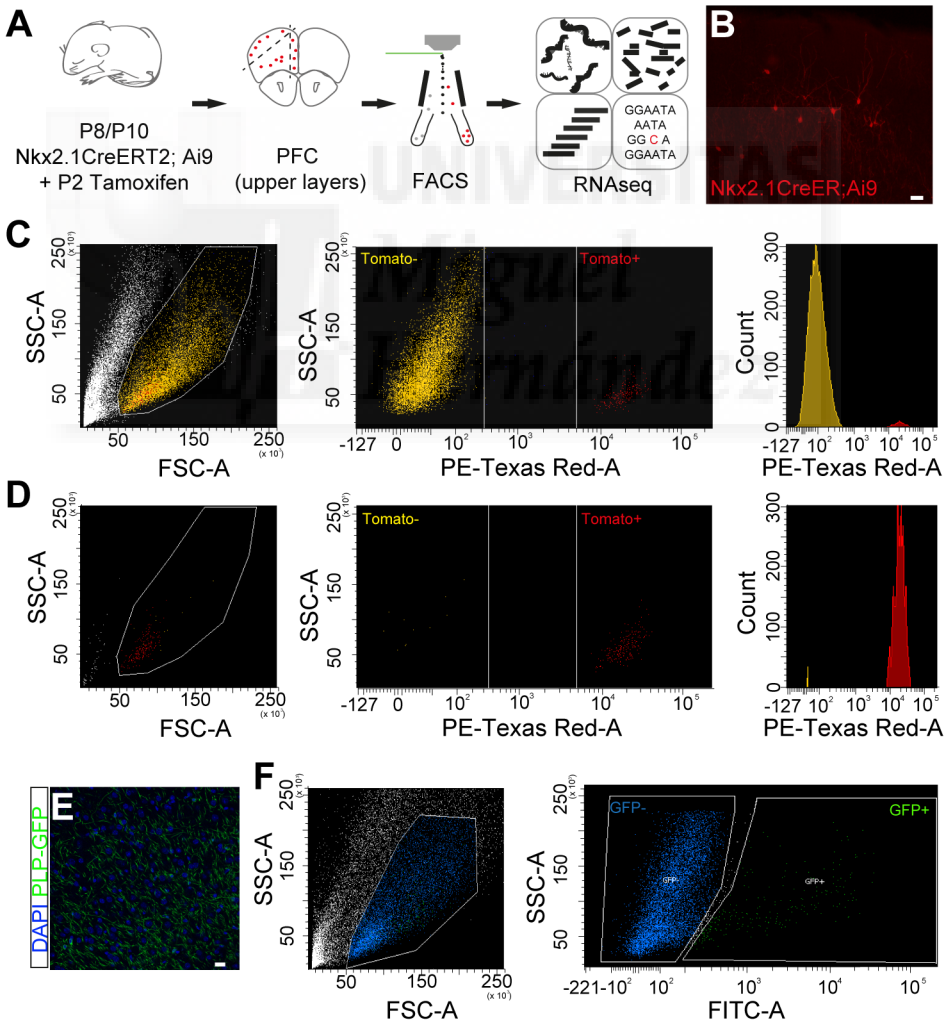

Figure 5. Isolation of different cell populations to perform gene expression profiling of different interneuron types across development.
(A) Schematic of the experimental design.

(B-D) FACS sorting of Tomato+ cells from P8 *Nkx2.1CreERT2;Ai9* mice. Note the difference in the relative fraction of Tomato+ and Tomato- cells before (C) and after sorting (D), showing the high efficiency of the isolation even with a low number of fluorescently labeled cells as in the case of chandelier cells. Scale bar equal 60 µm.
(E and F) FACS sorting of GFP+ cells from P10 *PLP-GFP* mice. Note the higher brightness of Tomato (C and D) compared to GFP (F). Scale bar equal 20 µm.

Next, we performed differential gene expression analysis (see Methods). As expected, the lower number of differentially expressed genes was found between different stages of the same subpopulation such as chandelier cells at P8 and at P10 (Figure 6A). It was also not surprising to find that oligodendrocytes have a very different expression profile as compared to all neuronal populations (Figure 6A). In addition, P12 pyramidal cells and P0 interneurons exhibited a high number of differentially expressed genes not only between them but also compared to the three interneuron subpopulations. Interestingly, pyramidal neurons shared more similarly expressed genes with P10 than P5 interneurons, whereas the opposite was observed for P0 interneurons, reflecting the significant influence that developmental processes have on gene expression.

Principal component analysis (PCA) revealed similar distinctions between populations and developmental stages (analysis performed by D. Exposito-Alonso, Figure 6B).

To assess the reproducibility of our data and conservation across biological replicates, we performed unsupervised hierarchical clustering based on the Jensen-Shannon distance of our complete RNA-Seq transcriptome data (analysis performed by D. Exposito-Alonso). We found low distance among replicates whereas higher distance was observed across differing cell types (Figure 6C) showing that the obtained gene expression profiles were internally consistent and subtype specific and thus ensuring the integrity of our dataset.

Control genes validate the transcriptome data

To further validate the purity of the isolated interneuron cell types, we probed the transcriptome data for expression of well-known cell type-specific genes for PV+ basket, e.g., Syt2 (Sommeijer and Levelt, 2012), and Somatostatin cells, e.g., Elfn1 (Sylwestrak and Ghosh, 2012). For chandelier cells, because of the lack of a specific known marker, we used genes that are expressed in all interneurons but are known to have a relatively higher (e.g., GAD1, ErbB4, GAT-1) or lower (e.g., GAD2) expression in chandelier cells compared to PV+ basket cells (Fazzari et al., 2010; Fish et al., 2011; Del Pino et al., 2013, 2017). We observed that subtype-specific genes were not expressed in the other samples (Figure 6D), indicating that these populations have minimal contamination with other cell subtypes. In addition, the mRNA expression ratio for genes that are enriched in chandelier versus PV+ basket cells or vice versa confirmed the successful purification of chandelier cells (Figure 6D).

We next sought to validate the suitability of our transcriptome data for identifying synaptogenic genes. To this aim, we looked at the expression of genes that are known to participate in synaptic processes across the two selected developmental time points. These classic synaptic genes consistently exhibited high increase in their expression levels between P5 and P10 for PV+ basket and somatostatin cells or P8 and P10 for chandelier cells, confirming the suitability of the selected developmental stages to identify genes involved in synapse formation (Figures 6D and 6E).

Altogether, our findings confirm the purity of the various isolated cell types and establish the feasibility of our transcriptome data for both resolving interneuron subtype-specific transcriptional dynamics and identifying genes that regulate the assembly of domain-restricted GABAergic synapses.

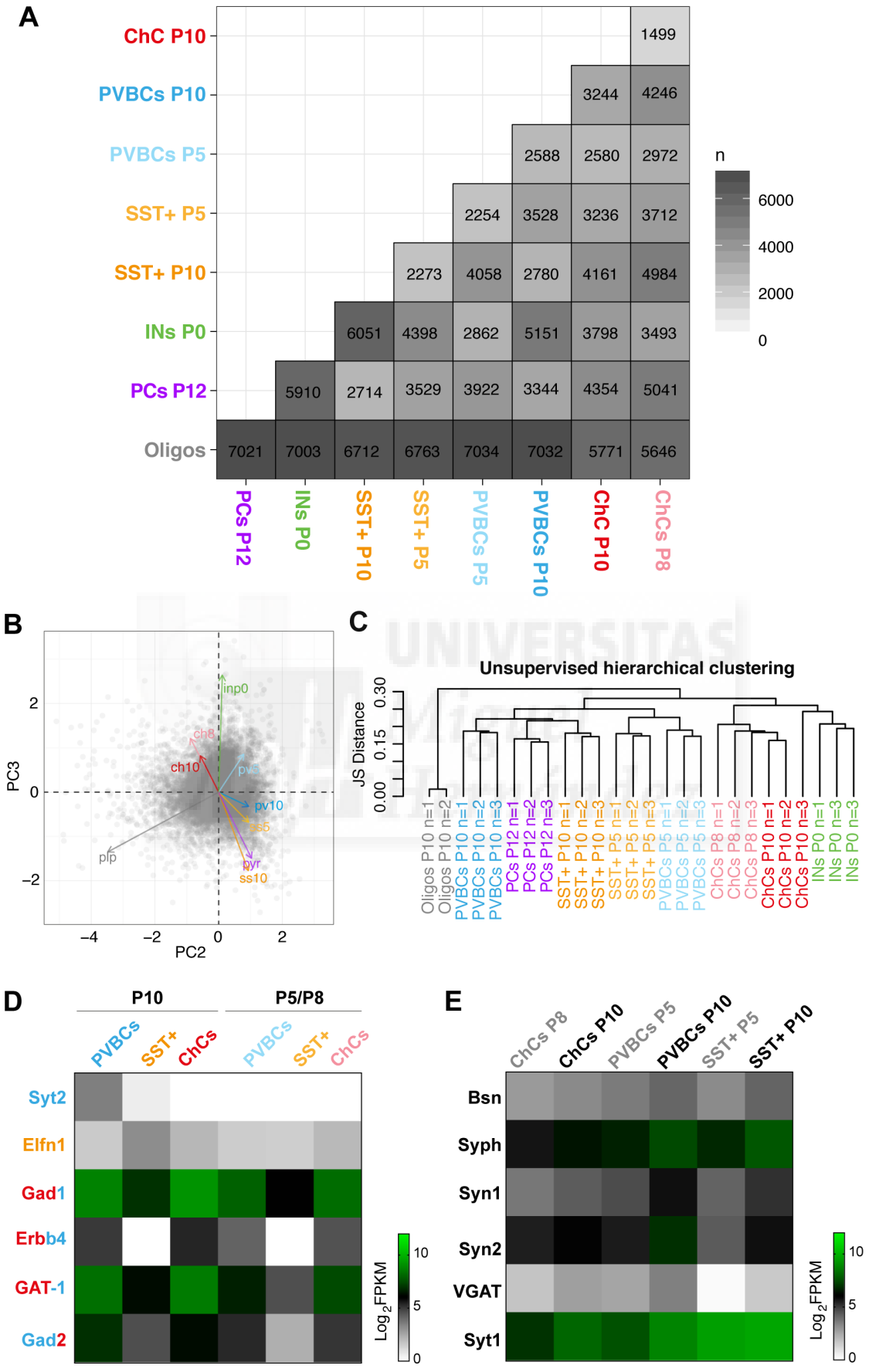

Figure 6. Comprehensive transcriptional analysis of different cell-types across development. *[Legend continues on next page]*

[Legend Figure 6 from the previous page]
(A) Heatmap showing the number of differentially expressed genes between cell-types at different stages using a False Discover Rate (FDR) of 5%.
(B) Principal component analysis on individual gene level indicates that cell-type and developmental stage were the greater sources of variability in gene expression.
(C) Unsupervised hierarchical clustering based on the Jensen-Shannon distance of our complete RNA-seq transcriptome data reveals low distance among replicates and higher distance across cell types.
(D) Analysis of the expression of well-known cell type-specific genes verifies that each cell-type has minimal contamination with other subtypes. Note that to verify the successful purification of chandelier cells we used genes that have a relatively higher (GAD1, ErbB4, GAT-1) or lower (GAD2) expression in chandelier cells compared to PV+ basket cells.
(E) The expression of well-known synaptogenic genes increases between the selected developmental stages, confirming the suitability of the transcriptome data to identify genes that regulate synapse development. Note that some of the genes in (D) are also involved in synapse formation and exhibit a similar increase in their expression across development.

4. Interneuron subtype-specific gene sets and pathway components

To explore which types of genes distinguish chandelier, PV+ basket or somatostatin cells at P10, we conducted a gene enrichment analysis with genes that share similar curated annotations but are uniquely expressed in one of the three subpopulations. To this end, we selected all genes differentially expressed between cell types at P10 and filtered them by a minimum normalized expression level (FPKM, see Methods) as well as a minimum specificity score ($\log_2$FC, analysis performed by D. Exposito-Alonso, see Methods). The pooled list was used as input for a preranked gene set enrichment analysis against the collection of GSEA canonical pathway gene sets (C2, KEGG, NABA and Reactome; MSigDB; Subramanian et al., 2005) (Figure 7A).

The pathway analysis revealed enrichment in genes that cover broad processes of neuronal function as well as genes associated with neurodegenerative diseases. However, several sets containing genes that play specific roles in the assembly and maturation of the neural circuits were also highly enriched. These sets included genes encoding extracellular matrix proteins, genes that regulate various aspects of neuronal communication, such as neurotransmission and ligand-receptor interactions, and also genes that control the emergence of the electrophysiological properties of cortical interneurons (Figure 7A).

To retrieve a functional profile of these gene sets, which will allow us to better understand the underlying biological processes, we performed a gene ontology (GO) term analysis (GSEA C5, GO gene sets; MSigDB; Subramanian et al., 2005). The GO analysis revealed that the predominant cellular component of P10 interneuron subtype-specific genes is the synapse, further supporting the suitability of our screening to seek genes involved in synapse formation (Figure 7B). In the GO term analysis, we also observed several enriched processes and functions, including signaling, ion transport as well as receptor and ion channel activity (Figure 7B).

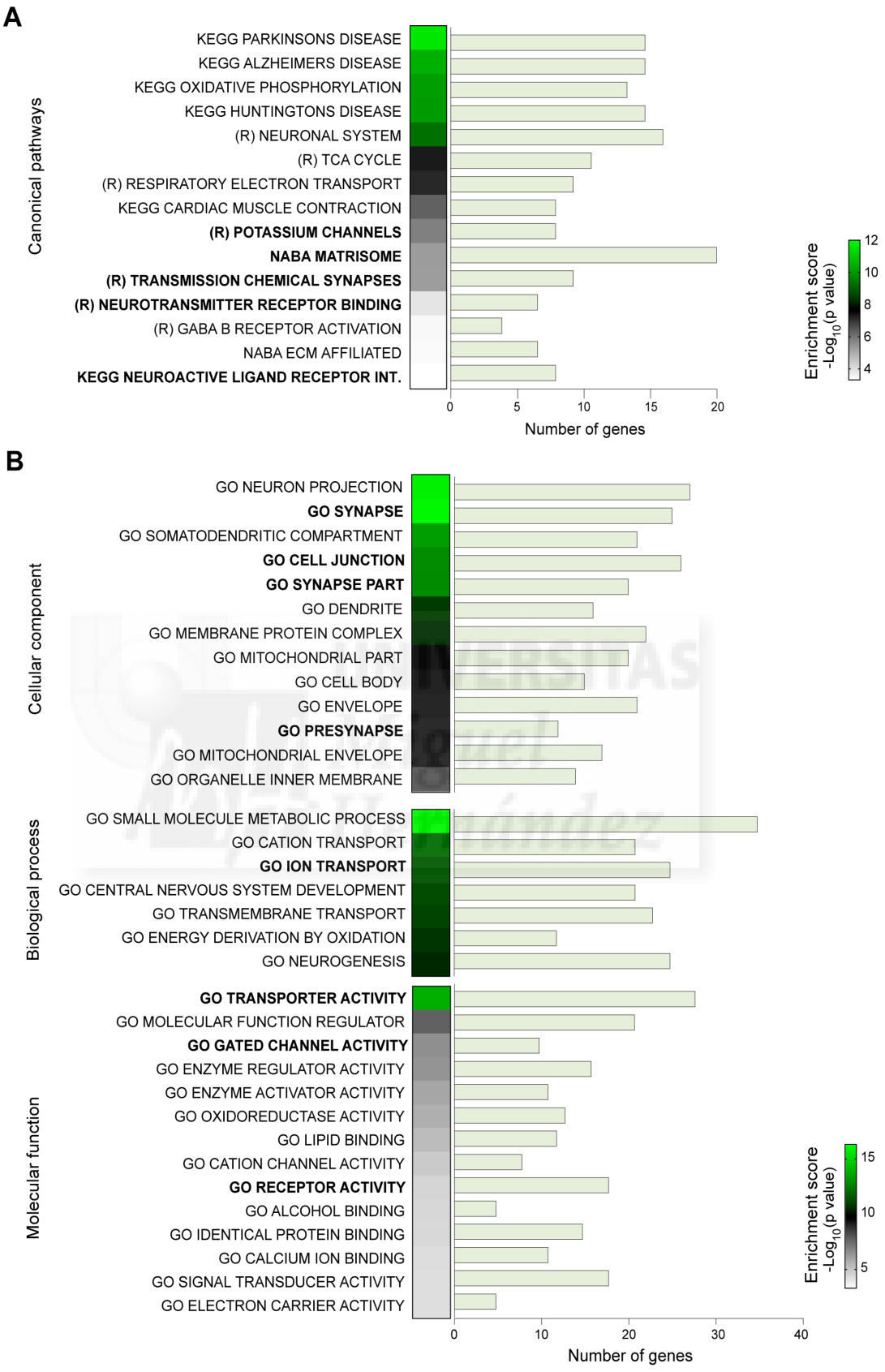

Figure 7. Interneuron subtype-specific gene sets and pathway components. *[Legend continues on next page]*

[Legend Figure 7 from the previous page]
Gene set enrichment analysis performed using a preranked pooled list of P10 interneuron subtype-specific genes and the GSEA software. (A) Gene set enrichment analysis against the Molecular Signatures Database (MSigDB) collection of KEGG, NABA and Reactome (R) pathway gene sets. (B) Comparative GO enrichment analysis for subtype-specific gene sets present in the GSEA collection arranged in cellular component, biological process and molecular function category. Given the vastness of the cellular component category, only GO terms that for such category are assigned to less than 1,200 and more than 500 genes in the mouse genome were considered.
In both (A) and (B), pathways (A) or GO terms (B) significantly enriched in P10 interneuron subtype-specific genes are shown on the left. *p* values for each pathway (A) or GO term (B) are color-coded as indicated. The bar graphs show the number of genes significantly associated with each pathway (A) or GO term (B). To avoid unnecessary complexity, when redundant terms appeared (e.g. 'transporter activity', 'cation transporter activity' and 'transmembrane transporter activity') only the hierarchically first pathway (A) or GO term (B) is shown.

To further explore the differential usage of genes across individual interneuron subtypes, we identified several gene sets with cell-type-specific enrichment. Analysis of manually curated groups of molecules revealed that the individual genes driving these signatures were differentially expressed between interneuron subtypes (Figure 8).

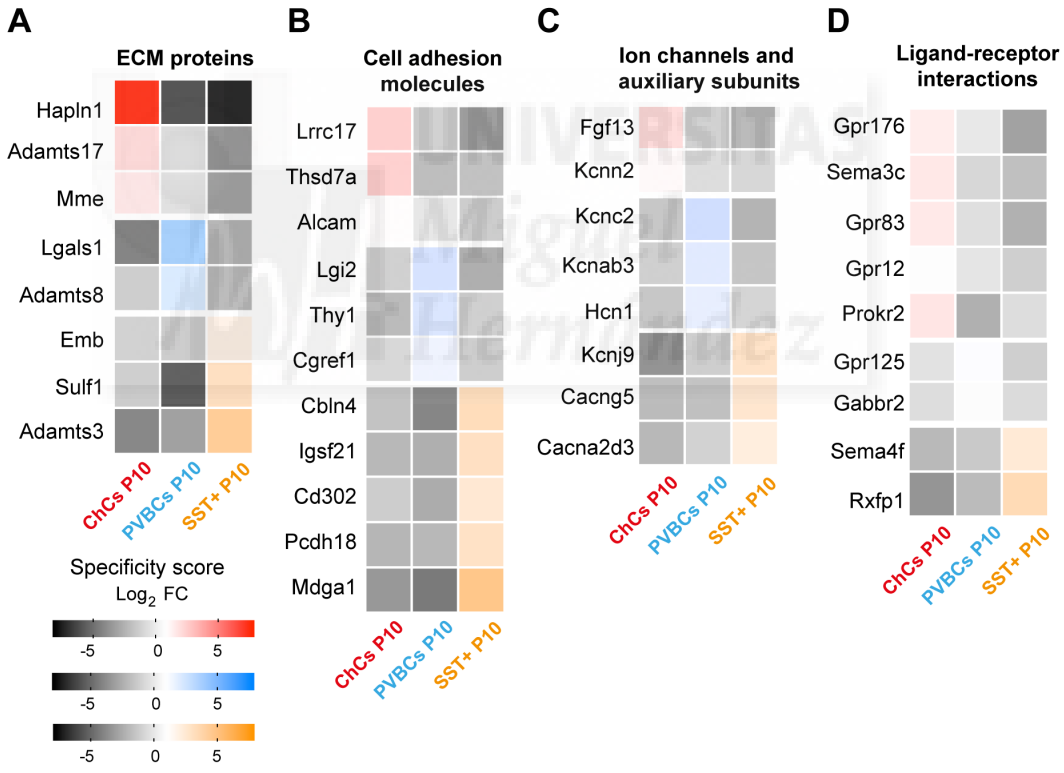

Figure 8. Extracellular matrix proteins, cell surface molecules, ion channels, ligands and receptors are the leading indicators of interneuron diversity at P10.
Analysis of manually curated groups of molecules revealed that individual interneuron subtypes use different codes of related molecules. Heatmaps showing the specificity score of individual genes driving matrisome (A), adhesion (B), ion transport (C) and ligand-receptor interaction (D) gene set enrichment and that are differentially expressed between interneuron subtypes.

For instance, consistent with the GO term analysis, we found that each interneuron subtype expressed a specific subset of genes involved in extracellular matrix (ECM) remodeling. A striking example is the differential use of ADAM metallopeptidase by each

interneuron subtype: chandelier cells specifically express ADAMTS17, PV+ basket cells use ADAMTS8 whereas ADAMTS3 is expressed in somatostatin cells (Figure 8A).

The concerted actions of cell surface proteins critically contribute to the precise assembly of neural circuits. The existence of unique surface molecule repertoires allows neurons to distinguish one another and connect with their appropriate target cells (de Wit and Ghosh, 2016). We identified a number of cell surface molecules with specific interneuron subtype expression, including protocadherin, immunoglobulin and leucine-rich repeat protein superfamilies (Figure 8B).

Apart from their subcellular targeting, interneurons can be distinguished based on their electrophysiological properties, which are determined by the different ion channels that they express. Ion channels and transporters were also among the main over-represented GO terms. We noticed that different interneurons indeed expressed different complements of voltage-gated ion channel subunits and ion channel-associated regulatory proteins (Figure 8C).

Finally, P10 chandelier, PV+ basket and somatostatin interneurons showed differential expression of individual genes involved in ligand-receptor interactions, such as G protein-coupled receptors (GPCRs) and members of the semaphorin family, highlighting their probable relevance for the wiring of inhibitory circuits (Figure 8D).

Our transcriptome database therefore provides an unprecedented opportunity to systematically identify interneuron subtype-specific expression of subsets of genes during synapse formation. Investigation of the function of these molecules and their dynamic changes during development would tremendously expand our knowledge of the assembly and function of the inhibitory circuits.

5. Identification of genes contributing to interneuron subtype synapse specificity

The gene enrichment analysis revealed that different codes of related molecules are expressed by particular P10 interneuron subtypes. To identify molecules that regulate interneuron synapse specificity, we selected genes with significant differences in gene-level expression both over time and between subtypes (see Methods).

Next, to detect those genes that exhibit the highest degree of subtype and stage specificity, we ranked all significantly differentially expressed genes using a specificity score (Figure 9, see Methods).

Moreover, we considered that the specificity of synaptic connections is the result of definite consecutive events such as axon guidance, synaptic cell adhesion, and stabilization of synaptic contacts (de Wit and Ghosh, 2016). Therefore, to identify cell-specific mechanisms that regulate synapse specificity, we focused our attention on genes that, in addition to being (1) developmentally upregulated and (2) specifically expressed in each interneuron subtype, had (3) demonstrated or putative roles in axon growth, axonal pathfinding, neuron-ECM communication or cell-cell adhesion.

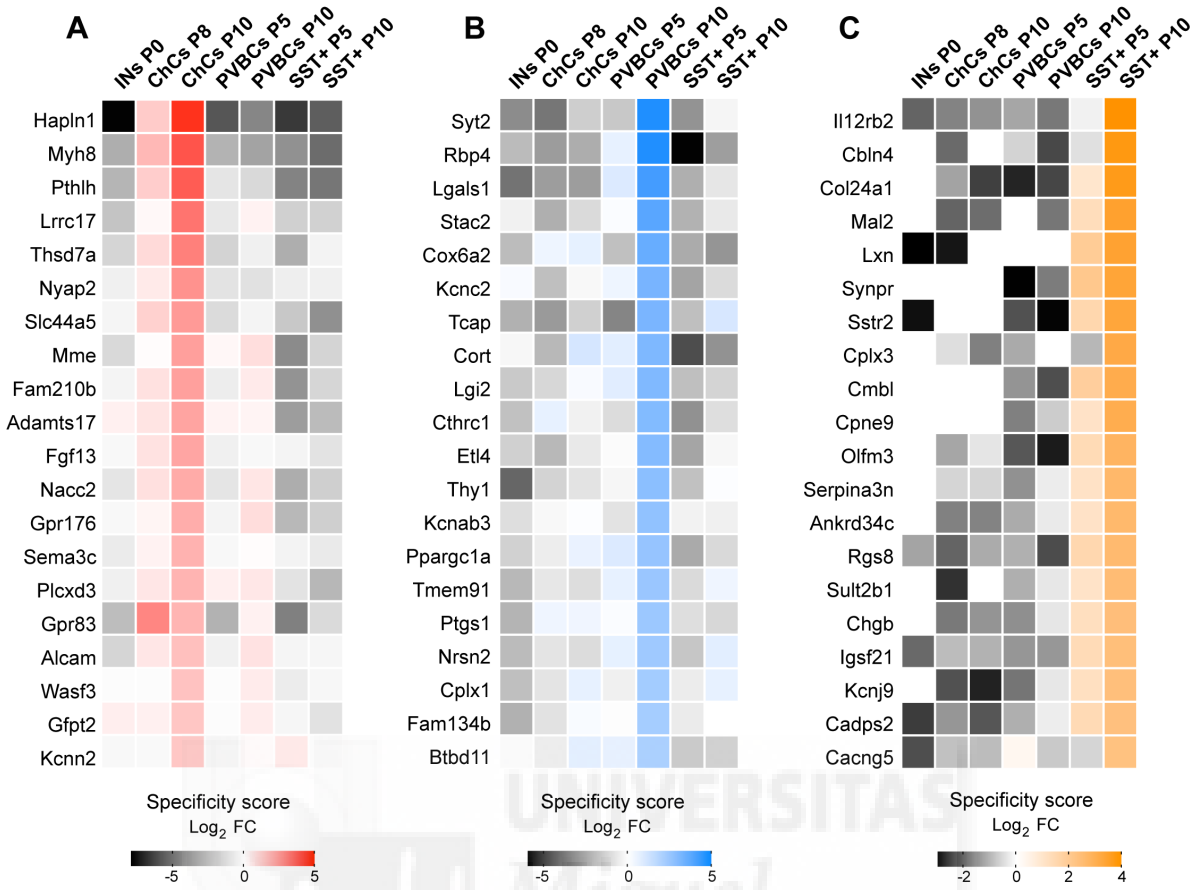

Figure 9. Cell-type specific genes significantly upregulated across development. Heatmaps showing the specificity score for the top 20 differentially expressed genes that exhibit the highest degree of subtype and stage specificity in chandelier, PV+ basket and SST+ cells.

For each interneuron subpopulation, the top 5 specific genes that met all these criteria were additionally ranked by a specificity ratio that further increased our specificity detection power (see Methods). The resulting hierarchically ordered list of candidate genes specifically expressed in chandelier, PV+ basket and somatostatin cells at the time of synapse formation is illustrated, along with their function, in Figure 10.

Subtype-specific candidate gene selection and validation

Our analysis (Figure 10) showed that Hyaluronan And Proteoglycan Link Protein 1 (*Hapln1*) was highly expressed in P10 chandelier cells and virtually absent in all other populations. Moreover, *Hapln1* exhibited significant upregulation in chandelier cells between P8 and P10. Published data reported that, in the visual cortex, *Hapln1* expression increases in PV+ cells along development, peaks at P14 and then, consistent with its role in regulating plasticity, decreases in the adult (Carulli et al., 2010). HAPLN1 is an ECM protein which contains an Ig-like V type domain that mediates cell-cell adhesion (Ivanova et al., 2009) and can also trigger intracellular signaling. *Hapln1*, therefore, stood out as the best candidate for playing a role in regulating chandelier synapse formation.

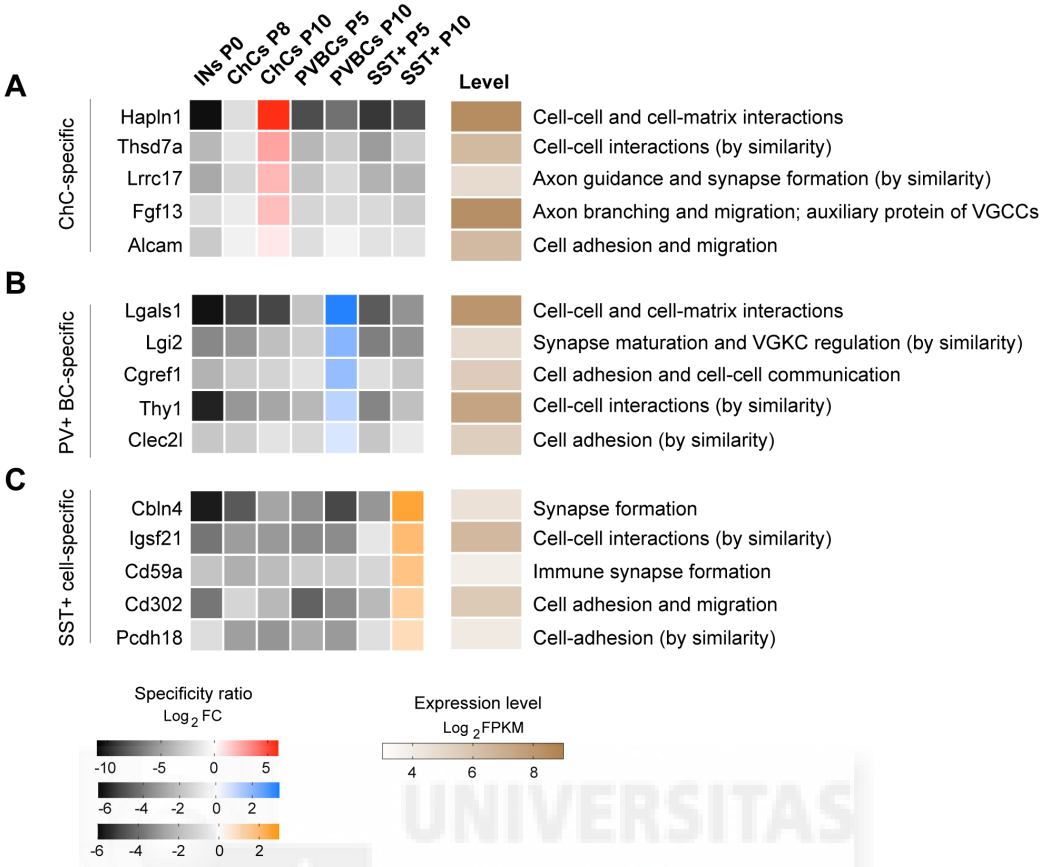

Figure 10. Candidate genes for mediating interneuron synapse specificity.
Heatmaps showing the specificity ratio for the top 5 candidate 'synaptic' genes that are specifically expressed in chandelier (A), PV+ basket (B) and SST+ cells (C) and are upregulated across development. The heatmap on the right shows the expression level of each gene at P10 in the population in which such genes are specifically expressed. The gene function which justified their selection as 'putative synaptic genes' is also briefly described.

Another ECM-associated molecule, Galectin-1 (*Lgas1*), was the more specific and abundant gene expressed in PV+ basket cells (Figure 10). However, since Galectin-1 does not regulate PV+ cell inhibitory synapse formation (A. Hinojosa, unpublished), based on the known role of LGI proteins in synapse maturation (Lovero et al., 2015; de Wit et al., 2011), we selected Leucine Rich Repeat LGI Family Member 2 (*Lgi2*) as a plausible candidate to regulate the specific development of perisomatic inhibitory synapses.

Finally, the leading candidate gene for somatostatin cells was Cerebellin 4 Precursor (*Cbln4*), a member of the Cbln subfamily, bidirectional synaptic organizers that regulate synapse development (Matsuda, 2017; Matsuda and Yuzaki, 2011; Siddiqui and Craig, 2011; Yuzaki, 2010).

To verify that the selected genes were indeed differentially expressed in distinct interneuron subpopulations and upregulated during development, we combined in situ hybridization (ISH) for *Hapln1*, *Lgi2* and *Cbln4* with immunohistochemistry (IHC) for the relevant interneuron markers. Fluorescent in situ hybridization histochemistry confirmed that *Cbln4* is only expressed in SST+ cells both at P10 and in the adult (data not shown, Rubén Deogracias, unpublished). At P10 *Cbln4*+SST+ are mostly distributed in superficial layers of the SSC. However, *Cbln4* expression increases along development and by P30 it is expressed in all SST+ interneurons, with the exception of a very small *Cbln4*-SST+ population in layer 4 (data not shown, Rubén Deogracias, unpublished).

Likewise, *Lgi2* expression increases along development and, although *Lgi2*+ PV+ basket cells are mainly located in cortical deep layers, *Lgi2* mRNA is almost exclusively found in PV+ basket cells both at P10 and at P30 (data not shown, André Marques-Smith, unpublished).

Chandelier-specific candidate gene selection and validation

Validation of the expression of candidate genes for playing a role in chandelier synapse formation was critical because, although the *Nkx2.1CreERT2* driver labeled a large percentage of chandelier cells (70%), *CreER*-induction also tagged a small percentage of PV+ basket cells, RELN+ interneurons and glial cells (Figure 3). Due to the lack of a specific marker, validation of the chandelier cell candidate genes relied on the morphological identification of chandelier cells after P12. As a proxy for identifying chandelier cells before that stage of development (or when performing ISH-IHC, see Methods), we estimated the match between the expected and observed ratio of fluorescently labeled cells that express the candidate gene in *Nkx2.1CreERT2* mice crossed with a reporter line.

In situ hybridization for *Hapln1* combined with immunohistochemistry for different markers showed that at P30 *Hapln1* was expressed in GABAergic cells and not in glial cells (Figure 11A-J). The gene was not expressed in somatostatin cells (Figure 11C), but the increased fraction of GFP+*Hapln1*+ cells in regions or layers enriched in chandelier cells (Figure 11H) suggested that it was expressed in a subset of putative chandelier cells. This was further confirmed by the low percentage of *Hapln1*+PV+ cells (Figure 11E and 11I), consistent with an expression in some chandelier but not PV+ basket cells. However, unexpectedly, only 9% of *Hapln1*-expressing cells were putative chandelier cells (labeled using *Nkx2.1CreERT2;RCE* mice, Figure 11D and 11J), whereas 52% of *Hapln1*-expressing cells were RELN+SST- interneurons (Figure 11F and 11J). Therefore, the pattern of expression of *Hapln1* suggested that it might play a general role in upper layer interneurons, such as neurogliaform (RELN+SST-) and chandelier cells, rather than specifically regulating chandelier synapse formation.

The next three candidate genes for chandelier cells were *Thsd7a*, *Lrrc17* and *Fgf13* (Figure 10). Thrombospondin Type 1 Domain Containing 7A (*Thsd7a*) is a membrane protein that mediates cell-cell interactions and has been shown to be involved in endothelial cell migration (Kuo et al., 2011; Wang et al., 2010). We found that the fraction of *Thsd7a*+GFP+ cells (putative chandelier cells) in *Nkx2.1CreERT2;RCE* mice at different developmental stages matched the prediction for a gene expressed in chandelier cells (Figures 11K and 11L). Of note, the similar ratio of PV+/chandelier and PV+/*Thsd7a*+ cells at P30 provided further evidence for its expression in chandelier cells (Figures 11K and 11M). In addition, consistent with the relatively small number of PV+ chandelier cells in the PFC, a very low fraction of PV+ cells expressed *Thsd7a* at P30 (Figures 11K and 11M). However, we also detected a strong reduction in the total number of *Thsd7a*+ cells along development (Figure 11N). The observation that this progressive developmental restriction of *Thsd7a* expression was not accompanied by parallel changes in the fraction of *Thsd7a*+ putative chandelier cells (Figure 11L), hinted that *Thsd7a* is also expressed in other cells at P10. Although we did not investigate the identity of non-chandelier *Thsd7a*+ cells, these results suggested that *Thsd7a* might play a specific role in chandelier cells only after inhibitory axo-axonic synapses are assembled, but is unlikely to specifically regulate chandelier synapse formation or to have such a role exclusively in chandelier cells.

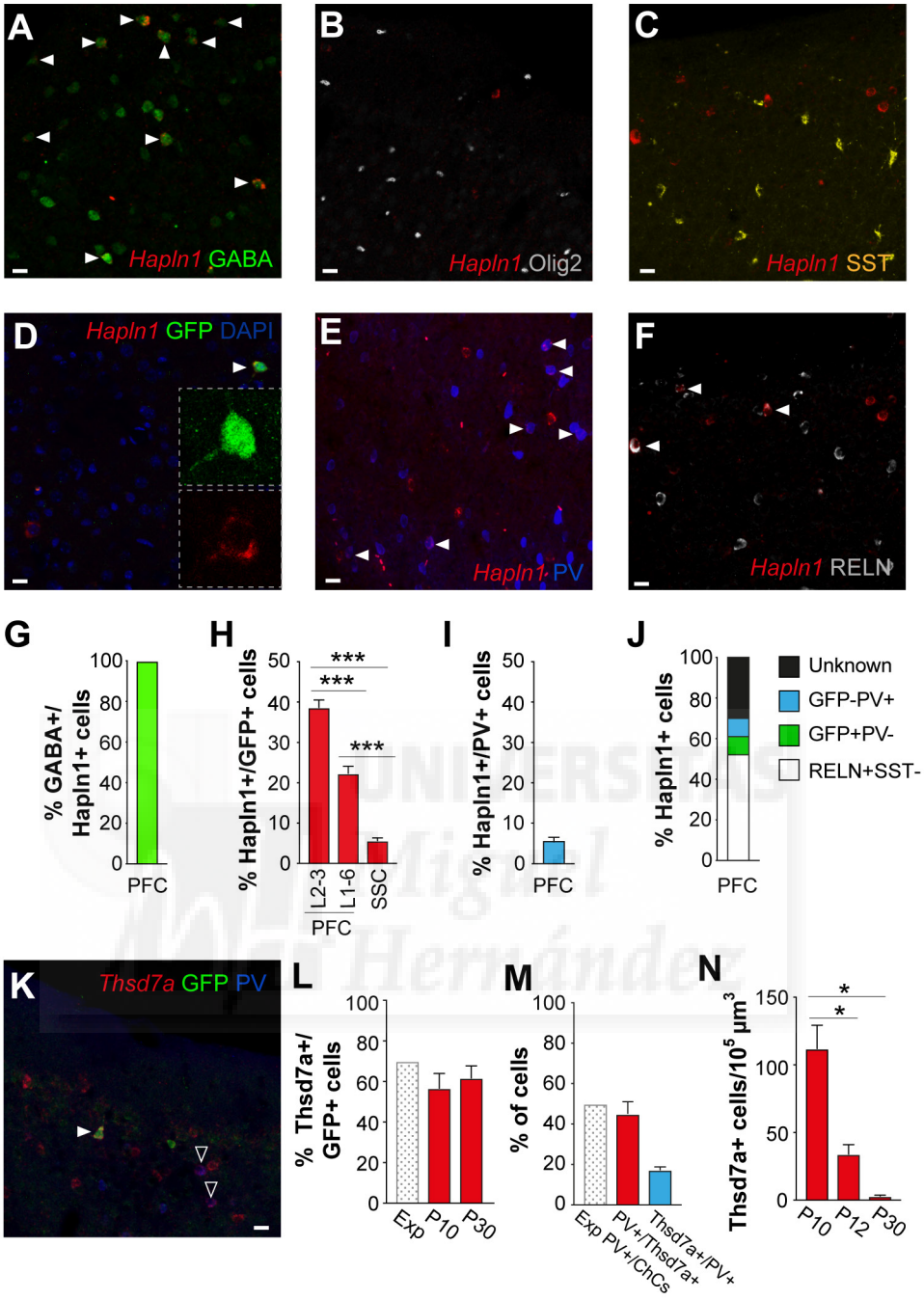

Figure 11. *Hapnl1* and *Thsd7a* are not good candidates for specifically regulating chandelier synapse development.

(A-F) Colocalization of *Hapln1* mRNA with different cell markers (arrowheads) at P30 in the mouse prefrontal cortex.

(G) Percentage of *Hapln1*+ cells that express GABA (n = 3 mice); note that all *Hapln1*+ cells are GABAergic.

(H) Percentage of GFP+ cells (labeled upon P2 tamoxifen *CreER* induction in *Nkx2.1CreERT2;RCE* mice) that express *Hapln1* in the upper and lower layers of the prefrontal cortex (PFC) as well as in the somatosensory cortex (SSC) at P30 (n = 3 mice). Note that the percentage of *Hapln1*+GFP+ cells increases in regions enriched in chandelier cells. One-way ANOVA ($p<0.001$), followed by Holm Sidak's multiple comparisons test ($p<0.001$ for all comparisons).

(I) Percentage of PV+ cells that express *Hapln1* in the prefrontal cortex (PFC) at P30 (n = 3 mice). Note the low colocalization, consistent with expression in some PV+ chandelier but not basket cells.
(J) Identification of cell types expressing *Hapln1* in the prefrontal cortex (PFC) at P30 (n = 3 mice per condition).
(K) Representative images showing *Thsd7a* mRNA colocalizing with GFP+ putative chandelier cells (arrowheads) and with PV+ cells (empty arrowheads).
(L) Percentage of GFP+ cells (labeled upon P2 tamoxifen *CreER* induction in *Nkx2.1CreERT2;RCE* mice) that express *Thsd7a* in the upper layers of the prefrontal cortex (PFC) at P10 and P30 (n = 3 mice per condition). Note that the percentage of *Thsd7a* +GFP+ cells matched the prediction for a gene expressed in chandelier cells (dotted white bar).
(M) Colocalization of *Thsd7a* mRNA with PV in the prefrontal cortex (PFC) at P30 (n = 3 mice per condition). The percentage of *Thsd7a*+ cells that express PV (red bar) is similar to that of PV+/chandelier (dotted white bar) supporting its expression in chandelier cells. The low percentage of *Thsd7a*+/PV+ cells (blue bar) also is consistent with an expression in PV+ chandelier but not basket cells. Note that this percentage is higher than the one found for *Hapln1* (I), suggesting that some basket cells might express *Thsd7a* and/or that *Hapln1* is not expressed in all PV+ chandelier cells.
(N) Density of *Thsd7a*+ cells in the prefrontal cortex across development (n = 3 mice per condition). Note the huge decrease in the number of cells after P12. One-way ANOVA ($p<0.05$), followed by Tukey's multiple comparisons (for both P10 vs P12 and P10 vs P30 $p<0.05$).
All scale bars in this figure are equal to 20 µm.

The next two genes, *Lrrc17* and *Fgf13*, had a similar specificity ratio. Whereas nothing is known about the role of *Lrrc17* in the brain, *Fgf13* is a member of the fibroblast growth factor (FGF) homologous factors (FHFs) that do not function as growth factors (Olsen et al., 2003). As other FHFs, FGF13 acts as an auxiliary protein of voltage-gated sodium channels, increases sodium current density and causes a depolarizing shift in the voltage dependence of the channel inactivation. As a result, FGF13 increases neuronal excitability and enables sustained high-frequency firing such as that of fast-spiking chandelier cells (Goldfarb et al., 2007; Musa et al., 2015; Pablo et al., 2016; Rush et al., 2006; Wang et al., 2017; Wittmack et al., 2004; Yang et al., 2017). FGF13 is also a microtubule stabilizing protein that regulates axon branching, neuronal polarization and migration (Wu et al., 2012a). In addition, *Fgf13* mutant mice exhibit enhanced susceptibility to epilepsy due to a reduction in inhibitory inputs onto pyramidal neurons and consequently altered excitatory/inhibitory balance (Puranam et al., 2015). In light of this, it is not surprising that mutations in *Fgf13* are associated with epilepsy (Puranam et al., 2015), X-chromosome-linked mental retardation (Wu et al., 2012a), autism (Yuan et al., 2017) and schizophrenia (Wang et al., 2015). Although *Lrrc17* was a very good candidate, the plausible function of *Fgf13* in maintaining the excitatory/inhibitory balance together with its high expression during circuit formation (Figure 10A) undoubtedly flagged it as a particularly promising gene for regulating chandelier synapse development.

Validation of FGF13 as a chandelier-specific gene

To validate FGF13 expression in chandelier cells, we used immunohistochemistry and colocalized FGF13 with fluorescently labeled chandelier cells in *Nkx2.1CreERT2;Ai9* mice. We found that all chandelier cells in the mouse PFC express FGF13 at P12, P15 and P30 (Figures 12A-12C). Published work had shown expression of *Fgf13* in pyramidal neurons at embryonic and early postnatal stages that decreased to barely detectable levels after P7 (Wu et al., 2012a), a time when chandelier cells start expressing high levels of the gene. Indeed, colocalization with gamma-aminobutyric acid (GABA) demonstrated that at P10 and P30 all FGF13-expressing cells are GABAergic

(Figures 12D-12F). Consistent with *Fgf13* developmental upregulation shown by our RNA-seq data, we found that the number of GABAergic cells expressing *Fgf13* dramatically increased from P5 to P10 (Figure 12E). Therefore, similar to *Cbln4* for somatostatin cells and *Lgi2* for PV+ basket cells, *Fgf13* is expressed in prefrontal chandelier cells, its expression increases during the time of chandelier synapse formation and is also maintained in the adult.

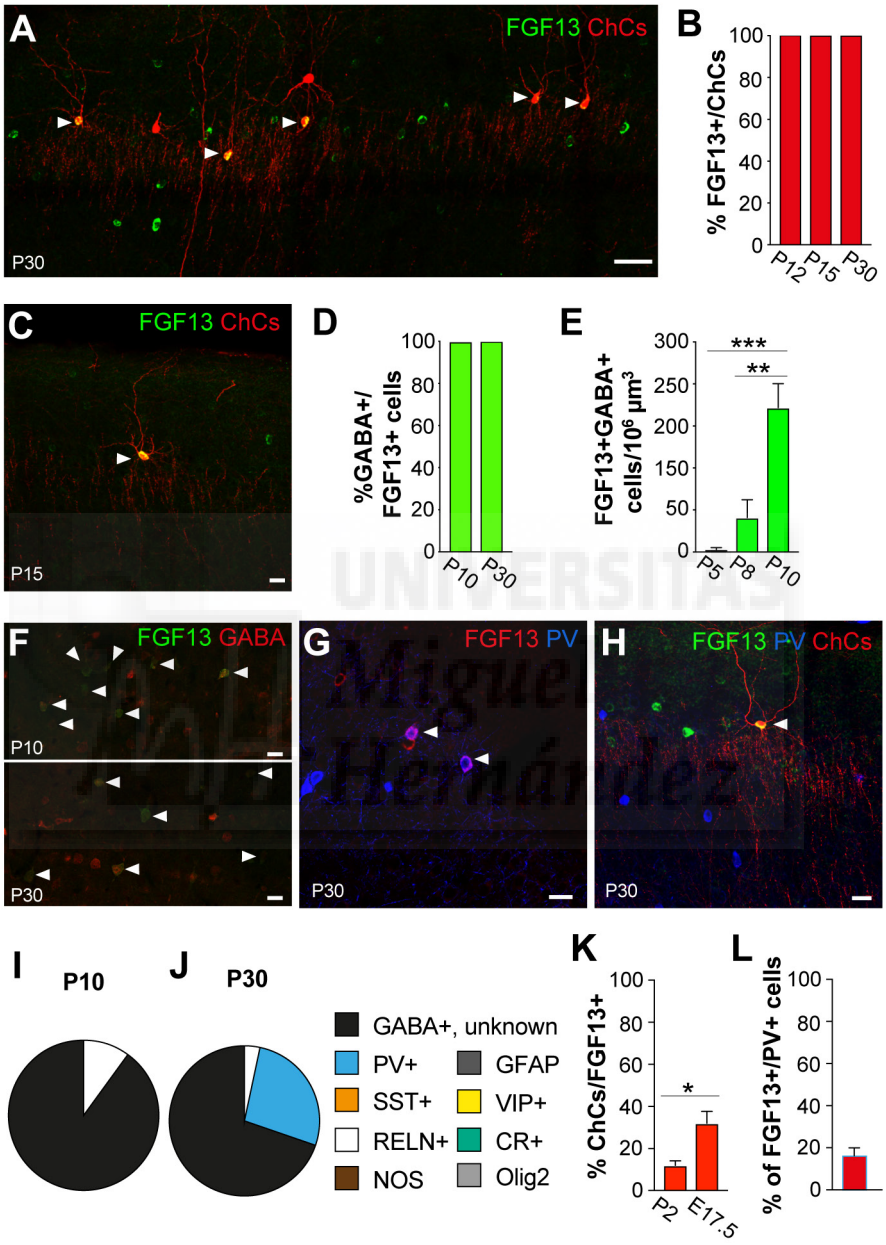

Figure 12. FGF13 is specifically expressed in all chandelier cells.
(A-C) Representative images (A and C) and quantification (B) showing expression of FGF13 in all chandelier cells at different stages of development (n = 3 mice in each condition). Scale bars equal 50 µm (A) and 20 µm (C).
(D) Percentage of FGF13+ cells that express GABA at P10 and P30 (n = 3 mice per condition); note that at both stages all FGF13+ cells are GABAergic.
(E) Density of FGF13+ cells in the prefrontal cortex across development (n = 3 mice per condition). Note the huge increase in the number of cells between P8 and P10. One-way ANOVA

(p<0.001), followed by Tukey's multiple comparisons (for P10 vs P5 p<0.001 and for P10 vs P8 p<0.01).
(F) Representative images showing FGF13+GABA+ cells at P10 and P30. Scale bars equal 20 μm.
(G) Colocalization of FGF13 and PV. Note that not all PV+ cells express FGF13 and not all FGF13+ cells express PV. Scale bar equal 20 μm.
(H) Representative image showing FGF13 expression in a PV- chandelier cell at P30. Scale bar equal 20 μm.
(I and J) Pie graphs showing the colocalization of FGF13 with different cell markers at P10 and P30 in the mouse prefrontal cortex (n = 3 mice per condition). FGF13 is not expressed at detectable levels in glial and pyramidal cells or in other interneurons, with the exception of a marginal percentage of RELN+ cells.
(K) Percentage of FGF13+ cells that are Tomato+ chandelier cells (labeled upon P2 or E17.5 tamoxifen *CreER* induction in *Nkx2.1CreERT2;Ai9* mice) in the upper layers of the prefrontal cortex at P30 (n = 3 mice per condition). Note that the colocalization rises when the total number of chandelier cells labeled increases. Student's t-test, p<0.05.
(L) Percentage of PV+ cells that express FGF13 (putative PV+ chandelier cells) in the prefrontal cortex (PFC) at P30 (n = 3 mice per condition). The low colocalization is consistent with the observed expression in PV+ chandelier but not basket cells. Note that this FGF13/PV colocalization suggests that, in the mouse prefrontal cortex, only 16% of PV+ interneurons are chandelier cells.

As expected for a gene expressed in chandelier cells, FGF13 was found in a subset of PV+ cells (Figure 12G). Colocalization of FGF13 with several markers showed that the gene was not expressed at detectable levels in glial and pyramidal cells or in other interneurons (Figures 12G-12L), with the exception of a marginal percentage of RELN+ cells (10% and 3% RELN+/FGF13+ cells at P10 and P30, respectively). These results strongly suggest that, at both P10 and P30, almost all FGF13+ cells are PV+ and PV- (Figure 12H) chandelier cells.

A caveat intrinsic to the *Nkx2.1CreERT2;Ai9* line is that only a subpopulation of chandelier cells is fluorescently labeled by *CreER*-induction. To further confirm that the rest of cells expressing detectable levels of FGF13 were unlabeled chandelier cells (ChCs), we compared the percentage of ChCs/FGF13+ cells in mice that were administered with Tamoxifen at P2 to that observed in mice induced at E17.5 when we label more chandelier cells. As expected, the percentage of colocalization increased in mice induced at E17.5 (Figure 12K), providing additional evidence that the 90-97% of cells showing clear immunoreactivity for FGF13+ can be considered *bona fide* chandelier cells. To the best of our knowledge, the specificity of FGF13 immunoreactivity is an unprecedented tool that allows estimation of the dimension of the whole chandelier cell population. Chandelier cells have always been considered to be a minority of PV+ interneurons but their exact percentage was unknown (Inan and Anderson, 2014). FGF13/PV colocalization showed that, in the mouse prefrontal cortex, only 16% of PV+ interneurons are chandelier cells (Figure 12L).

Altogether, the analyses performed with *Cbln4*, *Lgi2*, and *Fgf13* confirmed a highly restricted pattern of expression in PV+ basket, somatostatin and chandelier cells in the developing cortex and, consistent with their RNA-seq expression profile, revealed that the three genes are upregulated in the corresponding interneuron subpopulation during the time of synapse formation. Therefore, they appeared as promising candidates to play a role in the specific assembly of PV+ basket, somatostatin and chandelier cells synapses.

To investigate the role of *Fgf13*, *Lgi2* and *Cbln4* in regulating the development of different subtypes of GABAergic synapses, we used a systematic virus-mediated conditional gene knock-down strategy and performed cell-specific loss-of-function experiments *in vivo*.

FGF13 controls chandelier cartridge and bouton development

For chandelier cells, we engineered Cre-dependent conditional constructs expressing a short-hairpin RNA (shRNA) and in which recombination was reported by mCherry (Figure 13A). These constructs contained *shRNAs* targeting a common region for both FGF13 isoforms (*shFgf13*) or targeting LacZ as a control (Figure 13A). The ability of the *shRNAs* targeting FGF13 to efficiently downregulate FGF13 expression had been shown in previous work (Wu et al., 2012a). After confirming the functionality of our constructs *in vitro* (Figure 13B and 13C), we packed Cre-dependent shRNA-2 and shRNA-4 in adeno-associated viral vectors (AAV) and produced a mixture of both viruses.

Next, we injected Cre-dependent *shFgf13* or Cre-dependent control *shLacZ*-expressing viruses in the medial prefrontal cortex of *Nkx2.1CreERT2* mice at P2 and induced Cre translocation to the nucleus by simultaneous Tamoxifen injections (Figure 13D). Immunohistochemistry for FGF13 in the injected mice showed that *shFGF13* successfully down-regulated FGF13 expression in chandelier cells *in vivo* (Figure 13E and 13F).

The most distinctive feature of chandelier cells is that their axon terminals form a network of synaptic boutons that line up vertically onto the axon initial segment (AIS). Upon FGF13 knock-down, we observed a high disorganization of the chandelier axons at P30. This was particularly evident when infected chandelier cells were co-immunostained with AnkyrinG (AnkG), which labels the AIS of neighboring pyramidal neurons (Figures 13G and 13H). In control *shLacZ*-expressing chandelier cells, the axonal cartridges (labeled with mCherry) followed a single AIS and made multiple contacts onto it. In *shFgf13* cells, the cartridges formed tangles and crossed over horizontally from one AIS to another. Interestingly, in FGF13 knock-down cells each mCherry+ cartridge contacted more AISs compared to the control and this phenotype was accompanied by a small increase in cartridge length (Figure 13I and 13J). Although *shFgf13* did not prevent the formation of chandelier axons and we could still identify chandelier cells by morphology, *Fgf13* knock-down cells had a less dense arbor, as shown by a higher distance between cartridges compared to the controls (Figure 13K).

We next analyzed the density of chandelier synapses at P30 and found that expression of *shFgf13* led to a 50% decrease in the number of synapses that chandelier cells make onto the AIS compared to the control, whereas no significant difference in the number of total boutons per cartridge was observed (Figure 13L-13O). Altogether, these results show that FGF13 controls chandelier cartridge and bouton development. Remarkably, the number of somatic mCherry+ boutons from incidental infection of PV+ basket cells was unchanged, further supporting the specific role of FGF13 in the regulation of chandelier synapse formation (Figure 13P).

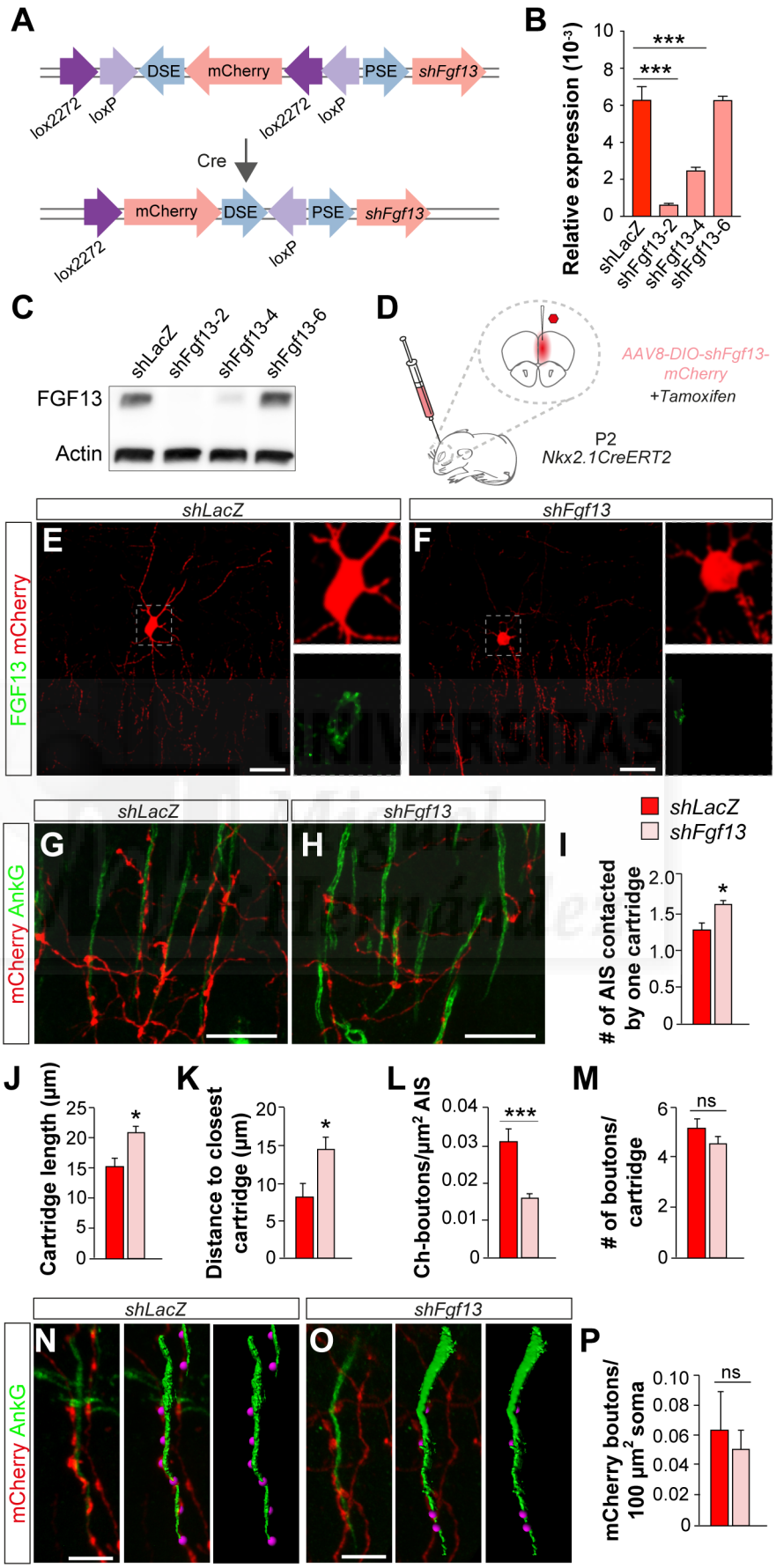

Figure 13. FGF13 controls cartridge and bouton development in chandelier cells. *[Legend continues on next page]*

[Legend Figure 13 from the previous page]

(A) Diagram of the AAV Cre-dependent constructs expressing mCherry and *shFgf13* (engineered by R. Deogracias).
(B and C) FGF13 mRNA (B) and protein (C) expression upon FGF13 downregulation using different *shRNAs in vitro* (n = 3, experiment performed by V. Gonzalez and R. Deogracias). For (B), one-way ANOVA followed by Holm-Sidak's multiple comparisons test ($p<0.001$ for the indicated comparisons).
(D) Schematic of AAVs stereotaxic injections in the prefrontal cortex of P2 *Nkx2.1CreERT2* mice.
(E and F) Representative images showing mCherry+ chandelier cells from sparse viral infection and the reduction of endogenous FGF13 protein in mCherry+ chandelier cells that express *shFgf13* (F) but not the *shLacZ* (E). Scale bars equal 20 µm.
(G and H) Representative images showing a less dense arborization and the disorganization of the chandelier axons at P30 in FGF13 knock-down cells (H) compared to control cells infected with a virus expressing *shLacZ* (G). These images were taken by V. Gonzalez. Scale bars equal 10 µm.
(I) Quantification of the number of axon initial segments contacted by one cartridge (defined as such when 3 consecutive presynaptic boutons were found on the same chandelier axon) in FGF13 knock-down cells (n = 16 cells from 3 mice) compared to *shLacZ*–expressing control cells (n = 13 cells from 3 mice). Mann Whitney test, $p<0.001$.
(J) Quantification of the average cartridge length in FGF13 knock-down cells (n = 6 cells from 3 mice) compared to controls (n = 3 cells from 3 mice). Mann Whitney test, $p<0.05$.
(K) Quantification of the 'distance to closest cartridge' (measured as the average distance between each cartridge and the cartridge that is closest to it and used as a proxy to estimate the density of the chandelier arbor) in FGF13 knock-down cells (n = 17 cells from 3 mice) compared to *shLacZ*–expressing control cells (n = 13 cells from 3 mice). Mann Whitney test, $p<0.001$.
(L) Quantification of the density of chandelier synapses per unit of axon initial segment in FGF13 knock-down cells (n = 16 cells from 3 mice) compared to *shLacZ*–expressing control cells (n = 14 cells from 3 mice). Student t-test, $p<0.001$.
(M) Quantification of the average number of chandelier presynaptic boutons in one cartridge in FGF13 knock-down cells (n = 3 cells from 3 mice) compared to *shLacZ*–expressing control cells (n = 5 cells from 3 mice). Student t-test, $p>0.05$.
(N and O) Representative images and Imaris reconstruction showing the lower density of chandelier AIS-synapses in FGF13 knock-down cells (O) compared to *shLacZ*–expressing control cells (N). These images were taken and reconstructed by V. Gonzalez. Scale bars equal 10 µm.
(P) Quantification of the density of mCherry+ somatic synapses per surface unit of pyramidal cell soma in FGF13 knock-down mice (n = 6 cells from 3 mice) compared to *shLacZ*–expressing control cells (n = 5 cells from 3 mice). Mann Whitney test, $p>0.05$.

FGF13B partially rescues the knock-down phenotype

FGF13 has two isoforms, FGF13A and FGF13B, that show a differential expression, subcellular localization, and function (Munoz-Sanjuan et al., 2000; Pablo et al., 2016; Wu et al., 2012a). FGF13B is highly expressed in the mouse cortex, whereas FGF13A is expressed at lower levels (Wu et al., 2012a). Although both isoforms bind directly to voltage-gated sodium channels (VGSCs), the effect of their modulation on cell excitability and firing frequency seems to be different (Pablo et al., 2016; Rush et al., 2006). In addition, FGF13B —but not FGF13A— interacts with microtubules and regulates axonal branching and neuronal migration (Wu et al., 2012a). FGF13A contains a nuclear localization signal (NLS) and has been found in the nucleus (Pablo et al., 2016; Wu et al., 2012a) which suggests a yet unidentified nuclear function. Since chandelier cells lacking FGF13 displayed defective cartridge and synapse development, we reasoned that the phenotype observed was likely due to the expression of the FGF13 isoform more related with the axonal branching, FGF13B.

A pilot experiment overexpressing a *Fgf13B* cDNA that has silent mutations which make it resistant to *shFgf13*-mediated RNA interference showed that the average number of chandelier synapses was still closer to the density found in knock-down cells (Figure 14A). Conversely, the cartridge length and the number of AISs contacted by one cartridge was more similar to the control (Figure 14B and 14C). Although the low number of cells analyzed did not provide enough power to allow detection of significant differences with either *shLacZ* or *shFgf13*, these preliminary results suggested that FGF13B might be able to rescue the chandelier arbor disorganization (Figure 13I-K) but not the decreased synapse density (Figure 13L). While more cells need to be analyzed, the data obtained so far hint that (1) the effects of *shFgf13* are likely to be specific, (2) the synaptic phenotype might not be the mere consequence of an abnormal morphological differentiation of the chandelier arbor and that (3) FGF13A or —more likely— a coordinated action of FGF13A and FGF13B may regulate chandelier synapse formation.

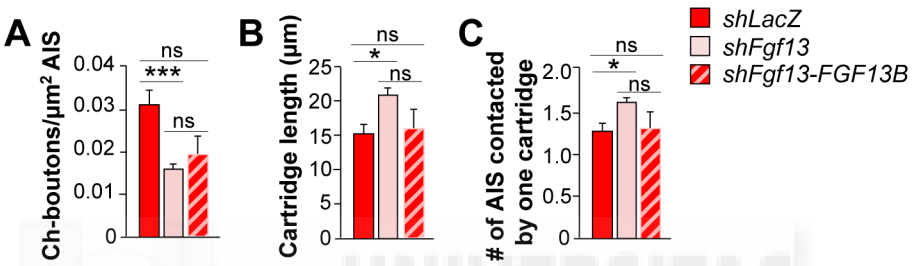

Figure 14. FGF13B seems to rescue the axonal phenotype but not the synaptic defect observed upon FGF13 downregulation.
(A) Quantification of the density of chandelier synapses per unit of axon initial segment in FGF13 knock-down cells (same data as in Figure 13L), *shLacZ*–expressing control cells (same data as in Figure 13L) and cells expressing both *shFgf13* and a mutated FGF13B isoform resistant to the shRNA (rescue, n = 4 cells from 2 animals). One-way ANOVA ($p<0.001$) followed by Tukey's multiple comparisons test (*shLacZ* vs FGF13B rescue $p=0.106$; *shFgf13* vs FGF13B rescue $p=0.784$).
(B) Quantification of the average cartridge length in FGF13 knock-down cells (same data as in Figure 13J), *shLacZ*–expressing control cells (same data as in Figure 13J) and FGF13B rescue (n = 4 cells from 2 animals). One-way ANOVA ($p<0.01$) followed by Tukey's multiple comparisons test (*shLacZ* vs FGF13B rescue $p=0.538$; *shFgf13* vs FGF13B rescue $p=0.233$).
(C) Quantification of the number of axon initial segments contacted by one cartridge in FGF13 knock-down cells (same data as in Figure 13I), *shLacZ*–expressing control cells (same data as in Figure 13I) and FGF13B rescue (n = 4 cells from 2 animals). One-way ANOVA ($p<0.001$) followed by Tukey's multiple comparisons test (*shLacZ* vs FGF13B rescue $p=0.891$; *shFgf13* vs FGF13B rescue $p=0.143$).

Cell-specific expression of Lgi2 and Cbln4 controls somatic and dendritic inhibitory synapse development

Chandelier cell-specific *Fgf13* knock-down experiments demonstrated that a cell-type specific program is responsible for the morphological differentiation of chandelier cells and regulates axo-axonic inhibitory synapse formation.

We used a similar approach to investigate the role of *Lgi2* and *Cbln4* in controlling the development of somatic and dendritic inhibitory synapses, respectively. Efficient downregulation of both proteins was achieved injecting Cre-dependent *shLgi2* or *shCbln4*-expressing virus in the somatosensory cortex of *Lhx-6-Cre* and *SST-Cre* mice,

respectively (data not shown, R. Deogracias, unpublished). We found that down-regulation of LGI2 in PV+ basket cells caused a decrease in the density of somatic inhibitory synapses and loss of function of CBLN4 in SST+ cells led to a reduction of dendritic synapses onto pyramidal cells (Figures 15A-E, R. Deogracias and A. Marques-Smith, unpublished). Remarkably, overexpression of CBLN4 in SST+ cells essentially yielded the opposite phenotype: an increase in inhibitory synapses onto the dendrites of pyramidal cells (Figure 15E; R. Deogracias, unpublished). Altogether, our findings demonstrated that three genes specifically expressed in different interneurons regulate the development of different types of inhibitory synapses.

It was however not clear whether FGF13, LGI2, and CBLN4 are components of entire cell-specific molecular programs that as a whole specify different patterns of connectivity. To get some insights into this question, we performed pilot experiments overexpressing an HA-tagged CBLN4 in chandelier using a conditional viral strategy in the *Nkx2.1CreERT2* line. We found that, whereas overexpression of CBLN4 in SST+ interneurons led to a gain of function phenotype, its overexpression in chandelier cells did not affect the number of chandelier synapses. Preliminary data showed that *Cbln4*-overexpressing chandelier cells innervated the AIS of pyramidal neurons, formed normal cartridges and made a number of axo-axonic synapses comparable to control chandelier cells (Figure 15F-15H). These results further confirmed that CBLN4 functions specifically in regulating the formation of dendritic synapses made by SST+ cells.

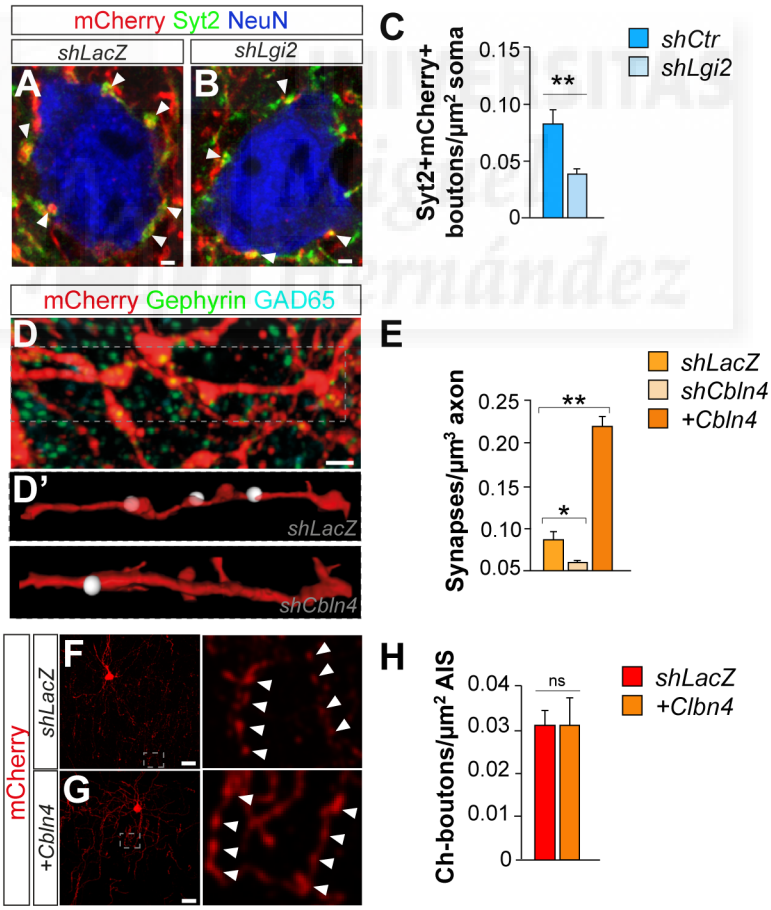

Figure 15. *Lgi2* regulates the development of PV+ somatic synapses and *Cbln4* specifically controls SST+ dendritic inhibitory synapses.
(A-C) Representative images (A and B) and quantification (C) of mCherry+Syt2+ somatic synapses per surface unit of pyramidal cell soma in LGI2 knock-down cells (n = 202 cells from 7

mice) and *shLacZ*–expressing control cells (n = 195 cells from 6 mice). Mann Whitney test, p<0.01. Images and graphs are from A. Marques-Smith. Scale bars equal 1 µm.
(D) Representative image and Imaris reconstruction used for quantification of mCherry+ boutons inside the axons of infected SST+ cells contacting Gephyrin+ postsynaptic clusters in layer I of the somatosensory cortex. Scale bar equal 1 µm.
(E) Quantification of GAD65+mCherry+Gephyrin+ synapses per unit of presynaptic mCherry+ axon in CBLN4 knock-down cells (n = 5 mice), *shLacZ*–expressing control cells (n = 5 mice) and CBLN4 overexpressing cells (n = 4 mice). Note that the graph does not start at zero. One-way ANOVA (p<0.001) followed by Tukey's multiple comparisons test (*shLacZ* vs *shCbln4* p<0.05; *shLacZ* vs CBLN4 overexpression p<0.001). Graphs are from R. Deogracias.
(F-H) Representative images (F and G) and quantification (H) of the density of chandelier synapses per unit of axon initial segment in CBLN4 overexpressing chandelier cells (n = 3 cells from 2 mice) compared to *shLacZ*–expressing control cells (n = 14 cells from 3 mice). Mann Whitney test, p>0.05. Scale bars equal 20 µm.

Collectively, *Fgf13*, *Lgi2* and *Cbln4* emerged as paradigmatic genes which support the existence of synaptic protein repertoires that are selective for each interneuron subtype. Altogether, these results illuminate how cell-specific molecular programs control the formation of different types of GABAergic synapses onto pyramidal neurons.

UNIVERSITAS Miguel Hernández

UNIVERSITAS
Miguel
Hernández

UNIVERSITAS Miguel Hernández

DISCUSSION

UNIVERSITAS
Miguel
Hernández

Understanding brain function (and dysfunction) begins with the knowledge of how neuronal connections are established and organized in functional networks. Identifying the mechanisms of synapse specificity is a key step in the greater endeavor of deciphering the brain connectome. In this study, we combined new methods for purifying different neuronal populations at various maturation stages together with parallel RNA sequencing to characterize the transcriptional dynamics of chandelier, PV+ basket and SST+ cells during synapse formation. Furthermore, we used a virus-mediated protein knockdown strategy to prove that the unveiled cell-specific molecular signatures translate functionally into the specification of different patterns of connectivity. The transcriptome data described in this work provide the neuroscience community with a valuable resource to better understand the relationship between cortical interneuron development and diversity.

1. Cell diversity: transcriptional signatures of developing interneurons

The analysis of our comparative transcriptome data showed that different developing interneuron populations express several cell type-specific genes. Many of these genes are critical to specify their synaptic and cellular properties. Indeed, our gene enrichment analysis revealed that of all genes differentially expressed in each interneuron subtype during cortical wiring, those broadly involved in circuit formation are predominant. In particular, axon guidance, cell adhesion and extracellular matrix molecules, in addition to G protein-coupled receptors (GPCRs), are the leading indicators of neuronal diversity in P10 interneurons. This is consistent with previous studies that have highlighted how cell surface molecules significantly contribute to cell type diversity (Doyle et al., 2008; Molyneaux et al., 2015). For example, P1 pyramidal cells that project to different regions have a different complement of G protein-coupled receptors (GPCRs) and members of the semaphorin family (Molyneaux et al., 2015).

Our analysis also showed a high enrichment in genes that control the emergence of the electrophysiological properties of neocortical interneurons. Electrophysiological maturation and connectivity are two concomitant and intimately related components of neuronal identity (Tremblay et al., 2016). During development, the properties of different interneurons undergo profound changes, ultimately leading to the phenotypic divergence that characterizes their mature profile (Petilla Interneuron Nomenclature Group et al., 2008; Tremblay et al., 2016). As the physiological maturation of each interneuron type relies on parallel trajectories of ion channel expression, it is not surprising that distinct repertoires of ion channels are expressed among different interneurons (Sugino et al., 2006) as well as in mature compared to developing interneurons (Okaty et al., 2009).

Although abundant and detailed information is available only for PV+ fast-spiking interneurons (Doischer et al., 2008; Goldberg et al., 2011; Itami et al., 2007; Okaty et al., 2009), we know that thousands of transcripts are developmentally regulated while interneurons undergo the tremendous physiological changes that characterize their maturation. Ion channel subunits are significantly overrepresented among both up- and downregulated genes; many of the upregulated ion channels show enriched expression in mature PV+ cells as compared to other interneuron subtypes, whereas downregulated genes are associated with PV- non-fast-spiking interneurons (Okaty et al., 2009; Sugino et al., 2006). Consistently, our transcriptome data show that already at P10 different interneurons exhibit cell-specific expression of ion channel subunits. It is particularly striking that such a difference also exists within the fast-spiking group, between chandelier and PV+ basket cells. Coupling a study of the expression of these cell-specific subunits with an analysis of how they change between two close stages of development (P5/P8 and P10) will allow a more detailed study of how cell type-specific

expression of ion channel subunits arises during development. Moreover, it would be interesting to complement this analysis by studying how post-transcriptional modifications, another key determinant of diversity in ion channel properties (Jan and Jan, 2012; Lipscombe et al., 2013a; Marques-Smith et al., 2016a; Onwuli and Beltran-Alvarez, 2016), contribute to the emergence of the unique mature physiological properties of different interneurons. Our transcriptome data would be an excellent valuable resource for both of these analyses, thus contributing to expand our knowledge on the developmental mechanisms underlying the constellation of interneuron subtype-specific features.

2. A dynamic picture of interneuron diversity across developmental stages

Interneuron diversity is a field under active investigation (Klausberger and Somogyi, 2008; Wamsley and Fishell, 2017). Recent progress in single-cell sequencing has complemented previous studies (Sugino et al., 2006) and has tremendously increased our knowledge on the roles of genetic programming in sculpting interneuron types (Jiang et al., 2015; Markram et al., 2015; Tasic et al., 2016; Zeisel et al., 2015). Conversely, a parallel understanding of how the unique properties of different interneurons emerge during development has lagged behind (Okaty et al., 2009). In particular, it is still unclear how cell-specific differences in gene expression support the exquisite specificity observed in the connectivity of different interneuron subtypes (Wamsley and Fishell, 2017).

In marked contrast with recent work (Jiang et al., 2015; Tasic et al., 2016), which provided a static —albeit useful— screenshot of the diversity exhibited by mature interneurons, our study not only revealed transcriptional differences between cell types but also provided a dynamic picture of the changes in gene expression between two close stages of early synaptic wiring.

This approach revealed that distinct genes with analogous molecular function are expressed in different interneurons and upregulated during circuit formation. In particular, we found that cell type-specific synaptic properties are encoded by different complements of molecules involved in axon growth as well as cell-cell and cell-matrix interactions. Consistently, upregulation or downregulation of similar types of molecules have been shown to distinguish maturing PV+ cells from their adult counterparts (Okaty et al., 2009).

Selective molecular programs support interneuron subtype-specific connectivity

As a proof of concept, we investigated the function of three putative synaptogenic genes that exhibited cell type-specific expression in chandelier, PV+ basket and SST+ cells and were upregulated across development. We proved that the three molecules — FGF13, LGI2 and CBLN4— regulate the assembly of, respectively, axo-axonic, somatic and dendritic inhibitory synapses (Figure D1). These results showed how cell-specific molecular signatures indeed trigger the specification of different patterns of connectivity. Interestingly, these molecules play a role in three different steps of synapse development: axon branching, synapse maturation and synapse assembly, suggesting that cell-specific mechanisms operate at all levels of interneuron circuit formation.

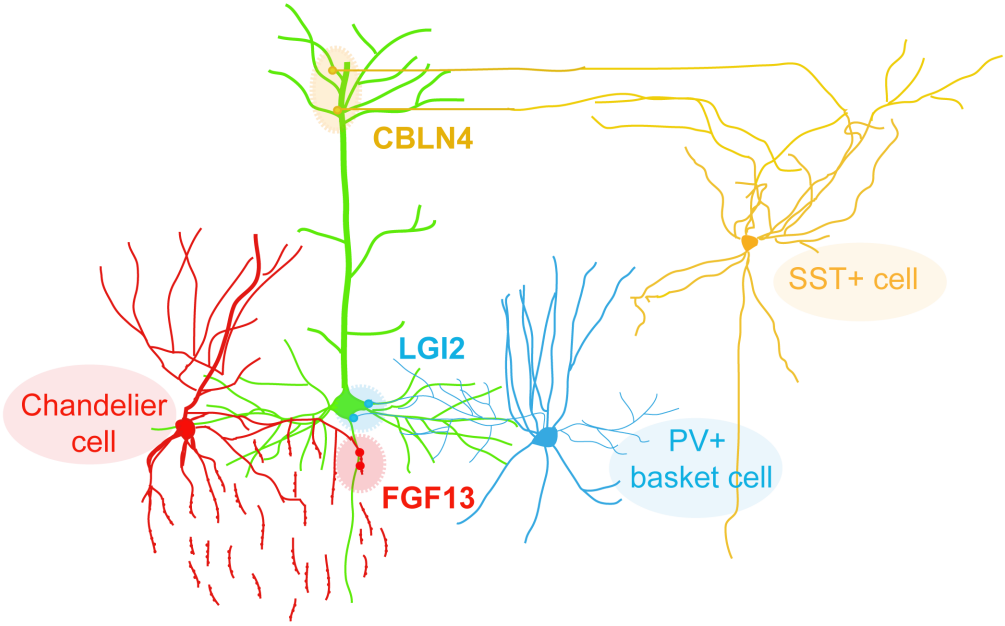

Figure D1. Selective molecular programs regulate interneuron subtype-specific connectivity.
FGF13, LGI2 and CBLN4 exhibit cell type-specific expression in chandelier, PV+ basket and SST+ cells and play a role in the assembly of axo-axonic, somatic and dendritic inhibitory synapses, respectively, thereby showing that cell-specific mechanisms regulate inhibitory circuit specificity.

In addition, we observed that overexpression of *Cbln4* in the cell type where it is exclusively expressed in the wild-type cortex —SST+ cells— leads to a huge increase in the density of dendritic synapses. However, forcing the expression of *Cbln4* in chandelier cells not only does not modify their target from the AIS to the dendrites but also has no effect on the number of chandelier synapses. Considering that *Cbln4* is a secreted molecule, one conceivable explanation is that chandelier cells do not express the presynaptic partners necessary for *Cbln4* to exert its potent synaptogenic effect. A second, not necessarily alternative, possibility is that *Cbln4* postsynaptic receptors are not positioned at the AIS where the terminals of chandelier cells make their synaptic contacts. The ability of *Cbln4* to selectively induce synapse formation only in SST+ cells further supports the existence of highly selective cell-type specific programs that shape not only one protein but entire molecular repertoires, such as synaptic protein complexes, in developing cortical interneurons.

Although our findings show that molecular diversity supports the exquisite specificity of interneuron subtype-specific synaptic connections, it is important to mention that ubiquitous molecules have been shown to regulate specific subtypes of inhibitory synapses, such as PV+ basket (Chattopadhyaya et al., 2013) or chandelier (Tai et al., 2014). This is however not surprising and supports the notion that molecules ubiquitously expressed can play unique roles in brain wiring because of the cell-specific molecular partners they interact with (Allan et al., 2005; Pawson and Nash, 2000).

3. Upregulation of metabolic genes in PV+ basket cells during brain wiring

Surprisingly, the pathway analysis also showed a high enrichment in genes associated with neurodegenerative diseases. A closer look to the individual genes driving this

enrichment reveals that that they are all involved in energy metabolism, which is a crucial pathological component in neurodegenerative disorders (Burté et al., 2015; Dunn et al., 2014; Gouarné et al., 2013; Gray et al., 2014; Knight et al., 2014; Lin and Sheng, 2015; Pathak et al., 2013; Schwarz, 2013). Indeed, the very same genes are also the source of the observed enrichment in oxidative phosphorylation, tricarboxylic acid (TCA) cycle and respiratory electron transport pathways.

Neuronal computation is energetically expensive. As such, most brain energy is used on different events of synaptic transmission, including transmitter release and recycling, generation of postsynaptic currents, and, predominantly, action potential initiation and frequency (Attwell and Laughlin, 2001; Carter and Bean, 2009; Harris et al., 2012; Rangaraju et al., 2014). In fact, activity-driven local ATP synthesis via both glycolysis and mitochondrial function is required for synaptic function (Jang et al., 2016; Rangaraju et al., 2014; Wang et al., 2004a). In light of this, the upregulation of metabolic genes during brain wiring appears as fundamental to fulfill the increased energy demand associated with the emergence of synaptic connectivity.

The metabolic genes are one of the very few instances in which *post hoc* analysis of the expressing cell-type reveals a predominant expression in one population only, PV+ basket cells. To support high-frequency neuronal firing and rapid action potential kinetics, PV+ interneurons are energetically demanding (Carter and Bean, 2009). This particularly high energy utilization requires optimal mitochondrial performance (Kann et al., 2011) and, indeed, PV+ cells have higher mitochondrial content compared to other neurons (Gulyás et al., 2006). As a result, mitochondrial dysfunction and metabolic deficits in PV+ cells alter their intrinsic physiology and network connectivity, as well as complex information processing (Galow et al., 2014; Inan et al., 2016; Kann et al., 2014).

Being PV+ basket and chandelier cells both fast-spiking, a legitimate question is why these metabolic genes are more specifically and abundantly expressed in PV+ basket than in chandelier cells. A possible explanation lies in their apparent differential contribution to the generation of gamma rhythm in the cortex. Fast-spiking cells have been shown to synchronize local assemblies of pyramidal cells in the gamma frequency (Cardin et al., 2009). However, although chandelier cells are active at gamma frequencies, their firing is not synchronized with the gamma rhythm and thus they do not seem to be critical for gamma oscillations (Dugladze et al., 2012; Massi et al., 2012). During gamma oscillations, the peak of oxygen consumption approaches the demand observed during seizures and mitochondrial oxidative capacity operates near its functional limit. As such, gamma band synchrony relies heavily on energy metabolism and is particularly sensitive to metabolic disruption (Kann et al., 2014). It is therefore possible that the metabolic machinery of PV+ basket but not chandelier cells is built to specifically cope with their high oxygen consumption and energy demands during gamma band synchrony.

While our knowledge on how cortical fast-spiking PV+ basket cells acquire their mature electrophysiological properties over the first postnatal weeks has considerably increased in the last years (Anastasiades et al., 2016; Doischer et al., 2008; Du et al., 1996; Goldberg et al., 2011; Itami et al., 2007; Okaty et al., 2009), a parallel understanding of how the metabolic machinery sustaining such properties develops has lagged behind. Consistent with previous work (Okaty et al., 2009), our screening highlights the physiological importance of the developmental upregulation of metabolism-related genes specifically in PV+ basket cells. In the future, our transcriptome data will be a useful tool to investigate the development of PV+ cell neuroenergetics over the course of their physiological and synaptic maturation.

4. The "*5 W's*" of FGF13 synaptic phenotype

To date, the low number of chandelier cells and the lack of a specific marker have severely hampered the identification of the mechanisms regulating chandelier cell development. Paraphrasing the words of a science writer, "because of the strategic importance of chandelier cells, it has been a source of frustration to neuroscientists that little has been learned about them since their discovery" (Tarr, 2012). Our findings show that FGF13 plays a critical role in chandelier axonal arbor, cartridge and bouton development. In particular, FGF13 deficient cells display a striking phenotype: (1) their axonal arbor is less dense with (2) tortuous, longer and more horizontally oriented cartridges. In their greater length, these abnormal cartridges (3) contain a similar number of total boutons compared to controls and (4) contact more axon initial segments (AISs), but yet (5) they make remarkably less axo-axonic synapses per unit of AIS.

Possible scenarios

Why, if FGF13 knockdown cartridges have the same number of boutons per cartridge and contact more AISs, the density of synapses on the AIS is reduced? Several – not mutually exclusive – scenarios are possible (Figure D2).

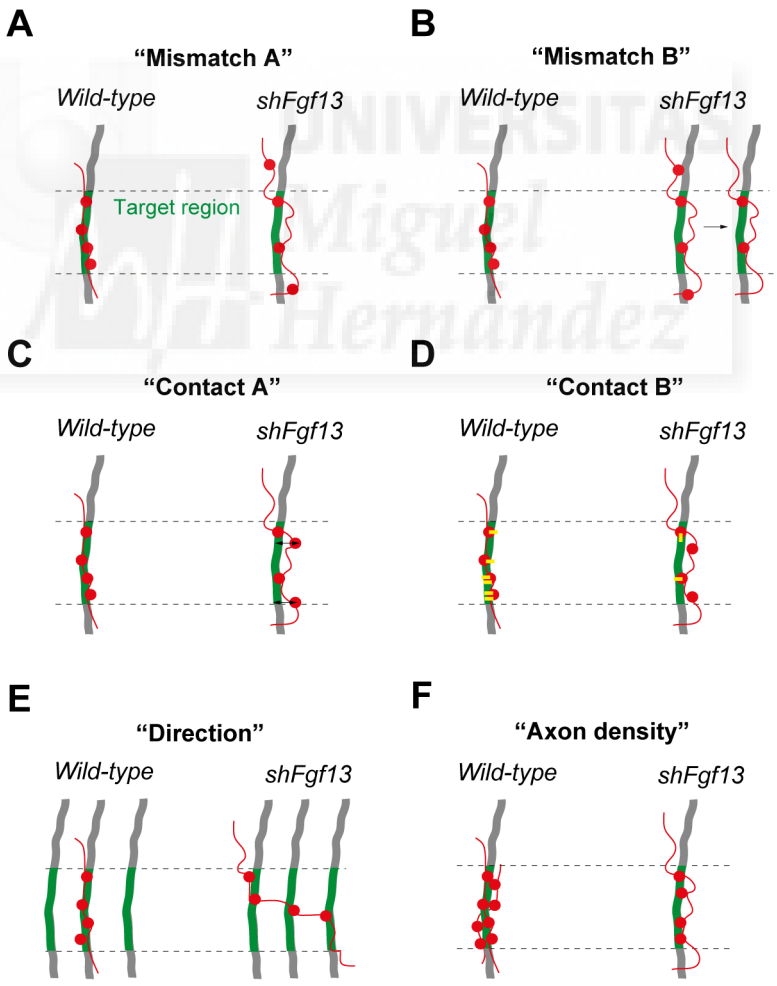

Figure D2. FGF13 regulates chandelier axonal arbor, cartridge and bouton development. Possible non mutually exclusive scenarios explaining the complex phenotype of FGF13 knockdown chandelier cells. FGF13 deficiency leads to the formation of tortuous, longer, less dense and more horizontally oriented cartridges. These cartridges contain a similar number of total

boutons compared to controls and contact more AISs but make less synapses. A potential explanation for the observed loss of synapses is related with the possibility of missing a specific target domain (A and B) or with a defective contact (C and D). Alternatively, the similar number of synapses per cartridge might be distributed over several AISs (E). Finally, the synaptic phenotype might simply be a consequence of the reduced chandelier axonal arborization (F). Note that most of these scenarios assume some degree of interdependence between the axonal and synaptic phenotype and are likely to co-exist.

(1) "**Mismatch**". In the cortex, chandelier synapses are not formed equally along the AIS but are instead biased toward the distal end (Inan et al., 2013; Wefelmeyer et al., 2015). Consequently, if the same number of boutons is distributed over a greater length, some of them may fall outside the domain where the postsynaptic partner is, thus impeding the synaptic contact (Figure D2A). An alternative inherent in this model is that the synaptic contact is actually made outside the target region but it is subsequently disassembled and retracted as inappropriate (Figure D2B). Live imaging of chandelier synapse formation in control and FGF13 knockdown cells would help to distinguish between these two possibilities.

(2) "**Contact**". A second scenario holds that all boutons in the cartridge have the potential to connect with the target domain but the contact does not occur due to (A) the curved and tortuous structure of FGF13 deficient cartridges. This hypothesis is based on the observation that synaptic cell adhesion can only operate at short distances (<100 nm) (Südhof, 2006). Consequently, once a first bouton has reached out the AIS, the following bouton may be too distant for a second contact to happen (Figure D2C). Alternatively, (B) all boutons may be close enough to allow the formation of synaptic connections within the target region but the lack of FGF13 could affect the expression or localization of presynaptic adhesion molecules, thus making on average the occurrence of synaptic contacts more difficult and, therefore, less likely (Figure D2D).

(3) "**Direction**". Although the tendency of FGF13 knockdown cartridges to have a horizontal orientation is still at the level of a mere qualitative observation, it might play an important role in determining the synaptic phenotype. Specifically, a possible explanation for the reduced density of axo-axonic synapses could be that the similar number of boutons per cartridge is distributed over several AISs. This possibility is consistent with both the increase in the number of AISs contacted by one cartridge and their horizontal orientation (Figure D2E). Implicit in such option is that the amount of inhibition provided by a single chandelier cell to a given pyramidal neuron would be lower but the overall inhibitory drive to the pyramidal cell network could be similar or even higher, depending on where these synapses are located at the AIS (Wefelmeyer et al., 2015). A different type of examination ('horizontal' as opposite to 'vertical'), for instance analyzing the number of bouton per AIS rather than per unit of AIS, can help to verify this fascinating scenario.

(4) "**Axon density**". A fourth possibility that deserves consideration is that the synaptic phenotype might be the mere consequence of the reduced chandelier axonal arborization. The higher distance found between neighbor cartridges suggests that the total number of cartridges made by individual chandelier cells lacking FGF13 may be reduced. Since each AIS is innervated by more than one cartridge (Inan et al., 2013), it is plausible to hypothesize that the resulting average synapse density onto the AIS will be correspondingly scaled down (Figure D2F). To rule out this option, it would be useful to study how a late FGF13 downregulation (for example using the relatively late *PV-Cre* driver) affects both the number of synapses and the axonal morphology.

As stated above, it is plausible that the synaptic phenotype is indeed the result of several of these scenarios combined. To parse among these possibilities, it would be

important to investigate whether the axonal and synaptic phenotypes observed upon FGF13 deficiency are related or if they reflect two different functions of the protein. Even in the last scenario, some degree of interdependence between the axonal and synaptic phenotype is nevertheless likely to occur.

Molecular perspective on the role of FGF13 in chandelier cells

So far only two molecules have been shown to regulate chandelier synapse formation, the tyrosine kinase receptor ErbB4 (Fazzari et al., 2010; Del Pino et al., 2013) and a cytoplasmic modulator of ErbB4 activity, the guanine nucleotide exchange factor (GEF) DOCK7 (Tai et al., 2014). Interestingly, whereas ErbB4 promotes the formation of axo-axonic inhibitory synapses but does not regulate chandelier axonal morphology (Fazzari et al., 2010), DOCK7 plays two distinct roles in chandelier cells regulating both cartridge and bouton development (Tai et al., 2014). In fact, the effects of DOCK7 deficiency closely resemble the phenotypes observed upon FGF13 knockdown (Tai et al., 2014). In addition, like FGF13 (Wu et al., 2012a), DOCK7 also controls axon formation and polarization of newborn pyramidal neurons at early stages of development (Watabe-Uchida et al., 2006). Whether DOCK7 and FGF13 interact is currently unknown and should be verified in the future.

The diverse functions of both FGF13 and DOCK7 support the notion that multiple interactions of the same molecule can drive different pathways. The fact that a molecule plays different roles in the same cell or similar roles in different cells is a recurrent theme in biology that shows how the specificity of its effects lays in the different molecular complexes it engages in (Allan et al., 2005; Pawson and Nash, 2000). In the case of FGF13, it regulates polarization in pyramidal cells at embryonic stages and then, later in development, it is specifically expressed in chandelier cells where it regulates both axon differentiation and synapse formation. Future studies exploring the molecular mechanisms underlying specific aspects of FGF13-mediated regulation of the morphological differentiation of chandelier cells will help to better understand how these peculiar inhibitory neurons mature.

Net effect of the multiple roles of FGF13

It is difficult to estimate how the intricate combination of the morphological changes observed upon FGF13 downregulation will ultimately affect their inhibitory drive onto both individual target pyramidal cells and at the network level. For example, can a 30% increase in the number of AISs contacted by one cartridge compensate, at the network level, for a 50% reduction in both axon and synapse density?

Patch-clamp electrophysiological recordings would be extremely informative. Performing pair-recordings between FGF13 knockdown chandelier cells and pyramidal neurons could reveal a lower connection probability if the arborization defect is predominant, or exactly the opposite if what prevails is the increase in AISs contacted by one cartridge. In addition, based on the results of the structural analysis, in the connected pairs one might expect to find altered inhibitory postsynaptic current dynamics.

However, the answers to these questions cannot be anticipated without taking into account the effect of FGF13 on the intrinsic properties of neurons. A large amount of evidence has shown that FGF13 binds and modulates voltage-gated sodium channels (VGSCs). As such, it profoundly influences their properties, leading to an increase in neuronal excitability and firing frequency (Ali et al., 2016; Goetz et al., 2009; Goldfarb et al., 2007; Laezza et al., 2009; Musa et al., 2015; Pablo et al., 2016; Rush et al., 2006; Wang et al., 2017; Wittmack et al., 2004; Yang et al., 2017). In light of this, we would predict that FGF13 knockdown makes chandelier cells more excitable and slower.

This scenario is nevertheless further complicated by the differential modulation of neuronal firing rate via the two FGF13 isoforms, both apparently expressed in chandelier cells (data not shown). FGF13B facilitates high-frequency spiking whereas FGF13A hampers it. The different effects of FGF13 isoforms on channel properties is remarkable as it may allow specific sub-populations of chandelier cells to fine-tune their firing properties via alternative splicing of FGF13. Once again, predicting the net effect of FGF13 deficiency in this context is not trivial and could only be investigated using deletion mutants that segregate the two functions —axonal growth and channel regulation— of this complex protein.

Of note, an analogous warning should also be raised for LGI2, as LGI proteins can influence cell excitability by modulating Kv1.1, a voltage-gated presynaptic potassium channel subunit that critically controls neurotransmitter release probability and neuronal excitability (Johnston et al., 2010; Schulte et al., 2006).

Value of FGF13 to gain insights into homeostatic plasticity

The remarkable phenotype exhibited by chandelier cells upon FGF13 knockdown also raises broader scale questions that should be answered in the future. One particularly interesting subject for future investigation concerns the compensatory mechanisms that might be triggered to satisfy the requirements for network homeostasis.

Cortical networks have the extraordinary ability to maintain stability despite perturbations. Homeostatic changes involve nearly any aspect of neuron and network function, from neuronal intrinsic excitability to synaptic inputs and outputs (Burrone, 2003; Marder and Taylor, 2011; Turrigiano and Nelson, 2000). As such, one would expect broad compensatory changes to be elicited by the large loss of chandelier synapses observed upon FGF13 deficiency.

For example, it would be interesting to explore whether wild-type chandelier cells attempt to compensate the reduced inhibition from knockdown cells and, if so, how. Do they make more synapses? Is their axonal arbor wider? Is it denser? Do they contact more AISs? Do they increase their excitability?

Alternatively, FGF13 knockdown chandelier cells might also correspondingly re-adjust their excitability. Although confirming such a compensatory effect would be greatly complicated by the additional direct role of FGF13 in regulating cell excitability, rescue experiments using deletion mutants or a comparison between acute (e.g. using small peptide inhibitors *in vitro*) and chronic FGF13 downregulation would allow discriminating between these possibilities.

The interaction between the position of the AIS and its synapses plays a critical role in determining the homeostatic adaptation of neurons to changes in network activity. Specifically, in response to an increase in activity, a combination of distal relocation of the AIS and activation of axo-axonic synapses in the proximal axonal region efficiently decreases neuronal excitability (Grubb and Burrone, 2010a, 2010b; Grubb et al., 2011; Wefelmeyer et al., 2015). What happens then to the AIS of pyramidal cells contacted by FGF13 deficient cells? Does the AIS undergo structural reorganization to compensate the changes in pyramidal cell excitability that are likely to result from the loss of chandelier synapses? In this context, a comparison between the effect of a cell-autonomous manipulation of FGF13 in chandelier cells and the use of an FGF13 conditional knock-out strain (Wang et al., 2017; Wu et al., 2012a) will certainly prove useful.

Given the paucity of information about chandelier cells and considering that what is known is not free from controversy and debate (Inan and Anderson, 2014; Szabadics et al., 2006; Wang et al., 2016; Woodruff et al., 2009, 2010), it is difficult to predict what compensatory mechanisms can be triggered by a reduction in such a strategical but enigmatic subtype of inhibitory inputs. We envision that teasing out in what way cortical

networks adapt to a loss of chandelier synapses will provide further insights into the function of these mysterious interneurons and how they are integrated in the cortical circuits.

5. Role of LGI2 and CBLN4 for subtype-specific synapse formation

Our findings showed that LGI2 and CBLN4 regulate the formation of, respectively, somatic and dendritic inhibitory synapses onto pyramidal cells.

LGI2 may regulate PV+ synapse maturation and properties

LGI2 is a secreted Leucine Rich Repeat (LRR)-containing protein. Whereas cell adhesion proteins containing LRR domains have fundamental roles in initiating synaptogenesis (de Wit and Ghosh, 2014, 2016; de Wit et al., 2011), secreted LRR-proteins have been shown to be critical in later stages of synapse development. For example, LGI1 —another member of the LGI family found at excitatory synapses— is an important regulator of excitatory synaptic transmission, a key step in the maturation of a nascent synapse (Südhof, 2013). By forming a synaptic complex with ADAM22 and PSD95, secreted LGI1 enhances AMPAR-mediated synaptic transmission. Likewise, at the PV+ synapses, LGI2 may interact with fundamental components of the synapse and therefore promote synapse potentiation and stabilization of a specific subtype of inhibitory synapses. The selective presence of LGI2 at the PV+ terminals may also be important to impart specificity at the level of their synaptic properties, in the same way that the LRR protein Elfn1 regulates presynaptic release in a subtype-specific manner (Sylwestrak and Ghosh, 2012).

Putative role of CBLN4 as synaptic organizer

CBLN4 is a member of the Cbln subfamily, bidirectional synaptic organizers that regulate synapse development (Matsuda, 2017; Matsuda and Yuzaki, 2011; Siddiqui and Craig, 2011; Yuzaki, 2010). The molecular identity of CBLN4 suggests a putative role as a subtype-specific synaptic organizer. Synaptic organizers typically play a cohesive role in the initial establishment of a synaptic contact. In addition, they also have a fundamental instructive role in initiating trans-synaptic signaling events that trigger synapse formation (Siddiqui and Craig, 2011).

So far, Neuroligin 2 is the only synaptic organizer known to drive inhibitory synapse formation owing to its ability to interact with gephyrin and recruit gephyrin-associated proteins to the inhibitory postsynapse (Poulopoulos et al., 2009). None of the synaptic organizers identified so far have been shown to unequivocally and purposely drive subtype-specific synaptogenesis. This observation, together with the relatively stereotyped pattern that characterizes the very first stages of synapse formation, provided the basis for the prevalent idea that cell subtype- and synapse subtype-specific identities emerge in later stages of synapse formation (Emes and Grant, 2012; de Wit and Ghosh, 2016). This idea is further supported by the various molecules involved in different aspects of late synapse formation, maturation or function that are able to impart specificity on synaptic connections (Sylwestrak and Ghosh, 2012; Williams et al., 2011). Although these molecules undoubtedly play a unique and essential role in the emergence of synapse diversity, our data hint at the exciting possibility that subtype-specific synaptic organizers might also exist.

Such hypothesis is in apparent contradiction with the inability of CBLN4 to increase the density of chandelier synapses when ectopically expressed in this interneuron subtype. However, the synaptogenic effect of other members of the Cbln subfamily, such as CBLN1, depends on their ability to form a complex with other synaptic proteins.

In the case of CBLN1, for instance, its ability to induce synapse formation depends on the interaction of CBLN1 with both neurexin and GluRδ2 receptors (Matsuda et al., 2010; Uemura et al., 2010). Similarly, CBLN4 might form a complex with a specific neurexin isoform expressed in SST+ cells and, on the post-synaptic side, with a specific GABA receptor subunit. As such, identification of CBLN4 binding partners on both sides of the synapse would be key to confirm that it is indeed a newly discovered —not only cell-specific but also, and more importantly, subtype-specific— synaptic organizer.

6. Technical and methodological considerations

Paucity of universal PV+ basket cell-specific genes

Validation of the transcriptome data revealed that the PV+ basket cell genes present in our list display exquisite specificity for this interneuron type. However, the majority of PV+ basket cell-specific genes also consistently showed expression in defined supopulations only. Increasing evidence has demonstrated that cortical PV+ basket cells exhibit a high degree of intra-group heterogeneity with regard to their birth-date, properties, input and output connectivity, and recruitment during behavior [(Akgul and Wollmuth, 2013; Dehorter et al., 2017; Donato et al., 2013, 2015; Lagler et al., 2016; Lee et al., 2014a, 2014c; Varga et al., 2014), see also part II of the thesis].

In particular, the strong propensity of PV+ basket cells to form subnetworks with distinct pyramidal cell subtypes (Lee et al., 2014a, 2014c) suggests that genes regulating the formation of inhibitory perisomatic synapses might also have a parallel early network organizer role. As such, they would instruct on not only which domain but also which cell subtype to contact. In light of this, it is conceivable to hypothesize that there might not be many of such “PV-specific all-encompassing” synaptogenic genes.

It is important to mention, though, that all parsed genes (*Lgas1*, *Lgi2* and *PGC-1α*) are expressed mainly by PV+ basket cells distributed in deep layers (A. Marques-Smith and A. Hinojosa, unpublished). Since in our screening we performed transcriptome analysis of lower layer PV+ basket cells to avoid incidental isolation of chandelier cells, we cannot rule out that this approach introduced a bias towards genes enriched in lower layer PV+ cells. However, the presence of Synaptotagmin 2 (Syt2) —a well-known marker of all PV+ basket inhibitory terminals (Sommeijer and Levelt, 2012)— as the most specific gene on our list (Figure 9) suggests that our strategy has the potential to identify, if there is any to identify, universal PV+ basket cell-specific genes.

Use of transcriptome data to identify a marker for chandelier cells

The urge for a molecular marker for chandelier cells in the scientific community is undoubted. Standard immunohistochemistry and in situ hybridization methods do not seem to have enough sensitivity to detect FGF13 expression in cells other than chandelier cells. Consequently, FGF13 could be used to label the entire population of chandelier cells in studies that require validation of the expression pattern of given molecules.

However, a note of caution should be sounded concerning the specificity of FGF13 expression and its suitability as a marker of chandelier cells. First, at embryonic stages FGF13 is abundantly expressed in pyramidal cells. Second, at postnatal stages, we detected that a minor fraction of FGF13-expressing cells are Reelin+ interneurons (3-10 %). Third, we have analyzed FGF13 expression in the mouse PFC; the specificity of its expression in other cortical regions remains to be determined. Fourth, although FGF13 is 3.5-folds more enriched in chandelier cells as compared to other cell types, its expression cannot be considered entirely absent in other interneurons or pyramidal

cells, thus hampering the possibility of generating a FGF13-CreERT2 driver to visualize and manipulate chandelier cells. Indeed, we expect that even low FGF13 expression levels will produce Cre-mediated recombination also in other non-chandelier cells. Therefore, although FGF13 represents an immediately available tool, it does not have the ideal features needed for a chandelier cell marker.

Nevertheless, our database is a promising resource to identify putative chandelier cell markers. Eliminating some of the restrictions introduced to reach our specific goals (e.g. molecular function, significant developmental upregulation, absence of expression at P0) would yield a higher number of chandelier cell-specific genes. Plotting their specificity versus expression values (Figure D3) will prove useful to search for highly expressed specific genes and might ultimately lead to the identification of a molecular marker for chandelier cells.

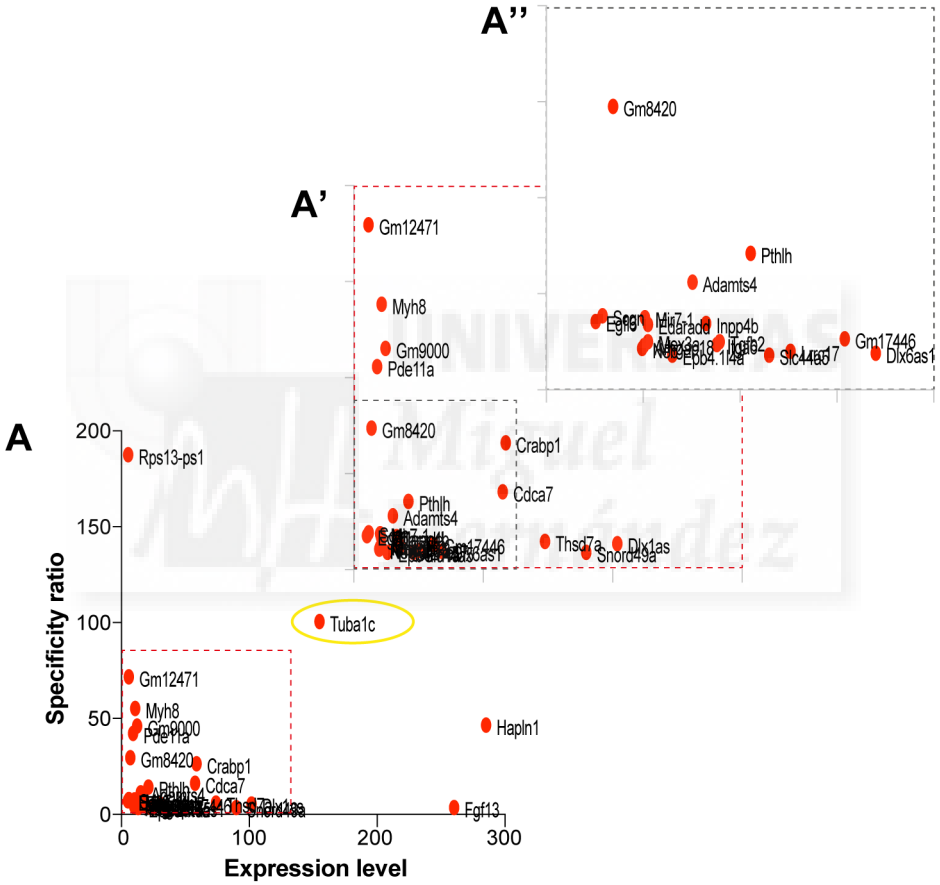

Figure D3. Plots showing the specificity versus expression values of several genes selectively expressed in chandelier cells.
(A') and (A'') are consecutive magnifications of (A) and the dotted line indicates the area of the graph that is magnified. Eliminating some of the restrictions introduced to expressly identify synaptic genes yields a high number of chandelier cell-specific genes. Some of these genes are also highly expressed and are promising candidates as cell markers or enhancers.

7. An enduring legacy: venues for future studies

Our findings reveal that cell-specific transcriptional programs operate in different interneurons across development to determine their exquisitely specific pattern of

connectivity in the mature cortex. While this information critically integrates our current knowledge on the fundamental mechanisms underlying the emergence of interneuron diversity and connectivity, the ultimate strength of our work lays in the plethora of perspectives it offers for further studies.

Rescuing homophilic interactions: genes specifically expressed in cell pairs

A large number of molecules mediating homophilic adhesion, such as cadherins or Ig-like cell adhesion molecules (Ig-CAMs), have demonstrated roles in synapse formation (Abbas, 2003; Shapiro et al., 2007; Togashi et al., 2009; Yamada and Nelson, 2007).

One of our criteria to select interneuron subtype-specific genes was a low expression in cell populations other than the one of interest, including pyramidal neurons. Consequently, our analysis excluded all molecules that mediate homophilic interactions, as the same molecule would have been expressed in pyramidal cells. To expand our knowledge on the cell-specific mechanisms regulating the assembly of different types of inhibitory synapses, it would be interesting to rescreen our gene profiles omitting pyramidal cells when calculating the specificity score. It is probable that genes ubiquitously involved in synapse formation, such as synaptic structural genes, will be anyway filtered out through the comparison with other interneuron subpopulations. Conversely, further genes necessary for forming connections between interneuron subtypes and pyramidal cells would be likely detected.

With a large amount of evidence coming from studies on visual circuit formation, homophilic cell adhesion molecules have also a remarkable role in target selection (Missaire and Hindges, 2015; Shapiro et al., 2007; Williams et al., 2010). In addition to revealing new genes mediating cell specificity, a study involving genes specifically expressed in pairs of cell types (e.g. chandelier and pyramidal cells) may also shed light on the mechanisms by which different interneurons select their target subdomain (subcellular specificity).

Finally, besides homophilic molecules, a study involving families of genes expressed in pairs of cell types may also highlight a critical role for heterophilic interactions between members of the same family that have cell-specific patterns of expression.

Interneuron subtype-specific alternative splicing

The generation of molecular diversity at the post-transcriptional level is likely to constitute an additional mechanism underlying the selective synaptic connectivity of chandelier, PV+ basket and SST+ interneurons.

In particular, an additional focus for future studies should be the investigation of specific subsets of isoforms that are developmentally regulated and enriched in individual interneuron subtypes. Alternative RNA splicing represents a fundamental mechanism that allows a single gene to generate multiple protein isoforms and thus regulates multiple aspects of nervous system development (Raj and Blencowe, 2015). Indeed, cell-specific alternative splicing of transmembrane proteins and ion channels has recently emerged as a potent post-transcriptional modulator of synaptic development and plasticity (Missaire and Hindges, 2015; Poskanzer et al., 2003; Sanes and Yamagata, 2009; Shapiro et al., 2007; Yamagata and Sanes, 2008; Yamagata et al., 2002). In this context, our transcriptome is an unparalleled resource for identifying alternatively spliced isoforms in different interneurons across developmental stages that may play a functional role in specializing their connectivity patterns.

Subtype-specific master regulators of interneuron wiring

The analysis of genes that undergo differential alternative splicing is likely to multiply the number of identified interneuron subtype-specific molecules involved in synapse formation. However, an additional related level of regulation that deserves to be studied in the future is the coordinated action of interneuron subtype-specific transcription factors and RNA-binding proteins (Marko et al., 2014).

Transcription factors act broadly to control the expression of many genes involved in the development and connectivity of specific neuron types. Likewise, regulators of alternative splicing control splicing choices in hundreds of RNA transcripts, thereby simultaneously tuning amounts and functions of large numbers of proteins. Therefore, the coordination of transcriptional and post-transcriptional events can multiply the coding power of the genome and quite possibly constitutes the ultimate level of cell identity (Deneris and Hobert, 2014; Grabowski and Black, 2001; Hobert, 2016; Kratsios et al., 2015; Lipscombe et al., 2013b; Marko et al., 2014; Miura et al., 2013). There seems little doubt that our data can provide considerable insights into how subtype-specific master regulators tailor the transcriptome to promote the maturation and integration of specific interneuron subtypes into developing cortical circuits.

Interneuron subtype-specific enhancers

The existence of genetically modified mice in which *Cre* expression is restricted to given subpopulations of GABAergic cortical neurons has galvanized the scientific community and tremendously increased our understanding of the cortical circuits. However, the use of transgenic mice to target interneurons at specific stages of development and/or in a subtype-specific manner is still limited. In some cases, targeting and manipulation of specific interneuron subtypes relies on the combinatorial use of transgenic mice expressing Cre and Flp recombinases in defined populations (Fenno et al., 2014; Madisen et al., 2015; Taniguchi et al., 2011), which is limited by the time-consuming associated breedings. In other cases, the specificity of targeting is hampered by the availability of flawless driver lines. In particular, it is still not possible to distinguish and efficiently manipulate chandelier and PV+ basket cells. These limitations are exemplified by the partial and not fully specific labeling of the chandelier cell population upon Cre-induction in the *Nkx2.1CreERT2* line or by the relatively late expression of Cre recombinase in the *PV-Cre* strain that, in addition, labels both PV+ basket and chandelier cells.

Enhancers are short DNA regions containing transcription factor binding sites that are responsible for tissue-specific transcriptional regulation of gene expression. The combination of enhancers with conditional viral strategies recently allowed to efficiently target, visualize and manipulate GABAergic interneurons (Dimidschstein et al., 2016). Our transcriptome is a promising dataset to search for interneuron subtype-specific enhancers. Plotting the specificity versus expression values (Figure D3) could guide the search for efficient enhancers that might ultimately allow fast and efficient manipulation of specific interneuron subtypes at early postnatal stages.

Outlook

Evolution has maximized the cortex's genetic material for the diversity and complexity of computational circuits to blossom exponentially. As such, a fundamental question in developmental neuroscience is how different cell types wire together with exquisite specificity to ensure the formation of sophisticated cortical circuits. Implicit in this question is both the desire to understand the grounds that support animal behavior and the urge to reveal what goes awry in neurodevelopmental disorders.

A critical step toward reaching these goals is represented by a full understanding of connectivity and circuit properties of different cell types, besides their contribution to information processing. Given the power of interneurons to shape cortical activity, a particular emphasis needs to be placed on understanding their development and diversity.

In this framework, our study supports the fascinating concept that evolution generates complexity and diversity by combining specific building blocks with superb finesse.

UNIVERSITAS Miguel Hernández

Part II

Activity-dependent gating of parvalbumin interneuron function by the perineuronal net protein Brevican[1]

Favuzzi E, Marques-Smith A, Deogracias R, Winterflood CM, Sánchez-Aguilera A, Mantoan L, Maeso P, Fernandes C, Ewers H & Rico B

Article in press in Neuron

[1] The protein studied in this second part, Brevican, does not appear in our screening, which is focused on molecules that mediate the assembly —but not maturation or plasticity— of the neural circuits. To investigate the role of molecules expressed in specific interneuron types and involved in the maturation and plasticity of neural circuits we took a candidate approach. Perineuronal net proteins —such as Brevican, Aggrecan or Neurocan— play a critical role in plasticity (Pizzorusso et al., 2002; Gogolla et al., 2009), have been shown to be developmentally upregulated between P7 and mature (P40) PV+ interneurons (Okaty et al., 2009) and, therefore, emerged as ideal candidates.

UNIVERSITAS
Miguel
Hernández

Article

Neuron

Activity-Dependent Gating of Parvalbumin Interneuron Function by the Perineuronal Net Protein Brevican

Highlights

- PNN proteins gate classes of neurons to support experience-dependent plasticity
- The PNN protein Brevican modulates cellular and synaptic plasticity in PV+ cells
- Brevican levels are dynamically regulated by network activity
- Brevican is required for normal cognitive function

Authors

Emilia Favuzzi, André Marques-Smith, Rubén Deogracias, ..., Cathy Fernandes, Helge Ewers, Beatriz Rico

Correspondence

beatriz.rico@kcl.ac.uk

In Brief

Favuzzi et al. unravel an activity-regulated cell-specific molecular program in PV+ interneurons. By simultaneously regulating the excitatory inputs and firing properties of PV+ cells, a perineuronal net protein drives PV+ interneuron wiring as well as network adaptation to experience.

UNIVERSIDAD Miguel Hernández

Favuzzi et al., 2017, Neuron *95*, 1–17
August 2, 2017 © 2017 Elsevier Inc.
http://dx.doi.org/10.1016/j.neuron.2017.06.028

CellPress

Please cite this article in press as: Favuzzi et al., Activity-Dependent Gating of Parvalbumin Interneuron Function by the Perineuronal Net Protein Brevican, Neuron (2017), http://dx.doi.org/10.1016/j.neuron.2017.06.028

Neuron
Article

Activity-Dependent Gating of Parvalbumin Interneuron Function by the Perineuronal Net Protein Brevican

Emilia Favuzzi,[1,2,3] André Marques-Smith,[1,2,8] Rubén Deogracias,[1,2,3,8] Christian M. Winterflood,[4] Alberto Sánchez-Aguilera,[1,2] Laura Mantoan,[5] Patricia Maeso,[1,2,3] Cathy Fernandes,[2,6] Helge Ewers,[5,7] and Beatriz Rico[1,2,3,9,*]

[1]Centre for Developmental Neurobiology, Institute of Psychiatry, Psychology and Neuroscience, King's College London, London, SE1 1UL, UK
[2]MRC Centre for Neurodevelopmental Disorders, King's College London, London, SE1 1UL, UK
[3]Instituto de Neurociencias, Consejo Superior de Investigaciones Científicas & Universidad Miguel Hernández, Sant Joan d'Alacant 03550, Spain
[4]Randall Division of Cell and Molecular Biophysics, King's College London, London, SE1 1UL, UK
[5]Clinical Neurosciences Department, King's College, NHS Foundation Trust, Denmark Hill, London, SE5 9RS, UK
[6]MRC Social, Genetic and Developmental Psychiatry Centre, Institute of Psychiatry, Psychology and Neuroscience, King's College London, London, SE5 8AF, UK
[7]Institute for Chemistry and Biochemistry, Free University Berlin, 14195 Berlin, Germany
[8]These authors contributed equally
[9]Lead Contact
*Correspondence: beatriz.rico@kcl.ac.uk
http://dx.doi.org/10.1016/j.neuron.2017.06.028

SUMMARY

Activity-dependent neuronal plasticity is a fundamental mechanism through which the nervous system adapts to sensory experience. Several lines of evidence suggest that parvalbumin (PV+) interneurons are essential in this process, but the molecular mechanisms underlying the influence of experience on interneuron plasticity remain poorly understood. Perineuronal nets (PNN) enwrapping PV+ cells are long-standing candidates for playing such a role, yet their precise contribution has remained elusive. We show that the PNN protein Brevican is a critical regulator of interneuron plasticity. We find that Brevican simultaneously controls cellular and synaptic forms of plasticity in PV+ cells by regulating the localization of potassium channels and AMPA receptors, respectively. By modulating Brevican levels, experience introduces precise molecular and cellular modifications in PV+ cells that are required for learning and memory. These findings uncover a molecular program through which a PNN protein facilitates appropriate behavioral responses to experience by dynamically gating PV+ interneuron function.

INTRODUCTION

Experience-dependent plasticity endows neural circuits in the cerebral cortex with the flexibility required for adapting to a continuously changing environment, thereby contributing to sensory perception, cognition, and behavior. The maintenance of precise neuronal coding during fluctuations in activity requires the balanced interaction between excitation and inhibition (Froemke, 2015; Hensch et al., 1998), a process that is dynamically sustained by the function of cortical parvalbumin-expressing (PV+) interneurons (Xue et al., 2014). Although several lines of evidence emphasize pivotal roles for PV+ cells in controlling the gain of sensory-related responses and learning (Wilson et al., 2012; Yazaki-Sugiyama et al., 2009), the molecular and cellular mechanisms by which PV+ interneurons influence these processes are poorly understood.

PV+ cells can adapt their intrinsic properties (cellular plasticity) and outputs (synaptic plasticity) in response to sensory experience. These cells display a remarkable dynamism that allows them to exist in different "cell states" or configurations, depending on the behavioral context (Bloodgood et al., 2013; Dehorter et al., 2015; Donato et al., 2013; Lagler et al., 2016). While the functional relevance of this novel form of experience-dependent plasticity during behavior is clear (Donato et al., 2013), the molecular mechanisms regulating the adaptability of PV+ interneurons to changing levels of neuronal activity are largely unknown. The lack of information about these processes is particularly striking because PV+ cell dysfunction has been linked to impaired cognition in psychiatric disorders (Cardin et al., 2009; Hu et al., 2014; Sohal et al., 2009). Hence, the identification of the relevant molecular mediators of this form of plasticity may offer novel therapeutic strategies to recover from deficits in perception, learning, and memory associated with a repertoire of diseases.

The induction and expression of neural plasticity—cellular and synaptic—relies on complex interactions between neurons and their extracellular environment. The extracellular matrix contains potential candidates for modulating neuronal responses to

activity changes. For instance, most cortical PV+ interneurons are wrapped by a specialization of the extracellular matrix known as perineuronal nets (PNNs), which includes chondroitin sulfate proteoglycans (CSPGs) (Deepa et al., 2006). The maturation of PNNs around PV+ cells coincides with the closure of the critical period, a window of enhanced plasticity across different brain regions during early postnatal life (Takesian and Hensch, 2013). It has been suggested that PNNs contribute to this process by promoting synapse stabilization and limiting synaptic rearrangements beyond the critical period for plasticity (Pizzorusso et al., 2002). Consistently, pharmacological degradation of CSPGs in the adult reactivates cortical plasticity and enhances learning (Gogolla et al., 2009). However, in spite of the unequivocal role of PNNs in the regulation of cortical plasticity, the precise mechanism through which PNNs mediate this process remains a mystery.

Brevican (BCAN) is one of the most abundant CSPGs in the brain and a fundamental component of the PNNs (Frischknecht et al., 2014). It is expressed in several brain regions from early postnatal development, mostly inside glial cells and around neurons (Seidenbecher et al., 2002). Though its function is currently unclear, three lines of evidence suggest that BCAN may play a key role regulating experience-dependent plasticity in cortical circuits: (1) BCAN is a component of PNNs surrounding PV+ cells (Valenzuela et al., 2014); (2) BCAN is present in cell membranes and synaptosomal fractions (Seidenbecher et al., 2002); and (3) BCAN is required for long-term potentiation (LTP) in the hippocampus (Brakebusch et al., 2002).

Here we identify the molecular mechanism through which the PNN protein BCAN influences cellular and synaptic plasticity in response to changes in the environment. We demonstrate that BCAN shapes the intrinsic properties of PV+ interneurons and sculpts their synaptic inputs by controlling the localization of potassium channels and the levels of synaptic AMPA receptors, respectively. Moreover, in contrast to the long-standing view that PNN proteins are static and function just as a break for synaptic plasticity (Nabel and Morishita, 2013; Takesian and Hensch, 2013), we show that BCAN is dynamically regulated by activity and that its function is fundamentally required for spatial working and short-term memories. These results therefore reveal that BCAN plays a key role in gating the function of PV+ interneurons, thereby enabling coordinated circuit responses to experience. Our findings clarify the molecular and cellular events underlying the function of PNN proteins in neuronal plasticity.

RESULTS

Brevican Is Expressed in PV+ Interneurons and Has a Synaptic Localization

Brevican protein (BCAN) has been found in several brain regions and its expression is described as a diffuse, dense net-like structure around mostly PV+ cells (Valenzuela et al., 2014). However, the precise source of BCAN remains unclear. We found that in the hippocampus, Brevican transcripts (*Bcan*) are restricted to glial and PV+ cells (Figures 1A–1D and S1A–S1D). BCAN has different splicing isoforms encoding secreted (BCAN1) and GPI-anchored (BCAN2) proteins (Seidenbecher et al., 1995). We observed that whereas both isoforms were co-expressed in glia and PV+ interneurons, the latter population of cells showed a bias toward *Bcan2* expression (Figures 1D–1G). The percentage of PV+ cells that expressed BCAN increased substantially in the second postnatal week, when the maximum fraction of BCAN+/PV+ cells was found (Figures 1H, 1I, and S1E). BCAN kept accumulating around PV+ cells after the third postnatal week (Figure S1F). Interestingly, we observed that BCAN+/PV+ cells exhibit higher PV levels than BCAN−/PV+ cells (Figures 1J, 1K, and S2A). Of note, although Brevican is also expressed throughout the neocortex (Figures S1G and S1H), no trace of BCAN was detected in chandelier cells (0 out of 9 cells, Figure S1B).

It has been shown that PNNs ensheath synaptic contacts, suggesting a possible role during synapse formation (Hockfield and McKay, 1983). We observed that the frequency and intensity of BCAN staining in PV+ cells increased concurrently with the development of synaptic inputs onto these cells (Figures S1E, S1F, and S1I). In the hippocampus, the soma of PV+ basket cells receives both excitatory inputs from pyramidal cells and inhibitory inputs from interneurons. Among these synapses, we found that BCAN was particularly enriched in excitatory terminals (VGlut1+) (Figures 1L–1N). In contrast, only a small percentage of inhibitory puncta (Syt2+ PV+ or GAD65+ PV−) contacting PV+ cells were BCAN+ (Figures S1J–S1O). To analyze the subcellular location of BCAN with nanoscale resolution in hippocampal sections, we developed a novel method for multi-color single-molecule localization-based super-resolution microscopy (Betzig et al., 2006), termed SD-dSTORM (spectral-demixing stochastic optical reconstruction microscopy) (Winterflood et al., 2015) (Figures 1O–1R and S1P–S1S). We first identified somatic synapses apposed to PV+ cells by immunolabeling the synaptic proteins Bassoon (pre-synapse) and Homer1 (post-synapse). As described before (Dani et al., 2010), we observed typical focal planes with Bassoon and Homer1 flanking the synaptic cleft (Figure 1P). Using Bassoon as a reference, we focused on the axial distribution of BCAN and found that it was located both pre- and postsynaptically (Figures 1O–1R). Next, we observed that the average radial position of BCAN relative to the center of the synaptic complex is predominantly peripheral (Figures 1P and 1R). Altogether, our findings reveal that BCAN—mostly BCAN2—is expressed in a large fraction of PV+ cells and that it flanks the excitatory synapses received by these cells.

Brevican Identifies a Subpopulation of PV+ Basket Cells

PV+ basket cells comprise a highly diverse population of interneurons that integrate in multiple microcircuits and exhibit diverse firing patterns and molecular programs (Dehorter et al., 2015). In addition to the different PV levels exhibited by BCAN+ and BCAN− PV+ cells (Figures 1J, 1K, and S2A), using pre- (VGlut1) and postsynaptic (PSD95) markers we found that BCAN+/PV+ cells receive a higher number of excitatory inputs than BCAN−/PV+ cells (Figures 2A–2C, S2B, and S2C).

We then enquired whether BCAN+ and BCAN− PV cells could be distinguished on the basis of their electrophysiological properties (Figures 2D–2M). BCAN+/PV+ cells are less excitable, showing lower input resistance than BCAN−/PV+

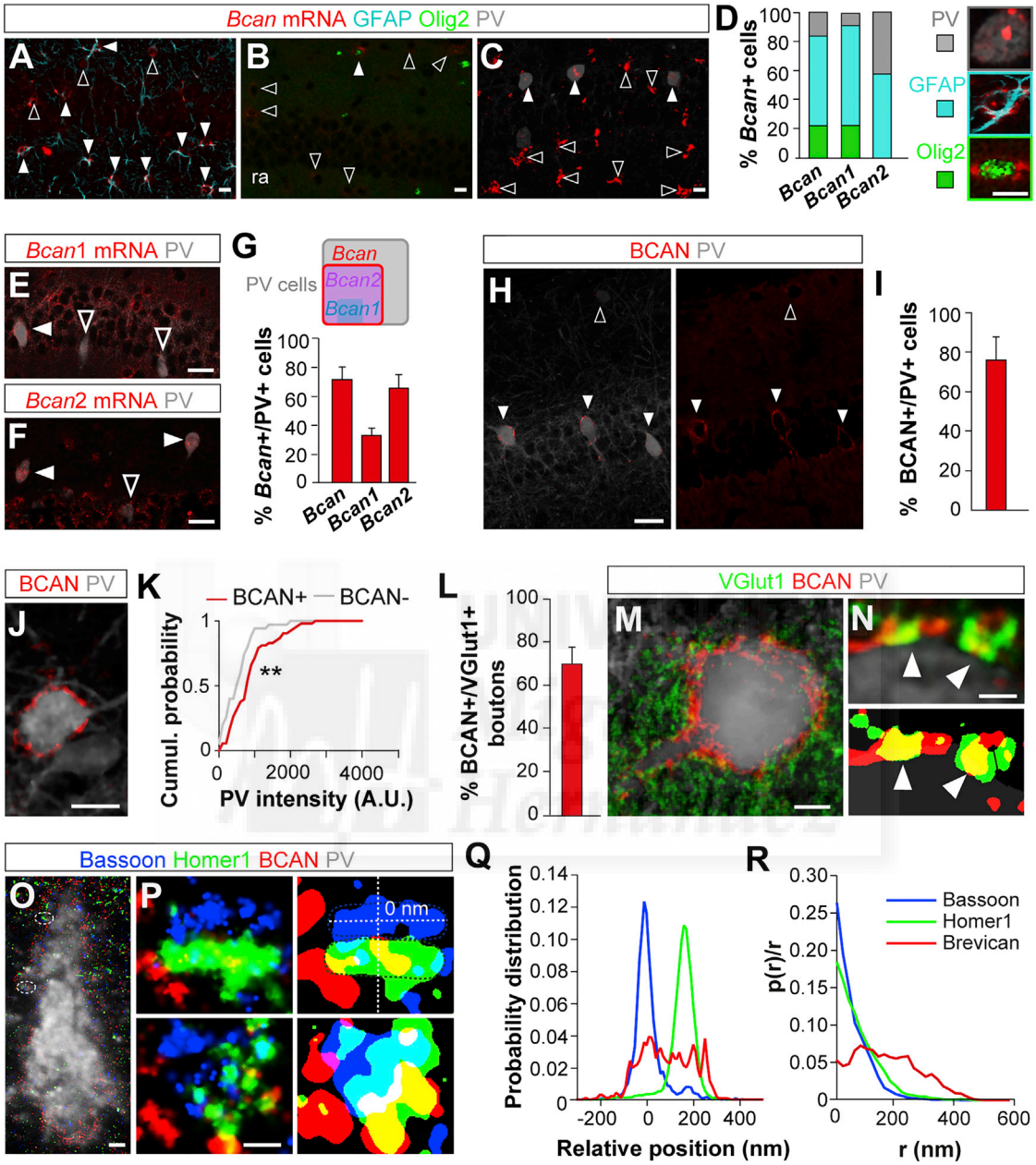

Figure 1. Characterization of BCAN Expression in the Hippocampus at P30

(A–D) Identification of cell types expressing *Bcan* mRNA. (A–C) PV+ cells, astrocytes, and oligodendrocytes among *Bcan*+ cells and percentage (D). *Bcan* common probe for both *Bcan* isoforms, *Bcan1* and *Bcan2* for secreted and membrane-bound isoforms, respectively (n = 3 mice).

(E–G) PV+ cells expressing either (*Bcan1*/*Bcan2*) or both *Bcan* isoforms (*Bcan*) (E and F) and its percentage (G). The diagram in (G) interprets the data in the bar graph (n = 3 mice).

(H and I) PV+ cells wrapped by BCAN protein (H) and percentage (I) (n = 3 mice).

(J) Image of high-PV BCAN+ and low-PV BCAN− cells.

(K) Cumulative probability plots in BCAN+ (n = 42 cells, 4 mice) and BCAN-PV+ cells (n = 29 cells, 4 mice). Kolmogorov-Smirnov test.

(L–N) VGlut1+ somatic inputs on PV+BCAN+ cells (M and N) and percentage (L) (n = 6 mice).

(O) BCAN+ PV+ cell (conventional wide-field) overlaid with three-color STORM image of BCAN, Bassoon, and Homer1.

(P) High-magnification images and thresholded masks of (O) showing single synapses.

(Q) Distribution of BCAN along the *trans*-synaptic axis. Analysis of 37 side-view synapses from 5 experiments.

(R) Radial distribution of BCAN at the synapse. P(r)/r: probability density of localization at the radial position r. Analysis of 52 face-view synapses from 6 experiments.

Full and open arrowheads show colocalization and no colocalization, respectively. Data are presented as mean. In this and all subsequent figures, error bars represent SEM. Scale bars represent 10 μm (A–D), 20 μm (E, F, and H), 5 μm (J and M), 1 μm (N), 2 μm (O), and 250 nm (P).

See also Figure S1.

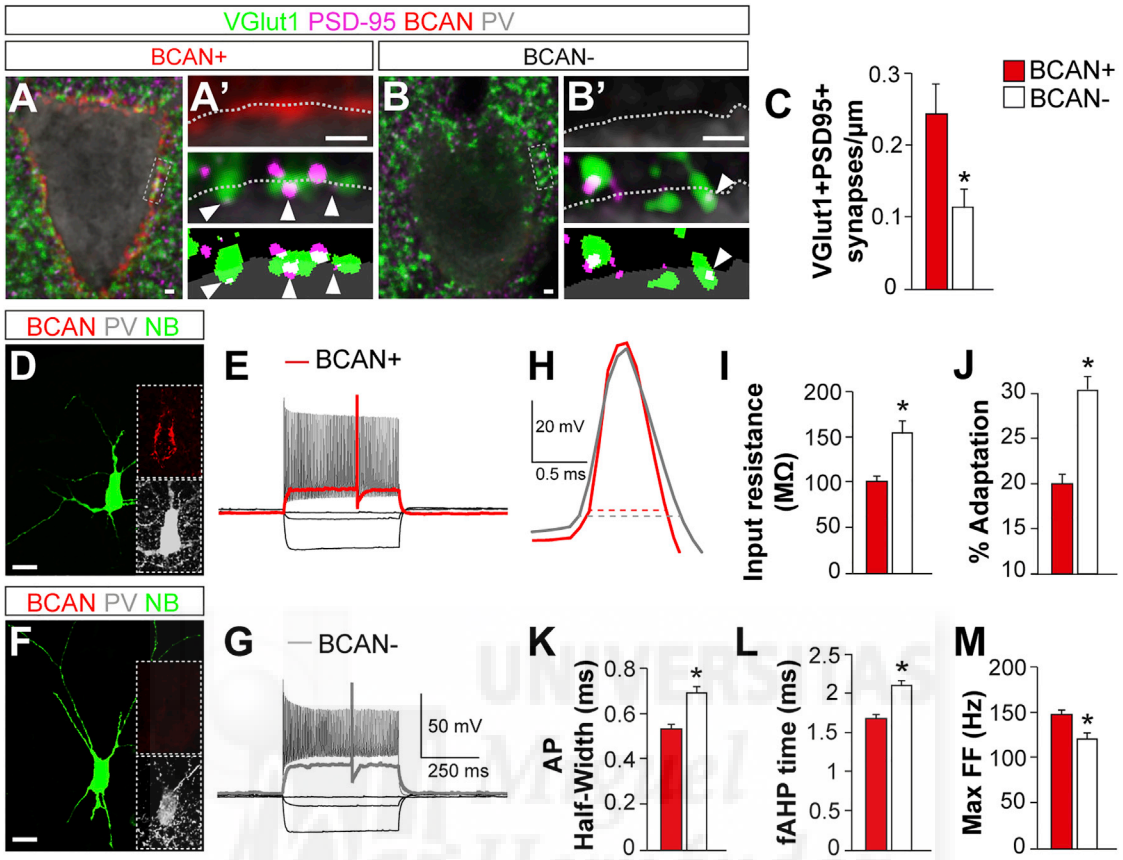

Figure 2. BCAN Expression Segregates Subpopulations of PV+ Cells

(A and B) High magnifications and thresholded masks (A′ and B′) showing VGlut1+PSD95+ somatic synapses on the soma of BCAN+ (A) and BCAN− (B) PV+ cells (arrowheads). In (A′), (B′), and all subsequent similar images, the opacity of the soma (dotted line) has been reduced to better visualize the synapses.

(C) Density of VGlut1+PSD95+ somatic synapses on BCAN+ and BCAN− PV cells (n = 7 mice).

(D–G) Images and firing traces for BCAN+ (D and E) and BCAN− (F and G) PV+ cells.

(H) Inset from (E) and (G). NB, Neurobiotin.

(I–M) Intrinsic properties of BCAN+ (n = 22 cells, 9 mice) and BCAN− (n = 13 cells, 9 mice) PV+ cells. AP, action potential; fAHP, fast after hyperpolarization; Max FF, maximum firing frequency. Student's t test except for (I) and (K) where Mann-Whitney test was used. In this and subsequent figures, *p < 0.05, **p < 0.01, ***p < 0.001, n.s., p > 0.05. Scale bars represent 1 µm (A and B) and 5 µm (D and F).

See also Figure S2 and Table S1.

cells (Figures 2I and Table S1). However, BCAN+/PV+ cells also seem better tuned to operate at higher spiking frequencies than their counterparts, as they display higher maximum firing frequency, less spike frequency adaptation, narrower action potential half-width, and an earlier fast after-hyperpolarization (fAHP) time than BCAN−/PV+ cells (Figures 2D–2M). Our findings reveal that PV+ cells expressing BCAN have a distinct profile: they receive more glutamatergic synapses, are less excitable, and have faster responses than PV+ cells lacking BCAN.

Brevican Controls Synapses and Intrinsic Properties of PV+ Basket Cells

BCAN locates at the flanks of excitatory synapses and its peak of expression coincides with the maturation of these inputs to PV+ cells (Figure S1I). To test a potential function of BCAN in the wiring of PV+ cells, we analyzed the impact of BCAN deletion on the synaptic inputs these interneurons receive. Whereas the density of excitatory synapses impinging on the soma of PV+ cells and the levels of PV expression were comparable in control and *Bcan* mutant mice at early stages of synaptic development (postnatal day 15 [P15]), PV+ cells received less excitatory inputs in *Bcan* knockout mice at P30 (Figures 3A–3D, S3A, and S3B). Consistently, *Bcan* mutants exhibited a lower frequency—but not amplitude—of miniature excitatory postsynaptic currents (mEPSCs), which also had a slower decay (Figures 3E–3I). These findings indicated that, although BCAN is dispensable for the initial contact of excitatory boutons with PV cells, it is critical for their maturation. Of note, we detected a reduction in PV protein levels at P30 but not at P15, while the total density of PV+ cells remained unaltered (Figures 3J–3M and S3C). We observed a similar reduction in the density of excitatory puncta in adult mice (P60; Figures S3D–S3F), which rules out a potential delay in synapse formation.

To test whether BCAN function is also required for the formation of perisomatic inhibitory synapses in PV+ cells, we

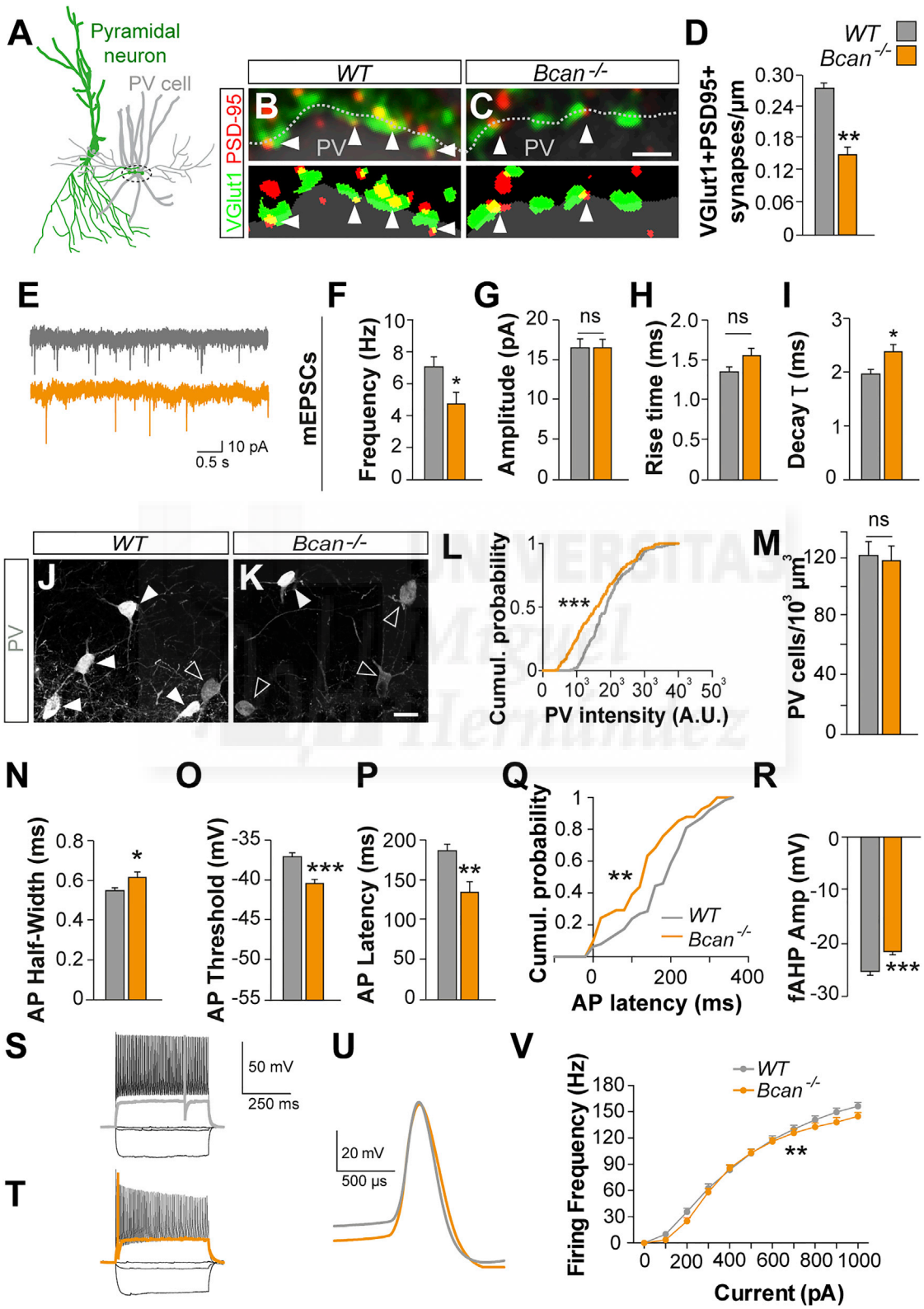

(legend on next page)

examined inputs from other PV+ and Cholecystokinin-positive (CCK+) basket cells (Karson et al., 2009). We observed that the density and size of Syt2+ (a presynaptic marker of PV+ cells) terminals contacting the soma of PV+ cells as well as the density of Syt2+/Gephyrin+ synapses were similar between both genotypes (Figures S3G–S3K). To analyze the contribution of CCK+ interneurons, we combined the GAD65 synaptic protein with the presynaptic receptor CB1, highly enriched in CCK+ axon terminals (Katona et al., 1999) (Figures S3G and S3L–S3N). We found no significant differences in the density of GAD65+/CB1+ synapses between control and *Bcan* mutant mice (Figures S3L–S3N). Consistent with these results, we found no differences in miniature inhibitory postsynaptic currents (mIPSCs) (Figures S3O–S3S). In agreement with its highly specific location at excitatory synapses, these results revealed that BCAN regulates the maturation of excitatory—but not inhibitory—inputs onto PV+ cells.

Since BCAN+/PV+ cells exhibit different electrophysiological properties than BCAN−/PV+ interneurons, we examined whether loss of BCAN would alter the intrinsic properties of BCAN+/PV+ cells. We found that PV+ interneurons in *Bcan* mutant mice exhibited broader action potentials with smaller fAHP phase (Figures 3N–3V and Table S2). Consistently, the input-output curve was below that of $Bcan^{+/+}$ cells (Figures 3V). Moreover, we found that deletion of BCAN enhanced the intrinsic excitability of PV+ cells by decreasing the action potential threshold and latency to first action potential (Figures 3O–3Q and Table S2). To examine how the changes in the excitatory drive and excitability of *Bcan* mutant PV+ interneurons ultimately influenced the flow of information from pyramidal to PV+ cells, we recorded spontaneous excitatory postsynaptic currents (sEPSCs) in PV+ cells (Figures S3T–S3X). We observed a decreased frequency of sEPSCs and slower decay kinetics in *Bcan* mutant mice (Figures S3U and S3X). Our findings therefore demonstrate that BCAN is necessary for the maturation of excitatory inputs onto PV+ interneurons, as well as for the expression of their normative intrinsic properties.

A Cell-Autonomous Function for Brevican in Parvalbumin Cells

BCAN is found around the soma of PV+ cells, but its source is unclear, as is its precise cellular contribution to the *Bcan* mutant phenotype. To investigate this, we first explored whether cell-type-specific knockdown of BCAN in PV+ interneurons was sufficient to mimic the synaptic and cellular phenotype found in *Bcan* mutant mice. We engineered Cre-dependent conditional constructs expressing a short-hairpin RNA (shRNA) targeting a common region for both *Bcan1* and *Bcan2* (*shBcan*, Figure S4A). We packed this construct in adeno-associated viral vectors (AAV) in which recombination was reported by mCherry (Figures 4A–4C), and the functionality of these constructs was assayed *in vitro* (Figures S4A–S4F). We co-injected low titer Cre-dependent *shBcan* and YFP-expressing viruses into the hippocampal CA1 region of *PV-Cre* mice at P12 and analyzed the density of synapses in sparsely labeled PV+ cells at P30 (Figures 4A–4G). Expression of *shBcan* led to a loss of BCAN in PV+ cells, causing a decrease in the number of excitatory—but not inhibitory—afferents onto knockdown (mCherry+) compared to control (YFP+) PV+ cells (Figures 4C–4G, S4G, and S4H) and a shift toward lower PV levels (Figure 4H).

We next used a similar approach to explore how PV-specific loss of BCAN affects the intrinsic properties of PV+ cells. We found that PV+ cells that expressed *shBcan* mimicked *Bcan* mutants for some variables but with a stronger trend when compared to $Bcan^{+/+}$ mice (Figures 4I–4U and Table S3). Altogether, these experiments demonstrated that cell-autonomous expression of BCAN in PV+ interneurons controls their excitatory inputs and some of their intrinsic properties.

Isoform-Specific Roles for Brevican

To explore which BCAN isoform is required for the maturation of excitatory synapses, we attempted to rescue cell-autonomously the synaptic deficit observed in *Bcan* mutant interneurons by overexpressing Cre-dependent HA-tagged *Bcan1* or *Bcan2* in hippocampal PV+ cells (Figures 5A–5C and S4B). HA reported BCAN1 and BCAN2 expression accurately (Figure S5A). Remarkably, whereas BCAN1 resembled other classical PNN markers, BCAN2 expression was dotted, similar to that commonly observed for synaptic markers (Figures 5D, 5I, and S5A). We observed that while *Bcan1* expression does not rescue the synaptic phenotype found in *Bcan* mutant PV+ cells, *Bcan2* does (Figures 5E–5H, 5J–5M, and S5B–S5G). The synaptic function of BCAN2 required the GPI-anchor, since overexpression of a *Bcan2* that lacks the GPI-domain led to an even more pronounced synaptic phenotype compared to *Bcan*−/− mice (Figures S5D–S5F). Interestingly, both *Bcan1* and *Bcan2* were able to rescue PV levels (Figures 5H and 5M), suggesting that it could change both as a result of modifications in the excitatory drive of PV+ cells as well as by independent cellular mechanisms. Altogether, these results reveal an isoform-specific function for *Bcan2* in the maturation of the excitatory synapses on PV+ interneurons.

Figure 3. Deletion of BCAN Changes Inputs and Properties of PV+ Cells

(A–D) Schematic (A), images (B and C, upper panels), thresholded mask (B and C, lower panels), and density (D) of somatic VGlut1+PSD95+ synapses (arrowheads) on PV+ cells (B, n = 6 WT, C, 5 $Bcan^{-/-}$).

(E–I) Traces (E), frequency (F), amplitude (G), rise (H), and decay time (I) of mEPSCs in WT (n = 12 cells, 4 mice) and $Bcan^{-/-}$ PV+ cells (n = 16 cells, 3 mice).

(J–L) Images (J and K) and cumulative probability plots (L) of PV fluorescence intensity in WT (n = 147 cells, 4 mice) and $Bcan^{-/-}$ (n = 164 cells, 4 mice).

(M) Density of PV+ cells in the CA1 region of the hippocampus in WT (n = 6) and $Bcan^{-/-}$ (n = 4) mice.

(N–U) Intrinsic properties (N–P and R), cumulative probability plot for the spike latency (Q) comparing WT (n = 63 cells, 10 mice) and $Bcan^{-/-}$ (n = 41 cells, 6 mice) PV+ cells, firing traces for WT (S) and $Bcan^{-/-}$ (T) PV+ cells. (U) Inset from (S) and (T).

(V) I/O curves showing the spike frequency of WT (n = 63 cells, 10 mice) and $Bcan^{-/-}$ (n = 41 cells, 6 mice) PV+ cells in response to current injections.

Student's t test (D, F, G, I, O, and R), Mann-Whitney test (H, M, N, and P), Kolmogorov-Smirnov test (L and Q), and two-way ANOVA (V). Scale bars represent 1 μm (B and C) and 20 μm (J and K).

See also Figure S3 and Table S1.

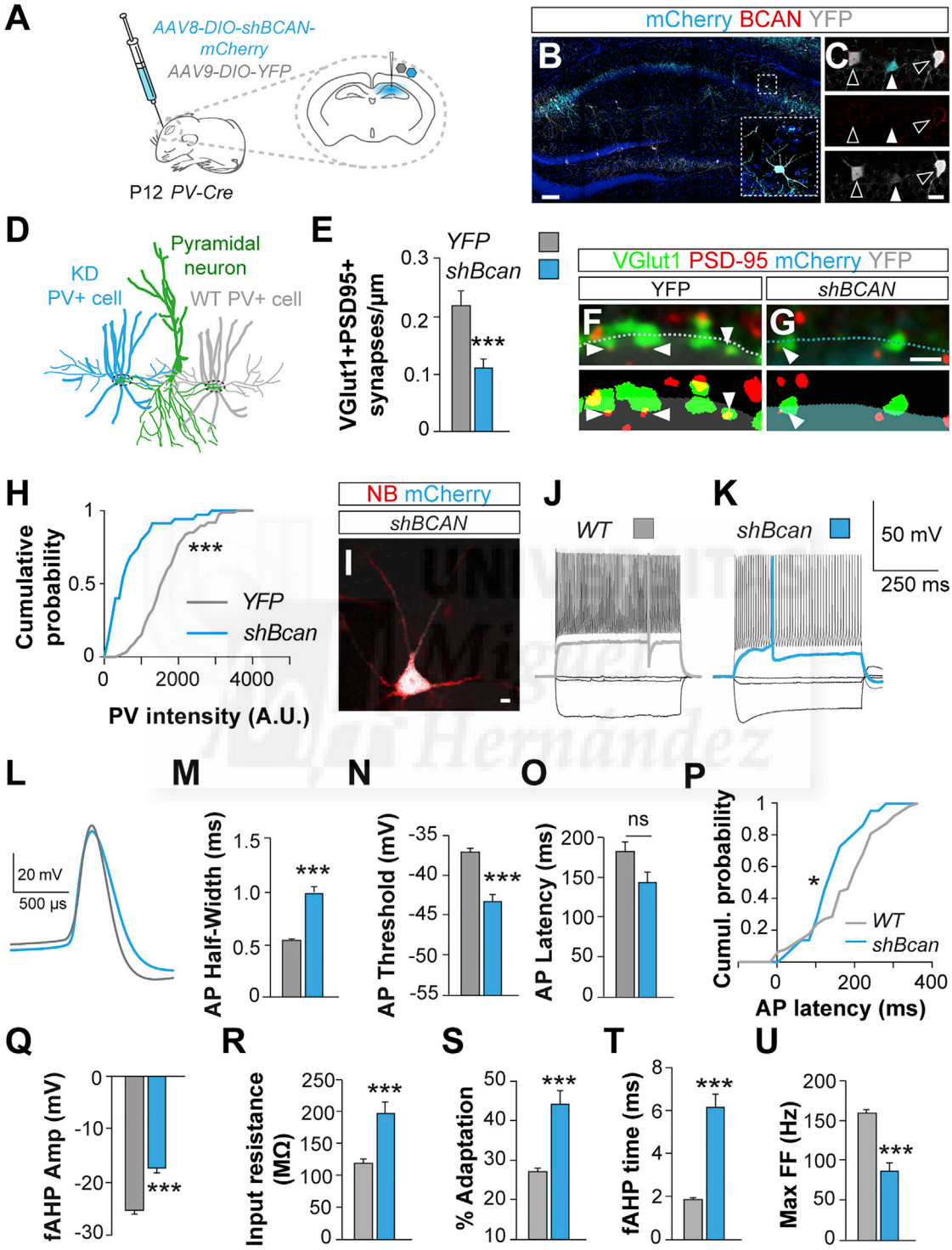

Figure 4. Cell-Autonomous Role of BCAN in PV+ Cells

(A) Schematic of AAVs injections in the hippocampus of P12 *PV-Cre* mice.

(B and C) mCherry and YFP low (B) and high (C) magnification from sparse infection and reduction of endogenous BCAN in *shBcan*-expressing PV+ mCherry+ (full arrowheads) but not mCherry− cells (open arrowheads).

(D) Schematic of BCAN knockdown (KD) PV+ cells in a WT background.

(E–G) Density (E), images (F and G, upper panel), and thresholded masks (F and G, lower panel) of VGlut1+PSD95+ somatic synapses on WT (F, n = 22 cells, 3 mice) and *shBcan* (G, n = 23 cells, 3 mice) PV+ cells.

(legend continued on next page)

Interestingly, we observed a milder reduction of excitatory inputs contacting *Bcan* knockdown compared to *Bcan* knockout PV+ cells (Figures S4G and S5H). Consistently, expression of *Bcan2* in PV+ cells only partially rescued the density of VGlut1+ puncta (Figure S5C). As BCAN is also expressed in glial cells (Figure 1) and astrocytes contribute to synapse development (Clarke and Barres, 2013), we attempted to rescue the *Bcan* mutant PV+ cells wiring phenotype by driving *Bcan1* or *Bcan2* expression in astrocytes (Figures 5N–5X). BCAN1 was secreted from astrocytes and concentrated around both a small number of PV+ cells (Figures 5Q, 5R, and S5I) and few pyramidal cells (Figure S5J), as described before (Carstens et al., 2016). BCAN2 was instead cleaved and released from astrocytes in the tissue without displaying any cell-type bias (Figures 5S and 5T). When expressed in astrocytes, *Bcan2*—but not *Bcan1*—rescued the synaptic phenotype found in *Bcan* mutant PV+ cells (Figures 5U–5X and S5M). However, neither *Bcan1* nor *Bcan2* expression in astrocytes led to a rescue of PV levels (Figure S5L). Altogether, our results suggest that *Bcan2* expression in PV+ cells regulates the maturation of their excitatory inputs, along with a potential contribution from astrocytes.

The marked alteration in the intrinsic properties of PV+ cells upon *Bcan* knockdown suggested a cell-autonomous role for BCAN in the regulation of the firing properties of PV+ cells. To determine whether this was due to the lack of a specific *Bcan* isoform, we asked whether expression of either *Bcan1* or *Bcan2* alone was sufficient to rescue the phenotype found in *Bcan* mutant mice (Figures 5A–5C). Our results revealed that none of the two isoforms was by itself sufficient to restore normative intrinsic properties in *Bcan* mutant mice (Figures S5M–S5W and Table S4), suggesting that either both isoforms may cooperatively regulate the firing behavior of PV+ interneurons or a more complex scenario may be taking place.

Brevican Controls AMPA Receptors and Voltage-Gated Potassium Channels in PV+ Cells

Our results demonstrate that BCAN—more specifically, BCAN2—is necessary for the maturation (Figure 3D) but not initial assembly (Figure S3B) of excitatory synapses onto PV+ cells. These findings prompted us to investigate how BCAN may regulate the differentiation of excitatory synapses.

During postnatal development, neurons edit the composition of their glutamate receptors (Hu et al., 2014). This process is particularly important in PV+ interneurons, where transmission is primarily mediated by GluA2-lacking, calcium-permeable AMPA receptors (AMPARs) with GluA1 and GluA4 subunits (Fuchs et al., 2007; Matta et al., 2013). The slower decay of mEPSCs and sEPSCs found in *Bcan* mutant mice suggested an altered subunit composition of AMPARs (Figures 3I and S3X). To investigate whether BCAN may contribute to the regulation of AMPARs in PV+ cells, we performed co-immunoprecipitation (coIP) experiments in hippocampal lysates. We found that BCAN protein co-immunoprecipitated with different AMPAR subunits but not with NMDA or metabotropic glutamate receptors (Figures 6A and S6A). We next examined whether BCAN is required for the expression of GluA1 and GluA4-containing AMPARs at synapses. Analysis of hippocampal synaptosome fractions obtained from *Bcan* mutant mice revealed a reduction of synaptic GluA1 compared to controls (Figures 6B, 6C, and S6E). This reduction was accompanied by an increase of GluA1 in the non-synaptic plasma membrane fraction, while no differences were observed in total or cytoplasmic GluA1 protein (Figures 6B, 6C, S6D, and S6E). In contrast, levels of GluA4 were unchanged (Figures S6B and S6C). Interestingly, although *Bcan2*—but not *Bcan1*—is responsible for the synaptic phenotype found in *Bcan* mutants (Figures 5G and 5L), both BCAN1 and BCAN2 co-immunoprecipitated with GluA1 *in vitro* (Figure S6I). Altogether, these results suggested that BCAN may be involved in the trafficking of GluA1 AMPAR subunits from extrasynaptic to synaptic sites.

Since GluA1 subunits are expressed in both pyramidal cells and interneurons, we sought to investigate the neuronal population responsible for the changes in GluA1 subcellular location. Using three-color STORM microscopy in brain sections of wild-type mice, we measured the radial position of BCAN and GluA1 in relation to the synaptic marker Bassoon contacting PV+ cells. We observed that BCAN and GluA1 partially overlap in the outer domain of Bassoon (Figures 6D and 6E). We next analyzed the density of GluA1+ synaptic clusters (Figures 6F–6M and S6F) and found a 50% reduction in *Bcan* mutant and *Bcan* knockdown PV+ cells (Figures 6H and 6L). Cell-type-specific loss of GluA1 is in itself sufficient to decrease the excitatory afferents onto PV+ cells, as the density of excitatory synapses was reduced in *PV-Cre;GluA1$^{F/F}$* mice compared to controls (Figures 6N–6P and S6G). This suggests that the PV-specific loss of GluA1 consequent to disruption of BCAN expression would suffice to produce a deficit in excitatory synaptic inputs. Consistent with the synaptic function of *Bcan2*, only this isoform's expression restored the density of synaptic GluA1+ clusters in *Bcan* mutant PV+ cells (Figures 6I, 6J, and 6M). Our results thus demonstrate that BCAN regulates excitatory inputs contacting PV+ interneurons at least in part by controlling the normal localization and levels of GluA1 AMPAR subunits.

BCAN also regulates the electrophysiological properties of PV+ cells. Some such properties are regulated by fast-activating voltage-gated K^+ conductances mediated by K_v1 and K_v3 potassium channels (Hu et al., 2014). We focused our analysis in the $K_v1.1$ and $K_v3.1$ subunits, which are enriched in PV+ cells and are key for the characteristics of their action potential waveform (Du et al., 1996; Goldberg et al., 2008). We found that

(H) Cumulative probability plots (WT, n = 87 cells, 3 mice and *shBcan* PV+ cells, n = 35 cells, 3 mice).

(I–L) Images and firing traces for WT (J, same as in Figure 3S) and BCAN KD (I and K) PV+ cells. (L) Inset from (J) and (K). NB, Neurobiotin.

(M–U) Intrinsic properties: AP Half-Width (M), AP Threshold (N), AP Latency (O), cumulative probability plot (P), fAHP Amp (Q), input resistance (R), percentage of Adaptation (S), fAHP time (T), and maximum firing frequency (U) for spike latency comparing WT (n = 63 cells, 11 mice) and *shBcan* KD (n = 22 cells, 4 mice) PV+ cells.

Student's t test (E, N, Q, S, and U), Mann-Whitney test (M, O, R, and T), and Kolmogorov-Smirnov test (H and P). Scale bars represent 100 μm (B), 20 μm (C), 1 μm (F and G), and 10 μm (I). See also Figure S4.

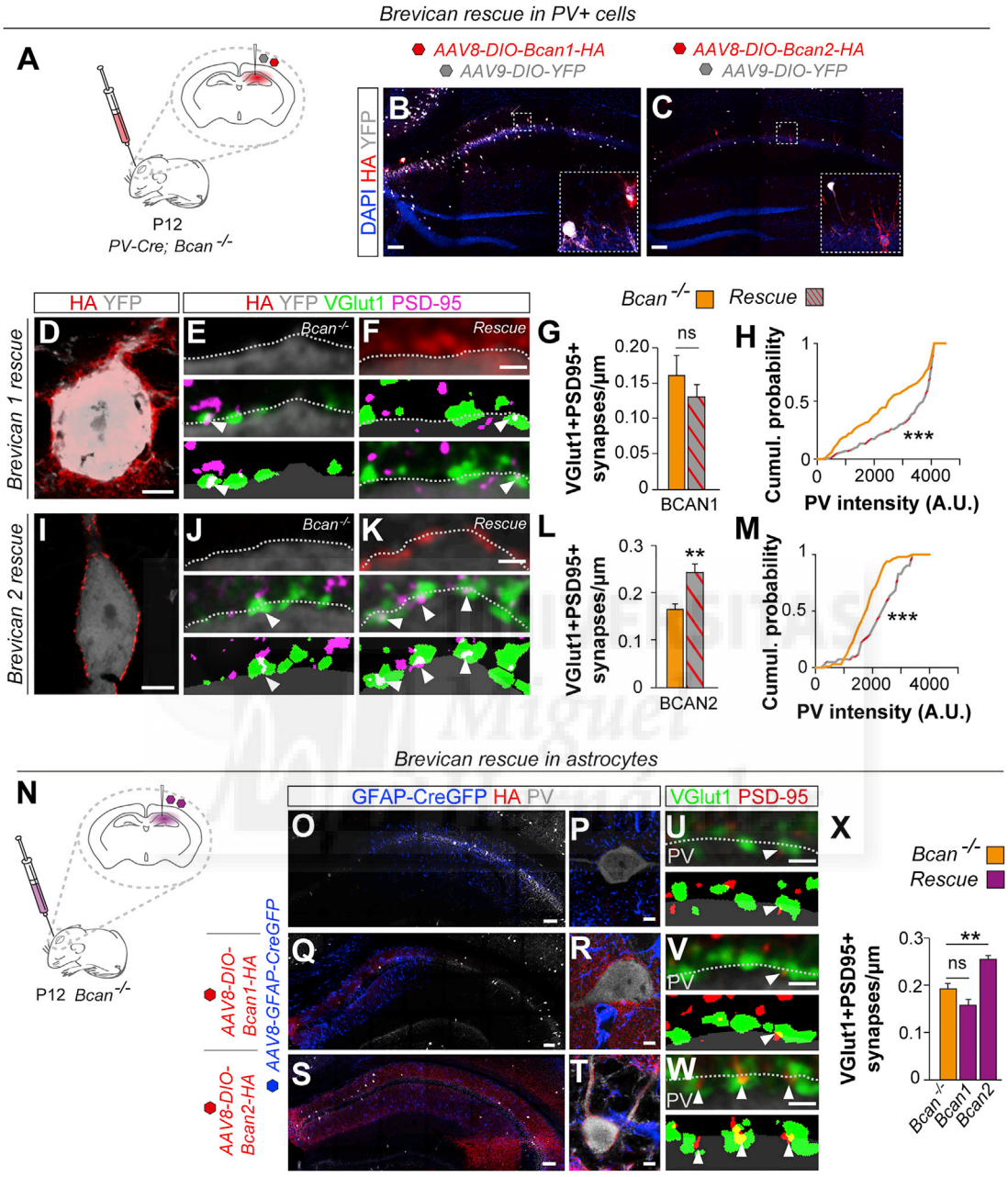

Figure 5. Specific Roles for *Bcan* Isoforms in PV+ Cells and Astrocytes

(A–C) Schematic of AAVs injections (A) and images showing YFP and BCAN1-HA (B) or BCAN2-HA (C).

(D) BCAN1-HA overexpressing cell.

(E–G) Images (E and F) and density (G) of VGlut1+PSD95+ somatic synapses onto *Bcan*$^{-/-}$ (n = 40 cells, 5 mice) and BCAN1-rescued (n = 40 cells, 5 mice) PV+ cells.

(H) Cumulative probability plots (*Bcan*$^{-/-}$, n = 155 cells, 4 mice and BCAN1 rescued, n = 127 cells, 4 mice).

(I) BCAN2-HA overexpressing cell.

(J–L) Images (J and K) and density (L) of VGlut1+PSD95+ somatic synapses on *Bcan*$^{-/-}$ (n = 50 cells, 4 mice) and BCAN2-rescued (n = 34 cells, 4 mice) PV+ cells.

(M) Cumulative probability plots (*Bcan*$^{-/-}$, n = 98 cells, 3 mice and BCAN2 rescued, n = 41 cells, 3 mice).

(N–T) Schematic of AAVs injections (N) and images (O–T) showing CreGFP expression in astrocytes and BCAN1-HA (Q) or BCAN2-HA (S) in the surrounding tissue. (P, R, and T) High-magnification images showing only CreGFP or BCAN1 or BCAN2 accumulation around PV+ cells.

(U–X) Images (U, V, and W) and density (X) of VGlut1+PSD95+ somatic synapses on PV+ cells in *Bcan*$^{-/-}$ mice infected with the control virus only (U, GFAP-CreGFP, n = 6 mice) or together with BCAN1 (V, n = 4 mice) or BCAN2 (W, n = 6 mice) virus.

Mann-Whitney test (G and L), Kolmogorov-Smirnov test (H and M), one-way ANOVA (X). Scale bars represent 100 µm (B, C, O, Q, and S), 5 µm (D, I, P, R, and T), and 1 µm (E, F, J, K, U, V, and W).

See also Figure S5.

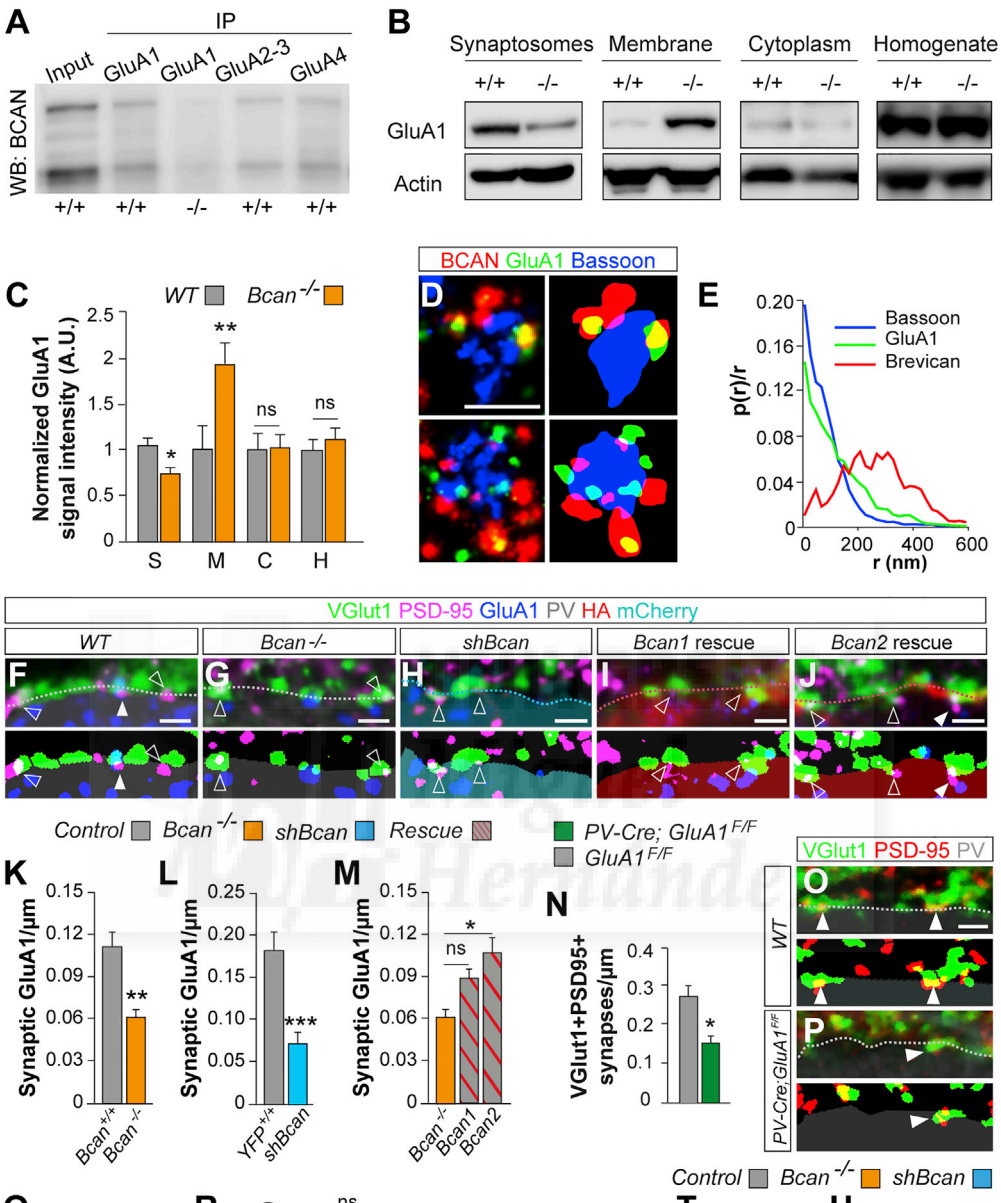

(legend on next page)

both BCAN1 and BCAN2 form protein complexes with K_v1.1 and K_v3.1b (Figures S6H and S6I). Consistently, we observed a prominent decrease in the density of K_v3.1b membrane clusters—but not in the total K_v3.1b protein—in *Bcan*-deficient PV+ cells (Figures 6Q–6U), which may support deficits in spike waveform, duration, and frequency found in the mutants (Figures 3N, 3U, and 3V). We also found a decrease in the density of K_v1.1 membrane clusters in PV+ cells—as well as in K_v1.1 total protein—in *Bcan* mutant mice (Figures 6V–6Y), a finding that is consistent with the reduction in action potential threshold and latency observed in the mutants (Figures 3O–3Q). BCAN knockdown in PV+ interneurons also reduced the density of K_v3.1b but not K_v1.1 clusters in these cells (Figures 6S, 6U, 6X, and 6Z). Altogether, these results suggest that cell-autonomous expression of BCAN in PV+ cells controls fundamental properties of the action potential by regulating the composition of specific channels, including K_v3.1b-containing potassium channels.

Brevican Expression Is Dynamically Regulated by Activity

AMPA glutamate receptors, particularly those containing GluA1 subunits, are recruited to the synapse in an activity-dependent manner (Henley and Wilkinson, 2016) but the molecular mechanisms by which they are trafficked to and held there are not fully understood (Turrigiano, 2012). Since BCAN controls the expression of GluA1 at the synapse, we hypothesized that it might coordinate GluA1 subunit clustering by dynamically responding to changes in activity. To test this idea, we analyzed the expression of BCAN in three different experimental paradigms of altered network activity. First, we used pharmacology in hippocampal cultures: increasing activity with the $GABA_A$ receptor antagonist Gabazine led to a 47% decrease in BCAN levels (Figures 7A and 7B). Reducing activity via L-type calcium channel blockade (Nifedipine) resulted in an increase in BCAN (Figures 7A and 7B).

Second, we obtained tissue from surgical resections of patients with temporal lobe seizures, a pathological model of excessive neural activity. We observed that BCAN was decreased in epilepsy patients compared to controls, suggesting that BCAN levels are controlled by activity also in the human cortex (Figures 7C and 7D). This decrease was not due to a reduction in the number of interneurons, as protein levels for the interneuron marker Lhx6 were similar in both conditions (Figures S7A and S7B).

To confirm that BCAN is dynamically regulated by activity under more physiological conditions, we analyzed changes in BCAN levels associated to training (Figures S7C and S7D). Previous studies have shown shifts in hippocampal PV+ cell network configuration after spatial learning (Dehorter et al., 2015; Donato et al., 2013). Consistently, 4 days of Morris Water Maze (MWM) training caused a shift to low PV expression in PV+ cells (Figure S7E). During the learning phase of the task (day 4), BCAN expression also shifted to lower levels, leading to a decrease in the proportion of BCAN+ cells among the PV+ interneuron population (Figures 7E–7H). Interestingly, upon learning accomplishment (day 10), PV expression shifted to a high-PV network configuration and BCAN expression returned to baseline levels (Figures 7H and S7F–S7H). To strengthen these observations, we analyzed BCAN levels in mice exposed to an enriched environment (EE). We observed that 30 days of EE caused a shift to low PV expression compared to mice housed in standard conditions (Figure S7J). Consistent with a remodeling of the PV+ interneuron network, we also found that EE decreases the levels of BCAN compared to controls (Figures 7I–7K). Consequently, the percentage of BCAN+/PV+ cells was also reduced (Figure 7L). Such changes in the BCAN levels led to synaptic modifications onto PV+ cells (Figure 7M), as observed in *Bcan* mutants (Figure 3). We next demonstrated that both BCAN isoforms were regulated by activity. A decrease in both *Bcan2* and *Bcan1* levels was detected since 4 days of EE (Figures 7N and 7O) when no change in the PV and BCAN levels or in the density of excitatory synapses were yet observed (Figures S7K–S7O). Noteworthy, the reduction of *Bcan2*—but not *Bcan1*—was still maintained after 30 days of EE (Figures 7N, 7O, S7N, and S7O). Although both *Bcan* isoforms seem to be regulated by activity, the

Figure 6. BCAN Controls AMPARs and Kv Channels

(A) CoIP blots from WT hippocampal lysates illustrating pull-down of AMPARs and BCAN (n = 3 mice).

(B and C) Blots (B) and quantification (C) of GluA1 in synaptosomes (S), non-synaptic membranes (M), cytoplasm (C), and total homogenate (H) from $Bcan^{-/-}$ and WT mice (n = 6–13 mice per genotype).

(D) Three-color STORM images of BCAN, Bassoon, and GluA1 at single synapses onto PV+ cells.

(E) Radial distribution of BCAN and GluA1 relative to Bassoon. Analysis of 117 face-view synapses from 11 experiments.

(F–J) Images and thresholded masks illustrating GluA1+ (full arrowheads) and GluA1− (open arrowheads) excitatory somatic synapses on WT, $Bcan^{-/-}$, *Bcan* KD, BCAN1, and BCAN2-rescued PV+ cells.

(K–M) Density of GluA1+ clusters at VGlut1+PSD95+ synapses onto PV+ cells in (K) *Bcan* mutants (n = 5 mice) compared to WT mice (n = 6 mice) and in the cell-autonomous experiments: (L) *Bcan* KD (n = 23 cells, 3 mice) compared to WT cells (n = 22 cells, 3 mice) and (M) BCAN1 (n = 42 cells, 5 mice) and BCAN2-rescued (n = 22 cells, 5 mice) compared to $Bcan^{-/-}$ cells (n = 29 cells, 5 mice).

(N–P) Density (N), control (O) and mutant (P) images (upper panels), and thresholded masks (lower panels) of VGlut1+PSD95+ synapses (arrowheads) contacting PV+ cells in *PV-Cre; GluA1* conditional mutants (n = 10 mice) compared to controls (n = 6 mice).

(Q and R) Blots (Q) and quantification (R) of K_v3.1b in WT (n = 5 mice) and $Bcan^{-/-}$ (n = 4 mice) hippocampal lysates.

(S–U) Images (S) and density of K_v3.1b clusters in (T) WT (n = 5 mice) compared to $Bcan^{-/-}$ (n = 6 mice) mice and in (U) *Bcan* KD (n = 13 cells, 3 mice) compared to WT cells (n = 23 cells, 3 mice).

(V and W) Blots (V) and quantification (W) of K_v1.1 in WT (n = 9 mice) and $Bcan^{-/-}$ (n = 5 mice) hippocampal lysates.

(X–Z) Images (X) and density of K_v1.1 clusters in (Y) WT (n = 5 mice) compared to $Bcan^{-/-}$ (n = 5 mice) mice and in (Z) *Bcan* KD (n = 11 cells, 3 mice) compared to WT cells (n = 25 cells, 3 mice).

Student's t test (C, K, and L), one-way ANOVA (M), and Mann-Whitney test (N, R, T, U, W, Y, and Z). Scale bars represent 500 nm (D) and 1 μm (F–J, O, P, S, and X). See also Figure S6.

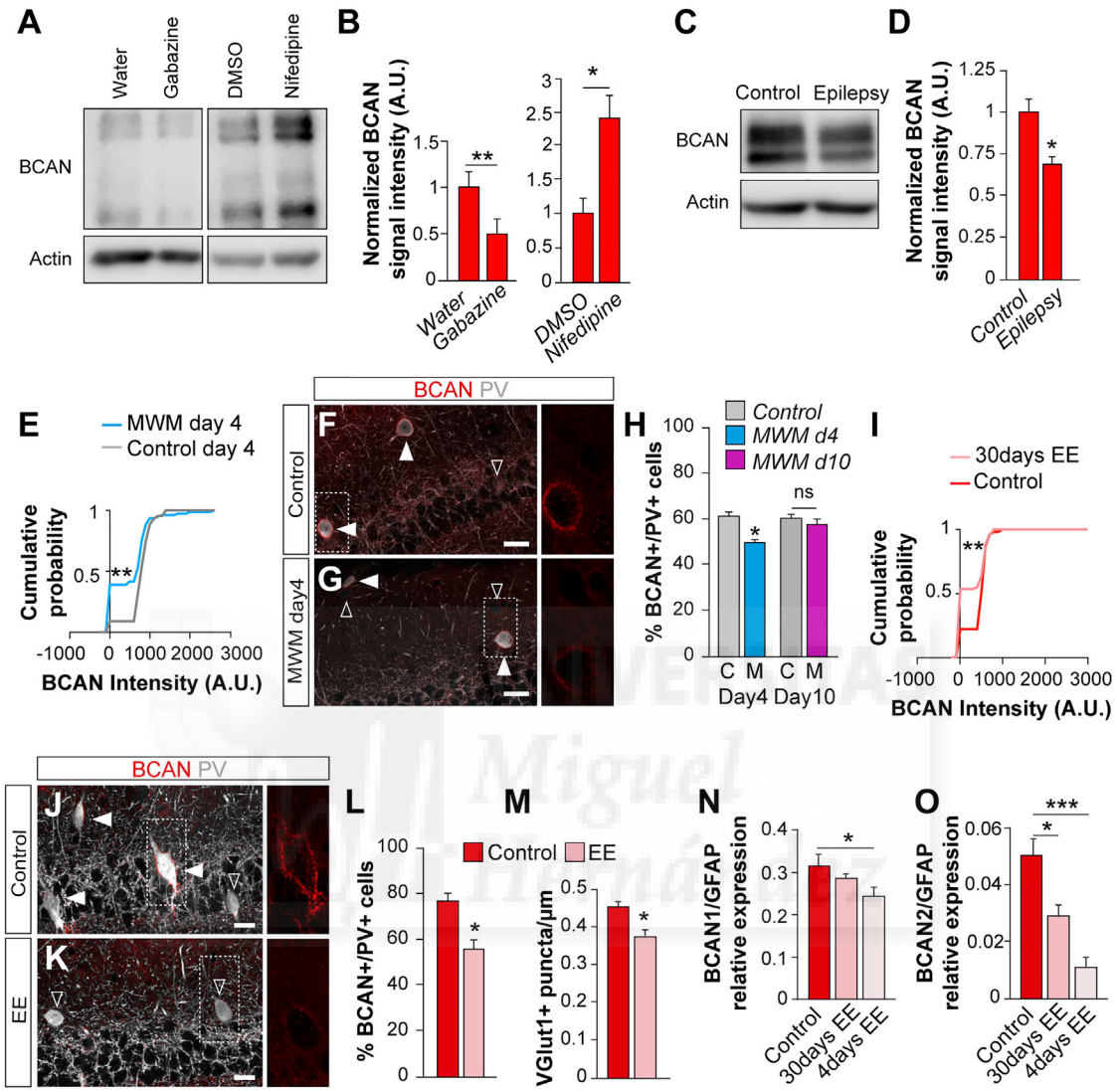

Figure 7. BCAN Expression Is Dynamically Regulated by Activity

(A and B) Blots (A) and quantification (B) of BCAN levels in hippocampal cultures treated for 48 hr with vehicle, Gabazine, or Nifedipine ($n \geq 7$ wells from 6 independent cultures).

(C and D) Blots (C) and analysis (D) of BCAN protein in the hippocampus of epilepsy patients (n = 4) compared to controls (n = 4).

(E) Cumulative probability plots (control, n = 44 cells, 3 mice; and trained mice, n = 79 cells, 4 mice).

(F and G) Images of BCAN levels in the hippocampus of mice trained for 4 days in the MWM (G) and swimming controls (F).

(H) Percentage of PV+ cells wrapped by BCAN after 4 days (n = 3 controls and 4 trained mice) and 10 days (n = 4 controls and 4 trained mice) of MWM.

(I) Cumulative probability plots (control, n = 54 cells, 3 mice; and EE mice, n = 71 cells, 3 mice).

(J and K) Images of BCAN level in the hippocampus of mice housed in an EE (K) compared to controls (J).

(L) Percentage of PV+ cells enwrapped by BCAN in control (n = 5 mice) and EE mice (n = 3 mice).

(M) Density of VGlut1+ somatic puncta on PV+ cells in control (n = 5 mice) and EE mice (n = 3 mice).

(N and O) *Bcan1* (N) and *Bcan2* (O) mRNA expression relative to that of GFAP in control (n = 5 mice) and in mice housed in an EE for 4 (n = 5 mice) and 30 (n = 5 mice) days. Scale bars represent 15 µm (F, G, J, and K).

Mann-Whitney test (B, D, H, L, and M), Kolmogorov-Smirnov test (E and I) and one-way ANOVA (N and O).

See also Figure S7.

increase in the *Bcan1*/*Bcan2* ratio suggests that *Bcan2* may be the main isoform that responds to changes in activity (Figure S7P). Altogether, these experiments demonstrate that BCAN levels are dynamically regulated by activity under physiological conditions.

Brevican Mutants Have Cognitive Deficits

The activity-dependent dynamics of BCAN could be a critical mechanism for regulating plasticity during learning and behavior. GluA1-containing AMPARs are essential for several hippocampal-dependent forms of memory (Fuchs et al., 2007; Reisel

et al., 2002; Sanderson et al., 2009). Since BCAN regulates GluA1 at excitatory synapses contacting PV+ cells (Figure 6), we next examined how the loss of BCAN affects learning and memory (Figures 8 and S8). We assessed spatial working memory on the T-maze and found a moderate impairment in *Bcan* mutant mice (Figures 8A and 8B) that resembles the phenotype of mice lacking GluA1 in PV+ cells (Fuchs et al., 2007).

GluA1 mutants also exhibit impaired short-term spatial memory (Sanderson et al., 2007). To assess whether the lack of BCAN leads to a similar phenotype, we used a novelty preference test on the Y-maze (Figures 8C–8H and S8E–S8L) (Sanderson et al., 2007). As expected, control mice showed a strong preference for the novel arm (Figures 8E–8H). In contrast, *Bcan* mutant mice were incapable of discriminating between familiar and novel arms (Figures 8E–8H). Interestingly, when tested for novelty preference after incremental training (Figures S8E–S8L), *Bcan* mutant mice preferred the novel to the familiar arm, showing higher discrimination indexes than control mice (Figures S8K and S8L).

In contrast to the short-term deficiencies, long-term memories seem to be enhanced in GluA1 mutants (Fuchs et al., 2007; Sanderson et al., 2009). Thus, we reasoned that alterations in GluA1 subunit mobility due to lack of BCAN might also alter memory consolidation. To explore this possibility, we designed a novel object recognition (NOR) protocol to consecutively assess the effect of BCAN deletion on short-term and long-term memories (Figures 8I–8M, S8M, and S8N). After a short retention interval, we observed that while control mice preferred the novel over the familiar object, *Bcan* mutant mice devoted similar time to exploring both novel and familiar objects (Figures 8J and 8K). In contrast, *Bcan* mutants were able to remember the familiar object after a longer retention time and spent more time exploring the novel object (Figure 8L). Interestingly, the discrimination index was higher in $Bcan^{-/-}$ mice than in controls (Figure 8M), suggesting potentially enhanced long-term memory in absence of BCAN.

Since BCAN expression in astrocytes may contribute to the synaptic phenotype found in $Bcan^{-/-}$ mice (Figure 1), we next investigated whether the specific depletion of BCAN in PV+ cells was sufficient to cause short-term memory defects as observed in *Bcan* mutant mice. *PV-Cre* mice were injected at P12 with Cre-dependent *shBcan*- or control YFP-expressing viruses into the dorsal hippocampus and spatial short-term memory was assessed at P60 by the novelty preference test (Figures 8C, 8D, 8N–8Q, and S8O–S8S). We found that *Bcan* knockdown mice displayed the same short-term memory deficit exhibited by *Bcan* mutant mice (Figures 8E–8H and 8N–8Q), demonstrating that normal levels of BCAN specifically in PV+ cells are required for short-term memory. Altogether, these results demonstrate that BCAN regulates plasticity-dependent events that are essential for learning and memory.

DISCUSSION

Several of studies have revealed a critical role for PNNs in experience-dependent plasticity, learning, and memory (Gogolla et al., 2009; Pizzorusso et al., 2002). However, how PNNs regulate the function of PV+ interneurons has remained enigmatic. Here we demonstrate that the PNN protein BCAN is expressed by a large fraction of PV+ cells. Expression of BCAN confers PV+ interneurons with specific synaptic and firing properties through the direct regulation of AMPARs and voltage-gated potassium channels. The levels of BCAN vary in response to changes in network activity that are required for learning and memory. Consistently, loss of BCAN leads to deficits in spatial working memory and short-term memory. These results demonstrate that the PNN protein BCAN orchestrates a dedicated molecular program that dynamically gates the drive of PV+ cells and underlies learning and memory.

Since the extracellular matrix (ECM) influences cell-cell interactions, it is conceivable that specific components of the ECM may promote cellular and synaptic plasticity in a cell-specific manner. ECM molecules and associated proteins have been shown to regulate receptor clustering and shape synaptic differentiation, function, and plasticity (Chang et al., 2010; Frischknecht et al., 2009; de Wit et al., 2013). In this study, we have shown that PV+ interneurons expressing BCAN receive more glutamatergic inputs than similar cells lacking BCAN. Specifically, expression of the GPI-anchored isoform of BCAN by PV+ cells is responsible for regulating the density of their excitatory synapses. In addition, release of BCAN2 from astrocytes may also contribute to synapse maturation onto PV+ cells. While astrocytes are well known to critically regulate the development of glutamatergic inputs onto pyramidal neurons (Clarke and Barres, 2013), our results hint at a possible role for these cells at the excitatory synapses of the PV+ interneurons. Future studies will need to address their function on interneuron wiring in more detail. Intriguingly, although our findings show a distinct function for BCAN1 and BCAN2 at the synapses, both BCAN isoforms are able to shift PV levels. One conceivable explanation is that the levels of the calcium binding protein PV change in response to different mechanisms: modifications in both the excitatory drive of PV+ cells that may affect intracellular calcium concentration and the diffusion of local extracellular calcium. Consistently, PNNs are highly negatively charged and have been proposed to function as a buffering system for cations surrounding fast-firing neurons (Brückner et al., 1993).

BCAN affects excitatory synaptic differentiation, at least in part by modulating the levels of GluA1 receptor at the synapse. In absence of BCAN, GluA1 fails to cluster in postsynaptic densities and this seems to cause a loss of excitatory synaptic contacts onto PV+ interneurons. Since the specific depletion of GluA1 from PV+ cells causes a similar phenotype, it is unlikely that the reduction in GluA1 observed in *Bcan* mutants is due to the loss of synapses by a GluA1-independent mechanism. Nevertheless, it is conceivable that other proteins interacting with BCAN also contribute to the synaptic phenotype described in the present study. Further studies will be needed to elucidate the contribution of other BCAN partners to the maturation of these synapses.

BCAN identifies a dynamic population of PV+ interneurons that not only receives more excitatory synapses but also has distinctive intrinsic properties. PV+ cells expressing BCAN are less excitable, but they are more efficient once recruited. Consistently, we observed deficits in the $K_v1.1$ and $K_v3.1b$ channels in absence of BCAN. Worth mentioning, in *Bcan* mutants,

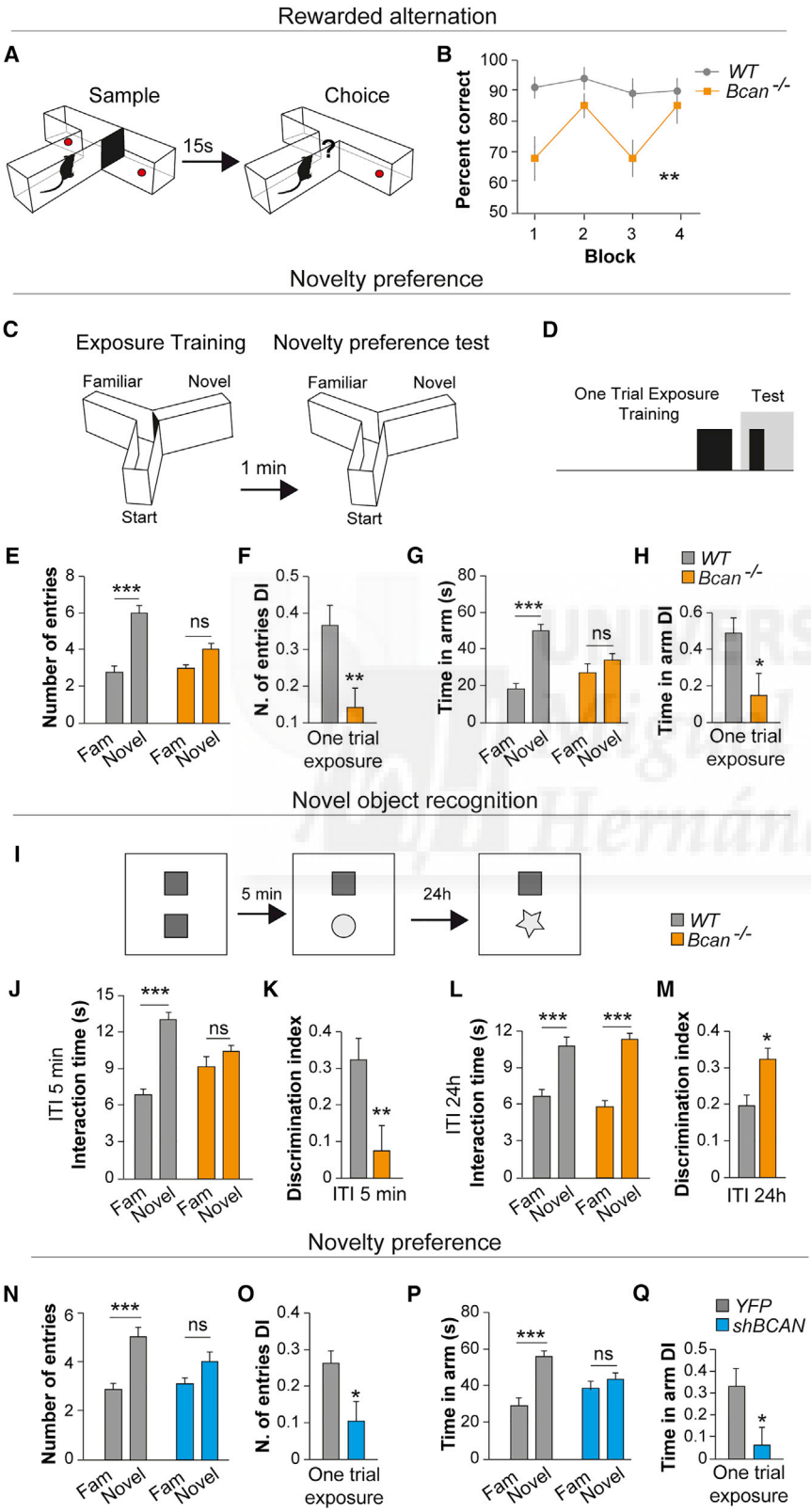

Figure 8. BCAN Deletion Impairs Working and Short-Term Memory

(A) Schematic of the T-maze test.

(B) Percentage of correct responses for wild-type (WT, n = 8) and *Bcan*$^{-/-}$ (n = 10).

(C and D) Schematic of the Y-maze test. (C) Y maze, (D) experimental protocol.

(E–H) Number of entries (E), its discrimination index (DI) (F), total time spent (G), and its discrimination index (H) in the "familiar" and "novel" arms for WT (n = 10) and *Bcan*$^{-/-}$ (n = 10) mice.

(I) Schematic of the novel object recognition test.

(J and K) Analysis of short-time recognition memory in WT (n = 19) and *Bcan*$^{-/-}$ (n = 20). Time spent exploring the "familiar" and "novel" object (J). Discrimination index (K).

(L and M) Analysis of long-time recognition memory in WT (n = 18) and *Bcan*$^{-/-}$ (n = 16). Time spent exploring the "familiar" and "novel" object (L). Discrimination index (M).

(N–Q) Number of entries (N), its discrimination index (DI) (O), total time spent (P), and its discrimination index (Q) in the "familiar" and "novel" arms for WT (n = 11) and *Bcan* KD (n = 13) mice in the novelty preference test.

Two-way repeated-measures ANOVA (A). One-way ANOVA (E, G, J, L, N, and P). Student's t test (F, H, K, M, O, and Q). See also Figure S8.

homeostatic adaptations of PV+ interneurons in response to the decreased number of excitatory inputs seem to trigger changes in Kv1.1. Conversely, a cell-autonomous decrease in Kv1.1 has been previously shown to cause homeostatic changes in connectivity (Dehorter et al., 2015). Altogether, these data support a novel interesting notion that connectivity and cell excitability are reciprocally regulated at the circuit level. Nevertheless, ECM molecules have been implicated in synaptic plasticity through the regulation of ion channels (Kochlamazashvili et al., 2010). As such, BCAN may directly regulate ion channel density, position, or function. Indeed, the changes in spike shape and Kv3.1b clustering appear more directly related with the absence of BCAN. Specifically, these properties seem to depend on BCAN expression in PV+ interneurons, as the PV+ cell-specific knockdown revealed a particularly strong and broad phenotype when compared to the full *Bcan* knockout that might be explained by the different timing of the experimental manipulations. The mature fast-spiking (FS) properties of PV+ interneurons emerge gradually over the first postnatal weeks and are ultimately determined by elaborate interactions among the complements of ion channels that they express (Okaty et al., 2009). Likewise, the first PNNs are observed around P7 and their maturation continues until P28 (Schweizer et al., 1993). In *Bcan* mutant cells, the absence of BCAN during this maturational progression may lead to the compensatory activation of parallel gene expression programs, including the previously reported Neurocan upregulation (Brakebusch et al., 2002). In *Bcan* knockdown cells, however, BCAN downregulation takes place after the emergence of most of their mature FS physiological features, therefore missing the precise time window for a potential compensation. The presence of developmental adaptations in *Bcan* mutant PV+ cells, might also explain why the relatively late expression of *Bcan1* or *Bcan2* is unable to rescue the electrophysiological phenotype. A complementary explanation is that the presence of both BCAN isoforms is required for PV+ cells to have normal intrinsic properties. Future work addressing the consequences of an earlier *Bcan* deletion and rescue, as well as the developmental emergence of FS properties in *Bcan* mutant PV cells, will help to further decompose the complex electrophysiological phenotype displayed by *Bcan*-deficient PV cells.

Growing evidence over the last two decades has shown that the synaptic expression of GluA1 is regulated by activity. For instance, activity-dependent AMPAR insertion at the synapse is the substrate for the expression of the synaptic scaling (Turrigiano, 2012). Interestingly, it was reported that the expression of CSPG proteins requires normal patterns of neural activity (Lander et al., 1997). In the present study, we have shown that BCAN expression is up- or downwardly scaled in response to activity changes. Cortical networks are dynamically regulated by activity *in vivo* (Donato et al., 2013), but little is known about how neurons sense and adapt to the dynamics alterations in network activity at the level of synapses and spiking properties. Recent studies have shown that some of these changes might be mediated by transcription factors (Bloodgood et al., 2013; Dehorter et al., 2015), but the mechanisms through which external signals directly control this process have remained elusive. Here we expose a novel molecular mechanism that simultaneously mediates modifications in the intrinsic properties and synaptic inputs of PV+ interneurons and that is regulated by experience.

Our data provide evidence that BCAN, one of the major components of PNNs, allows PV+ cells to adapt their responses to different types of sensory experience. Specifically, BCAN plays a crucial role in spatial working memory and short-term episodic-like memory but is dispensable, if not obstructive, for long-term memory. How do assemblies of neurons encode and represent different types of memory? It is worth mentioning that BCAN is enriched in the soma and proximal dendrites of PV+ cells, suggesting that it might regulate specific inputs arriving to PV+ cells. Indeed, in the hippocampus, different inputs have distinct subcellular specificity (Klausberger and Somogyi, 2008) and are involved in different aspects of memory (Kitamura et al., 2015). Experience could therefore drive context-specific activation of BCAN+/PV+ cells, where BCAN would contribute to strengthen their excitatory inputs and filter weak and asynchronous stimuli. This positive feedback loop might thus promote the synchronization of pyramidal neurons leading to the formation of short-term memories. On the contrary, prolonged sensory experience, such as that linked to an enriched environment, would attenuate the levels of the PNN protein BCAN. As a consequence, the excitatory drive onto PV+ interneurons would be reduced, further releasing pyramidal cells from inhibition and triggering the plastic rearrangements in the principal cell network that underlie memory consolidation.

A growing amount of research is aiming to reveal the relationship between PNNs, memory and cognition (Tsien, 2013). The newly discovered function of BCAN in PV+ cell plasticity may represent a general principle through which activity-regulated PNN proteins orchestrate selective modifications in specific classes of neurons, thereby influencing network plasticity outcomes upon changes in the environment.

STAR★METHODS

Detailed methods are provided in the online version of this paper and include the following:

- KEY RESOURCES TABLE
- CONTACT FOR REAGENT AND RESOURCE SHARING
- EXPERIMENTAL MODEL AND SUBJECT DETAILS
  - Mice
- METHOD DETAILS
  - Perfusions and Immunohistochemistry
  - Fluorescent *In Situ* Hybridization Histochemistry
  - Super-Resolution Image Acquisition and Analysis
  - Cell Culture, Transfection, Pharmacology and Immunocytochemistry
  - Generation of AAV Expression Vectors
  - AAV Production and Intracranial Injections
  - Western blot and Fractionation
  - Co-immunoprecipitation Assays
  - *In vitro* Patch Clamp Recordings
  - Image Acquisition and Analysis
  - In utero electroporation and Tamoxifen Induction
  - Quantitative real-time PCR
  - Epilepsy human samples

- Behavioral procedures
- Statistical analysis

SUPPLEMENTAL INFORMATION

Supplemental Information includes eight figures and five tables and can be found with this article online at http://dx.doi.org/10.1016/j.neuron.2017.06.028.

AUTHOR CONTRIBUTIONS

Conceptualization, E.F. and B.R.; Methodology, E.F., R.D., C.M.W., B.R.; Formal Analysis, E.F., A.M.-S., A.S.-A., C.M.W., Investigation, E.F., A.M.-S., R.D., A.S.-A., P.M., C.M.W.; Resources, C.M.W., C.F., L.M., H.E., B.R.; Writing, E.F. and B.R.; Visualization, E.F., A.M.-S., C.M.W., B.R.; Funding Acquisition, B.R.

ACKNOWLEDGMENTS

We are thankful to N. Carvajal and D. Baeza for technical assistance and lab support, Ian Andrew for mouse management, R. Fässler for *Bcan*$^{-/-}$ mice, S. Arber for *PV-Cre* mice, R. Frischknecht for BCAN antibodies, E. Fuchs, A. Herb, and H. Monyer for *PV-Cre;GluA1*$^{F/F}$ brains, A. Navarro for electroporated brains, A. Kirby for helping with the Kv experiments, and the London Neurodegenerative Diseases Brain Bank and Brains for Dementia Research (C. Troakes, S. Selvackadunco, and S. Al-Sarraj) for human tissue. We are grateful to O. Marín, N. Dehorter, C. Bernard, and J. Burrone for critical reading of the manuscript and members of Rico and Marín laboratories for stimulating discussions and ideas. Supported by grants from European Research Council (ERC-2012-StG 310021) to B.R. E.F. was supported by JAE-Pre fellowship (CSIC) and King's College London funds. B.R. is Wellcome Trust investigator.

Received: October 31, 2016
Revised: June 2, 2017
Accepted: June 16, 2017
Published: July 13, 2017

REFERENCES

Betzig, E., Patterson, G.H., Sougrat, R., Lindwasser, O.W., Olenych, S., Bonifacino, J.S., Davidson, M.W., Lippincott-Schwartz, J., and Hess, H.F. (2006). Imaging intracellular fluorescent proteins at nanometer resolution. Science *313*, 1642–1645.

Bloodgood, B.L., Sharma, N., Browne, H.A., Trepman, A.Z., and Greenberg, M.E. (2013). The activity-dependent transcription factor NPAS4 regulates domain-specific inhibition. Nature *503*, 121–125.

Brakebusch, C., Seidenbecher, C.I., Asztely, F., Rauch, U., Matthies, H., Meyer, H., Krug, M., Böckers, T.M., Zhou, X., Kreutz, M.R., et al. (2002). Brevican-deficient mice display impaired hippocampal CA1 long-term potentiation but show no obvious deficits in learning and memory. Mol. Cell. Biol. *22*, 7417–7427.

Brückner, G., Brauer, K., Härtig, W., Wolff, J.R., Rickmann, M.J., Derouiche, A., Delpech, B., Girard, N., Oertel, W.H., and Reichenbach, A. (1993). Perineuronal nets provide a polyanionic, glia-associated form of microenvironment around certain neurons in many parts of the rat brain. Glia *8*, 183–200.

Cardin, J.A., Carlén, M., Meletis, K., Knoblich, U., Zhang, F., Deisseroth, K., Tsai, L.-H., and Moore, C.I. (2009). Driving fast-spiking cells induces gamma rhythm and controls sensory responses. Nature *459*, 663–667.

Carstens, K.E., Phillips, M.L., Pozzo-Miller, L., Weinberg, R.J., and Dudek, S.M. (2016). Perineuronal Nets Suppress Plasticity of Excitatory Synapses on CA2 Pyramidal Neurons. J. Neurosci. *36*, 6312–6320.

Chang, M.C., Park, J.M., Pelkey, K.A., Grabenstatter, H.L., Xu, D., Linden, D.J., Sutula, T.P., McBain, C.J., and Worley, P.F. (2010). Narp regulates homeostatic scaling of excitatory synapses on parvalbumin-expressing interneurons. Nat. Neurosci. *13*, 1090–1097.

Clarke, L.E., and Barres, B.A. (2013). Emerging roles of astrocytes in neural circuit development. Nat. Rev. Neurosci. *14*, 311–321.

Dani, A., Huang, B., Bergan, J., Dulac, C., and Zhuang, X. (2010). Superresolution imaging of chemical synapses in the brain. Neuron *68*, 843–856.

de Wit, J., O'Sullivan, M.L., Savas, J.N., Condomitti, G., Caccese, M.C., Vennekens, K.M., Yates, J.R., 3rd, and Ghosh, A. (2013). Unbiased discovery of glypican as a receptor for LRRTM4 in regulating excitatory synapse development. Neuron *79*, 696–711.

Deepa, S.S., Carulli, D., Galtrey, C., Rhodes, K., Fukuda, J., Mikami, T., Sugahara, K., and Fawcett, J.W. (2006). Composition of perineuronal net extracellular matrix in rat brain: a different disaccharide composition for the net-associated proteoglycans. J. Biol. Chem. *281*, 17789–17800.

Dehorter, N., Ciceri, G., Bartolini, G., Lim, L., del Pino, I., and Marín, O. (2015). Tuning of fast-spiking interneuron properties by an activity-dependent transcriptional switch. Science *349*, 1216–1220.

Donato, F., Rompani, S.B., and Caroni, P. (2013). Parvalbumin-expressing basket-cell network plasticity induced by experience regulates adult learning. Nature *504*, 272–276.

Du, J., Zhang, L., Weiser, M., Rudy, B., and McBain, C.J. (1996). Developmental expression and functional characterization of the potassium-channel subunit Kv3.1b in parvalbumin-containing interneurons of the rat hippocampus. J. Neurosci. *16*, 506–518.

Frischknecht, R., Heine, M., Perrais, D., Seidenbecher, C.I., Choquet, D., and Gundelfinger, E.D. (2009). Brain extracellular matrix affects AMPA receptor lateral mobility and short-term synaptic plasticity. Nat. Neurosci. *12*, 897–904.

Frischknecht, R., Chang, K.-J., Rasband, M.N., and Seidenbecher, C.I. (2014). Neural ECM molecules in axonal and synaptic homeostatic plasticity. Prog. Brain Res. *214*, 81–100.

Froemke, R.C. (2015). Plasticity of cortical excitatory-inhibitory balance. Annu. Rev. Neurosci. *38*, 195–219.

Fuchs, E.C., Zivkovic, A.R., Cunningham, M.O., Middleton, S., Lebeau, F.E.N., Bannerman, D.M., Rozov, A., Whittington, M.A., Traub, R.D., Rawlins, J.N.P., and Monyer, H. (2007). Recruitment of parvalbumin-positive interneurons determines hippocampal function and associated behavior. Neuron *53*, 591–604.

Gogolla, N., Caroni, P., Lüthi, A., and Herry, C. (2009). Perineuronal nets protect fear memories from erasure. Science *325*, 1258–1261.

Goldberg, E.M., Clark, B.D., Zagha, E., Nahmani, M., Erisir, A., and Rudy, B. (2008). K+ channels at the axon initial segment dampen near-threshold excitability of neocortical fast-spiking GABAergic interneurons. Neuron *58*, 387–400.

Gu, S., Jin, L., Zhang, Y., Huang, Y., Zhang, F., Valdmanis, P.N., and Kay, M.A. (2012). The loop position of shRNAs and pre-miRNAs is critical for the accuracy of dicer processing in vivo. Cell *151*, 900–911.

Henley, J.M., and Wilkinson, K.A. (2016). Synaptic AMPA receptor composition in development, plasticity and disease. Nat. Rev. Neurosci. *17*, 337–350.

Hensch, T.K., Fagiolini, M., Mataga, N., Stryker, M.P., Baekkeskov, S., and Kash, S.F. (1998). Local GABA circuit control of experience-dependent plasticity in developing visual cortex. Science *282*, 1504–1508.

Hippenmeyer, S., Vrieseling, E., Sigrist, M., Portmann, T., Laengle, C., Ladle, D.R., and Arber, S. (2005). A developmental switch in the response of DRG neurons to ETS transcription factor signaling. PLoS Biol. *3*, e159.

Hockfield, S., and McKay, R.D. (1983). A surface antigen expressed by a subset of neurons in the vertebrate central nervous system. Proc. Natl. Acad. Sci. USA *80*, 5758–5761.

Hu, H., Gan, J., and Jonas, P. (2014). Interneurons. Fast-spiking, parvalbumin^{+} GABAergic interneurons: from cellular design to microcircuit function. Science *345*, 1255263.

Karson, M.A., Tang, A.-H., Milner, T.A., and Alger, B.E. (2009). Synaptic cross talk between perisomatic-targeting interneuron classes expressing cholecystokinin and parvalbumin in hippocampus. J. Neurosci. *29*, 4140–4154.

Katona, I., Sperlágh, B., Sík, A., Käfalvi, A., Vizi, E.S., Mackie, K., and Freund, T.F. (1999). Presynaptically located CB1 cannabinoid receptors regulate GABA release from axon terminals of specific hippocampal interneurons. J. Neurosci. *19*, 4544–4558.

Kitamura, T., Sun, C., Martin, J., Kitch, L.J., Schnitzer, M.J., and Tonegawa, S. (2015). Entorhinal Cortical Ocean Cells Encode Specific Contexts and Drive Context-Specific Fear Memory. Neuron *87*, 1317–1331.

Klausberger, T., and Somogyi, P. (2008). Neuronal diversity and temporal dynamics: the unity of hippocampal circuit operations. Science *321*, 53–57.

Kochlamazashvili, G., Henneberger, C., Bukalo, O., Dvoretskova, E., Senkov, O., Lievens, P.M.-J., Westenbroek, R., Engel, A.K., Catterall, W.A., Rusakov, D.A., et al. (2010). The extracellular matrix molecule hyaluronic acid regulates hippocampal synaptic plasticity by modulating postsynaptic L-type Ca(2+) channels. Neuron *67*, 116–128.

Lagler, M., Ozdemir, A.T., Lagoun, S., Malagon-Vina, H., Borhegyi, Z., Hauer, R., Jelem, A., and Klausberger, T. (2016). Divisions of Identified Parvalbumin-Expressing Basket Cells during Working Memory-Guided Decision Making. Neuron *91*, 1390–1401.

Lander, C., Kind, P., Maleski, M., and Hockfield, S. (1997). A family of activity-dependent neuronal cell-surface chondroitin sulfate proteoglycans in cat visual cortex. J. Neurosci. *17*, 1928–1939.

Matta, J.A., Pelkey, K.A., Craig, M.T., Chittajallu, R., Jeffries, B.W., and McBain, C.J. (2013). Developmental origin dictates interneuron AMPA and NMDA receptor subunit composition and plasticity. Nat. Neurosci. *16*, 1032–1041.

Nabel, E.M., and Morishita, H. (2013). Regulating critical period plasticity: insight from the visual system to fear circuitry for therapeutic interventions. Front. Psychiatry *4*, 146.

Okaty, B.W., Miller, M.N., Sugino, K., Hempel, C.M., and Nelson, S.B. (2009). Transcriptional and electrophysiological maturation of neocortical fast-spiking GABAergic interneurons. J. Neurosci. *29*, 7040–7052.

Pizzorusso, T., Medini, P., Berardi, N., Chierzi, S., Fawcett, J.W., and Maffei, L. (2002). Reactivation of ocular dominance plasticity in the adult visual cortex. Science *298*, 1248–1251.

Platonova, E., Winterflood, C.M., and Ewers, H. (2015). A simple method for GFP- and RFP-based dual color single-molecule localization microscopy. ACS Chem. Biol. *10*, 1411–1416.

Reisel, D., Bannerman, D.M., Schmitt, W.B., Deacon, R.M.J., Flint, J., Borchardt, T., Seeburg, P.H., and Rawlins, J.N.P. (2002). Spatial memory dissociations in mice lacking GluR1. Nat. Neurosci. *5*, 868–873.

Sanderson, D.J., Gray, A., Simon, A., Taylor, A.M., Deacon, R.M.J., Seeburg, P.H., Sprengel, R., Good, M.A., Rawlins, J.N.P., and Bannerman, D.M. (2007). Deletion of glutamate receptor-A (GluR-A) AMPA receptor subunits impairs one-trial spatial memory. Behav. Neurosci. *121*, 559–569.

Sanderson, D.J., Good, M.A., Skelton, K., Sprengel, R., Seeburg, P.H., Rawlins, J.N.P., and Bannerman, D.M. (2009). Enhanced long-term and impaired short-term spatial memory in GluA1 AMPA receptor subunit knockout mice: evidence for a dual-process memory model. Learn. Mem. *16*, 379–386.

Schweizer, M., Streit, W.J., and Müller, C.M. (1993). Postnatal development and localization of an N-acetylgalactosamine containing glycoconjugate associated with nonpyramidal neurons in cat visual cortex. J. Comp. Neurol. *329*, 313–327.

Seidenbecher, C.I., Richter, K., Rauch, U., Fässler, R., Garner, C.C., and Gundelfinger, E.D. (1995). Brevican, a chondroitin sulfate proteoglycan of rat brain, occurs as secreted and cell surface glycosylphosphatidylinositol-anchored isoforms. J. Biol. Chem. *270*, 27206–27212.

Seidenbecher, C.I., Smalla, K.H., Fischer, N., Gundelfinger, E.D., and Kreutz, M.R. (2002). Brevican isoforms associate with neural membranes. J. Neurochem. *83*, 738–746.

Sohal, V.S., Zhang, F., Yizhar, O., and Deisseroth, K. (2009). Parvalbumin neurons and gamma rhythms enhance cortical circuit performance. Nature *459*, 698–702.

Takesian, A.E., and Hensch, T.K. (2013). Balancing plasticity/stability across brain development. Prog. Brain Res. *207*, 3–34.

Tsien, R.Y. (2013). Very long-term memories may be stored in the pattern of holes in the perineuronal net. Proc. Natl. Acad. Sci. USA *110*, 12456–12461.

Turrigiano, G. (2012). Homeostatic synaptic plasticity: local and global mechanisms for stabilizing neuronal function. Cold Spring Harb. Perspect. Biol. *4*, a005736.

Valenzuela, J.C., Heise, C., Franken, G., Singh, J., Schweitzer, B., Seidenbecher, C.I., and Frischknecht, R. (2014). Hyaluronan-based extracellular matrix under conditions of homeostatic plasticity. Philos. Trans. R. Soc. Lond. B Biol. Sci. *369*, 20130606.

Wilson, N.R., Runyan, C.A., Wang, F.L., and Sur, M. (2012). Division and subtraction by distinct cortical inhibitory networks in vivo. Nature *488*, 343–348.

Winterflood, C.M., Platonova, E., Albrecht, D., and Ewers, H. (2015). Dual-color 3D superresolution microscopy by combined spectral-demixing and biplane imaging. Biophys. J. *109*, 3–6.

Xue, M., Atallah, B.V., and Scanziani, M. (2014). Equalizing excitation-inhibition ratios across visual cortical neurons. Nature *511*, 596–600.

Yazaki-Sugiyama, Y., Kang, S., Câteau, H., Fukai, T., and Hensch, T.K. (2009). Bidirectional plasticity in fast-spiking GABA circuits by visual experience. Nature *462*, 218–221.

Neuron, Volume *95*

Supplemental Information

Activity-Dependent Gating of Parvalbumin Interneuron Function by the Perineuronal Net Protein Brevican

Emilia Favuzzi, André Marques-Smith, Rubén Deogracias, Christian M. Winterflood, Alberto Sánchez-Aguilera, Laura Mantoan, Patricia Maeso, Cathy Fernandes, Helge Ewers, and Beatriz Rico

SUPPLEMENTAL FIGURES

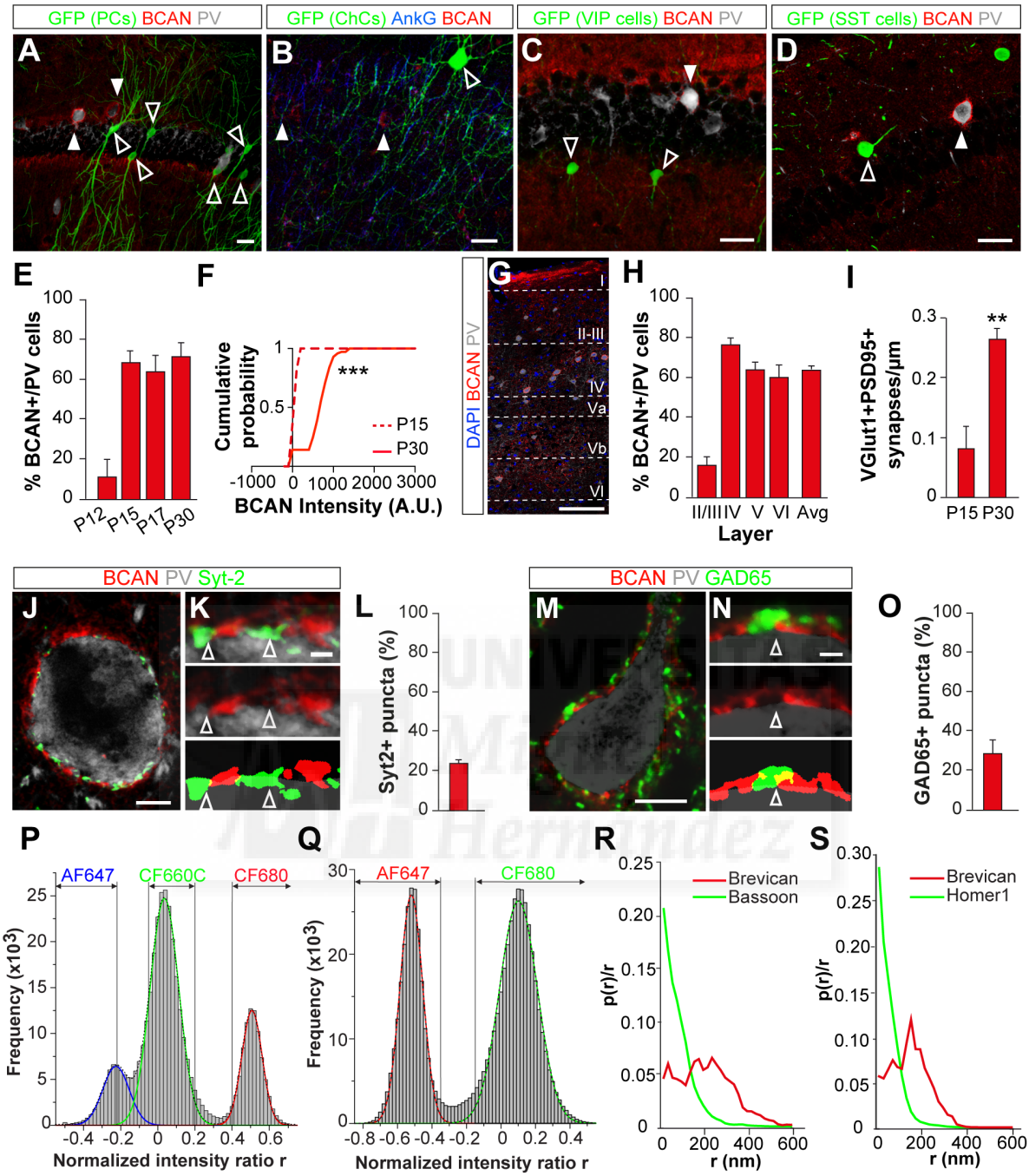

Figure S1. Expression and localization of Brevican in the cerebral cortex, related to Figure 1

(A-D) Representative images showing the absence of Brevican sheath surrounding pyramidal cells or interneuron subtypes (empty arrowheads) other than PV+ basket cells (arrowheads). PCs: GFP-electroporated pyramidal cells, ChCs: chandelier cells in *Nkx2.1CreERT2;RCE*, VIP cells: *VIP-Cre; RCE*, SST cells: *GIN* mice.

(E) Percentage of PV+ interneurons enwrapped by Brevican protein at different postnatal developmental stages in the hippocampus (n = 3 mice). P30 data are the same as in Figure 1I.

(F) Cumulative probability plot comparing Brevican fluorescence intensity levels at P15 (n = 55 cells, 3 mice) and P30 (n = 142 cells, 4 mice) mice; Kolmogorov-Smirnov test.

(G and H) Representative image (G) and percentage (H) of PV+ interneurons enwrapped by Brevican protein in the somatosensory cortex (n = 4 mice).

(I) Density of VGlut1+PSD95+ synapses contacting the soma of PV+ cells at P15 (n = 7 mice) and P30 (n = 6 mice); Mann-Whitney test. P15 and P30 data are the same as the controls in Figure S3E and Figure 3D, respectively.
(J-O) Representative images and percentage of Syt2+ (J-L, n = 4 mice) and GAD65+ (M-O, n = 3 mice) inhibitory terminals contacting the soma of PV+BCAN+ cells.
(P and Q) Histograms of normalized intensity ratios and dye separation for a three-color STORM experiment using Bassoon-AF647, Homer-CF660 and Brevican-CF680 (P) and for a two-color STORM experiment using Brevican-AF647 and Bassoon-CF680 (Q).
R and S) Radial (lateral) distribution of Brevican and Bassoon (R) or Homer1 (S). Analysis of 51 (R) and 41 (S) face-view synapses from 6 experiments. Scale bars equal 20 μm (A-D), 100 μm (G), 5 μm (J, M), 1 μm (K, N).

UNIVERSITAS Miguel Hernández

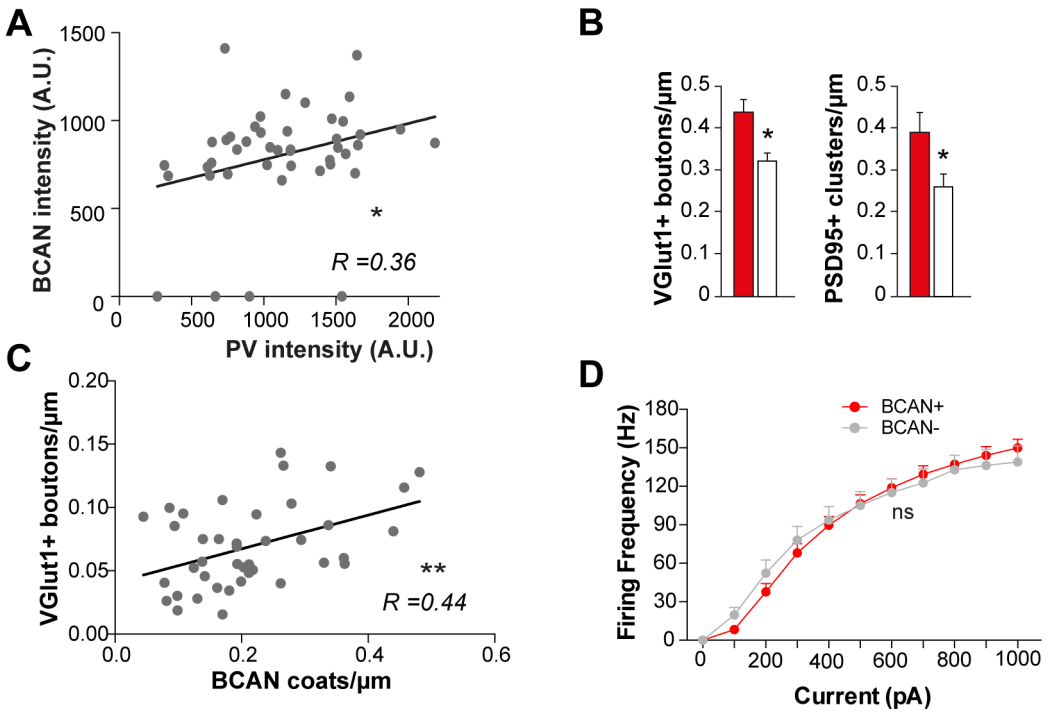

Figure S2. Characterization of Brevican+ and Brevican- cells, related to Figure 2

(A) Correlation between the PV and Brevican protein intensities in PV+ cells (Spearman correlation, n = 44 cells, 3 mice).

(B) Density of VGlut1+ boutons (n = 7 mice) and PSD95+ clusters (n = 9 mice) contacting the soma of BCAN+ and BCAN- PV cells. Student t-test.

(C) Correlation between the number of Brevican "coats" (see supplemental experimental procedures for details) and the number of VGlut1+ inputs contacting PV+ interneurons (Pearson correlation, n = 41 cells, 3 mice).

(D) I/O curves showing the spike frequency of BCAN+ (n = 22 cells, 9 mice) and BCAN- (n = 13 cells, 9 mice) PV+ cells in response to current injections (left Y-axis, solid lines). Note that the input-output curve was similar between the two populations of basket PV+ cells. Two-way ANOVA, F (1, 346) = 0.0170.

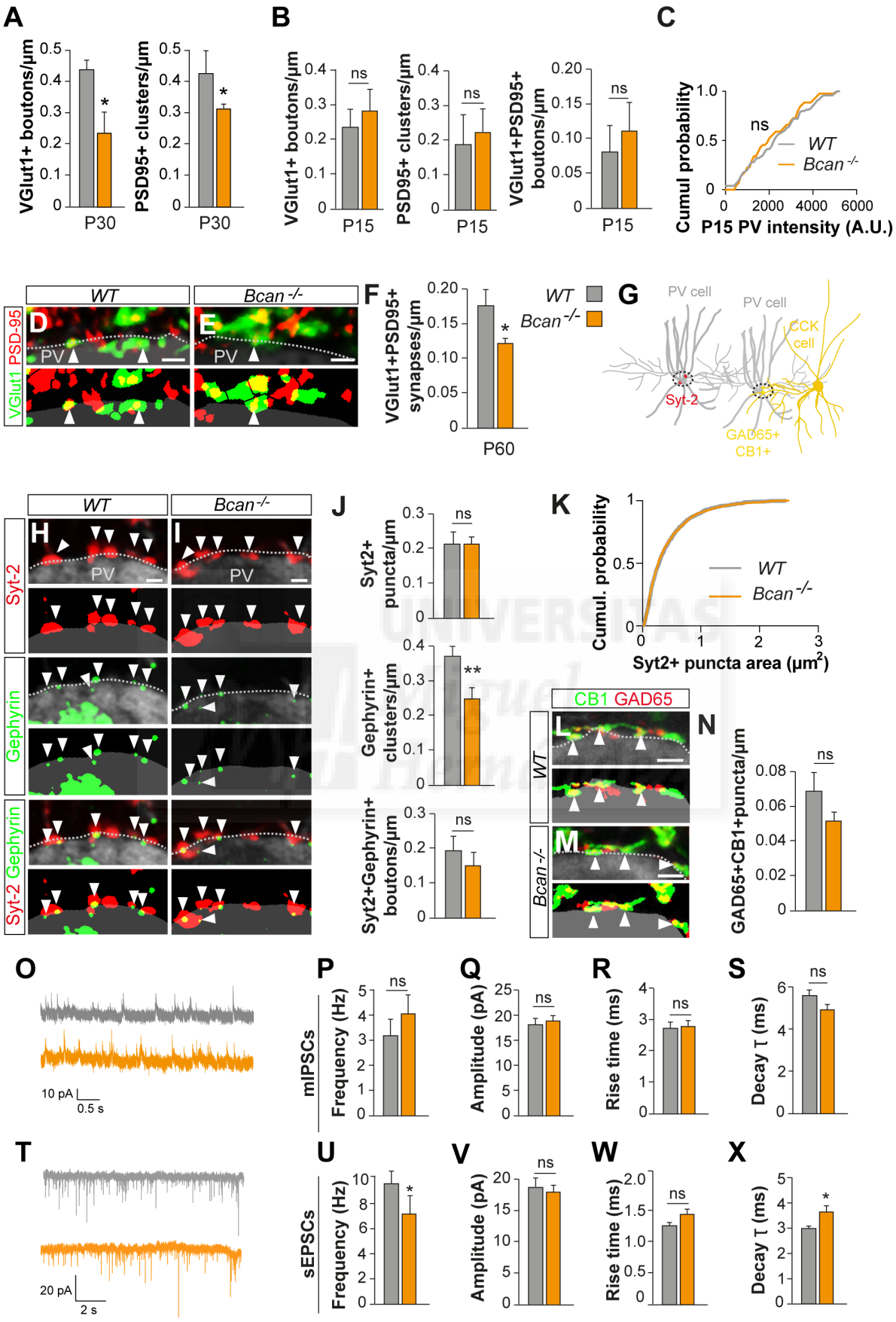

Figure S3. Effect of Brevican deletion on the wiring of PV+ interneurons, related to Figure 3

(A) Density of VGlut1+ boutons (n = 6 WT, 4 *Bcan*$^{-/-}$) and PSD95+ clusters (n = 7 WT, 7 *Bcan*$^{-/-}$) contacting the soma of PV+ cells at P30.
(B) Density of VGlut1+ boutons, PSD95+ clusters and VGlut1+PSD95+ synapses contacting the soma of PV+ cells in P15 wild type (WT, n = 7 mice) and *Bcan*$^{-/-}$ (n = 7 mice) mice.
(C) Cumulative probability plots comparing PV fluorescence intensity levels in P15 wild type (WT, n = 75 cells, 8 mice) and *Bcan*$^{-/-}$ (n = 44 cells, 3 mice) mice; ns: no significant difference.
(D-F) Representative images and thresholded binary images (D and E) illustrating VGlut1+PSD95+ synapses contacting the soma of PV+ cells, and synaptic density (F), in WT (n = 6 mice) and *Bcan*$^{-/-}$ (n = 8 mice) mice at P60.
(G) Schematic drawing highlighting the synapses analyzed in the following experiments.
(H-J) Representative images, thresholded binary images (H and I) and synaptic density (J). Images illustrate Syt2+ boutons (n= 5 WT, 4 *Bcan*$^{-/-}$), Gephyrin+ clusters (n = 12 WT, 11 *Bcan*$^{-/-}$) and Syt2+Gephyrin+ synapses (n = 5 WT, 4 *Bcan*$^{-/-}$) contacting the soma of PV+ cells.
(K) Cumulative probability plots comparing the size of Syt2 puncta in wild type (WT, n = 61 cells, 6 mice) and *Bcan*$^{-/-}$ (n = 82 cells, 4 mice) mice.
(L-N) Representative images and thresholded binary images (L and M) illustrating CB1+GAD65+ boutons contacting the soma of PV+ interneurons, and synaptic density (N) in WT (n = 5 mice) and *Bcan*$^{-/-}$ (n = 6 mice) mice .
(O-S) Representative traces, frequency, amplitude, rise and decay time of mIPSCs in WT (n = 11 cells, 4 mice) and *Bcan*$^{-/-}$ PV+ cells (n = 16 cells, 3 mice).
(T-X) Representative traces, frequency, amplitude, rise and decay time of sEPSCs in WT (n = 11 cells, 1 mouse) and *Bcan*$^{-/-}$ PV+ cells (n = 10 cells, 2 mice).
Student t-test (A, F, N, R, S, V, W, PSD95+ clusters in C, and Gephyrin+ clusters in J), Mann-Whitney test for (J, P, Q, U, X and VGlut1+ boutons in C). Kolmogorov-Smirnov test (B and K). Scale bars equal 1 µm (D, E, H, I), 2 µm (L, M).

UNIVERSITAS Miguel Hernández

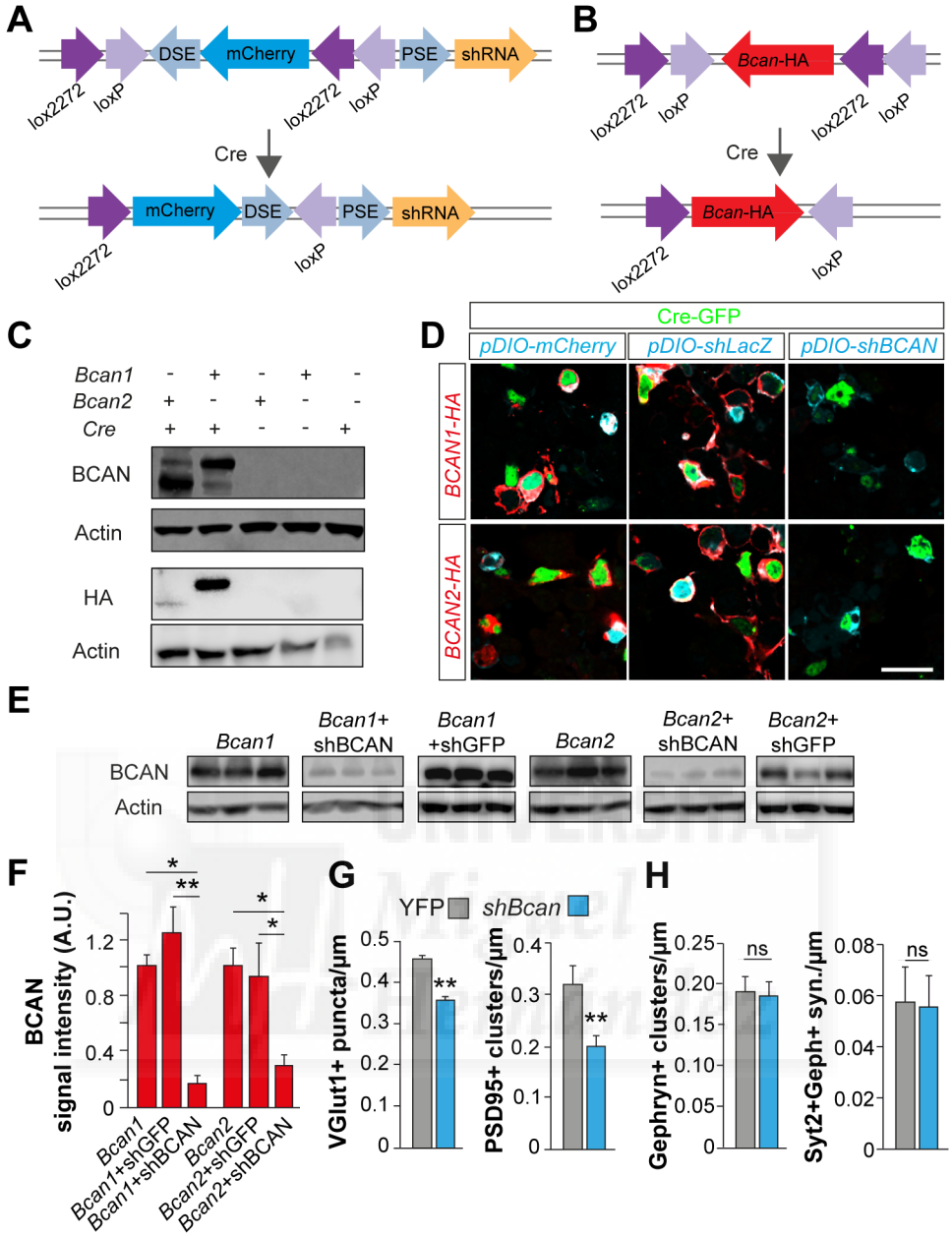

Figure S4. Strategy to knockdown Brevican in PV+ interneurons, related to Figure 4

(A and B) Diagram of the AAV cre-dependent constructs expressing *mCherry* and *shBcan* (A), or Brevican isoforms tagged with HA (B).

(C) Representative immunoblots from HEK293T cells co-transfected with *Cre-GFP* and *Brevican1-HA* or *Brevican2-HA* (n = 2 independent wells).

(D-F) Representative immunocytochemistry images (D) and immunoblots (E and F) illustrating downregulated Brevican expression upon co-transfection with plasmids expressing *shRNA* for Brevican (shBCAN). Cells were co-transfected with *Cre-GFP*, *shBrevican*, and *Bcan1-HA* or *Bcan2-HA*; n = 6 independent wells except *Bcan1*+shGFP and *Bcan1*+shBCAN where n = 9. Kruskal-Wallis test for *Bcan1* and one-way ANOVA for *Bcan2*. Scale bar 20 µm.

(G) Density of VGlut1+ boutons (n = 67 WT cells and 45 Brevican KD cells, from 5 mice) and PSD95+ clusters (n = 22 WT cells and 23 Brevican KD cells, from 3 mice) contacting the soma of PV+ cells. Student t-test.

(H) Density of Gephyrin+ clusters and Syt2+Gephyrin+ synapses (n = 28 WT cells and 25 Brevican KD cells, from 3 mice) contacting the soma of PV+ cells. Mann-Whitney test.

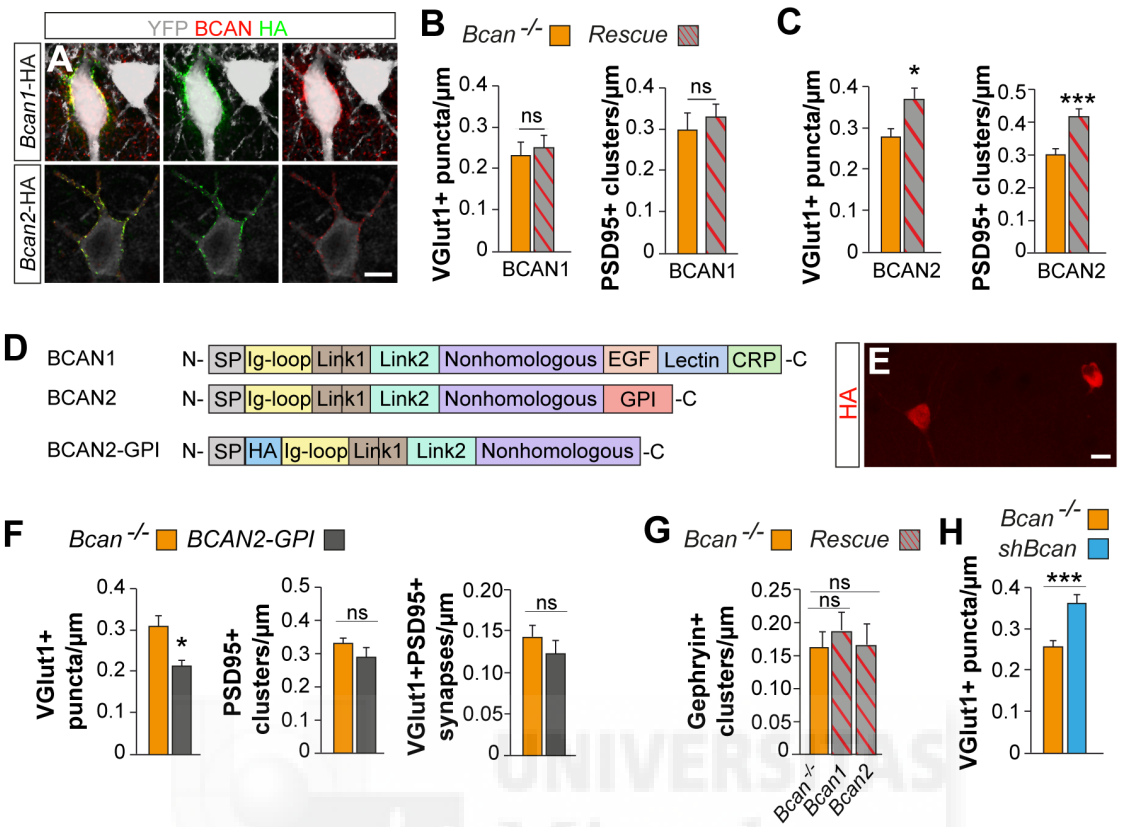
YFP BCAN HA
A
Bcan1-HA
Bcan2-HA
B
Bcan -/-
Rescue
VGlut1+ puncta/µm
PSD95+ clusters/µm
ns
BCAN1
C
*
***
BCAN2
D
BCAN1 N- SP Ig-loop Link1 Link2 Nonhomologous EGF Lectin CRP -C
BCAN2 N- SP Ig-loop Link1 Link2 Nonhomologous GPI -C
BCAN2-GPI N- SP HA Ig-loop Link1 Link2 Nonhomologous -C
E
HA
F
BCAN2-GPI
VGlut1+ puncta/µm
PSD95+ clusters/µm
VGlut1+PSD95+ synapses/µm
G
Gephryin+ clusters/µm
Bcan1
Bcan2
H
shBcan
***

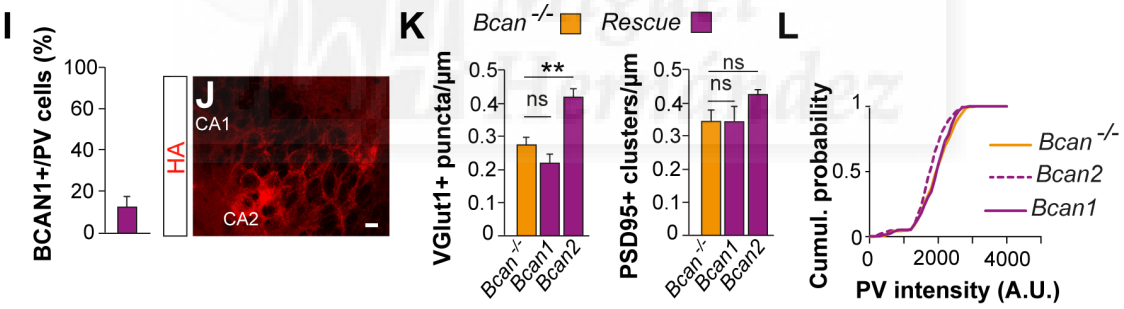
I
BCAN1+/PV cells (%)
HA
J
CA1
CA2
K
Bcan -/-
Rescue
VGlut1+ puncta/µm
PSD95+ clusters/µm
**
ns
L
Cumul. probability
Bcan -/-
Bcan2
Bcan1
PV intensity (A.U.)

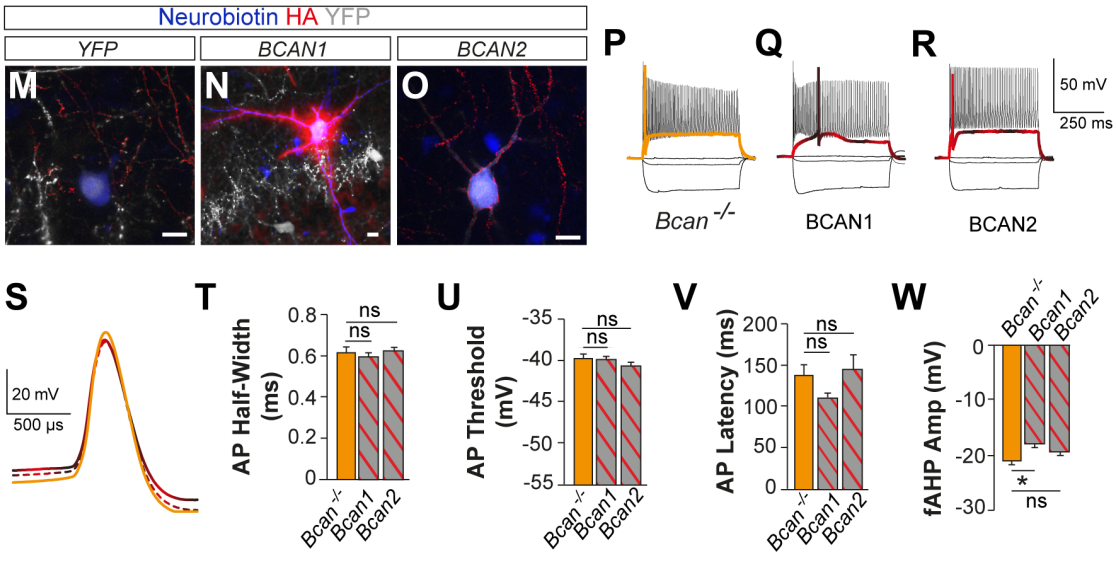
Neurobiotin HA YFP
YFP
BCAN1
BCAN2
M
N
O
P
Q
R
50 mV
250 ms
Bcan -/-
BCAN1
BCAN2
S
20 mV
500 µs
T
AP Half-Width (ms)
U
AP Threshold (mV)
V
AP Latency (ms)
W
fAHP Amp (mV)
Bcan1
Bcan2

Figure S5. Overexpression of Brevican in PV+ interneurons and astrocytes, related to Figure 5

(A) Representative images of PV+ interneurons infected *in vivo* with AAVs expressing *Brevican1-HA* or *Brevican2-HA* and immunostained with BCAN antibody.

(B) Density of VGlut1+ boutons (n = 25 *Bcan*$^{-/-}$cells and 23 BCAN1 rescued cells, from 5 mice) and PSD95+ clusters (n = 40 WT cells and 40 BCAN1 rescued cells, from 5 mice) contacting the soma of PV+ cells.

(C) Density of VGlut1+ boutons (n = 24 *Bcan*$^{-/-}$cells and 23 BCAN2 rescued cells, from 6 mice) and PSD95+ clusters (n = 50 WT cells and 34 BCAN2 rescued cells, from 5 mice) contacting the soma of PV+ cells.

(D) Functional protein domains in BCAN1 and BCAN2 sequences and design of a BCAN2 mutant that lacks the GPI-anchor (BCAN2-GPI).

(E) Representative image showing how BCAN2-GPI is retained in the cytoplasm of PV+ cells.

(F) Density of VGlut1+ boutons, PSD95+ clusters and VGlut1+PSD95+ synapses (n = 30 *Bcan*$^{-/-}$, 21 BCAN2-GPI expressing cells, 4 mice) contacting the soma of PV+ cells.

(G) Density of Gephyrin+ clusters in *Bcan*$^{-/-}$ (n = 19 cells, 5 animals), BCAN1 (n= 13 cells, 4 animals) and BCAN2 (n = 17 cells, 3 animals) PV+ cells.

(H) Comparison between the density of VGlut1+ boutons in Brevican KD cells (45 cells, from Figure S4G) and *Bcan*$^{-/-}$ cells (49 cells, pool of data from Figure 5B and S5C).

(I) Percentage of PV+ cells that are surrounded by BCAN1-HA secreted from astrocytes infected with GFAP-CreGFP and BCAN1-HA expressing viruses.

(J) Representative image showing CA2 pyramidal neurons surrounded by BCAN1 secreted from astrocytes that had been infected with GFAP-CreGFP and BCAN1-HA Cre-dependent virus.

(K) Density of VGlut1+ boutons and PSD95+ clusters contacting the soma of PV+ cells in *Bcan*$^{-/-}$ mice infected with the control virus only (GFAP-CreGFP, n = 8 for VGlut1+ boutons and 6 mice for PSD95+ clusters) or together with BCAN1 (n = 4 mice) or BCAN2 (n = 3 mice for VGlut1+ boutons and 6 mice for PSD95+ clusters) expressing virus.

(L) Cumulative probability plots comparing PV fluorescence intensity levels in *Bcan*$^{-/-}$ mice in which astrocytes had been infected with the control virus only (GFAP-CreGFP, n = 360 cells, 6 mice) or together with BCAN1 (n = 202 cells, 4 mice) or BCAN2 (n = 227 cells, 3 mice) expressing virus. Note that neither BCAN1 nor BCAN2 were able to rescue the PV level, however the PV level in mice that overexpressed *Bcan2* in astrocytes was even lower than in *Bcan*$^{-/-}$ mice, Kolmogorov-Smirnov test ($p<0.0001$) whereas no significant differences were observed between *Bcan1* and *Bcan*$^{-/-}$ mice, Kolmogorov-Smirnov test ($p>0.05$).

(M-R) Representative images (M-O) and firing traces (P-R) for *Bcan*$^{-/-}$ (same as in Figure 3O), BCAN1 and BCAN2 overexpressing PV+ cells. (S) are insets from (P-R) illustrating the similar spike shape of *Bcan*$^{-/-}$, BCAN1 and BCAN2 rescued cells.

(T-W) Intrinsic electrophysiological properties comparing *Bcan*$^{-/-}$ (n = 53 cells, 13 mice), BCAN1 (n = 13 cells, 4 mice) and BCAN2 (n = 32 cells, 5 mice) overexpressing PV+ cells. Note that *Bcan*$^{-/-}$ cells used for comparison were a pool of the cells shown in Figure 3 and YFP+HA- cells from the injected mice. Mann-Whitney test (B, C, H, VGlut1+PSD95+ synapses in F), one-way ANOVA (G, K, U, V, W), Student t-test (F, VGlut+ boutons and PSD95+ clusters), Kolmogorov-Smirnov test (L), Kruskal–Wallis test (T). Scale bars equal 10 µm (A, E, J, M, N, O).

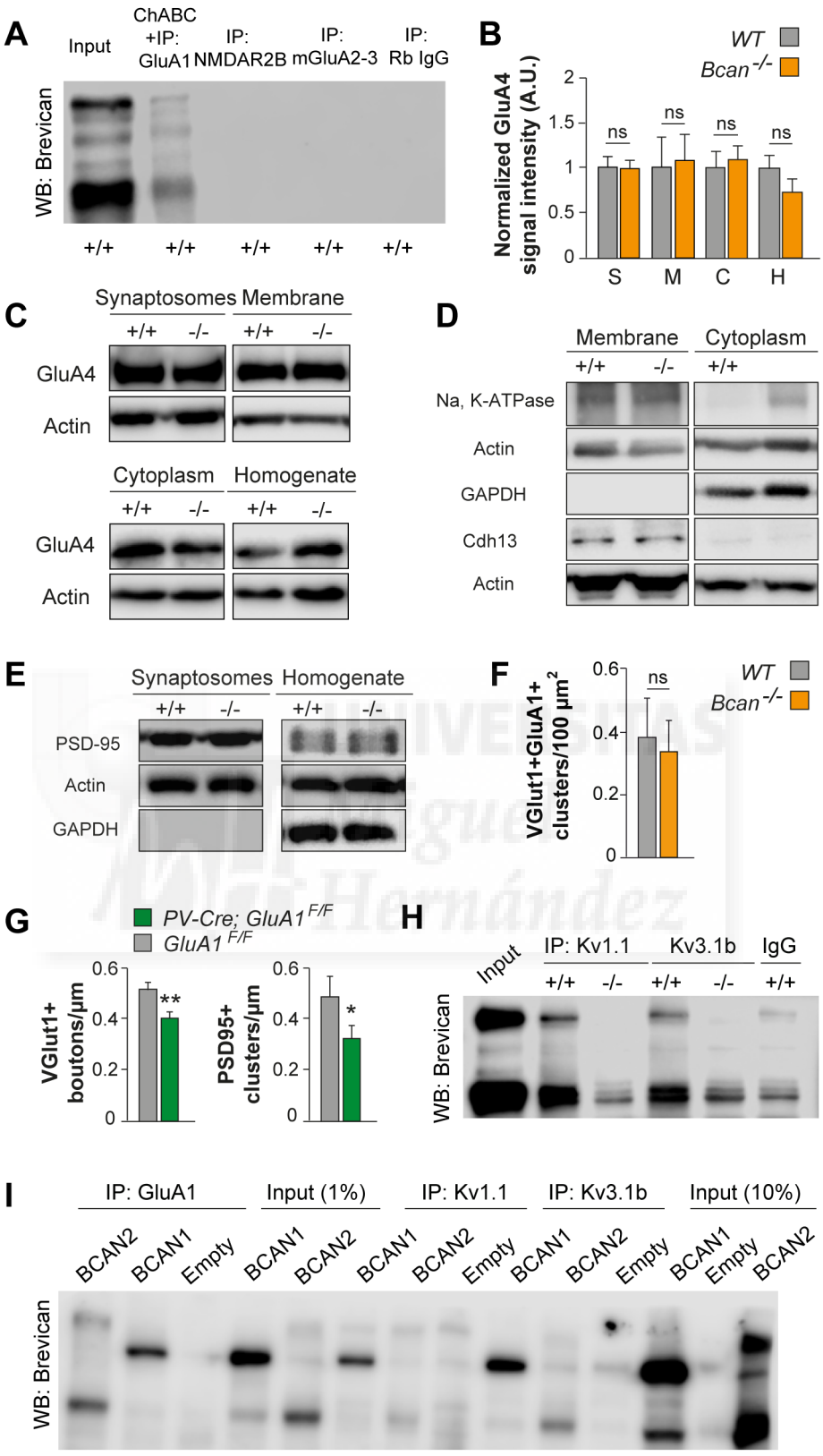

Figure S6. Role of Brevican in the late formation of excitatory synapses, related to Figure 6
(A) Representative immunoblot illustrating that pull-down of GluA1 from wild type hippocampal lysates previously digested with ChABC co-immunoprecipitates Brevican whereas pull-down of NMDA2B, mGluA2-3 or control IgG fails to co-immunoprecipitate Brevican (n = 2 Co-IP independent experiments).

(B and C) Quantification (B) and representative immunoblots (C) of GluA4 protein in the indicated cell fractions (n = 7-11 mice per genotype).
(D and E) Immunoblots of the fractionation controls showing enrichment of GAPDH in cytoplasmic fractions, of Na,K-ATPase and Cadherin13 in membrane fractions, and of PSD95 in synaptosomes.
(F) Density of GluA1+VGlut1+ clusters in the stratum radiatum of WT (n = 3 mice) and *Bcan*$^{-/-}$ (n = 3 mice) mice.
(G) Density of VGlut1+ boutons and PSD95+ clusters contacting the soma of PV+ cells in *PV-Cre; GluA1* conditional mutants (n = 10 mice) compared to controls (n = 6 mice).
(H) Representative immunoblots illustrating that pull-down of Kv1.1 and Kv3.1b from WT hippocampal lysates co-immunoprecipitate Brevican (n = 2 mice). Note that although a non-specific band is detected, the difference in its intensity indicates that Kv1.1 and Kv3.1b fail to co-immunoprecipitate Brevican in *Bcan*$^{-/-}$ hippocampal lysates.
(I) Representative immunoblots illustrating that pull-down of GluA1, Kv1.1 and Kv3.1b from *Bcan*$^{-/-}$ hippocampal lysates co-immunoprecipitate BCAN1 and BCAN2 from transfected HEK cells (n = 1 Co-IP experiment from 2 independent transfections.
Student t-test (B) and Mann-Whitney test (F and G).

UNIVERSITAS Miguel Hernández

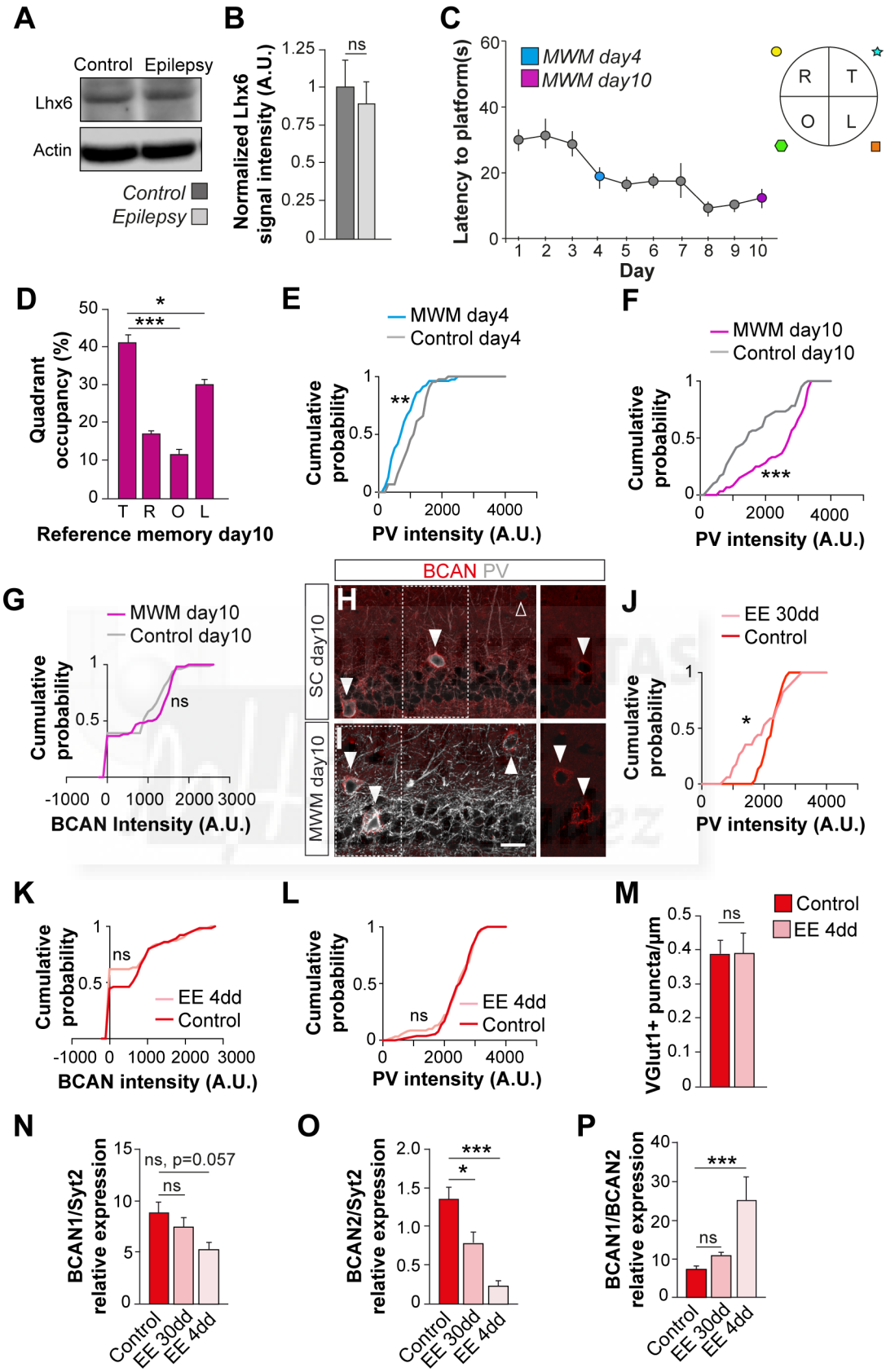

Figure S7. Experience can modify PV and Brevican expression, related to Figure 7

(A and B) Representative immunoblots (A) and analysis (B) of Lhx6 protein levels in hippocampal lysates from epilepsy patients (n = 4) compared to controls (n = 4).

(C) Morris Water maze (MWM) learning curve (symbols indicate spatial cues).

(D) Reference spatial memory on day 10 during the probe test in the Morris Water Maze (MWM) (n = 5 mice).
(E) Cumulative probability plots comparing PV fluorescence intensity levels in control (n = 44 cells, 3 mice) and MWM trained mice (n = 79 cells, 4 mice) at day 4.
(F and G) Cumulative probability plots comparing the PV (F) and Brevican (G) fluorescence intensity levels in control (n = 60 cells, 4 brains) and MWM trained (n = 60 cells, 4 mice) mice after 10 days.
(H and I) Representative images illustrating Brevican levels in the hippocampus of mice that were trained for 10 days in the MWM compared to swimming controls. Full arrowheads show colocalization, open arrowheads show no colocalization. Scale bar, 20 μm.
(J) Cumulative probability plots comparing PV fluorescence intensity levels in control (n = 30 cells, 3 mice) and mice housed in an enriched environment (EE) for 30 days (n = 34 cells, 3 mice).
(K and L) Cumulative probability plots comparing Brevican (K, n = 65 control, 63 EE cells) and PV (L, 183 control, 149 EE cells) fluorescence intensity levels in control (5 mice) and mice housed in an enriched environment (EE) for 4 days (5 mice).
(M) Density of VGlut1+ boutons contacting the soma of PV+ cells in control (n = 3 mice) and mice housed in an enriched environment (EE) for 4 days (3 mice).
(N and O) *Bcan1* (N) and *Bcan2* (O) mRNA expression relative to that of Syt-2 in control (n = 5 mice) and in mice housed in an enriched environment (EE) for 4 (n = 5 mice) and 30 (n = 5 mice) days.
(P) Ratio between the mRNA expression of *Bcan1* and *Bcan2* in control (n = 5 mice) and mice housed in an enriched environment (EE) for 4 (n = 5 mice) and 30 (n = 5 mice) days.
Mann-Whitney test (B, M), Kolmogorov-Smirnov test (E, F, G, J, K, L), and one-way ANOVA (D, N, O, P).

UNIVERSITAS Miguel Hernández

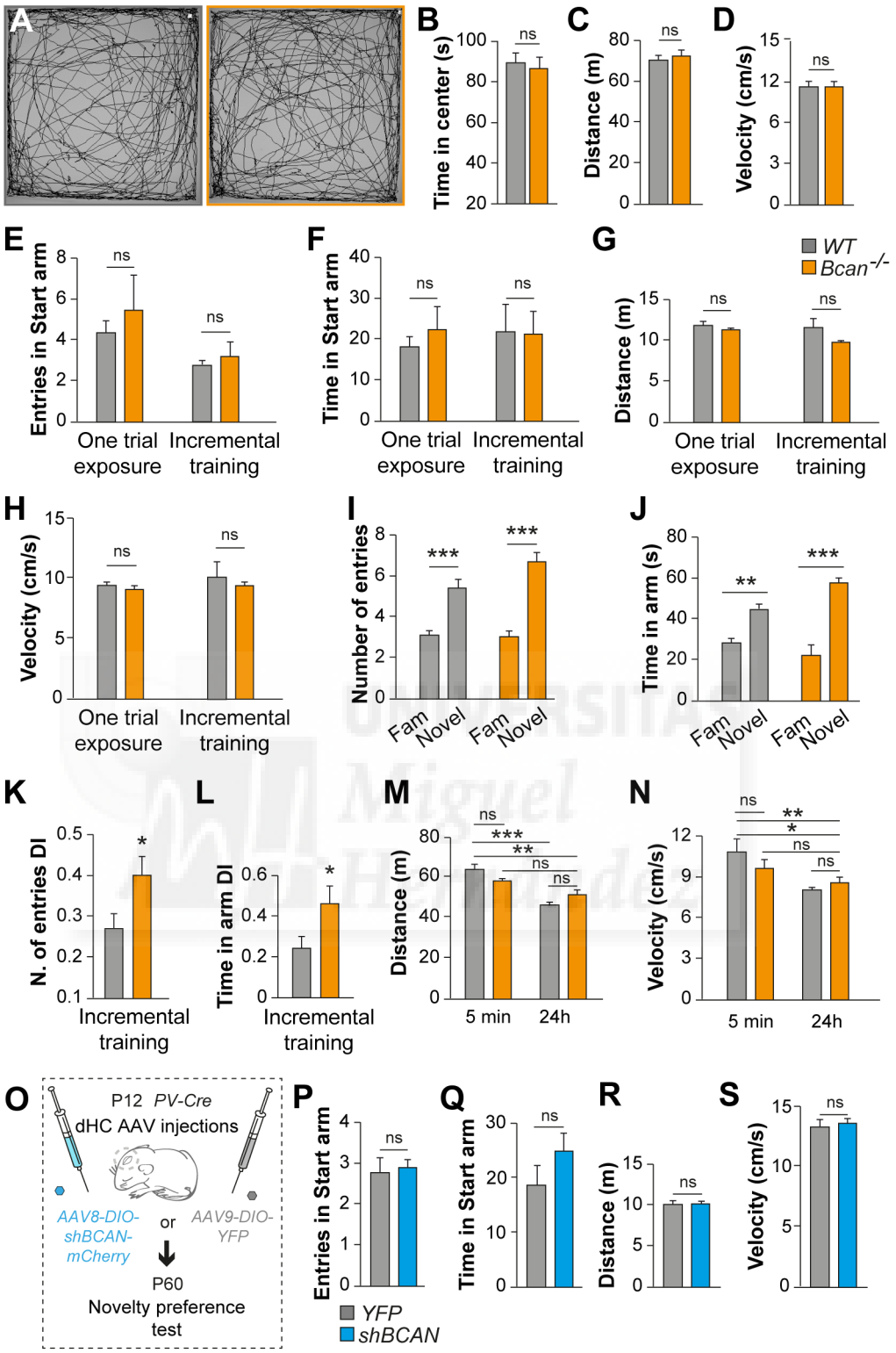

Figure S8. Brevican deletion does not affect spontaneous locomotor activity, related to Figure 8

(A-D) Behavior of wild type (WT, n = 19) and *Bcan*$^{-/-}$ (n = 20) mice showing representative movement paths of individual mice (A), as well as time spent in the center (B), total distance traveled (C) and velocity (D) across the entire session in the open-field. ns: no significant difference.

(E-H) Analysis of the one trial and incremental exposure novelty preference test showing the number of entries (E), time spent (F) distance traveled and velocity (H) in the "start" arm (n = 5

mice per genotype). Number of entries made in the “familiar” and “novel” arms (I), the total time spent in the “familiar” and “novel” arms (J), and the discrimination index for the number of entries (K) and the time spent in the arms (L), for WT (n = 11) and *Bcan*$^{-/-}$ (n = 10) mice.
(M and N) Distance traveled and velocity for WT and *Bcan*$^{-/-}$ mice during the novel object recognition test after 5 minutes ITI (n = 19 WT and n = 20 *Bcan*$^{-/-}$) and 24 hours ITI (n = 18 WT and n = 16 *Bcan*$^{-/-}$).
(O) Schematic illustration of the experiment shown in Figure 8N-Q. *PV-Cre* mice received multiple bilateral injections with one of the indicated AAVs in the dorsal hippocampus at P12 and were tested for the novelty preference.
(P-S) Number of entries, time spent in the “start” arm, distance traveled and velocity for WT (n = 11) and *Bcan* KD mice (n = 13) in the novelty preference test.
One-way ANOVA (E, F, G, H, I, J, M, N), Student t-test (A, K, L, R, S), and Mann-Whitney test (B, C, D, P, Q).

UNIVERSITAS Miguel Hernández

SUPPLEMENTAL TABLES

	Brevican+	Brevican-	*p* value
Vrest (mV)	-61.77 ± 0.65	-61.85 ± 1.23	0.9510
Rheobase (pA)	135.30 ± 15.62	95.62 ± 18.87	0.0520
First spike latency (ms)	183.40 ± 13.28	168.10 ± 19.17	0.4720
AP Threshold (mV)	-36.35 ± 1.02	-36.43 ± 1.04	0.9560
AP Height (mV)	62.49 ± 1.94	61.11 ± 2.22	0.6530
AP Half-Width (ms)	0.5455 ± 0.0194	0.6462 ± 0.0313	0.0130 (*)
fAHP time (ms)	1.818 ± 0.069	2.123 ± 0.096	0.0130 (*)
fAHP Amplitude (mV)	-26.83 ± 1.11	-24.91 ± 1.79	0.3420
Max FF (Hz)	148.70 ± 6.59	123.70 ± 11.35	0.0480 (*)
Adaptation (%)	19.65 ± 2.15	28.53 ± 3.18	0.0220 (*)
Input resistance (MΩ)	106.3 ± 8.0	155.4 ± 19.0	0.0320 (*)
Time constant (ms)	10.80 ± 0.59	13.95 ± 1.49	0.2600
N	22	13	

Table S1. Summary comparing the intrinsic properties of BCAN+ and BCAN- PV+ interneurons, Related to Figure 2.

Values are provided for each measurement as mean ± SEM. The column to the right indicates the p value (Student's t-test or Mann-Whitney test) of statistical comparisons for each row's variable between BCAN+ and BCAN- cells. Abbreviations: Vrest – Resting Membrane Potential, AP – Action Potential, fAhP – fast-Afterhyperpolarisation, MaxFF – Saturating Firing Frequency. N indicates number of cells in each condition.

	WT	Brevican$^{-/-}$	*p* value
Vrest (mV)	-60.67 ± 0.63	-60.40 ± 0.80	0.7965
Rheobase (pA)	151.20 ± 13.44	145.60 ± 9.92	0.3971
First spike latency (ms)	181.90 ± 11.44	132.40 ± 14.59	0.0084 (**)
AP Threshold (mV)	-36.75 ± 0.54	-40.31 ± 0.57	<0.0001 (***)
AP Height (mV)	61.64 ± 1.08	63.04 ± 1.53	0.223
AP Half-Width (ms)	0.55 ± 0.01	0.61 ± 0.03	0.0227 (*)
fAHP time (ms)	1.85 ± 0.05	2.07 ± 0.08	0.052
fAHP Amplitude (mV)	-25.45 ± 0.73	-21.72 ± 0.58	0.0004 (*)
Max FF (Hz)	158.20 ± 5.28	149.70 ± 6.15	0.3078
Adaptation (%)	20.87 ± 1.37	24.17 ± 1.82	0.1465
Input resistance (MΩ)	118.60 ± 7.14	127.00 ± 8.65	0.453
Time constant (ms)	11.58 ± 0.56	11.97 ± 0.79	0.9433
N	63	41	

Table S2. Summary comparing the intrinsic properties of wild-type and *Bcan-/-* PV interneurons, Related to Figure 3.

Values are provided for each measurement as mean ± SEM. The column to the right indicates the p value (Student's t-test or Mann-Whitney test) of statistical comparisons for each row's variable between wild-type (WT) and *Bcan-/-* PV interneurons. Abbreviations: Vrest – Resting Membrane Potential, AP – Action Potential, fAhP – fast-Afterhyperpolarisation, MaxFF – Saturating Firing Frequency. N indicates number of cells in each condition. The WT group includes all cells in BCAN+ and BCAN- groups (Table S1), plus 14 cells for which Brevican immunostaining was inconclusive.

	WT	shBrevican	*p* value
Vrest (mV)	-60.67 ± 0.63	-60.35 ± 1.43	<0.0001 (**)
Rheobase (pA)	151.20 ± 13.44	69.27 ± 11.16	<0.0001 (**)
First spike latency (ms)	181.90 ± 11.44	143.20 ± 13.84	0.0698
AP Threshold (mV)	-36.75 ± 0.54	-42.70 ± 0.96	<0.0001 (**)
AP Height (mV)	61.64 ± 1.08	72.56 ± 1.72	<0.0001 (**)
AP Half-Width (ms)	0.55 ± 0.01	0.99 ± 0.07	<0.0001 (**)
fAHP time (ms)	1.85 ± 0.05	6.12 ± 0.63	<0.0001 (**)
fAHP Amplitude (mV)	-25.45 ± 0.73	17.47 ± 0.99	<0.0001 (**)
Max FF (Hz)	158.20 ± 5.28	86.36 ± 9.54	<0.0001 (**)
Adaptation (%)	20.87 ± 1.37	42.73 ± 3.58	<0.0001 (**)
Input resistance (MΩ)	118.60 ± 7.14	196.30 ± 18.43	<0.0001 (**)
Time constant (ms)	11.58 ± 0.56	14.91 ± 1.13	0.0045
N	63	22	

Table S3. Summary comparing the intrinsic properties of wild-type and *Bcan* KD (shBrevican) PV interneurons, Related to Figure 4.

Values are provided for each measurement as mean ± SEM. The column to the right indicates the p value (Student's t-test or Mann-Whitney test) of statistical comparisons for each row's variable between wild-type (WT) and *Bcan* KD PV interneurons. Abbreviations: Vrest – Resting Membrane Potential, AP – Action Potential, fAhP – fast-Afterhyperpolarisation, MaxFF – Saturating Firing Frequency. N indicates number of cells in each condition. The WT group is the same as in Table S2.

Variable	Genotype	N	Mean	SEM	Test	p value	Multiple Comp. vs Bcan-/-
Vrest (mV)	Bcan -/-	53	-58.30	0.85	One-way ANOVA	0.2996	
	Bcan1 rescue	13	-59.40	1.42			
	Bcan2 rescue	32	-60.50	1.21			
Rheobase (pA)	Bcan -/-	53	154.00	10.80	Kruskal-Wallis test	0.4214	
	Bcan1 rescue	13	189.00	27.10			
	Bcan2 rescue	32	152.00	13.10			
First spike latency (ms)	Bcan -/-	53	139.00	13.50	One-way ANOVA	0.5983	
	Bcan1 rescue	13	112.00	28.30			
	Bcan2 rescue	32	147.00	16.60			
AP Threshold (mV)	Bcan -/-	53	-40.80	0.57	One-way ANOVA	0.5876	
	Bcan1 rescue	13	-40.50	0.90			
	Bcan2 rescue	32	-39.90	0.61			
AP Height (mV)	Bcan -/-	53	64.10	1.33	One-way ANOVA	0.5418	
	Bcan1 rescue	13	64.40	2.76			
	Bcan2 rescue	32	61.90	1.47			
AP Half-Width (ms)	Bcan -/-	53	0.62	0.02	Kruskal-Wallis test	0.758	
	Bcan1 rescue	13	0.59	0.02			
	Bcan2 rescue	32	0.62	0.02			
fAHP time (ms)	Bcan -/-	53	2.40	0.19	Kruskal-Wallis test	0.0001	
	Bcan1 rescue	13	2.82	0.35			0.0257 (*)
	Bcan2 rescue	32	2.83	0.16			0.0001 (***)
fAHP Amplitude (mV)	Bcan -/-	53	-20.80	0.61	One-way ANOVA	0.0309	
	Bcan1 rescue	13	-17.90	0.65			0.0402 (*)
	Bcan2 rescue	32	-19.50	0.48			0.2161
Max FF (Hz)	Bcan -/-	53	138.00	6.56	One-way ANOVA	0.9467	
	Bcan1 rescue	13	134.00	11.80			
	Bcan2 rescue	31	138.00	7.76			
Adaptation (%)	Bcan -/-	53	-19.30	2.00	One-way ANOVA	0.0183	
	Bcan1 rescue	13	-30.80	3.96			0.0219 (*)
	Bcan2 rescue	31	-25.70	2.62			0.0526
Input Resistance (MΩ)	Bcan -/-	53	130.00	8.82	Kruskal-Wallis test	0.4686	
	Bcan1 rescue	13	122.00	16.20			
	Bcan2 rescue	32	143.00	11.50			
Time constant (ms)	Bcan -/-	53	13.00	0.94	Kruskal-Wallis test	0.6804	
	Bcan1 rescue	13	12.30	1.11			
	Bcan2 rescue	32	11.30	0.88			
V-Sag (mV)	Bcan -/-	52	-3.81	0.38	Kruskal-Wallis test	0.6961	
	Bcan1 rescue	13	-5.03	1.03			
	Bcan2 rescue	32	-3.97	0.49			

Table S4. Summary comparing the intrinsic properties of *Bcan-/-*, BCAN1 and BCAN2 overexpressing PV interneurons, Related to Figure 5.

Values are provided for each measurement as mean ± SEM. The columns to the right indicate the p value (one-way ANOVA or Kruskal–Wallis test) of statistical comparisons for each row's variable between *Bcan-/-*, BCAN1, and BCAN2 overexpressing PV interneurons followed by Holm-Sidak's multiple comparison test when significant differences were found. Abbreviations: Vrest – Resting Membrane Potential, AP – Action Potential, fAhP – fast-Afterhyperpolarisation, MaxFF – Saturating Firing Frequency. N indicates number of cells in each condition. The *Bcan-/-* group includes all cells in *Bcan-/-* group from Table S2, plus 12 YFP+HA- cells from the injected mice.

UNIVERSITAS
Miguel
Hernández

APPENDIX

In the second part of the thesis, we have shown that cell-type specific expression of Brevican in PV+ cells critically specifies intrinsic properties and glutamatergic afferent synapse maturation, and also impacts mouse behavior (Figure Ax1). In response to activity, Brevican mediates cellular and synaptic forms of plasticity in PV+ interneurons by regulating the localization of potassium channels and AMPA receptors, respectively (Figure Ax1).

In this appendix, we will present and discuss preliminary or conflicting results not included in the published article but also additional data that could guide future studies further investigating the underpinnings of interneuron plasticity.

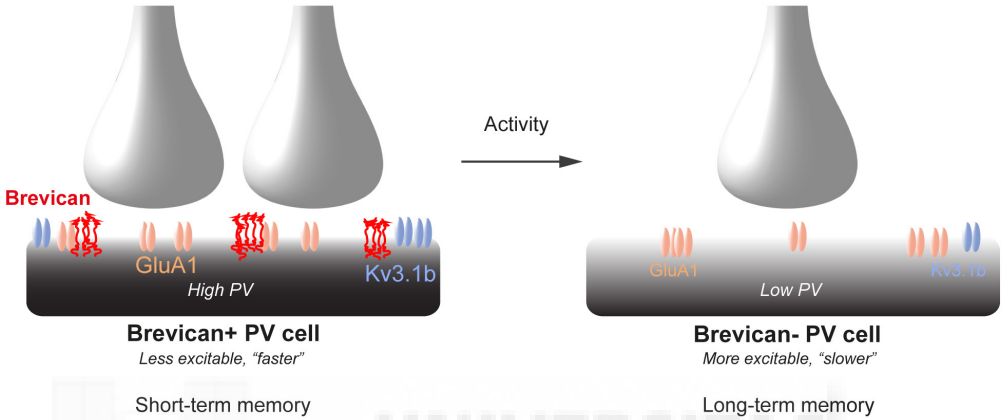

Figure Ax1. Working model illustrating the function of Brevican.
This model summarizes and visually integrates the results showed in Part 2 of this thesis. Brevican simultaneously regulates cellular and synaptic plasticity of PV cells. *Bcan* expressing cells receive more excitatory inputs and have specific, tunable, intrinsic properties. Brevican is located at the periphery of the excitatory synapses where it interacts with Kv3.1b-containing channels and with GluA1 subunits, and regulates GluA1 activity-dependent synaptic delivery thus promoting the maturation of excitatory synapses. Upon experience, Brevican senses changes in activity and orchestrates molecular rearrangements that underlie different types of memory.
(B) Same model as in (A) but including a complement of proteins that, based on the results of the proteomic screening, might interact with Brevican and participate in regulating the maturation of excitatory synapses at the postsynaptic side. The model also includes putative Brevican interactors that might mediate a presynaptic, GluA1-independent, role of Brevican.

RESULTS AND DISCUSSION

1. PV+ cells secrete their own Brevican sheath in vitro

Brevican is found around the soma of PV+ interneurons which, like glial cells, also express *Bcan* mRNA (Figure 1). *In vivo* overexpression of *Bcan1* and *Bcan2* in astrocytes led to the accumulation of both proteins around PV+ cells (Figure 5), suggesting that astrocytes are a potential additional source of Brevican. To explore whether endogenous (as opposed to overexpression) levels of Brevican expression also lead to its secretion into the PNNs by glial cells, we generated mosaic primary hippocampal cultures from wild type and *Bcan* mutant embryos (Figure Ax2A). We used a PV green fluorescence protein (GFP) reporter (*PV-Cre;RCE*) to identify wild type interneurons so that the cultures contained both GFP+ (wild type) and GFP- (*Bcan* mutant) PV+ interneurons (Figure Ax2A). Immunohistochemical staining for glial fibrillary

acidic protein (GFAP) confirmed the presence of astrocytes in the cultures (Figure Ax2B). Consistent with our *in vivo* analysis (Figure 1), we observed that Brevican encapsulated 64% of wild type PV+ interneurons (GFP+) (Figures Ax2C, 2D). In contrast, all *Bcan* mutant PV+ interneurons (GFP-) lacked a Brevican case (Figures Ax2C, 2D), suggesting that PV+ basket cells may be the main source of their own Brevican sheath.

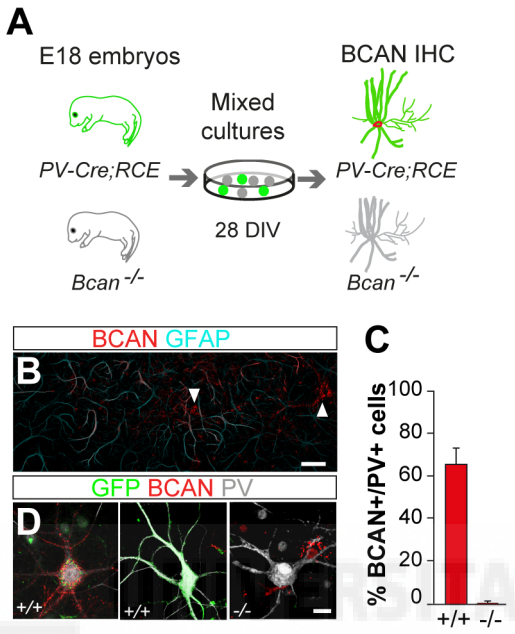

Figure Ax2. PV+ cells secrete their own Brevican sheath *in vitro*.
(A) Experimental design of the mosaic primary hippocampal cultures.
(B) Representative image showing GFAP+ astrocytes in the mixed cultures. The arrowheads point to BCAN+ cells. Scale bar equal 50 µm.
(C and D) Percentage (C) and representative images (D) of wild type (WT, PV+GFP+) and *Bcan*$^{-/-}$ cells (PV+GFP-) enwrapped by Brevican (290 cells, n = 3 experiments). Scale bar equal 20 µm.

Discussion of the results

The *in vivo* astrocyte-rescue experiments showed that astrocytes might be a second source of Brevican protein found around PV+ interneurons. These findings are challenged by our *in vitro* results from the mixed primary cultures. In this experiment, Brevican did not enclose mutant PV+ interneurons, in spite of having neighboring wild-type astrocytes that expressed normal Brevican levels. Given the relatively low number of PV+ interneurons that survive *in vitro*, one possible reason is that we missed BCAN+ PV+ cells in the mixed culture experiments. Alternatively, the *in vitro* system may not have been appropriate to allow accumulation of Brevican from wild-type astrocytes around mutant PV+ cells. In terms of yield, the optimal age to obtain astroglial-enriched primary cultures is while astrogenesis peaks; in mice, this window spans a period from 2-3 days prenatal to 2-3 days postnatal for cortex and most CNS regions (Conn, 1990). Since our cultures were obtained from E18 embryos and we consistently observed astrocytes in our mixed cultures, it is unlikely that the lack of BCAN+ PV+ mutant cells is due to a low number of *Bcan*-expressing astrocytes. A more probable explanation is that the aggregation of astrocytic Brevican around PV+ cells requires both cell types to be embedded in the ultrastructural microenvironment of the brain. Indeed, the astrocyte

rescue experiments showed that both BCAN1 and BCAN2 can be released from astrocytes and deposited in the neighboring tissue perhaps waiting for its potential target. Therefore, the lack of surrounding brain tissue in the *in vitro* system may have contributed to the failed detection of BCAN+ mutant cells. This shall constitute a warning that primary cultures —widely used to study perineuronal nets (Hedstrom et al., 2007; John et al., 2006; Valenzuela et al., 2014)— may instead not constitute an appropriate system to investigate their development and function.

However, we cannot rule out that the localization of astrocytic Brevican around PV+ cells is the consequence of its over- rather than endogenous expression. By definition, overexpression leads to particularly high protein levels that may not recapitulate the localization of endogenous Brevican produced by astrocytes. Although not conclusive, the astrocyte-rescue experiments suggested a very interesting scenario, that a coordinated expression of Brevican from PV+ cells and astrocytes regulates excitatory synapse development onto PV+ cells as well as PV+ cell function. More importantly, they provide a framework for future work addressing the consequences of *Bcan* knock-down in astrocytes. These studies will help not only to solve the inconsistency between the *in vitro* and *in vivo* experiments but also to examine in more detail the potential contribution of astrocyte to the *Bcan* mutant phenotype.

2. Unbiased, proteomics-based identification of synaptic Brevican interactors

Although BCAN2 expression in PV+ cells fully rescued the density of GluA1 synaptic clusters and the number of excitatory synapses, it only partially rescued the presynaptic phenotype (Figures 6M, 5L and S5C). Similarly, when overexpressed in astrocytes, BCAN2 restored the presynaptic phenotype and the density of VGlut+PSD95+ synapses but did not rescue the density of PSD95+ clusters (Figures 5X and S5K). These observations raised the possibility of an additional presynaptic mechanism by which Brevican from PV cells, and potentially astrocytes, may regulate the excitatory inputs that contact PV interneurons. Supporting this idea, analysis of the axial distribution of Brevican using three-color STORM microscopy showed that it was located both pre- and postsynaptically (Figure 1O-1R). It is, therefore, conceivable to hypothesize that Brevican may also have a presynaptic binding partner and that its synaptic role may extend beyond the regulation of GluA1.

To identify candidate Brevican interactors, we took an unbiased, discovery-based approach (Savas et al., 2014). We purified a recombinant ecto-Fc protein for BCAN1 and used it to identify interacting proteins in detergent-solubilized whole-brain homogenate from 3- to 4-week-old rats by affinity chromatography (Ecto-Fc MS experiment, performed by Joris de Wit & Jeff Savas, VIB Center for the Biology of Disease, K.U. Leuven). Bound proteins were then analyzed by tandem mass spectrometry (MS/MS). The resulting list of putative binding partners was ranked by spectral counts (a measure of protein abundance) and only proteins with a spectral count higher than 2 were considered for further analysis. We then filtered the list by eliminating known MS/MS contaminants (Weber et al., 2012) and proteins that copurified with the Fc protein alone. The proteomic experiment revealed a high number of putative partners (Figure Ax3A). Worth mentioning, this is an *in vitro* proteomics-based approach. As such, sharing BCAN isoforms all their domains except the GPI, proteins that bound BCAN1 in our experiment may interact with either or both BCAN isoforms *in vivo*. To have an overview of the proteins that copurified with Brevican, we performed a GO term analysis (Panther GO-Slim Cellular Component, Figure Ax3A). In addition to cytosolic proteins, which likely do not interact with Brevican *in vivo*, several extracellular matrix molecules as well as membrane and synaptic proteins bound to Brevican (Figure Ax3A).

Judging by the number of peptides and spectra hits, some proteins related to synaptic vesicle fusion and neurotransmitter release were identified as potential binding partners (Figure Ax3B). This result was unexpected because pyramidal neurons do not express *Bcan* mRNA (Figure S1) and because we found BCAN protein at the presynaptic membrane but not inside the presynaptic terminal of excitatory synapses (Figure 1P), where a vesicle-associated protein would be. A possible explanation for the presence of vesicle-related proteins in our list is that Brevican also locates to the presynaptic terminals of PV+ cells, suggesting that it might have a yet unidentified role in regulating the output of PV+ interneurons. Furthermore, we identified a few transporters (Figure Ax3C) which might be useful to better understand how BCAN1 and BCAN2 influence the firing properties of PV+ cells (Figures 3, 4 and S5) or how they both rescue the PV levels (Figures 5H-5M).

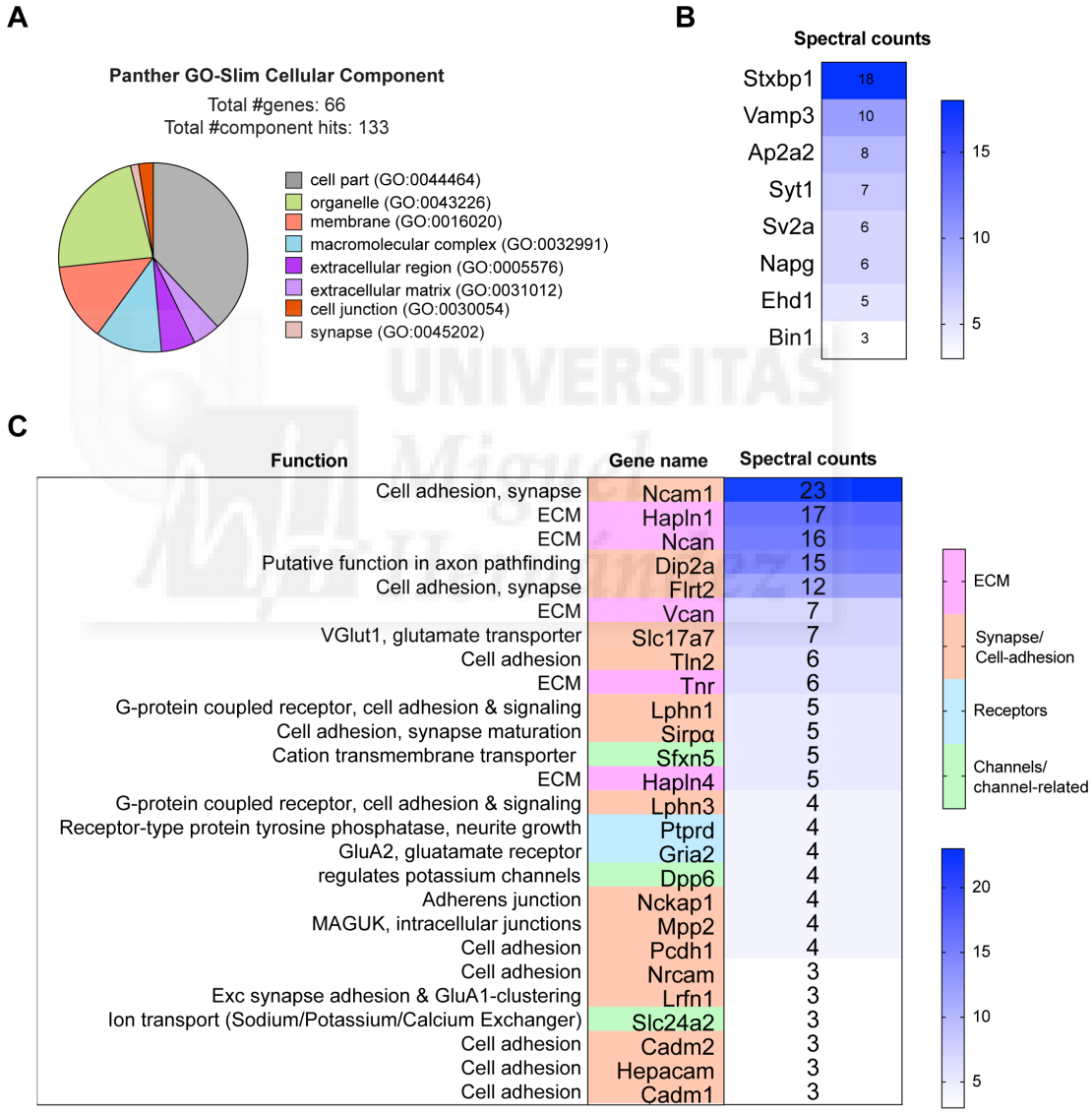

Figure Ax3. Proteomics-based identification of synaptic Brevican interactors.
(A) Gene ontology (GO) term analysis showing the cellular localization of proteins that copurified with the ectodomain of BCAN1-Fc.
(B) Heat-map showing vesicle-related proteins that selectively bound to ecto-BCAN1-Fc. The numbers inside the cell indicate the spectral counts.
(C) Heat-map showing the function and abundance of ECM molecules, receptors, ion channels, transporters, and synaptic proteins that copurified with Brevican.

Of the proteins that selectively bound to ecto-BCAN1-Fc, molecules involved in cell-cell interaction and synapse development were the most abundant (Figure Ax3C). Among the postsynaptic proteins that co-purified with Brevican, MPP2 is a molecular constituent of AMPA receptor complexes (Rademacher et al., 2016). LRFN/SALM2 controls the clustering of several postsynaptic proteins, including GluA1 receptors, and is an important regulator of the differentiation of excitatory synapses (Ko et al., 2006). A particularly abundant protein that co-purified with the ectodomain of BCAN1 is Dip2a, a cell-surface receptor whose function has not been studied in the mammalian brain. Moreover, we identified the presynaptic receptors LPHN1and LPHN3 as well as the postsynaptic ligand FLRT2 as putative Brevican interactors (Figure Ax3C). Since the interaction between Latrophilins (LPHNs) and fibronectin leucine-rich repeat transmembrane (FLRT) proteins mediates excitatory synapse development (Jackson et al., 2015; O'Sullivan et al., 2012; de Wit and Ghosh, 2014), Brevican binding to LPHNs-FLRTs may be relevant for its synaptic role. An interesting molecule that stood out as candidate Brevican presynaptic binding partner is SIRPα. Remarkably, activity-dependent regulation of SIRPα drives the maturation of the presynaptic terminal (Toth et al., 2013). Another potential presynaptic partner of Brevican is Talin2 that is found at the presynapse where it regulates synaptic vesicle endocytosis (Morgan et al., 2004). Finally, neural cell adhesion molecule NCAM was the most abundant protein identified as potentially binding Brevican. NCAM is expressed both pre- and postsynaptically and plays key roles in excitatory synapse formation, maturation, maintenance, and plasticity (Südhof, 2006). All these putative post- and presynaptic interactors are of particular interest not only because they could complement our understanding on how Brevican regulates the synaptic delivery of GluA1-containing receptors at the postsynapse but also because they may shed light on possible additional presynaptic mechanisms by which Brevican regulates synapse maturation. Although validation will be required, our proteomic database provides a useful tool to further explore the role of Brevican in the regulation of neural circuit maturation and plasticity.

Discussion of the results

The unbiased search for proteins that interact with Brevican *in vitro*, allowed us to identify putative new players involved in the molecular rearrangements orchestrated by Brevican at the excitatory synapses of PV+ cells. Specifically, this approach revealed neural cell adhesion molecule NCAM as a strong candidate Brevican partner. NCAM is the first described member of cell adhesion molecules from the immunoglobulin superfamily and is involved in almost all aspects of synapse development, function, and remodeling (Berezin, 2010; Südhof, 2006). NCAM polysialylated form (PSA-NCAM) exhibits de-adhesive properties and critically regulates activity-dependent synaptic remodeling, neuron-glia interactions, as well as learning and memory (Bonfanti and Theodosis, 2009; Senkov et al., 2012; Sytnyk et al., 2006, 2017). In addition to interacting homophilically with each other, NCAM molecules bind and regulate ion channels, cytokine and neurotransmitter receptors, including AMPA receptors (Potschka et al., 2008; Vaithianathan et al., 2004).

Worth mentioning, NCAM also controls inhibitory PV+ synapse formation onto pyramidal neurons (Chattopadhyaya et al., 2013). Since there are major differences between the effect of NCAM deficiency on excitatory synapse development (Dityatev et al., 2000) and the phenotype observed in absence of Brevican, NCAM and Brevican are more likely to interact at the PV+ inhibitory synapses contacting pyramidal neurons. As we did not investigate if Brevican plays a role in regulating the development of the output

of PV+ interneurons onto pyramidal cells, the functional significance of this NCAM-BCAN putative interaction has yet to be explored.
How could BCAN and NCAM work together? Previous work showed that PSA-NCAM interacts with chondroitin sulfate proteoglycans (CSPGs), such as Neurocan and Phosphacan (Senkov et al., 2012), although the biological significance of these interactions is not well understood (Berezin, 2010). NCAM can interact with both chondroitin sulfate chains and the core protein of PNN molecules, and the resulting effect – adhesion or repulsion – seems highly dependent on the context (Berezin, 2010). Brevican expression is regulated by activity and, similarly, delivery of PSA-NCAM to the cell surface is activity-dependent (Kiss et al., 1994; Muller et al., 1996). In addition, BCAN can occur as both CSPG and CS-free non-proteoglycan (Seidenbecher et al., 2002). Accordingly, the biological responses upon interactions between these two molecules will reflect the local balance between them and their post-translational modifications, providing a mechanism for fine-tuning processes like synapse development and plasticity. One possibility is that CS-BCAN may prevent PSA-NCAM molecules from clustering too densely. Alternatively, Brevican might competitively inhibit both hemophilic and heterophilic NCAM interactions. A third possible scenario is that NCAM-BCAN interaction works as a “trap” to allow peripheral accumulation of synaptic proteins. The increase in neuronal activity may, therefore, function as a switch: NCAM polysialylation and/or BCAN downregulation would uncage these synaptic molecules allowing them to diffuse at the synapse. More experiments will be needed to verify these hypotheses and the role of such potential BCAN-NCAM complexes in synapse development and plasticity.

The proteomic screening also revealed potential candidates mediating a presynaptic role of Brevican at the excitatory synapses. Of all presynaptic putative Brevican partners, SIRPα appears as the most prominent because it bears remarkable resemblances to Brevican. SIRPα is a target-derived glutamatergic presynaptic organizer in the hippocampus that, like Brevican, (1) is enriched at excitatory, but not inhibitory, synapses and (2) is regulated by activity. (3) SIRPα functions in late but not early stages of excitatory synapse development and it regulates (4) the number and size of VGlut1 puncta as well as (5) the frequency, but not the amplitude, of miniature excitatory postsynaptic currents (mEPSCs). In addition, (6) SIRPα does not control PSD95 clustering, although (7) it does influence the colocalization between VGlut1 and PSD95 (Toth et al., 2013). Strikingly, the *Bcan2* astrocyte-rescue of the density of excitatory synapses onto PV+ cells that we observed in *Bcan* mutants closely mirrors the function of SIRPα. It is therefore tempting to hypothesize that astrocyte-derived Brevican might target SIRPα at the excitatory synapses contacting PV+ interneurons and thus promote their presynaptic maturation.

The fibronectin leucine-rich repeat transmembrane (FLRT) protein FLRT2 was one of the most abundant proteins that copurified with BCAN in our Ecto-Fc MS experiment. FLRT proteins are cell-adhesion molecules that regulate cortical development and synapse formation. Their extracellular regions interact with Latrophilins (LPHNs) to mediate synapse development and with Uncoordinated-5 (UNC5)/netrin receptors to control the migration of neurons in the developing cortex (Lu et al., 2015). Although FLRTs seem to regulate early stages of synapse assembly (de Wit and Ghosh, 2014), it is possible that they also have a yet unidentified role in synapse maturation. The presence of Latrophilin3 (LPHN3), one of the presynaptic receptors for FLRT2 (Lu et al., 2015), in the list of putative Brevican binding partners suggests that this may indeed be the case. In the future, it will be interesting to validate BCAN-FLRT2 binding and investigate how Brevican modulates LPHN3-FLRT2 interaction and function.

The proteomic screen also uncovered some other putative postsynaptic Brevican interactors. Remarkably, most of these proteins are related to AMPA receptors, confirming the importance of GluA1 for Brevican-mediated regulation of excitatory inputs onto PV+ interneurons. The absence of GluA1 in our list could be explained by the limitations of Ecto-Fc MS which is particularly weak at identifying low-affinity interactions (Savas et al., 2014). Alternatively, the ecto-Fc proteins might be saturated by highly expressed binding partners and may not copurify detectable amounts of less abundant proteins (Savas et al., 2014). Nevertheless, it is important to mention that we were able to copurify the GluA2 subunit of AMPARs which we also previously identified as a Brevican binding partner (Figure 6A). Of all postsynaptic putative Brevican partners, LRFN/SALM2 appears of particular interest because of the similarities it shares with Brevican. LRR and Fibronectin Type III Domain Containing proteins (also known as Synaptic Cell Adhesion-Like proteins; LRFN/SALM1–5) were identified as PSD-family-interacting proteins (Ko et al., 2006; Morimura et al., 2006; Wang et al., 2006). Alike Brevican, the role of SALM2 in synapse maturation is restricted to excitatory, but not inhibitory, synapses and is executed by regulating GluA1 clustering (Ko et al., 2006). In addition to the observation that both Brevican and SALM2 selectively regulate the density of excitatory synapses via a GluA1-dependent mechanism, SALM2 knockdown leads to a phenotype that is strikingly comparable to that of Brevican deficiency: it reduces the number of excitatory synapses and the frequency, but not amplitude, of mEPSCs (Ko et al., 2006). The regulation of SALM2 might, therefore, be the mechanism by which Brevican regulates GluA1-subunit synaptic delivery. In addition, the role of SALM proteins in regulating synapse function is still largely unknown and their trans-synaptic binding partners have not been identified. It is, therefore, appealing to hypothesize that Brevican might also link SALM2 to its receptor on the presynaptic membrane. Future studies confirming and further investigating the physical and functional interaction of Brevican with SIRPα, LPHN3-FLRT2, and SALM2 (Figure Ax4) will broaden our knowledge about how the excitatory drive of PV+ interneurons in the mature neural circuits is finely shaped.

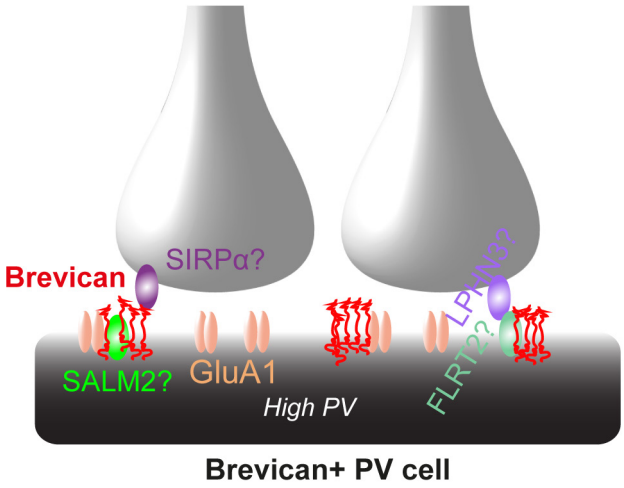

Figure Ax4. Working model illustrating putative pre- and postsynaptic Brevican interactors. Similar model as in FigureAx2 but including a complement of proteins that, based on the results of the proteomic screening, might interact with Brevican and participate in regulating the maturation of excitatory synapses at the postsynaptic side. The model also includes putative Brevican interactors that might mediate a presynaptic, GluA1-independent, role of Brevican.

3. Role of Brevican at the PV+ cell output

The presence of NCAM and the relatively high number of vesicle-related proteins found in the Ecto-Fc MS screening suggested a possible role of Brevican in the regulation of the outputs of PV+ interneurons. Brevican is not involved in regulating PV+ synapse onto other PV+ cells (Figure S3), but it may control the development of PV+ inhibitory synapses contacting pyramidal cells. To investigate whether the lack of Brevican affects the outputs of the PV+ interneurons, we assessed the density and distribution of Syt2+ presynaptic inputs, postsynaptic Gephyrin+ clusters and alpha1-containing $GABA_A$ receptors (α1-$GABA_A$Rs), as well as their colocalization at the pyramidal cell soma (Figures Ax5A-5H). Quantitative analysis revealed that, although the average density of presynaptic inputs and postsynaptic clusters did not change, their relative frequency was altered in opposite directions (Figures Ax5I-5M): the distribution of Syt2+ boutons was slightly shifted towards lower values, whereas the distribution of postsynaptic Gephyrin+ clusters and α1-$GABA_A$Rs was increased (Figures Ax5I, 5J, 5L). However, these pre- and post-synaptic changes did not affect the distribution of Syt2+/Gephyrin+ synapses which was similar between genotypes (Figure Ax5K). The relative frequency of α1-$GABA_A$Rs containing synapses was instead increased in *Bcan* mutants (Figure Ax5M). These findings indicate that Brevican might also have a minor role in regulating the formation of inhibitory synapses on pyramidal cells. However, since the observed increase is largely due to an alteration in postsynaptic GABAergic clusters in pyramidal cells, an alternative explanation for the observed changes might be that they are secondary to the deficits found in PV+ interneurons.

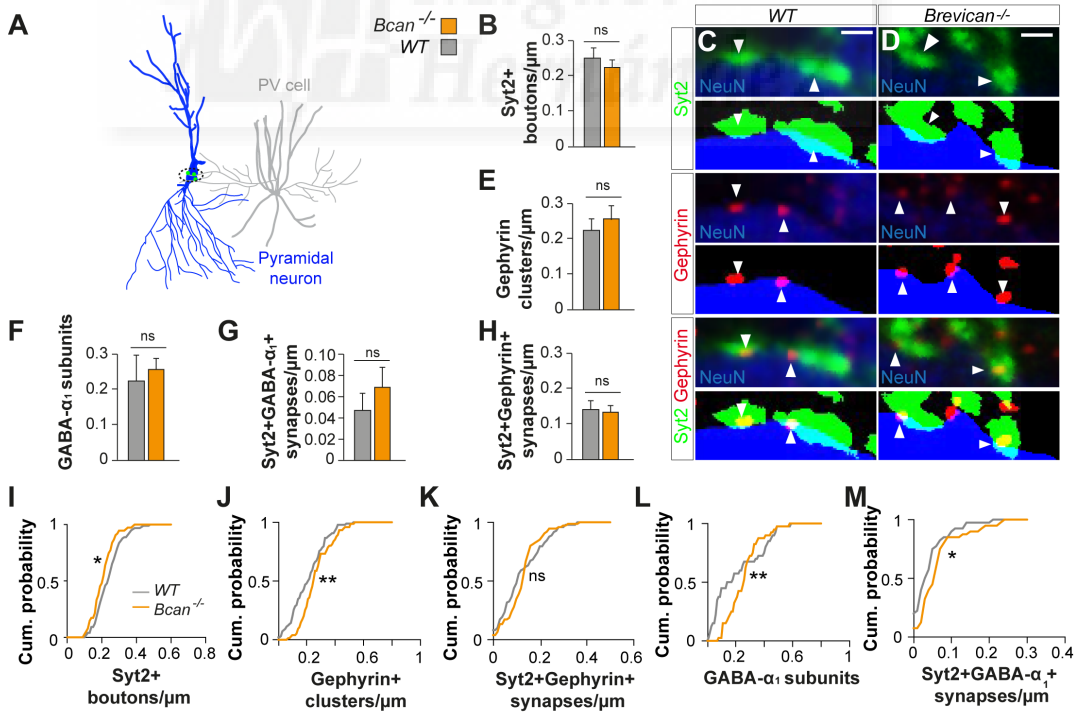

Figure Ax5. Subtle changes in PV+ inhibitory synapses contacting pyramidal cells upon *Bcan* deletion.

(A) Schematic drawing highlighting the synapses analyzed in this experiments (black ellipse).

(B-H) Synaptic density (B, E, H), representative images and their corresponding binary images (C and D) illustrating Syt2+ boutons (n= 6 WT, 4 Bcan-/-), Gephyrin+ clusters (n = 6 WT, 4 Bcan-/-)

and Syt2+Gephyrin+ synapses (n = 6 WT, 4 Bcan-/-) contacting the soma of pyramidal cells. Mann-Whitney test. Scale bars equal 0.5 µm.
(F and G) Density of α1-GABA$_A$Rs (F) and α1-GABA$_A$Rs- containing inhibitory synapses (G) in pyramidal neurons (n = 4 WT, 4 Bcan-/-). Mann-Whitney test.

4. Brevican protects PV cells against oxidative stress

The high metabolic requirements of fast-spiking cells make them susceptible to redox dysregulation and oxidative stress (Carter and Bean, 2009). In addition to their role in synaptic plasticity, perineuronal nets protect PV+ interneurons against oxidative stress (Cabungcal et al., 2013a). We reasoned that, if Brevican contributes to this neuroprotection, its absence would make PV+ cells more vulnerable to oxidative stress. To test this hypothesis, we first analyzed the levels of oxidative stress revealed by the presence of 8-oxo-7,8-dihydro-20-deoxyguanine (8-oxo-dG), a product of DNA oxidation, in *Bcan* mutants compared to controls. We observed barely detectable 8-oxo-dG immunoreactivity in both wild-type and *Bcan* mutant PV+ cells at P30 (Figure Ax6A), showing that the basal levels of oxidative stress in PV+ cells are not affected by the absence of Brevican.

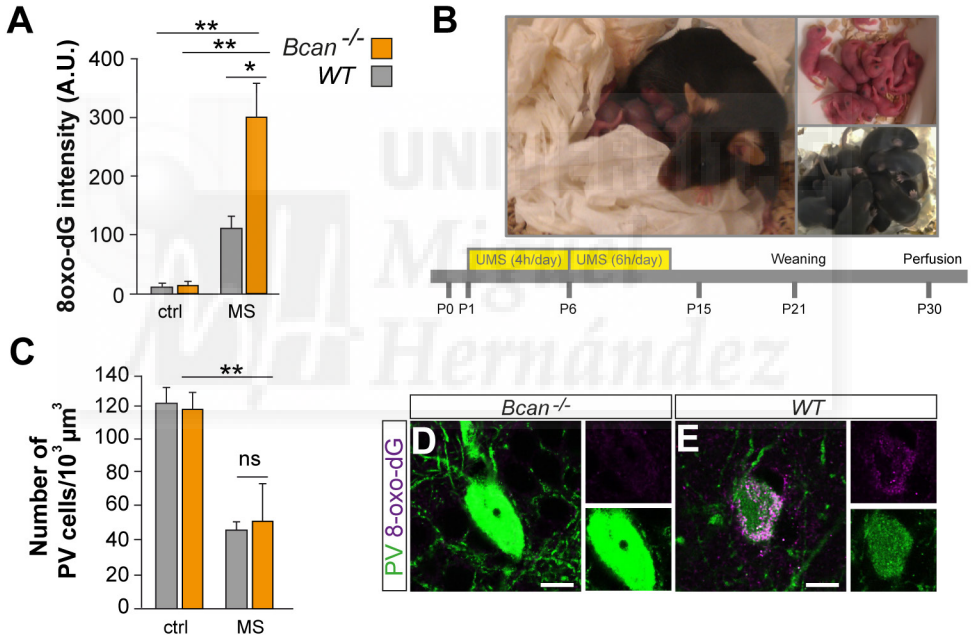

Figure Ax6. Brevican has a neuroprotective role against oxidative stress
A. Fluorescence intensity levels of 8-oxo-dG in *Bcan*-/- and wild-type mice subjected or not to maternal separation (MS) (n = 3 for each condition). One-way ANOVA followed by Sidak's multiple comparisons test.
B. Schematic of the unpredictable maternal separation (UMS) procedure. Pups were separated from the mothers at different times during the day for 4h daily on post-natal day (PND) 1 to PND 6 and for 6h on PND 7 to PND 14.
C. Quantification of the density of PV+ interneurons in the CA1 region of the hippocampus in WT (n = 3) and Bcan-/- (n = 3) mice subjected to MS. The control data (left bars) are the same as in Figure 3. One-way ANOVA followed by Holm-Sidak's multiple comparisons test.
D and E. Representative images showing 8-oxo-dG levels exhibited by *Bcan*-/- (D) and WT (E) PV cells. Scale bars equal 5 µm.

The deleterious effect of oxidative stress on PV+ cells is particularly prevalent during specific developmental time windows. Early-life insults inducing oxidative stress in pre-weaning or pubertal – but not young adult – mice reduces the number of PV+

interneurons and have long-term detrimental consequences on their maturation (Cabungcal et al., 2013b). For instance, severe psychosocial trauma caused by maternal separation (MS) induces oxidative stress (Daniels et al., 2012; Diehl et al., 2012), reduces PV expression in the hippocampus (Brenhouse and Andersen, 2011), alters synaptic development and plasticity (Aisa et al., 2009; Andersen and Teicher, 2004; Hsu et al., 2003; Monroy et al., 2010; Xie et al., 2013), and ultimately affects behavior and cognition (Aisa et al., 2009; Brenhouse and Andersen, 2011; Diehl et al., 2012; Hsu et al., 2003; Lippmann et al., 2007; Millstein and Holmes, 2007). We, therefore, explored whether the lack of Brevican makes PV+ cells more susceptible to redox dysregulation when an oxidative challenge, such as MS, is applied at early stages of development. We daily removed *Bcan* mutant and wild-type pups from their mothers during the neonatal and preweaning period (P1-P14) and assessed the levels of oxidative stress at P30 (Figures Ax6A-D). Consistent with previous reports (Brenhouse and Andersen, 2011; Cabungcal et al., 2013b), we observed a lower number of PV+ cells in both *Bcan* mutant and wild-type mice subjected to MS compared to controls (Figure Ax6C) but no difference between genotypes. In addition, MS increased the levels of 8-oxo-dG in *Bcan* mutant PV+ cells compared to wild-type MS PV+ interneurons as well as to wild-type and mutant PV+ cells from mice not subjected to MS (Figures Ax6A, 6D and 6E). Altogether, these results show that Brevican protects immature PV+ interneurons against oxidative stress caused by environmental insults during particularly sensitive developmental windows.

Discussion of the results

Our work hints at a different function of BCAN1 and BCAN2 in PV+ interneurons. Whereas BCAN2 regulates the maturation of excitatory synapses onto PV+ cells, BCAN1 does not seem to play such a role. However, the rescue of PV levels by BCAN1 suggests that it influences the concentration of the calcium binding protein PV without causing any change in the density of excitatory inputs. A growing amount of evidence has highlighted that PV levels are the litmus test of how several different events ultimately affect PV+ interneuron function (Brenhouse and Andersen, 2011; Cabungcal et al., 2013a, 2013b; Donato et al., 2013). One of these events is oxidative stress which negatively alters PNNs and, as a result, the PV levels (Brenhouse and Andersen, 2011; Cabungcal et al., 2013a, 2013b). To support their high-frequency firing, PV+ interneurons are energy demanding. This requires enhanced metabolic activity, which may lead to elevated mitochondria-generated reactive oxygen species (ROS). As a result, PV+ cells are particularly vulnerable to redox dysregulation and need well-regulated antioxidant systems to neutralize ROS and maintain proper redox state. Interestingly, this vulnerability of PV+ cells is associated with the absence of fully mature PNNs which protects them against oxidative stress. In turn, excess oxidative stress also affects PNN which reciprocally impact PV+ interneurons (Do et al., 2015). Remarkably, in addition to the well-known contribution of oxidative stress to neurodegenerative diseases (Qureshi and Parvez, 2007) and consistent with the pivotal role that PV+ interneurons play in cognitive functions (Hu et al., 2014), PV+ cell impairment caused by severe redox imbalance has been recently linked to psychiatric disorders (Do et al., 2015; O'Donnell et al., 2014). It is, however, unknown whether all PNN proteins play a similar role in protecting PV+ cells against oxidative stress. By using a paradigm that was both physiological and ethologically relevant, we induced oxidative stress during a particularly sensitive period in brain development and uncovered a neuroprotective role for Brevican against oxidative damage in PV+ interneurons. Although the lack of Brevican does not increase oxidative stress *per se*, it makes PV+ cells susceptible to

insults during specific sensitive time windows that have a long-lasting impact over the lifespan.

How does Brevican protect PV+ interneurons against oxidative stress? Brevican, as other PNNs, is a polyanionic molecule that can function as a buffering system for cations (Brückner et al., 1993). Whereas buffering calcium and sodium is likely to be important to regulate the firing properties of PV+ cells, iron chelation may limit the formation of iron-generated reactive hydrogen radicals. In addition, hyaluronan and chondroitin sulfate which are bound to Brevican have antioxidant properties (Campo et al., 2004). The low expression of BCAN2, its punctate appearance and its restricted synaptic localization suggests that it is unlikely to have a main role as a cation chelator. BCAN1, instead, is expressed at higher levels (Figure 7) and resembles other classical PNNs: it is secreted and it densely encloses PV+ interneurons. As such, BCAN1 appears tailored to fulfill BCAN neuroprotective function. Future work investigating whether overexpression of BCAN1 – but not BCAN2 – in *Bcan* mutant PV+ cells is able to prevent the high oxidative stress found in *Bcan* knock-out mice subjected to maternal separation will help to further address the different, complementary roles of BCAN1 and BCAN2.

Worth to mention, these experiments might also direct novel therapeutic approaches aimed at thwarting oxidative stress damage in neurodegenerative diseases and psychiatric disorders. Indeed, neurodevelopmental disorders result precisely from disrupting early processes that are crucial for brain development. In particular, GABAergic interneurons have emerged as key regulators of some of these developmental milestones in the assembly of neural circuits and, consistently, have been implicated in several neurological and psychiatric disorders (Hu et al., 2014; Marín, 2012, 2016). Therefore, identifying the mechanisms that regulate the assembly, dynamics and functioning of inhibitory circuits may provide fundamental insights not only into the development of our brain but also on its pathological alterations.

UNIVERSITAS
Miguel
Hernández

METHODS

UNIVERSITAS
Miguel
Hernández

Mice

Brevican$^{-/-}$ mice (Brakebusch et al., 2002), *PV-Cre* (Hippenmeyer et al., 2005), *PLP-GFP* (Fuss et al., 2000), *Nkx2.1-Cre* (Xu et al., 2008), *Nex-Cre* (Goebbels et al., 2006), *VIP-Cre,* and *RCE* (Jackson Laboratories #010908 and #032037), were maintained in a C57B/6 background (Charles River Laboratories); *Nkx2.1CreERT2* mice (Jackson Laboratories #014552) were maintained in a 129S2/SV background, G42 mice (Jackson Laboratories #007677) were maintained in a CB6F1/J background and *GIN* mice (Jackson Laboratories #003718) were maintained in an FVB/NJ background. All experimental procedures were performed on male mice, except the work performed with chandelier cells (Part I, Figure 13), the analysis of synapse density in *PV-Cre;GluA1*$^{F/F}$ mice (Part II, Figures 6N and S6G) and of the intrinsic properties in *Bcan* knock-down PV+ cells (Part II, Figures 4I-4U) where mice of both sexes were used. Animals were maintained under standard, temperature controlled, laboratory conditions, or in an enriched environment with free access to colored tunnels, mazes, climbing materials, and running wheels. Mice were kept on a 12:12 light/dark cycle and received water and food *ad libitum* with the exception of the rewarded alternation test. Animal procedures were approved by ethical committees (IN-CSIC and King's College London) and conducted in accordance with Spanish and European regulations, and Home Office personal and project licenses under the UK Animals (Scientific Procedures) 1986 Act.

Tissue dissociation and FACS

To isolate individual cells, we euthanized the corresponding transgenic mice (Table 1), extracted the brain and microdissected the region of interest in cold pH 7.35 dissociation media (16 mM HEPES, 20M glucose, 0.8M kynurenic acid, 0.05mM APV, 50 U/ml penicillin–0.05 mg/ml streptomycin, 2 mM NaOH, 0.09M Na_2SO_4, 0.03M K_2SO_4, and 0.014M $MgCl_2$). To generate single-cell suspensions, 1 mm^3 tissue pieces from 1-3 brains were pooled and enzymatically digested in dissociation medium containing 0.1 mg/ml DNAse, 0.16 gm/l L-cysteine HCl and 6.8 U/ml papain at 37°C for 30 min. Papain digestion was then blocked with dissociation medium containing 5 mg/ml ovomucoid (Sigma, St. Louis, MO) and 5 mg/ml bovine serum albumin (BSA) at room temperature. Neurons were mechanically dissociated to create a single cell suspension by gentle trituration in iced OptiMem (Life Technologies, Gaithersburg, MD) containing 20 mm glucose, 0.1 mg/ml DNAse and both 0.4 mM kynurenic acid and 0.025 mM APV to protect against glutamate-induced neurotoxicity. Fluorescently labeled individual cells were then purified from the suspension by fluorescence-activated cell sorting (FACS) using a BD FACSAria III cytometer. Cells from 1-3 consecutive experiments were collected in 350 µl of RLT buffer (QIAGEN, #79216) containing 0.01% 2-Mercaptoethanol (BioRad, #1610710) and stored at -80°C for RNA extraction.

RNA sequencing and differential expression analysis

RNA was extracted using the QIAGEN RNeasy Micro Kit, according to the manufacturer's instructions. Library preparation and RNA-seq experiments were performed by the Genomic Unit of the Centre for Genomic Regulation in Barcelona. Depending on the cell type and stage, approximately 7,000-30,000 cells were required to obtain 1-2 ng of total RNA, which served as input for the library preparation using the SMARTer Ultra Low RNA Kit for ultra-low amount of RNA. The Illumina HiSeq 2000 platform was used to sequence libraries to a mean of approximately 50 million mapped 50 base pair single-end reads per sample. In the RNA-seq experiment, three biological replicates were ascertained for each dataset, except for oligodendrocytes where two replicates were used.

Bioinformatic analysis of RNA-seq data was performed by the Bioinformatic Unit of the Centre for Genomic Regulation in Barcelona. RNA-seq quality check was performed using the tool FastQC (Babraham Bioinformatics). The goal of this step was to provide an overview of the quality of the data such as: per base sequence quality, GC content,

duplication level, amount of overrepresented regions and presence of adapters. To confirm a low amount of rRNA contaminations, we extracted a subset of 1 million reads for every sample and aligned them against a database of rRNAs using the tool ribopicker (Schmieder et al., 2012). Consistent with the presence of a step for filtering by polyA selection in the RNA-seq protocol, we obtained a low amount of reads mapping to rRNAs (0.6-4.1%). Next, reads were aligned to the reference genome (Ensembl version 66 corresponding to NCBIM37 from iGenome database) using Tophat2 (Kim et al., 2013), a splice aware mapper for RNA-seq reads that uses known information of splicing events to align reads spamming the junction of two exons. We successfully mapped 75.2 ± 13.5% of the fragments to the genome.

For the matter of an accurate comparison, a normalized value of expression called FPKM (Fragments Per Kilobase of exon per Million fragments mapped) was used. The FPKM corresponds to the number of reads aligned per kilobases of the transcript per million aligned reads from the total dataset. The software Cuffdiff2 (version 2.1.1) was used to compute FPKM values (Trapnell et al., 2013). FPKMs and read counts were scaled via the median of the geometric means of fragment counts across all libraries. Each replicated condition was used to build dispersion models, then these models were averaged to provide a single global model for all conditions in the experiment. Cuffdiff2 was also used to perform differential expression analysis between cell populations by using a False Discover Rate (FDR) of 5%. Individual replicates were found to be highly reproducible with a low squared coefficient of variation (CV^2) and clustered tightly together across all genes.

Data were visualized using the cummeRbund package from Bioconductor (Trapnell et al., 2012). Principal component analysis was performed by D. Exposito-Alonso using the cummeRbund package in R. Principal components 2 and 3 are plotted in Figure 6. We also measured the Jensen-Shannon distance between replicates as well as between samples and used it for plotting a dendrogram with the cummeRbund package (Figure 6, performed by D. Exposito-Alonso).

Specificity indexes

To calculate the specificity scores showed in Figure 7 and Figure 8, we first selected all genes differentially expressed between P10 chandelier, P10 PV+ basket, P10 SST+ cells and P12 pyramidal cells. To remove genes with high specificity owing to barely detectable expression, we additionally filtered them by a minimum normalized expression level (FPKM) of 10. Next, we ranked all significantly differentially expressed genes using a specificity score based on the fold change between the gene's normalized expression in a given subpopulation and the average normalized expression of that gene in all the other P10/P12 populations. In particular, for each gene, we calculated the fold change (FC) between the FPKM value of that gene in each of the three P10 interneuron subpopulations and the average FPKM value in the other populations at P10/P12. The specificity score was calculated as the $\log_2$ transform of the fold change ($\log_2$FC).

To detect the genes that exhibit the highest degree of both subtype and stage specificity showed in Figure 9, we calculated the specificity scores following similar steps but including all populations and stages in the calculations. In particular, we selected genes differentially expressed between each of the three P10 interneuron subtypes (e.g. P10 chandelier cells) and the same subtype at P5/P8 (e.g. P8 chandelier cells) as well as all other populations at different stages when applicable (e.g. P5 and P10 PV+ basket cells, P5 and P10 SST+ cells, P0 interneurons, P12 pyramidal cells and P10 oligodendrocytes). Next, all genes were filtered by a minimum FPKM expression level of 10 and the specificity score was calculated between a given subpopulation and all other populations (e.g. P8 chandelier cells, P5 and P10 PV+ basket cells, P5 and P10 SST+ cells, P0 interneurons, P12 pyramidal cells and P10 oligodendrocytes). Next, we

selected those genes that were specific for each of the three interneuron subpopulations by additionally filtering out genes with a specificity score lower than 0 for the cell type of interest and higher than 1 in the other populations (excluding the same subtype at P5/P8).

To rank the genes shown in Figure 10, of all genes exhibiting both subtype and stage specificity we selected those that had demonstrated or putative roles in axon growth, axonal pathfinding, neuron-ECM communication or cell-cell adhesion, according to the gene ontology analysis or a manual MEDLINE® search. Additionally, for each interneuron subpopulation, the top 5 most specific genes were further ranked by a specificity ratio between the gene's normalized expression (FPKM) in the population of interest and the maximum FPKM value of that gene found in any of the other cell populations.

The specificity score highlights as specific those genes that are highly expressed in one population but low on average in all other populations. Because the average dilutes the contribution of individual cell populations, genes that are relatively highly expressed in a second population but particularly low in all others will still have a comparatively high specificity score. This is, for instance, the case for several genes shared between chandelier and PV+ basket cells. Conversely, the specificity ratio is particularly powerful in detecting as relatively 'not specific' those genes that are low in all other populations on average but specifically high in a second population only. However, because it only considers the expression level in the second expressing population, the specificity ratio lacks the power to additionally lower the ranking position of a gene that is widespread in all other populations. The fact that these two specificity indexes are complementary justified the use of both to increase our specificity detection power.

Gene Ontology and pathway analysis

The Gene Ontology and pathway enrichment analysis shown in Figure 7 was performed to identify which types of genes distinguish chandelier, PV+ basket or somatostatin cells at P10 but minimizing the effects of differences across developmental time. Because the number of genes specifically expressed in one of the three subpopulations was relatively low and enrichment can be significantly detected only when the input list contains a high number of genes, we pooled the lists of genes uniquely expressed in each of the three subpopulations. The pooled list was used as input for a preranked gene set enrichment analysis against the collection of GSEA canonical pathway gene sets (C2, KEGG and Reactome; MSigDB; Subramanian et al., 2005). The example of the metabolic gene set (Figure 7, see Discussion) indicates that, although more powerful, performing a gene enrichment analysis using a pool of all genes specific for each interneuron subpopulation has a disadvantage: enrichment may be driven by genes expressed in a given population only. However, this limitation was overcome by *post hoc* manual analysis of the individual genes driving the highlighted signatures. The list of manually curated gene groups revealed that the majority of enriched gene sets were cell-type-specific thus verifying that all interneuron subpopulations contributed to such subtype-specific signatures and confirming the differential use of similar molecules across our three interneuron subtypes.

Chandelier cell imaging and analysis

For the analysis of chandelier morphology and synapse density shown in Figure 13, confocal image stacks (100X oil immersion objective, 1.4 NA, 2.2 digital zoom, 0.2 µm step size) were analyzed with IMARIS 7.5.2 software. The axon initial segment (AIS, labeled with AnkyrinG) was reconstructed with the "create surface" tool as described above. Briefly, AISs included within the tissue sections with optimal staining were isolated in three dimensions. Three-dimensional isosurfaces were created using the "create surface" tool and volume was quantified automatically. A threshold was selected to include as much of the neuron as possible while excluding any background. A size

filter was applied with the minimum size being related to the volume of the AIS. For bouton density, the chandelier presynaptic boutons were detected with the “spot” tool using a spot diameter of 0.7 µm and a threshold was selected to accurately detect as many spots as possible without creating artifacts. The radius of the spot was used as a threshold distance to define the contact with the AIS and the “Find spots close to surface” tool (ImarisXT extension) was used to count the number of presynaptic boutons (“spots”) that were contacting the surface of the AIS.

A cartridge was defined as such when at least 3 consecutive presynaptic boutons were found on the same chandelier axonal segment. For each cartridge, we measured length, number of boutons per cartridge, number of AISs contacted by one cartridge and the ‘distance to closest cartridge’ parameter. Cartridge length was quantified by tracing a line that joined all consecutive varicosities found on each cartridge and automatically measuring its length. The number of boutons in each cartridge was determined by counting the number of varicosities found in the entire length of each cartridge. The number of AISs contacted by one cartridge was assessed by calculating the total number of AISs contacted by one cartridge (with ‘cartridge’ and ‘contact’ defined as above) within the field of view. The ‘distance to closest cartridge’ indicates the average distance between each cartridge and the cartridge that is closest to it. This parameter is considered diagnostic of the overall density of the cartridges in a given volume and was used as a proxy to estimate the density of the chandelier arbor (Fazzari et al., 2010).

Analysis of the number of somatic mCherry+ boutons from incidental infection of PV+ basket cells (Figure 13P) was analyzed as explained below (Image Acquisition and Analysis) for the correlation analysis shown in Figure S2B (Part II), with the only difference of defining the soma using NeuN instead of PV.

Analysis of somatic and dendritic synapses upon *Lgi2* and *Cbln4* downregulation were performed by A. Marques-Smith and R. Deogracias, respectively, and the details of their analysis are not included in this thesis.

Perfusions and Immunohistochemistry

Animals were deeply anesthetized with sodium pentobarbital by intraperitoneal injection and then transcardially perfused with PBS followed by 4% paraformaldehyde (PFA) in PBS. Brains were dissected out and postfixed for two hours at 4°C, cryoprotected in a series of sucrose-PBS solutions overnight at 4°C. Then, tissue was sectioned at 40 µm on a sliding microtome (Leica). Free-floating brain sections were permeabilized by incubating with 0.2% Triton X-100 in PBS for 1 hour and then blocked for 3 hours (0.3% Triton X-100, 1% Normal Goat Serum and 5% BSA), followed by incubation with primary antibodies in 0.3% Triton X-100, 1% Normal Goat Serum and 2% BSA overnight at 4°C. The next day, brains were rinsed in PBS and incubated with the appropriated secondary antibodies for 2 hours at room temperature, rinsed in PBS, and then incubated with DAPI. The following primary antibodies were used: rabbit anti-GAT-1 (1:250, Chemicon #AB1570), mouse anti-GAD67 (1:5000, Chemicon #MAB5406), mouse anti-AnkyrinG (1:500, NeuroMab #75-146), rat anti-somatostatin (1:250, Chemicon #MAB354), mouse anti-Reelin (1:250, MBL International #D223-3), rabbit anti-VIP (1:1000, ImmunoStar #20077), rabbit anti-nNOS (1:1000, ImmunoStar #24287), rabbit anti-calretinin (1:200, Chemicon #AB149), rabbit anti-GABA (1:2000, Sigma #A-2052), rabbit anti-Olig2 (1:250, Millipore #AB9610), goat anti-mCherry (1:500, Antibodies-Online #ABIN1440057), rabbit anti-NeuN (1:500, Millipore #ABN78), mouse anti-NeuN (1:500, Millipore # MAB377), goat anti-FGF13 (1:500, Santa Cruz #sc-16811), mouse anti-parvalbumin (1:1000, Sigma #P-3088), rabbit anti-parvalbumin (1:2000, Swant #PV-25); goat anti-parvalbumin (1:500, Swant #PVG-214); chicken anti-parvalbumin (1:500, SySy #195 006); guinea-pig anti-VGlut1 (1:2000, Millipore #AB5905), mouse anti-PSD95 (1:500, NeuroMab #70-028), guinea-pig and rabbit anti-Brevican (1:1000, a gift from R. Frischknecht), rabbit anti-GluA1 (1:1000, Millipore #04-855), mouse anti-HA (1:500, Covance #MMS-101P),

rabbit anti-DsRed (1:500, Clontech #632496), chicken anti-GFP (1:1000, Aves Lab #1020), mouse anti-GAD65 (1:500, Millipore #MAB351R), mouse anti-Synaptotagmin-2 (1:1000, ZFIN #ZDB-ATB-081002-25), goat anti-CB1 (1:400, Frontier Science #Af450-1), mouse anti-gephyrin (1:500, Synaptic Systems #147 011), mouse anti-Kv3.1b (1:1000, NeuroMab #75-041), mouse anti-Kv1.1 (1:500, NeuroMab #75-007).

Fluorescent *In Situ* Hybridization Histochemistry

For dual-color fluorescent in situ hybridization combined with immunohistochemistry, mice were perfused and brains were fixed overnight in 4% PFA in PBS followed by cryoprotection in 30% sucrose-RNase free PBS. 30 µm sliding microtome sections were mounted on RNAse-free SuperFrost Plus slides (Fisher Scientific) with PBST (0.5%Tween20 in PBS), allowed to dry and postfixed in 4% PFA for 5 minutes. After three rinses with PBST, sections were treated with 5 µg/ml proteinase K in PBST (Invitrogen) for 5 minutes, briefly transferred to 4% PFA, and rinsed with PBST. Sections were then incubated for 1 hour at 62°C with hybridization solution (50% formamide, 10% dextran sulfate, 0.2% tRNA, 4% Denhardt's solution, 200 mM NaCl, 10 mM Tris, 5 mM NaH2PO4, 5 mM Na_2HPO_4, 5 mM EDTA, pH 7.5) and hybridized overnight at 62°C with 0.2-0.5 µg of digoxigenin (DIG)-labeled probes diluted in hybridization solution. The next day, sections were rinsed with 50% formamide, 0.5× SSC, and 0.5% Tween 4x30 minutes at 62°C and 1x30 minutes at room temperature. Sections were then blocked for 1 hour in 3% BSA, 20% blocking solution (Roche), 10% sheep serum in MABT (0.1 M maleic acid, 0.2 M NaOH, 0.2 M NaCl, 0.5% Tween) followed by incubation overnight at 4°C with anti-DIG antibody (1:5000; Roche) together with primary antibodies diluted in blocking solution. On the following day, sections were rinsed 12x15 minutes in MABT, incubated with secondary antibodies for 2 hours at room temperature, rinsed 6x5 minutes in PBS, and incubated with DAPI. Sections were then rinsed twice with detection buffer (Tris HCl 100mM, 100 mM NaCl 5M, 10 mM $MgCl_2$ pH 8) and incubated for 3 hours at room temperature in the dark with 2-hydroxy-3-naphthoic acid 2'-phenylanilide phosphate (HNPP)/Fast Red mix (Roche) diluted 1:100 in detection buffer. Sections were rinsed with PBS-EDTA buffer, briefly transferred to 4% PFA, and rinsed twice with PBS. Then, sections were allowed to dry and covered with Mowiol/DABCO. Images were acquired in the following two days on an inverted Leica TCS-SP8 confocal with a 40x objective. The following DIG-labeled probes were used: *Hapln1* (primers: 5'-CATTACAGCGCAGTA GCATTTC-3' and 3'- GTGACAAAA TATGGCAGCAGTC-5'), *Thsd7a* (primers: 5'-GAAAA CCACAGAAGGGAAACAG-3' and 3'-GCTTTCGACAAGTAATGGCTCT-5'), *Bcan* (IMAGE: 5695027), *Bcan1* (primers: 5'-TGCACCCCTGAGGAGCAAGAC-3' and 3'-CG GGTAAAACCTGAGGCCCTTGTG-5') and *Bcan2* (primers: 5'-GTAATTCTGCTGA AGGCTCAA-3' and 3'-TGGGTACAAAGCAGTTTA ATACAG-5'). The probes used to detect the specific *Bcan* isoforms were obtained by RT-PCR amplification of P30 mouse hippocampal cDNA. The purified PCR product was A-tailed and cloned into the pGEMT-easy vector (Promega). The following primary antibodies were used: chicken anti-GFP (1:1000, Aves Lab #1020), rabbit anti-parvalbumin (1:500, Swant #PV-25), rabbit anti-Olig2 (1:250, Millipore #AB9610), mouse anti-GFAP (1:500, Sigma #G3893). Note that the relatively higher background and the lower signal of the IHC combined with ISH did not allow identification of the fine cartridge structure and hence of chandelier cells by morphology when using this technique.

Super-Resolution Image Acquisition and Analysis

For super-resolution imaging, mouse brains were fixed overnight in 4% PFA in PBS and cryoprotected in 30% sucrose-PBS. 20 µm sliding microtome sections were stained following immunohistochemistry procedure. The following primary antibodies were used: guinea-pig anti-Brevican (1:1000, a gift from R. Frischknecht), mouse anti-Bassoon

(1:500, Abcam #ab82958), rabbit anti-Homer1 (1:400, Synaptic Systems #160 002), rabbit anti-GluA1 (1:1000, Millipore #04-855).

Image Acquisition Single-molecule localization microscopy was performed on a custom-built setup as previously described (Platonova et al., 2015). In brief, a 473 nm laser (100 mW, Laserglow Technologies) was used for activation and a 643 nm laser (150 mW, Toptica Photonics) for imaging. Both lasers were focused onto the back-focal plane of an Olympus NA 1.49, 60x, TIRF-objective. A quad-edge dichroic beamsplitter (405/488/532/635 nm, Semrock) was used to separate fluorescence emission from excitation light. Emission light was filtered by two bandpass emission filters (700/75 nm, Chroma) and a long pass dichroic beamsplitter (690 nm, AHF Analysetechnik) was used to split the emission light. The emission was dually focused by two separate 500 mm tube lenses and onto a back-illuminated EM-CCD chip (Evolve, Photometrics) which was liquid-cooled to -80°C. Focusing was done by moving the objective with a piezo objective positioner (MIPOS100, Piezo Systems Jena). A focus lock was implemented by an electronic feedback loop (LabView, National Instruments), based on total internal reflection of a red laser at the cover slip and its detection on a quadrant photodiode. The *z* stability was better than ±10 nm over several hours. For SMLM imaging, the switching buffer consisted of 0.1 M MEA/0.2 M Tris, pH 8.0 with 5 % (*w*/*v*) glucose, 0.25 mg/ml glucose-oxidase and 20 µg/ml catalase. The imaging laser intensity of the 643 nm laser line used was ~2 kW/cm ^{2}. To keep the average number of localizations per frame constant (maximum intensity ~0.5 kW/cm^2), the intensity of the 473 nm activation laser was automatically adjusted. Imaging was performed in objective-type total internal reflection fluorescence (TIRF) mode. We recorded a minimum of 30,000 frames with an exposure time of 20-35 milliseconds. All data analysis was performed in MATLAB (Mathworks). The acquired raw camera frames were filtered using a running median filter (Hoogendoorn et al., 2014), a 50 frame filter radius and a keyframe separation of 20 frames. Single-molecule positions were determined by Gaussian fitting based on a maximum likelihood estimator (Smith et al., 2010) and only localizations with a maximum localization precision of 15 nm and a maximum PSF of 180 nm (1/*e*-intensity) were considered for further analysis. An image-correlation based drift-correction was employed. The first 25 frames of the dSTORM acquisition were used for a coarse estimate of the translational shift between the left and right side of the EMCCD chip. This was done using the phase difference of the Fast Fourier Transform, which was calculated using a pixel-reconstructed image from the single-molecule localization coordinates using a pixel-size of 100 nm. The localizations from the short-wavelength channel were coarsely mapped onto the localizations of the long-wavelength channel and paired. For pairing the localizations of the two channels in each frame had to be within a maximum search-radius of 8 camera pixels (~800 nm). The paired localizations were used to calculate an affine transformation matrix using the MATLAB built-in routine *cp2tform*. The transformation matrix was used to map the localizations from the short-wavelength onto the localizations of the long-wavelength channel. The overall registration precision was 25-35 nm. The localizations were paired again, but using a more stringent cut-off of 1 pixel for the search-radius. The normalized intensity ratio was calculated for all localization pairs for the color-assignment using $r=(I_l-I_s)/(I_l+I_s)$, where I_l and I_s are the fluorescence intensities determined by maximum-likelihood fitting for the long and short wavelength channels, respectively. The localization pair was assigned to AF647, CF660C or C680 by manually selecting the ranges for the normalized intensity ratio. Examples for the dye separation are provided in Figure S1.

Data analysis. Individual synapses contacting the soma of PV cells were manually selected from three-color dSTORM images. To determine the distribution between pre- and post-synaptic site (Figure 1M), “side” view synapses were chosen such that Bassoon and Homer1 were seen as parallel stripes. A line along the center of the pre-

synaptic Bassoon was drawn manually (position = 0 nm). The synapses were overlaid with Bassoon = 0 and Homer1 was used to determine the orientation of the synapse. The longitudinal profile of Bassoon/Brevican/Homer1 across the synapse was then determined straightforwardly. For the radial distribution analysis of Bassoon/Homer1/Brevican (Figure 1N) and Bassoon/GluA1/Brevican (Figure 5H), "face" view synapses were chosen such that Bassoon/Homer1 and Bassoon/GluA1 were seen as overlapping round or elliptical discs. The mean x,y position of the Bassoon localizations of each synapse (simplified and considered to be radially symmetric) was set to x,y = 0,0. The Euclidian distance of the Bassoon/Homer1/Brevican and Bassoon/GluA1/Brevican localizations was used to compute their radial distribution for each synapse. The two-color radial distribution analysis of Brevican with respect to Bassoon (Figure S1R) or Homer1 (Figure S1S) was done correspondingly, except that in the latter case the mean x,y position of Homer1 localizations was used to establish x,y = 0,0.

Cell Culture, Transfection, Pharmacology and Immunocytochemistry

Cell line cultures. HEK293T cells were cultured in Dulbecco's Modified Eagle's medium supplemented with 10% fetal bovine serum, 2 mM glutamine, penicillin (50 units/ml) and streptomycin (50 g/ml). The cultures were incubated at 37°C in a humidified atmosphere containing 5% CO_2. HEK293T cells were transfected using polyethylenimine (PEI, Sigma) at a 1:4 DNA:PEI ratio.

Primary hippocampal cultures. Hippocampi from E18 mouse embryos were dissected in ice cold Hank's Balanced Salt Solution (HBSS), digested with 1 mg/ml trypsin (Worthington) for 15 minutes at 37°C, treated with 0.1 mg/ml DNase I (Roche) and triturated to produce a single cell suspension. Cells were then plated at 100,000 cells/cm^2 on plastic dishes or at 50,000 cells/cm2 on glass coverslips pre-coated with 0.5 mg/ml poly-L-lysine (Sigma). Cells were cultured in Neurobasal (Invitrogen) supplemented with 2% B27 (Invitrogen), glutamine (2 mM) and 100 µg/ml penicillin-streptomycin (Gibco). For *in vitro* activity manipulations, 26DIV neuronal cultures were treated for 48 hours with 20 µM Gabazine or 20 µM Nifedipine, or their appropriated controls (H_2O, and DMSO, respectively).

Immunocytochemistry. HEK293T cells or 28 DIV neurons were fixed in 4% PFA/1% sucrose in PBS for 10 minutes, briefly washed in PBS and permeabilized with 0.2% Triton X-100 in PBS. Coverslips were blocked with 5% BSA in PBS for 1 hour and incubated with primary antibodies in blocking solution overnight at 4°C. Coverslips were then washed 6x5 minutes in PBS and incubated with secondary antibodies in blocking solution for 1h at room temperature. Coverslips were then washed 6x5 minutes in PBS, incubated with DAPI and mounted in Mowiol/DABCO. Primary antibodies used: chicken anti-GFP (1:3000, Aves Lab #1020), guinea-pig anti-Brevican (1:2000, a gift from R. Frischknecht), rabbit anti-Brevican (1:2000, a gift from R. Frischknecht), rabbit anti-DsRed (1:500, Clontech #632496), mouse anti-HA (1:500, Covance #MMS-101P), chicken anti-GFP (1:1000, Aves Lab #1020).

Generation of AAV Expression Vectors

To generate the *pDIO-shBCAN-mCherry*, the sequence containing the distal and proximal elements of the U6 promoter spaced by the CDS for mCherry was amplified by PCR (primers: 5'-TTCGCTAGCGGATCCGGAATAAC-3' and 3'-CCAGAGGTTGATTGG TTTATCAGGC -5'). The resulting PCR product was cloned into the *pAAV-EF1a-DIO-mCherry* vector (kindly provided by Prof. K. Deisseroth) and a TATA box was introduced in the U6 fragment (primers: 5'-TATGCTTACCGTAACTTGAAAGTATTTCGATTTCTTG GGTTTATATATCTTGTGGAAAGGACGCGGTTTCCTAGGTTTAAACTG-3' and 3'-TATG
CTTACCGTAACTTGAAAGTATTTCGATTTCTTGGGTTTATATATCTTGTGGAAAGGAC GCGGTTTCCTAGGTTTAAACTG-5'). The ssDNA primers to generate the shBCAN (5'-

CTAGGCAAGCAGAACCGCTTCAATGCCTGACCCACATTGAAGCGGTTCTGTTGCTT TTTG-3' and 3'-AATTCAAAAAGCAAGCAGAACCGCTTCAATGTGGGTCAGGCATTGAA GCGGTTCTGCTTGC-5') were obtained using the Block-it RNAi web tool (Thermo Scientific). To minimize the putative off-target effects of the shRNA, a miR-133 derived loop sequence was used (Gu et al., 2012). Moreover, the shRNA sequence was blasted and no other mouse mRNA apart from *Bcan* was predicted to be targeted. A similar strategy was followed to clone the shRNAs targeting FGF13 [shRNA-2 and shRNA-4 from (Wu et al., 2012a)]. The coding sequences for *Fgf13*, *Bcan1* and *Bcan2* full-length used in the rescue experiments were obtained from P30 mouse hippocampal cDNA and cloned into the pGEMT-easy vector (Promega). A canonical HA tag sequence was introduced after the signal peptide (primers: 5'-TCTAGAGCCACCATGATACCACTGCT TCTGTCCCTGCTGGCCGCTCTGGT-3' and 3'-TTGGGTCAGGACCAGAGCGGCCAGC AGGGACAGAAGCAGTGGTATCATGGTGGCCTAGAA-5'; 5'-CCTGACCCAAGCCCCTG CCGCCCTCGCTGATTACCCATACGATGTTCCAGATTACGCTAGATCTA-3' and 3'-AGA TCTAGCGTAATCTGGAACATCGTATGGGTAATCAGCGAGGGCGGCAGGGGC-5') and cloned in the *pAAV-EF1a-DIO-mCherry* vector (*Bcan1* and *Bcan2*) or in the *pDIO-shFgf13-mCherry* after adding a T2A sequence (*Fgf13B*). To generate a *Bcan2* mutant that lacks the GPI anchor (BCAN2-GPI), the DNA sequence coding for the protein region containing the C-terminal GPI-modification sites was removed from *Bcan2* full-length. The same sequence (P**S**SGNSAEGSM PAFLLFLLLQLWAT, the best predicted site is shown in bold and is underlined, the alternative site is underlined) was cloned after the last exon of *Bcan1* full-length to generate BCAN1+GPI.

AAV Production and Intracranial Injections

HEKs 293FT cells (ThermoScientific) were seeded on 15-cm plates and co-transfected with packaging plasmids AAV-ITR-2 genomic vectors (7.5µg), AAV-Cap8 vector pDP8 (30µg; PlasmidFactory GmbH, Germany, #pF478) using PEI (Sigma) at a ratio 1:4 (DNA:PEI). 72 hours post transfection, supernatants were incubated with ammonium persulfate (65g/200ml supernatant) for 30 minutes on ice and centrifuged for 45 minutes at 4000 RPM at 4°C. Transfected cells were harvested and lysed (150mM NaCl, 50mM Tris pH8.5), followed by three freeze-thaw cycles and Benzonase treatment (50U/ml; Sigma) for 1 hour at 37°C. Filtered AAVs (0.8 µm, 0.45 µm and 0.2 µm MCE filters) from supernatants and lysates were run on an iodixanol gradient by ultracentrifugation (Vti50 rotor, Beckmann Coultier) at 50,000 RPM for 1 hour at 12°C. The 40% iodixanol fraction containing AAV was collected, concentrated using 100 kDa-MWCO Centricon plus-20 and Centricon plus-2 (Merck-Millipore), aliquoted and stored at -80°C. The infectious titer of virus was measured by quantitative real-time PCR (primers: 5'-GGCACTGACAATTCC GTGGT-3' and 3'-CGCTGGATTGAGGGCCGAA-5'). AAVs with a titer equal or higher to 10^{11} genome copy/ml were used for in vivo injections. The AAV9-EF1a-DIO-eYFP was generated by and acquired from the Penn Vector Core, with a titer of 3.95 x 10^{13} genome copy/ml. The AAV8-GFAP(0.7)-EGFP-T2A-iCre was generated by and acquired from the Vector Biolabs, with a titer of 5.6 x 10^{13} genome copy/ml.

For intracranial injections, P2 or P12 mice were anesthetized with isoflurane and were mounted in a stereotactic frame. For experiments shown in Part I, 500 nl of AAV8-shFgf13-mCherry, AAV8-FGF13B-HA-T2A-shFgf13-mCherry or AAV8-Cbln4-HA-T2A-shLacZ-mCherry were unilaterally injected in the medial prefrontal cortex (anteroposterior −0.6 mm; mediolateral +0.2 mm; dorsoventral −0.4 and −0.8 mm relative to Bregma) at an injection rate of 100 nl/minute followed by 2 additional minutes to allow diffusion.

For synapse analysis in Part II, 250 nl of AAV8-shBcan-mCherry:AAV9-YFP in a 10:1 ratio, AAV8-Bcan1-HA:AAV9-YFP in a 10:1 ratio, AAV8-Bcan2-HA:AAV9-YFP in a 10:1 ratio, AAV8-Bcan2-HA:AAV8-GFAP-iCRE in a 1:1 ratio or AAV8-Bcan2-HA:AAV8-GFAP-iCRE in a 1:1 ratio were unilaterally injected into the dorsal region of the left hippocampus (anteroposterior −2.8 mm; mediolateral +1.2 mm; dorsoventral −1.3 mm relative to Bregma) at an injection rate of 50 nl/minute followed by 2 additional minutes to allow diffusion. For electrophysiology or behavioral experiments, 400 nl of AAV8-shBcan-mCherry:AAV9-YFP in a 10:1 ratio, 400 nl of AAV8-Bcan1-HA:AAV9-YFP in a 10:1 ratio or 400 nl AAV8-Bcan2-HA:AAV9-YFP in a 10:1 ratio (for electrophysiology experiments) or 500 nl of AAV8-shBcan-mCherry or 500 nl of AAV9-YFP (for behavioral experiments) were bilaterally injected into the dorsal region of the hippocampus (anteroposterior −2.5, −2.8, −3.2 mm; mediolateral +1.2 mm; dorsoventral −1.3 mm relative to Bregma) at an injection rate of 100 nl/minute. Post-recording immunocytochemistry was carried out to evaluate the recorded cell and the expansion of the injection. For behavioral experiments, injections massively targeted the majority of the PV cells in the dorsal hippocampus (data not shown).

Western blot and Fractionation

For Western blot analysis on neuronal cultures, DIV28 E17.5 hippocampal cultures or HEK293T were placed on ice and rinsed 1x in PBS. For Western blot analysis on mouse tissue, P30 hippocampi were rapidly dissected in ice cold PSB. Samples were homogenized in lysis buffer containing 25 mM Tris-HCl pH 8, 50mM NaCl, 1% Triton X-100, 0.5% sodium deoxycholate, 0.001 % SDS and protease inhibitor cocktail. For anti-Brevican Western blot, samples were digested with 1.7U/mg of ChABC (Sigma) for 2 hours at 37°C. For fractionation experiments, Syn-PER™ Synaptic Protein Extraction Reagent (ThermoScientific) or Subcellular Protein Fractionation Kit for Tissues (ThermoScientific) were used according to the manufacturer's instructions. Protein quantity was measured using bicinchoninic acid (BCA) assay (ThermoScientific). All samples were denatured, resolved by SDS-PAGE and transferred onto PVDF membranes. Membranes were blocked with 5% nonfat milk (Biorad) in TBST (20mM Tris-HCl pH7.5, 150mM NaCl and 0.1% Tween20) for 1 hour and probed with the following primary antibodies: mouse anti-PSD95 (1:500, NeuroMab #70-028), guinea-pig and rabbit anti-Brevican (1:1000, a gift from R. Frischknecht), rabbit anti-actin (1:1000, Sigma #A2066), rabbit anti-GluR1 (1:1000, Millipore #04-855), mouse anti-GAPDH (1:1000, Sigma # GAPDH-71.1), rabbit anti-T-cadherin (1:500, Millipore #ABT121), rabbit anti-Na,K-ATPase (1:1000, Abcam, #ab76020), mouse anti-HA (1:500, Covance #MMS-101P), mouse anti-Kv1.1 (1:500, NeuroMab #75-007). After incubation with HRP-conjugated secondary antibodies, protein levels were visualized by chemiluminescence. Blots were scanned using a LI-COR Odyssey® Fc Imaging System and band were quantified with Image Studio Software. For quantification, densitometry of protein bands of interest was normalized to that of actin.

Co-immunoprecipitation Assays

100 µg of hippocampal homogenates from P30 mice were pre-cleared by adding 50 µl of protein A-Sepharose (Sigma) bead slurry (50%). For Brevican isoform-specific Co-IP, 100 µg of hippocampal homogenates from P30 *Bcan* mutant mice were mixed with 50 µg of lysate from HEK293T co-transfected with CreGFP and a Cre-dependent Bcan1-HA or Bcan2-HA expressing plasmid. The pre-cleared lysate was then diluted in 1 ml of Co-IP buffer (0.3M sucrose, 10 mM Tris-HCl pH 8, 10 mM NaCl, 3 mM $MgCl_2$, 1% NP-40, 5% glycerol and protease inhibitor cocktail) and subsequently incubated overnight at 4°C with 2 µg of one of the following antibodies: rabbit anti-GluR1 (Millipore #04-855), rabbit anti-GluR2-3 (Millipore #AB1506), rabbit anti-GluR4 (Millipore #AB1508), rabbit anti-NMDAR2B (Millipore #AB1557P), Rabbit IgG-Isotype Control (Abcam #ab27478), rabbit anti-mGluR2-3 (Millipore #AB1553), mouse anti-Kv1.1 (NeuroMab #75-007), mouse anti-

Kv3.1b (NeuroMab #73-041), Mouse IgG-Isotype Control (Abcam # ab37355). 50 µl of protein A-Sepharose (Sigma) bead slurry was washed in Co-IP buffer and added to the mixture. After overnight incubation at 4°C with gentle rotation, the beads were pelleted and rinsed three times with Co-IP buffer. Immune complexes were then analyzed by western blot.

***In vitro* Patch Clamp Recordings**

Slice preparation. Postnatal day (P) 26-38 mice were deeply anesthetized with sodium pentobarbital and transcardially perfused with ice-cold sucrose-based cutting solution containing (in mM): 70 Sucrose, 86 NaCl, 4 KCl, 1 NaH_2PO_4, 7 $MgCl_2$, 26 $NaHCO_3$, 25 Glucose and 0.5 $CaCl_2$. After brain dissection, 300 µm coronal hippocampal slices were cut using a vibratome (Leica) in the same ice-cold solution. After cutting, slices were transferred to an incubation chamber filled with artificial cerebrospinal fluid (ACSF) heated to 34 ˚C and containing (in mM): 127 NaCl, 2.5 KCl, 0.6 NaH_2PO_4, 26 $NaHCO_3$, 13 Glucose, 1.3 $MgSO_4$, 2 $CaCl_2$. Slices were kept in this heated chamber for 30 minutes and then transferred to a second chamber containing the same solution at room temperature, where they were kept for an additional 30 minutes, and throughout the day, before recordings.

Patch clamp recordings. After recovery, slices were transferred to a recording chamber continuously superfused with ACSF heated to 34 ˚C. PV interneurons were viewed with infrared-differential interference optics (Hamamatsu camera controller) and fluorescence illumination (Cool Led 473nm) through a 40x water-immersion objective (Olympus). Patch microelectrodes (4–8 MΩ) were pulled from borosilicate glass (1.5 mm outer diameter x 0.86 mm inner diameter; Harvard Apparatus) using a vertical P10 puller (Narishige). Current-clamp and voltage-clamp (sEPSC) recordings were performed using an intracellular solution containing, in mM, 130 KGluconate, 5 KCl, 10 HEPES, 2 MgCl2, 10 Sodium Phosphocreatine, 2 Na2-ATP and 0.4 Na-GTP, as well as 1mg/ml neurobiotin. sEPSCs were recorded at a holding potential of -70 mV. During current-clamp recordings, membrane potential was biased towards -65 mV. Cells were kept under current-clamp or voltage-clamp configuration with a Multiclamp 700B amplifier operating in fast mode. For mEPSC and mIPSC recordings, the following intracellular solution was used (in mM): 135 Cesium Methanesulfonate, 8 KCl, 10 HEPES, 0.4 Mg-ATP, 2.0 Na2-ATP, 0.5 EGTA, 0.6 Na-GTP. 1 µM TTX was added to the bath. mEPSCs were recorded at -60 mV and mIPSCs at +10 mV, accounting for an estimated liquid-junction potential of 10.4 mV. No pharmacological blockade of transmission was performed, in order to allow recording mEPSCs and mIPSCs from the same cell. Data were filtered on-line at 2 kHz, and acquired at a 20 kHz sampling rate for current-clamp recordings in Figure 2 and 50kHz for all others using pClamp 6.0.2 software (Molecular Devices). For immunohistochemistry after patch clamp recording, slices were immediately drop-fixed in PFA 4% at room temperature for 30 mins and subsequently transferred into PBS with 0.05% sodium azide. For BCAN+ and BCAN- cells, only one cell was recorded per slice, as to allow for unequivocal identification between immunohistochemical staining and electrophysiological recording.

Data analysis. Intrinsic properties were measured rapidly after obtaining whole-cell configuration, following previously established protocols (Kawaguchi, 1995). A series of depolarizing or hyperpolarizing 500 milliseconds current steps were used at 0.5 Hz. Resting membrane potentials were measured just after patched membranes were ruptured by suction. Input resistance and membrane time constants were determined by passing hyperpolarizing current pulses inducing voltage shifts of 5-15 mV negative to resting membrane potential. Time constants were measured by fitting voltage responses with a single exponential function. Action potential (AP) threshold was determined as the voltage at which slope trajectory reached 20 mV/milliseconds (Stuart and Häusser, 1994). AP widths at half amplitude were measured for spikes elicited by depolarizing

current pulses of threshold strength. Rheobase was determined by initially injecting positive current generating near-threshold 15-25 mV depolarizations and subsequently applying 1 pA current steps until APs were elicited. Rheobase was considered to have been reached once three such steps consecutively produced an AP, with the lowest value of the AP-generating injected currents used. Delay to first AP was measured during the same procedure, as the time elapsed between onset of current injection and AP threshold and was calculated from the average of 4 repetitions of this procedure. AP height was calculated as the difference in membrane potential between AP threshold and the peak. Afterhyperpolarisation (AhP) amplitude was defined as the difference between AP threshold and the most negative potential attained within 5 milliseconds of AP threshold. AhP time was defined as the time elapsed between this point and AP threshold. For *Bcan*$^{-/-}$ recordings, since a change in AP threshold occurred, we corrected AhP amplitude accordingly. Saturating firing frequency and input-output curves were obtained by injecting steps of 100 pA current and counting spike number. AP frequency adaptation was calculated as the percent change in spike frequency during the last 100 milliseconds of the spike train compared to the first 100 milliseconds. Synaptic currents were analysed semi-automatically with Mini-Analysis (Synaptosoft), using detection parameters of 7 pA for event threshold, 10 ms for searching for a local maximum, 5 ms to search for baseline before peak, 50 ms to search for decay time and 0.37 as the fraction of peak amplitude to find a decay time. Rise-time was calculated as time elapsed between 10 and 90% of peak amplitude.

Image Acquisition and Analysis

Samples belonging to the same experiment were imaged during the same imaging session on an inverted Leica TCS-SP8 confocal. Imaging was performed with the same laser power, photomultiplier gain, pinhole and detection filter settings (1024x1024 resolution, 12 bits or 16 bits). For cell co-localization analyses, confocal image stacks (40X oil immersion objective, 1.4 NA, 0.2 µm step size) were used to create maximum intensity projections and analyzed using a custom macro in Fiji (ImageJ) software. For Brevican and PV level analyses, Cy3 and AF647 fluorophores were used, respectively, and confocal image stacks (40X oil immersion objective, 1.4 NA, 0.2 µm step size) were reconstructed and analyzed with IMARIS 7.5.2 software. PV neurons whose soma was included within the tissue sections with optimal staining were isolated in three dimensions. Three-dimensional isosurfaces were created around each PV-neuron soma using the “create surface” tool and volume and labeling intensities were quantified automatically. A threshold was selected to include as much of the neuron as possible while excluding any background. A size filter was applied with the minimum size being related to the volume of the PV cell. The PV surface was then used to define the cellular domain and create three-dimensional isosurfaces around the PV neuron in the Brevican channel. The threshold was selected so as to have no surface reconstruction outside the cellular domain of PV cells. Brevican volume and intensity were quantified automatically. For synaptic puncta/cluster analysis, images of z-planes with optimal staining of synaptic markers were acquired (100X oil immersion objective, 1.44 NA, 2.2 digital zoom). Analysis of excitatory and inhibitory synapses contacting PV cells was carried out in the stratum oriens of the CA1 region of the hippocampus. Analysis of synaptic puncta/cluster densities was performed using a custom macro in Fiji (ImageJ) software. Processing of all channels included background subtraction, Gaussian blurring, smoothing and contrast enhancement. All single channel images were converted to RGB. For the PV soma, a color threshold was selected to identify the cell soma. The border of the soma was automatically or manually drawn to automatically calculate its perimeter and create a mask with the cell body only. For the presynaptic boutons or postsynaptic clusters, a color threshold was selected to include as many putative synapses as possible while excluding any background. The same threshold in each channel was applied to all

images from the same experiment. The “Analyze Particles” (size 0.10-infinity, circularity 0.00-1.00) and “Watershed” tools were applied and a mask was generated. A merged image from all masks was created. Presynaptic boutons were defined as such when they were located outside the perimeter border but had ≥ 0.1 μm^2 colocalizing with the mask of the soma. The criterion to define postsynaptic clusters was that ≥ 0.2 μm^2 of the cluster area in the mask was located inside the perimeter border of the soma. Synapses were counted when an identified postsynaptic cluster was contacted by a presynaptic terminal (i.e. they had ≥ 1 pixel colocalizing) or when an identified presynaptic bouton was contacting (i.e. they had ≥ 1 pixel colocalizing) a postsynaptic cluster with ≥ 1/4 of its area located inside the perimeter border of the soma. For the four-color analysis of GluA1-containing synapses, GluA1 clusters in PV cells were considered located at the synapse when colocalising with a PSD-95 postsynaptic cluster that was contacted by a VGlut1 presynaptic terminal. For the correlation analysis shown in Figure S2B, confocal image stacks (100X oil immersion objective, 1.4 NA, 2.2 digital zoom, 0.2 µm step size) were reconstructed and analyzed with IMARIS 7.5.2 software. The PV cell soma was reconstructed with the “create surface” tool as described above. The VGlut1 presynaptic boutons and the Brevican coats were detected with the “spot” tool using a spot diameter of 0.68 µm for the VGlut1 boutons and of 0.5 µm for the Brevican coats. A threshold was selected to accurately detect as many spots as possible without creating artifacts. The radius of the spot was used as a threshold distance to define the contact and the “Find spots close to surface” tool (ImarisXT extension) was then used to count the number of presynaptic VGlut1 and Brevican spots that were contacting the surface of the soma.

In utero electroporation and Tamoxifen Induction

CA1 pyramidal cells were labeled by in utero electroporation of a GFP plasmid in *NEX-Cre* mice as described previously (Chacón et al., 2012; Fazzari et al., 2010).

Tamoxifen was dissolved in corn oil (10 mg/ml) at 37°C with constant agitation. Chandelier cells were labeled by intra-gastric tamoxifen injections of P2 post-natal *Nkx2.1CreERT2;RCE* mouse pups at a dose of 1mg/10g of body weight.

Quantitative real-time PCR

Total RNA was extracted from mouse hippocampi using TRIzol reagent (Invitrogen) followed by DNAse I treatment (Promega). cDNA synthesis was performed using the SuperScript IV First-Strand Synthesis System (Invitrogen) according to the manufacturer’s protocol. qPCR was carried out in triplicates on a LightCycler 480 Instrument (Roche) using SYBR Green PCR Master Mix (Roche). Normalized mRNA levels for *Bcan1* and *Bcan2* relatively to those of *Syt2* or *Gfap* were calculated using the comparative C_T method. The sequences of qPCR primers were as follows: *Bcan1* (Fw: CTATGTTTGCCAGGCTATGGG GG, Rv: TGCCTCCTCCCAACTCCTTCGTG), *Bcan2* (Fw: GTCCTGGCAGGCACCTC AGTG, Rv: GCATTGAGCCTTCAGCAGAA TTAC), *Syt2* (Fw: ACGTGCCCACAGCTGG GAAGCTC, Rv: GTCTCTTACCGTTCT GCATCAGG), *Gfap* (Fw: GGGACAACTTTGCACAGGACCTC, Rv: GGTGGCTTCATCTGCCTCCT GTC). The activity-dependent gene *Npas4* (Fw: TTCAAGCCAAGCATGGAGGCTGG, Rv: TAGCTGCTGGCGGAGGCTCC AGG) (Bloodgood et al., 2013), was used to confirm the increase in activity in the enriched environment experiment.

Epilepsy human samples

Frozen postmortem brain tissue from individuals with epilepsy and controls was kindly supplied by the MRC London Neurodegenerative Diseases Brain Bank. Control brains were from individuals with no history of epilepsy or psychiatric disease. The use of human sections was covered by ethics approval granted to the London Neurodegenerative Diseases Brain Bank. For biochemical analysis, 50 µg of tissue from

the CA1 region of the hippocampus were homogenized in lysis buffer and processed following Western blot procedures as described above.

Behavioural procedures

Animals were maintained under standard, temperature controlled, laboratory conditions and kept in 12 hours light-dark cycles with *ad libitum* access to food and water with the exception of the rewarded alternation test. For all behavioral tests, mice were housed singly and assessed during the light phase of the day.

Enriched environment. C57BL/6J male mice were housed together for 4 days (8-week old mice) or 1 month (4-week old mice) in an enrichment cage composed of colored tunnels, mazes, climbing materials, and tilted running wheels (Marlau Cage, ViewPoint Behavior Technology). Controls were age-matched littermates housed in standard conditions.

Morris Water Maze. Testing of 8-12 weeks old C57BL/6J (n = 10) was performed in a 130-cm pool filled with milky water, surrounded by four different objects placed as reference cues onto white curtains. A circular escape platform (10 cm diameter) was submerged 0.5 cm below the water surface. Mice were trained to find the platform during four trials a day, with inter-trial intervals of 5 minutes spent in their home cage. During training, mice were released from pseudo-randomly assigned start locations; they were allowed to swim for up to 60 seconds, when they were manually guided to the platform in the case of failures. Performance was scored as the average latency to find the platform in the four consecutive trials each day. On the last day, the reference memory was assessed as fraction of time spent in the target quadrant during one full trial (60 seconds) upon removal of the escape platform. Swim controls (n = 8) were age-matched mice that were allowed to swim in the pool without escape platform, in a comparable training regime (four trials per day; inter-trial intervals of 5 minutes). For swim controls, trial durations for each day were adjusted to average values of training animals. Trials were tracked using EthoVision software (Noldus Information Technology).

Rewarded alternation task in T-maze. Mice were maintained on a restricted feeding schedule at 85% of their free-feeding weight. Spatial working memory was assessed on a continuous black T-maze consisting of a start arm (60 x 10 cm), two identical goal arms (35 x 10 cm) and two return arms (90 x 10 cm), surrounded by a 14 cm high wall. Light sources in the room were adjusted in order to have the same light intensity in every arm of the maze (20 LUX) and the maze was surrounded by various prominent distal extra-maze cues. The mice were habituated to the maze and to drinking condensed milk pellets over two days for 8 minutes every day. After habituation, animals were pre-trained daily over several days until the consumption of the reward reached minimum 80%. Each pre-training daily session consisted of 4 trials and mice were run one trial at a time with an inter-trial interval (ITI) of approximately 10 minutes. During the pre-training, one milk pellet was available at the end of the two goal arms as reward and mice were allowed to consume the reward from both arms. For spatial nonmatching- to-place testing, mice were assessed in a counterbalanced order and each trial consisted of a sample run and a choice run. On the sample run, the mice were forced either left or right by the presence of a door, according to a pseudorandom sequence (with equal numbers of left and right turns per session, and with not more than two consecutive turns in the same direction). A reward consisting of one milk pellet was available at the end of the arm. The time interval between the sample run and the choice run was approximately 15 seconds. The animal was rewarded for choosing the previously unvisited arm (that is, for alternating). Criterion point for a correct trial was that the whole animal (including the tip of the tail) entered the rewarded arm. Maze was cleaned between trials to avoid any potential odor cues. Each daily session consisted of 4 trials and mice were run one trial at a time with an ITI of approximately 10 minutes.

Open field. The open field consisted of a white PVC enclosed arena (70 x 70 x 30 cm) under uniform lightning conditions (20 LUX). The arena was delimited into two regions using the EthoVision software: an outer zone and an inner zone, a central square area of 35 x 35 cm equidistant from the walls. Mice were placed individually into one corner of the arena facing the sidewalls and were allowed to explore for 10 minutes. The time spent, velocity and total distance moved were recorded and video-tracked using EthoVision software.

Novel object recognition task. The object recognition task took place in the open field apparatus. Mice were individually habituated to the arena for two days. During the training session, two identical objects A1 and A2 were placed into the open field at 20 cm from the walls and the mouse was allowed to explore for 10 minutes. On the short-term memory (STM) testing trial, after an ITI of 5 minutes spent in the home cage, the animals were placed back into the open field, where one of the familiar objects was replaced by a novel object B, and allowed to explore freely for 10 minutes. The position of the novel object (left or right) was randomized between each mouse and each group tested. On the long-term memory (LTM) testing trial (24 hours after the STM testing trial), mice were allowed to explore the open field for 10 minutes in the presence of two objects: the familiar object A and a second novel object C. The novel object (B or C) was randomized in the STM or LTM sessions between each mouse and each group tested. All objects presented similar textures and sizes, but distinctive shapes and colors. Between trials, the objects were washed with 1% Anistel® solution to avoid the use of odor cues. The mice did not show any object preference before trials. Exploratory behavior was videotaped and video-tracked with the EthoVision software and it was measured *post hoc* using two stopwatches to record the time spent exploring the objects during the experimental sessions. A 20 seconds criterion of total exploration (or 10 minutes/session when the criterion was not reached) was used to score exploratory behavior. Object exploration was assessed only if the total time of exploration for each mouse was higher than 5 seconds in the training session. Exploration was scored whenever the mouse sniffed or touched the object while looking at it (i.e., when the distance between the nose and the object was less than 2 cm). Climbing onto the object (unless the mouse sniffed the object it had climbed on) did not qualify as exploration. To measure recognition memory, a discrimination index (DI) was calculated as the difference in exploration time between the novel and familiar objects, divided by the total time spent exploring both objects [(novel arm – familiar arm) / (novel arm + familiar arm)].

Spatial novelty preference in a Y-maze. Spatial novelty preference was assessed as described previously (Bannerman et al., 2008; Sanderson et al., 2009). Briefly, the spontaneous spatial novelty preference test was conducted using an 8 arm radial maze made from transparent Perspex with arms of 22 x 7 x 20 cm. The maze was placed into a room containing a variety of extra-maze cues. Mice were assigned two arms (“start arm” and “familiar arm”) while the entrance to the third arm (the “novel arm” during the subsequent test phase) was blocked off with a black door. Allocation of arms (familiar and novel) to specific spatial locations was counterbalanced within each experimental group. During the exposure phase mice were allowed to explore the two arms for 5 minutes in the one trial exposure test or for 2 minutes five times, spaced by an ITI of 1 minute in the home cage, in the incremental training test. The mouse was then removed from the maze and returned to its home cage for a 1-minute interval between the exposure and test phases. During the test phase, mice were placed at the end of the start arm and allowed to explore all three arms for 2 minutes. An entry into an arm was defined by a mouse placing the forepaws inside an arm. Similarly, a mouse was considered to have left an arm if the forepaws were placed outside the arm. Exploratory behavior was videotaped and video-tracked with the EthoVision software and the

number of entries and the time that mice spent in each arm were recorded manually. For the test phase, a discrimination index DI = [novel arm – familiar arm] / [novel arm + familiar arm] was calculated for both arm entries and time spent in arms.

Ecto-Fc tandem mass spectrometry

The Ecto-Fc MS experiment was performed by Joris de Wit & Jeff Savas at the VIB Center for the Biology of Disease, K.U. Leuven as described previously (Savas et al., 2014). Briefly, the *Bcan1* sequence described above was cloned into an Ecto-Fc plasmid as described previously (Savas et al., 2014) and the purified Ecto-Fc-BCAN2 or the Ecto-Fc only as a control were mixed with detergent-solubilized whole-brain homogenate from 3- to 4-week-old rats. The resulting complexes were purified by affinity chromatography and bound proteins were then analyzed by tandem mass spectrometry (MS/MS). The resulting list of putative binding partners was ranked by spectral counts and only proteins with a spectral count higher than 2 were considered for further analysis. The list was then filtered by eliminating known MS/MS contaminants (Weber et al., 2012) and proteins that copurified with the Fc protein alone as described previously (Savas et al., 2014).

Maternal separation and oxidative stress analysis

An unpredictable maternal separation (UMS) procedure was used. Pups were separated from the mothers at different times during the day for 4h daily on post-natal day (PND) 1 to PND 6 and for 6h on PND 7 to PND 14. During the separation, all pups were placed together in a heat-block at 37°C.

Quantification of the fluorescence intensity levels of 8-oxo-dG in Bcan-/- and wild-type mice subjected or not to maternal separation (MS) was performed in ImageJ. The outline of the cell body was manually drawn and a raw intensity was automatically calculated. An identical outline was used to measure the background fluorescence (i.e. in regions devoid of somata or fluorescence) and the final intensity value was calculated as the subtraction between the raw intensity and the background.

Statistical analysis

All statistical analyses were performed using GraphPad Prism 6 (GraphPad Softwares) or SPSS (IBM Corp) softwares. Unless otherwise stated, parametric data were analyzed by *t*-test or one-way ANOVA followed by the Sidak or Tukey *post hoc* analysis for comparisons of multiple samples. Non-parametric data were analyzed by the Mann-Whitney rank sum test or Kruskal-Wallis one-way analysis of variance on ranks followed by the Dunn *post hoc* analysis for comparisons of multiple samples. Probability distributions were compared using the Kolmogorov-Smirnov test. P values <0.05 were considered statistically significant. Data are presented as mean ± SEM.

UNIVERSITAS
Miguel
Hernández

UNIVERSITAS Miguel Hernández

CONCLUSIONS

UNIVERSITAS Miguel Hernández

1) Different subpopulations of developing GABAergic neurons exhibit cell-specific molecular signatures underscoring a differential usage of related molecules across individual maturing interneuron subtypes.

2) Analysis of interneuron subtype-specific transcriptional dynamics between two close stages of early synaptic wiring revealed a subtype-specific upregulation of genes that specify various critical cellular properties.

3) Tightly regulated cell-type specific molecular programs support interneuron early wiring and underlie the specification of their different patterns of connectivity.

4) FGF13, LGI2 and CBLN4 are selectively and correspondingly expressed in chandelier, PV+ basket and SST+ cells and regulate the development of axo-axonic, somatic and dendritic inhibitory synapses, respectively.

5) In particular, FGF13 is expressed in all chandelier cells, is upregulated during development, and is responsible for the morphological differentiation of chandelier cells by controlling chandelier axonal arbor, cartridge and bouton formation.

6) The perineuronal net protein Brevican is expressed by only one interneuron type: a large fraction of PV+ basket cells, and confers them with specific cellular and synaptic properties.

7) Brevican is located at the excitatory synapses contacting PV+ cells where it regulates GluA1 trafficking and synaptic AMPA receptor composition to promote the stabilization and maturation of the excitatory inputs.

8) By regulating the localization of voltage-gated potassium channels, Brevican endows PV+ basket cells with distinctive intrinsic properties: Brevican-expressing PV+ cells are less excitable but more efficient when recruited.

9) Brevican expression is dynamically regulated by activity and by experience-dependent plasticity *in vivo* and its cell-autonomous function in PV+ cells is required for normal learning and memory.

10) An activity-regulated protein orchestrates cell-specific molecular programs to regulate the maturation of excitatory afferents onto PV+ interneurons and their properties during development but also dynamically gates their function in the adult, thereby facilitating appropriate behavioral responses to experience.

CONCLUSIONES (Spanish)

1) Diferentes subpoblaciones de neuronas GABAérgicas muestran, durante el desarrollo, improntas transcripcionales específicas que subyacen a un uso diferencial de moléculas relacionadas con la formación de los circuitos neuronales.

2) El análisis de la dinámica transcripcional de los subtipos específicos de interneuronas entre dos etapas cercanas del desarrollo neuronal reveló que los genes que especifican varias propiedades celulares críticas aumentan su expresión durante estas etapas.

3) Los programas moleculares específicos de cada tipo de célula apoyan la formación temprana de las interneuronas y subyacen a la especificación de sus diferentes patrones de conectividad.

4) FGF13, LGI2 y CBLN4 se expresan de forma selectiva y correspondiente en células candelabro, PV+ y SST+ y regulan el desarrollo de sinapsis inhibitorias axo-axónicas, somáticas y dendríticas, respectivamente.

5) En particular, FGF13 se expresa en todas las células candelabro, aumenta su expresion durante el desarrollo, y es responsable de la diferenciación morfológica de dichas células controlando el desarrollo del árbol axonal y la formación de sinapsis.

6) La proteína perineuronal Brevican se expresa exclusivamente en una fracción de células PV+ y les confiere propiedades celulares y sinápticas específicas.

7) Brevican se localiza en las sinapsis excitatorias en contacto con las células PV+ donde regula el tráfico de GluA1 y la composición sináptica de los receptores AMPA para promover la estabilización y maduración de las sinapsis excitatorias.

8) Mediante la regulación de la localización de canales de potasio, Brevican confiere propiedades intrínsecas distintivas a las células PV+: las células PV+ que expresan Brevican son menos excitables pero más eficientes cuando son reclutadas.

9) La expresión de Brevican está regulada dinámicamente por la actividad y la experiencia in vivo y su función de especificidad en dichas células PV+ es necesaria para que haya aprendizaje y memoria reglamentarias.

10) Una proteína regulada por actividad dirige programas moleculares específicos para regular la maduración de los aferentes excitatorios en las interneuronas PV+ y sus propiedades durante el desarrollo, pero también regula dinámicamente la función de dichas interneuronas en el adulto, facilitando así las respuestas conductuales apropiadas a la experiencia.

UNIVERSITAS Miguel Hernández

BIBLIOGRAPHY

UNIVERSITAS
Miguel
Hernández

Abbas, L. (2003). Synapse formation: let's stick together. Curr Biol *13*, R25–R27.

Adesnik, H., and Scanziani, M. (2010). Lateral competition for cortical space by layer-specific horizontal circuits. Nature *464*, 1155–1160.

Adesnik, H., Bruns, W., Taniguchi, H., Huang, Z.J., and Scanziani, M. (2012). A neural circuit for spatial summation in visual cortex. Nature *490*, 226–231.

Aisa, B., Elizalde, N., Tordera, R., Lasheras, B., Del Río, J., and Ramírez, M.J. (2009). Effects of neonatal stress on markers of synaptic plasticity in the hippocampus: implications for spatial memory. Hippocampus *19*, 1222–1231.

Akgül, G., and McBain, C.J. (2016). Diverse roles for ionotropic glutamate receptors on inhibitory interneurons in developing and adult brain. J Physiol (Lond) *594*, 5471–5490.

Akgul, G., and Wollmuth, L.P. (2013). Synapse-associated protein 97 regulates the membrane properties of fast-spiking parvalbumin interneurons in the visual cortex. J Neurosci *33*, 12739–12750.

Albrecht, D., Winterflood, C.M., Sadeghi, M., Tschager, T., Noé, F., and Ewers, H. (2016). Nanoscopic compartmentalization of membrane protein motion at the axon initial segment. J Cell Biol *215*, 37–46.

Alcamo, E.A., Chirivella, L., Dautzenberg, M., Dobreva, G., Fariñas, I., Grosschedl, R., and McConnell, S.K. (2008). Satb2 regulates callosal projection neuron identity in the developing cerebral cortex. Neuron *57*, 364–377.

Ali, S.R., Singh, A.K., and Laezza, F. (2016). Identification of Amino Acid Residues in Fibroblast Growth Factor 14 (FGF14) Required for Structure-Function Interactions with Voltage-gated Sodium Channel Nav1.6. J Biol Chem *291*, 11268–11284.

Allan, D.W., Park, D., St Pierre, S.E., Taghert, P.H., and Thor, S. (2005). Regulators acting in combinatorial codes also act independently in single differentiating neurons. Neuron *45*, 689–700.

Allène, C., Cattani, A., Ackman, J.B., Bonifazi, P., Aniksztejn, L., Ben-Ari, Y., and Cossart, R. (2008). Sequential generation of two distinct synapse-driven network patterns in developing neocortex. J Neurosci *28*, 12851–12863.

Anastasiades, P.G., Marques-Smith, A., Lyngholm, D., Lickiss, T., Raffiq, S., Kätzel, D., Miesenböck, G., and Butt, S.J.B. (2016). GABAergic interneurons form transient layer-specific circuits in early postnatal neocortex. Nat Commun *7*, 10584.

Andersen, S.L., and Teicher, M.H. (2004). Delayed effects of early stress on hippocampal development. Neuropsychopharmacology *29*, 1988–1993.

Ango, F., di Cristo, G., Higashiyama, H., Bennett, V., Wu, P., and Huang, Z.J. (2004). Ankyrin-based subcellular gradient of neurofascin, an immunoglobulin family protein, directs GABAergic innervation at purkinje axon initial segment. Cell *119*, 257–272.

Ango, F., Wu, C., Van der Want, J.J., Wu, P., Schachner, M., and Huang, Z.J. (2008). Bergmann glia and the recognition molecule CHL1 organize GABAergic axons and direct innervation of Purkinje cell dendrites. PLoS Biol *6*, e103.

Aoto, J., Martinelli, D.C., Malenka, R.C., Tabuchi, K., and Südhof, T.C. (2013). Presynaptic neurexin-3 alternative splicing trans-synaptically controls postsynaptic AMPA receptor trafficking. Cell *154*, 75–88.

Armijo-Weingart, L., and Gallo, G. (2017). It takes a village to raise a branch: Cellular mechanisms of the initiation of axon collateral branches. Mol Cell Neurosci.

Armstrong, C., and Soltesz, I. (2012). Basket cell dichotomy in microcircuit function. J Physiol (Lond) *590*, 683–694.

Attwell, D., and Laughlin, S.B. (2001). An energy budget for signaling in the grey matter of the brain. J Cereb Blood Flow Metab *21*, 1133–1145.

Ayzenshtat, I., Karnani, M.M., Jackson, J., and Yuste, R. (2016). Cortical control of spatial resolution by VIP+ interneurons. J Neurosci *36*, 11498–11509.

Babraham Bioinformatics, B.B. Babraham Bioinformatics - FastQC A Quality Control tool for High Throughput Sequence Data.

Bannerman, D.M., Deacon, R.M.J., Offen, S., Friswell, J., Grubb, M., and Rawlins, J.N.P. (2002). Double dissociation of function within the hippocampus: spatial memory and hyponeophagia. Behav Neurosci *116*, 884–901.

Bannerman, D.M., Niewoehner, B., Lyon, L., Romberg, C., Schmitt, W.B., Taylor, A., Sanderson, D.J., Cottam, J., Sprengel, R., Seeburg, P.H., et al. (2008). NMDA receptor subunit NR2A is required for rapidly acquired spatial working memory but not incremental spatial reference memory. J Neurosci *28*, 3623–3630.

Barrecheguren, P.J., Ros, O., Cotrufo, T., Kunz, B., Soriano, E., Ulloa, F., Stoeckli, E.T., and Araújo, S.J. (2016). SNARE proteins play a role in motor axon guidance in vertebrates and invertebrates. Dev Neurobiol.

Bartolini, G., Ciceri, G., and Marín, O. (2013). Integration of GABAergic interneurons into cortical cell assemblies: lessons from embryos and adults. Neuron *79*, 849–864.

Bashaw, G.J., and Klein, R. (2010). Signaling from axon guidance receptors. Cold Spring Harb Perspect Biol *2*, a001941.

Basu, J., Srinivas, K.V., Cheung, S.K., Taniguchi, H., Huang, Z.J., and Siegelbaum, S.A. (2013). A cortico-hippocampal learning rule shapes inhibitory microcircuit activity to enhance hippocampal information flow. Neuron *79*, 1208–1221.

Béïque, J.-C., Lin, D.-T., Kang, M.-G., Aizawa, H., Takamiya, K., and Huganir, R.L. (2006). Synapse-specific regulation of AMPA receptor function by PSD-95. Proc Natl Acad Sci U S A *103*, 19535–19540.

Bekku, Y., Su, W.-D., Hirakawa, S., Fässler, R., Ohtsuka, A., Kang, J.S., Sanders, J., Murakami, T., Ninomiya, Y., and Oohashi, T. (2003). Molecular cloning of Bral2, a novel brain-specific link protein, and immunohistochemical colocalization with brevican in perineuronal nets. Mol Cell Neurosci *24*, 148–159.

Bellone, C., and Nicoll, R.A. (2007). Rapid bidirectional switching of synaptic NMDA receptors. Neuron *55*, 779–785.

Ben-Ari, Y. (2002). Excitatory actions of gaba during development: the nature of the nurture. Nat Rev Neurosci *3*, 728–739.

Berezin, V.A. (2010). Structure and function of the neural cell adhesion molecule NCAM (New York: Springer).

Betzig, E., Patterson, G.H., Sougrat, R., Lindwasser, O.W., Olenych, S., Bonifacino, J.S., Davidson, M.W., Lippincott-Schwartz, J., and Hess, H.F. (2006). Imaging intracellular fluorescent proteins at nanometer resolution. Science *313*, 1642–1645.

Bian, W.-J., Miao, W.-Y., He, S.-J., Qiu, Z., and Yu, X. (2015). Coordinated Spine Pruning and Maturation Mediated by Inter-Spine Competition for Cadherin/Catenin Complexes. Cell *162*, 808–822.

Biederer, T., Sara, Y., Mozhayeva, M., Atasoy, D., Liu, X., Kavalali, E.T., and Südhof, T.C. (2002). SynCAM, a synaptic adhesion molecule that drives synapse assembly. Science *297*, 1525–1531.

Blackman, A.V., Abrahamsson, T., Costa, R.P., Lalanne, T., and Sjöström, P.J. (2013). Target-cell-specific short-term plasticity in local circuits. Frontiers in Synaptic Neuroscience *5*, 11.

Bloodgood, B.L., Sharma, N., Browne, H.A., Trepman, A.Z., and Greenberg, M.E. (2013). The activity-dependent transcription factor NPAS4 regulates domain-specific inhibition. Nature *503*, 121–125.

Blosa, M., Sonntag, M., Jäger, C., Weigel, S., Seeger, J., Frischknecht, R., Seidenbecher, C.I., Matthews, R.T., Arendt, T., Rübsamen, R., et al. (2015). The extracellular matrix molecule brevican is an integral component of the machinery mediating fast synaptic transmission at the calyx of Held. J Physiol (Lond) *593*, 4341–4360.

Bloss, E.B., Cembrowski, M.S., Karsh, B., Colonell, J., Fetter, R.D., and Spruston, N. (2016). Structured Dendritic Inhibition Supports Branch-Selective Integration in CA1 Pyramidal Cells. Neuron *89*, 1016–1030.

Bonfanti, L., and Theodosis, D.T. (2009). Polysialic acid and activity-dependent synapse remodeling. Cell Adh Migr *3*, 43–50.

Brakebusch, C., Seidenbecher, C.I., Rauch, U., Matthies, H., Meyer, H., Krug, M., Böckers, T.M., Zhou, X., Kreutz, R., Montag, D., et al. (2002). Brevican-Deficient Mice Display Impaired Hippocampal CA1 Long-Term Potentiation but Show No Obvious Deficits in Learning and Memory Brevican-Deficient Mice Display Impaired Hippocampal CA1 Long-Term Potentiation but Show No Obvious Deficits in Learning an.

Brenhouse, H.C., and Andersen, S.L. (2011). Nonsteroidal anti-inflammatory treatment prevents delayed effects of early life stress in rats. Biol Psychiatry *70*, 434–440.

Brückner, G., Brauer, K., Härtig, W., Wolff, J.R., Rickmann, M.J., Derouiche, A., Delpech, B., Girard, N., Oertel, W.H., and Reichenbach, A. (1993). Perineuronal nets provide a polyanionic, glia-associated form of microenvironment around certain neurons in many parts of the rat brain. Glia *8*, 183–200.

Burrone, J. (2003). Synaptic gain control and homeostasis. Curr Opin Neurobiol *13*, 560–567.

Burté, F., Carelli, V., Chinnery, P.F., and Yu-Wai-Man, P. (2015). Disturbed mitochondrial dynamics and neurodegenerative disorders. Nat Rev Neurol *11*, 11–24.

Buzsáki, G., and Draguhn, A. (2004). Neuronal oscillations in cortical networks. Science *304*, 1926–1929.

Cabungcal, J.-H., Steullet, P., Morishita, H., Kraftsik, R., Cuenod, M., Hensch, T.K., and Do, K.Q. (2013a). Perineuronal nets protect fast-spiking interneurons against oxidative stress. Proc Natl Acad Sci U S A *110*, 9130–9135.

Cabungcal, J.-H., Steullet, P., Kraftsik, R., Cuenod, M., and Do, K.Q. (2013b). Early-life insults impair parvalbumin interneurons via oxidative stress: reversal by N-acetylcysteine. Biol Psychiatry *73*, 574–582.

Campo, G.M., Avenoso, A., Campo, S., Ascola, A. D', Ferlazzo, A.M., and Calatroni, A. (2004). Reduction of DNA fragmentation and hydroxyl radical production by hyaluronic acid and chondroitin-4-sulphate in iron plus ascorbate-induced oxidative stress in fibroblast cultures. Free Radic Res *38*, 601–611.

Cancedda, L., Fiumelli, H., Chen, K., and Poo, M. (2007). Excitatory GABA action is essential for morphological maturation of cortical neurons in vivo. J Neurosci *27*, 5224–5235.

Cardin, J.A., Carlén, M., Meletis, K., Knoblich, U., Zhang, F., Deisseroth, K., Tsai, L.-H., and Moore, C.I. (2009). Driving fast-spiking cells induces gamma rhythm and controls sensory responses. Nature *459*, 663–667.

Carstens, K.E., Phillips, M.L., Pozzo-Miller, L., Weinberg, R.J., and Dudek, S.M. (2016). Perineuronal Nets Suppress Plasticity of Excitatory Synapses on CA2 Pyramidal Neurons. J Neurosci *36*, 6312–6320.

Carter, B.C., and Bean, B.P. (2009). Sodium entry during action potentials of mammalian neurons: incomplete inactivation and reduced metabolic efficiency in fast-spiking neurons. Neuron *64*, 898–909.

Carulli, D., Pizzorusso, T., Kwok, J.C.F., Putignano, E., Poli, A., Forostyak, S., Andrews, M.R., Deepa, S.S., Glant, T.T., and Fawcett, J.W. (2010). Animals lacking link protein have attenuated perineuronal nets and persistent plasticity. Brain *133*, 2331–2347.

Celio, M.R., Spreafico, R., De Biasi, S., and Vitellaro-Zuccarello, L. (1998). Perineuronal nets: past and present. Trends Neurosci *21*, 510–515.

Chacón, M.R., Navarro, A.I., Cuesto, G., del Pino, I., Scott, R., Morales, M., and Rico, B. (2012). Focal adhesion kinase regulates actin nucleation and neuronal filopodia formation during axonal growth. Development *139*, 3200–3210.

Chang, M.C., Park, J.M., Pelkey, K.A., Grabenstatter, H.L., Xu, D., Linden, D.J., Sutula, T.P., McBain, C.J., and Worley, P.F. (2010). Narp regulates homeostatic scaling of excitatory synapses on parvalbumin-expressing interneurons. Nat Neurosci *13*, 1090–1097.

Chattopadhyaya, B., Di Cristo, G., Higashiyama, H., Knott, G.W., Kuhlman, S.J., Welker, E., and Huang, Z.J. (2004). Experience and activity-dependent maturation of perisomatic GABAergic innervation in

primary visual cortex during a postnatal critical period. J Neurosci *24*, 9598–9611.

Chattopadhyaya, B., Di Cristo, G., Wu, C.Z., Knott, G., Kuhlman, S., Fu, Y., Palmiter, R.D., and Huang, Z.J. (2007). GAD67-mediated GABA synthesis and signaling regulate inhibitory synaptic innervation in the visual cortex. Neuron *54*, 889–903.

Chattopadhyaya, B., Baho, E., Huang, Z.J., Schachner, M., and Di Cristo, G. (2013). Neural cell adhesion molecule-mediated Fyn activation promotes GABAergic synapse maturation in postnatal mouse cortex. J Neurosci *33*, 5957–5968.

Chen, B., Schaevitz, L.R., and McConnell, S.K. (2005). Fezl regulates the differentiation and axon targeting of layer 5 subcortical projection neurons in cerebral cortex. Proc Natl Acad Sci U S A *102*, 17184–17189.

Chen, L.Y., Jiang, M., Zhang, B., Gokce, O., and Südhof, T.C. (2017). Conditional deletion of all neurexins defines diversity of essential synaptic organizer functions for neurexins. Neuron *94*, 611–625.e4.

Chen, W.G., Chang, Q., Lin, Y., Meissner, A., West, A.E., Griffith, E.C., Jaenisch, R., and Greenberg, M.E. (2003). Derepression of BDNF transcription involves calcium-dependent phosphorylation of MeCP2. Science *302*, 885–889.

Chih, B., Engelman, H., and Scheiffele, P. (2005). Control of excitatory and inhibitory synapse formation by neuroligins. Science *307*, 1324–1328.

Chih, B., Gollan, L., and Scheiffele, P. (2006). Alternative splicing controls selective trans-synaptic interactions of the neuroligin-neurexin complex. Neuron *51*, 171–178.

Chiu, C.Q., Lur, G., Morse, T.M., Carnevale, N.T., Ellis-Davies, G.C.R., and Higley, M.J. (2013). Compartmentalization of GABAergic inhibition by dendritic spines. Science *340*, 759–762.

Christensen, R., Shao, Z., and Colón-Ramos, D.A. (2013). The cell biology of synaptic specificity during development. Curr Opin Neurobiol *23*, 1018–1026.

Christopherson, K.S., Ullian, E.M., Stokes, C.C.A., Mullowney, C.E., Hell, J.W., Agah, A., Lawler, J., Mosher, D.F., Bornstein, P., and Barres, B.A. (2005). Thrombospondins are astrocyte-secreted proteins that promote CNS synaptogenesis. Cell *120*, 421–433.

Chung, W.-S., Clarke, L.E., Wang, G.X., Stafford, B.K., Sher, A., Chakraborty, C., Joung, J., Foo, L.C., Thompson, A., Chen, C., et al. (2013). Astrocytes mediate synapse elimination through MEGF10 and MERTK pathways. Nature *504*, 394–400.

Clarke, L.E., and Barres, B.A. (2013). Emerging roles of astrocytes in neural circuit development. Nat Rev Neurosci *14*, 311–321.

Colón-Ramos, D.A., Margeta, M.A., and Shen, K. (2007). Glia promote local synaptogenesis through UNC-6 (netrin) signaling in C. elegans. Science *318*, 103–106.

Conn, P.M. (1990). Isolation of Astrocytes and Schwann Cells for Culture. In Cell Culture, (San Diego : Academic Press, c1990.: Academic Press), pp. 47–56.

Cossart, R. (2011). The maturation of cortical interneuron diversity: how multiple developmental journeys shape the emergence of proper network function. Curr Opin Neurobiol *21*, 160–168.

Cotrufo, T., Pérez-Brangulí, F., Muhaisen, A., Ros, O., Andrés, R., Baeriswyl, T., Fuschini, G., Tarrago, T., Pascual, M., Ureña, J., et al. (2011). A signaling mechanism coupling netrin-1/deleted in colorectal cancer chemoattraction to SNARE-mediated exocytosis in axonal growth cones. J Neurosci *31*, 14463–14480.

Cottam, J.C.H. (2009). Identifying the functional role of Martinotti cells in cortical sensory processing. J Neurophysiol *102*, 9–11.

Di Cristo, G., Chattopadhyaya, B., Kuhlman, S.J., Fu, Y., Bélanger, M.-C., Wu, C.Z., Rutishauser, U., Maffei, L., and Huang, Z.J. (2007). Activity-dependent PSA expression regulates inhibitory maturation and onset of critical period plasticity. Nat Neurosci *10*, 1569–1577.

Dalva, M.B., Takasu, M.A., Lin, M.Z., Shamah, S.M., Hu, L., Gale, N.W., and Greenberg, M.E. (2000). EphB receptors interact with NMDA receptors and regulate excitatory synapse formation. Cell *103*, 945–956.

Danglot, L., Triller, A., and Marty, S. (2006). The development of hippocampal interneurons in rodents. Hippocampus *16*, 1032–1060.

Dani, A., Huang, B., Bergan, J., Dulac, C., and Zhuang, X. (2010). Superresolution imaging of chemical synapses in the brain. Neuron *68*, 843–856.

Daniels, W.M.U., Marais, L., Stein, D.J., and Russell, V.A. (2012). Exercise normalizes altered expression of proteins in the ventral hippocampus of rats subjected to maternal separation. Exp Physiol *97*, 239–247.

Deacon, R.M.J., and Rawlins, J.N.P. (2006). T-maze alternation in the rodent. Nat Protoc *1*, 7–12.

Deepa, S.S., Carulli, D., Galtrey, C., Rhodes, K., Fukuda, J., Mikami, T., Sugahara, K., and Fawcett, J.W. (2006). Composition of perineuronal net extracellular matrix in rat brain: a different disaccharide composition for the net-associated proteoglycans. J Biol Chem *281*, 17789–17800.

DeFelipe, J., and Fariñas, I. (1992). The pyramidal neuron of the cerebral cortex: morphological and chemical characteristics of the synaptic inputs. Prog Neurobiol *39*, 563–607.

DeFelipe, J., López-Cruz, P.L., Benavides-Piccione, R., Bielza, C., Larrañaga, P., Anderson, S., Burkhalter, A., Cauli, B., Fairén, A., Feldmeyer, D., et al. (2013). New insights into the classification and nomenclature of cortical GABAergic interneurons. Nat Rev Neurosci *14*, 202–216.

Deguchi, Y., Donato, F., Galimberti, I., Cabuy, E., and Caroni, P. (2011). Temporally matched subpopulations of selectively interconnected principal neurons in the hippocampus. Nat Neurosci *14*, 495–504.

Dehorter, N., Ciceri, G., Bartolini, G., Lim, L., del Pino, I., and Marín, O. (2015). Tuning of fast-spiking interneuron properties by an activity-dependent transcriptional switch. Science *349*, 1216–1220.

Dehorter, N., Marichal, N., Marín, O., and Berninger, B. (2017). Tuning neural circuits by turning the interneuron knob. Curr Opin Neurobiol *42*, 144–151.

DeNardo, L.A., de Wit, J., Otto-Hitt, S., and Ghosh, A. (2012). NGL-2 regulates input-specific synapse development in CA1 pyramidal neurons. Neuron *76*, 762–775.

Deneris, E.S., and Hobert, O. (2014). Maintenance of postmitotic neuronal cell identity. Nat Neurosci *17*, 899–907.

Dent, E.W., and Kalil, K. (2001). Axon branching requires interactions between dynamic microtubules and actin filaments. J Neurosci *21*, 9757–9769.

Dent, E.W., Gupton, S.L., and Gertler, F.B. (2011). The growth cone cytoskeleton in axon outgrowth and guidance. Cold Spring Harb Perspect Biol *3*.

Dickson, B.J. (2002). Molecular mechanisms of axon guidance. Science *298*, 1959–1964.

Diehl, L.A., Alvares, L.O., Noschang, C., Engelke, D., Andreazza, A.C., Gonçalves, C.A.S., Quillfeldt, J.A., and Dalmaz, C. (2012). Long-lasting effects of maternal separation on an animal model of post-traumatic stress disorder: effects on memory and hippocampal oxidative stress. Neurochem Res *37*, 700–707.

Dimidschstein, J., Chen, Q., Tremblay, R., Rogers, S.L., Saldi, G.-A., Guo, L., Xu, Q., Liu, R., Lu, C., Chu, J., et al. (2016). A viral strategy for targeting and manipulating interneurons across vertebrate species. Nat Neurosci *19*, 1743–1749.

Ding, J.B., Oh, W.-J., Sabatini, B.L., and Gu, C. (2011). Semaphorin 3E-Plexin-D1 signaling controls pathway-specific synapse formation in the striatum. Nat Neurosci *15*, 215–223.

Dityatev, A., Dityateva, G., and Schachner, M. (2000). Synaptic strength as a function of post- versus presynaptic expression of the neural cell adhesion molecule NCAM. Neuron *26*, 207–217.

Do, K.Q., Cuenod, M., and Hensch, T.K. (2015). Targeting oxidative stress and aberrant critical period plasticity in the developmental trajectory to schizophrenia. Schizophr Bull *41*, 835–846.

Doischer, D., Hosp, J.A., Yanagawa, Y., Obata, K., Jonas, P., Vida, I., and Bartos, M. (2008). Postnatal differentiation of basket cells from slow to fast signaling devices. J Neurosci *28*, 12956–12968.

Donato, F., Rompani, S.B., and Caroni, P. (2013). Parvalbumin-expressing basket-cell network plasticity induced by experience regulates adult learning. Nature *504*, 272–276.

Donato, F., Chowdhury, A., Lahr, M., and Caroni, P. (2015). Early- and late-born parvalbumin basket cell subpopulations exhibiting distinct regulation and roles in learning. Neuron *85*, 770–786.

Doyle, J.P., Dougherty, J.D., Heiman, M., Schmidt, E.F., Stevens, T.R., Ma, G., Bupp, S., Shrestha, P., Shah, R.D., Doughty, M.L., et al. (2008). Application of a translational profiling approach for the comparative analysis of CNS cell types. Cell *135*, 749–762.

Du, J., Zhang, L., Weiser, M., Rudy, B., and McBain, C.J. (1996). Developmental expression and functional characterization of the potassium-channel subunit Kv3.1b in parvalbumin-containing interneurons of the rat hippocampus. J Neurosci *16*, 506–518.

Dugladze, T., Schmitz, D., Whittington, M.A., Vida, I., and Gloveli, T. (2012). Segregation of axonal and somatic activity during fast network oscillations. Science *336*, 1458–1461.

Dunah, A.W., Hueske, E., Wyszynski, M., Hoogenraad, C.C., Jaworski, J., Pak, D.T., Simonetta, A., Liu, G., and Sheng, M. (2005). LAR receptor protein tyrosine phosphatases in the development and maintenance of excitatory synapses. Nat Neurosci *8*, 458–467.

Dunn, L., Allen, G.F., Mamais, A., Ling, H., Li, A., Duberley, K.E., Hargreaves, I.P., Pope, S., Holton, J.L., Lees, A., et al. (2014). Dysregulation of glucose metabolism is an early event in sporadic Parkinson's disease. Neurobiol Aging *35*, 1111–1115.

Durand, G.M., Kovalchuk, Y., and Konnerth, A. (1996). Long-term potentiation and functional synapse induction in developing hippocampus. Nature *381*, 71–75.

Ehrlich, I., Klein, M., Rumpel, S., and Malinow, R. (2007). PSD-95 is required for activity-driven synapse stabilization. Proc Natl Acad Sci U S A *104*, 4176–4181.

El-Husseini, A.E., Schnell, E., Chetkovich, D.M., Nicoll, R.A., and Bredt, D.S. (2000). PSD-95 involvement in maturation of excitatory synapses. Science *290*, 1364–1368.

Elias, G.M., and Nicoll, R.A. (2007). Synaptic trafficking of glutamate receptors by MAGUK scaffolding proteins. Trends Cell Biol *17*, 343–352.

Emes, R.D., and Grant, S.G.N. (2012). Evolution of synapse complexity and diversity. Annu Rev Neurosci *35*, 111–131.

Ethell, I.M., and Pasquale, E.B. (2005). Molecular mechanisms of dendritic spine development and remodeling. Prog Neurobiol *75*, 161–205.

Evers, M.R., Salmen, B., Bukalo, O., Rollenhagen, A., Bösl, M.R., Morellini, F., Bartsch, U., Dityatev, A., and Schachner, M. (2002). Impairment of L-type Ca2+ channel-dependent forms of hippocampal synaptic plasticity in mice deficient in the extracellular matrix glycoprotein tenascin-C. J Neurosci *22*, 7177–7194.

Fallon, J.R., and Hall, Z.W. (1994). Building synapses: agrin and dystroglycan stick together. Trends Neurosci *17*, 469–473.

Fannon, A.M., and Colman, D.R. (1996). A model for central synaptic junctional complex formation based on the differential adhesive specificities of the cadherins. Neuron *17*, 423–434.

Fazzari, P., Paternain, A.V., Valiente, M., Pla, R., Luján, R., Lloyd, K., Lerma, J., Marín, O., and Rico, B. (2010). Control of cortical GABA circuitry development by Nrg1 and ErbB4 signalling. Nature *464*, 1376–1380.

De Felipe, J., Marco, P., Fairén, A., and Jones, E.G. (1997). Inhibitory synaptogenesis in mouse somatosensory cortex. Cereb Cortex *7*, 619–634.

Fenno, L.E., Mattis, J., Ramakrishnan, C., Hyun, M., Lee, S.Y., He, M., Tucciarone, J., Selimbeyoglu, A., Berndt, A., Grosenick, L., et al. (2014). Targeting cells with single vectors using multiple-feature Boolean logic. Nat Methods *11*, 763–772.

Fish, K.N., Sweet, R.A., and Lewis, D.A. (2011). Differential distribution of proteins regulating GABA synthesis and reuptake in axon boutons of subpopulations of cortical interneurons. Cereb Cortex *21*, 2450–2460.

Fishell, G. (2013). Hurricane Sandy: After the deluge. Nature *496*, 421–422.

Flavell, S.W., Cowan, C.W., Kim, T.-K., Greer, P.L., Lin, Y., Paradis, S., Griffith, E.C., Hu, L.S., Chen, C., and Greenberg, M.E. (2006). Activity-dependent regulation of MEF2 transcription factors

suppresses excitatory synapse number. Science *311*, 1008–1012.

Fossati, M., Pizzarelli, R., Schmidt, E.R., Kupferman, J.V., Stroebel, D., Polleux, F., and Charrier, C. (2016). SRGAP2 and Its Human-Specific Paralog Co-Regulate the Development of Excitatory and Inhibitory Synapses. Neuron *91*, 356–369.

Frischknecht, R., and Seidenbecher, C.I. (2012). Brevican: a key proteoglycan in the perisynaptic extracellular matrix of the brain. Int J Biochem Cell Biol *44*, 1051–1054.

Frischknecht, R., Heine, M., Perrais, D., Seidenbecher, C.I., Choquet, D., and Gundelfinger, E.D. (2009). Brain extracellular matrix affects AMPA receptor lateral mobility and short-term synaptic plasticity. Nat Neurosci *12*, 897–904.

Frischknecht, R., Chang, K.-J., Rasband, M.N., and Seidenbecher, C.I. (2014). Neural ECM molecules in axonal and synaptic homeostatic plasticity. Prog Brain Res *214*, 81–100.

Fritschy, J.-M., Harvey, R.J., and Schwarz, G. (2008). Gephyrin: where do we stand, where do we go? Trends Neurosci *31*, 257–264.

Fritschy, J.-M., Panzanelli, P., and Tyagarajan, S.K. (2012). Molecular and functional heterogeneity of GABAergic synapses. Cell Mol Life Sci *69*, 2485–2499.

Froemke, R.C. (2015). Plasticity of cortical excitatory-inhibitory balance. Annu Rev Neurosci *38*, 195–219.

Frotscher, M., Heimrich, B., and Deller, T. (1997). Sprouting in the hippocampus is layer-specific. Trends Neurosci *20*, 218–223.

Fu, Y., Wu, X., Lu, J., and Huang, Z.J. (2012). Presynaptic GABA(B) Receptor Regulates Activity-Dependent Maturation and Patterning of Inhibitory Synapses through Dynamic Allocation of Synaptic Vesicles. Front Cell Neurosci *6*, 57.

Fuchs, E.C., Zivkovic, A.R., Cunningham, M.O., Middleton, S., Lebeau, F.E.N., Bannerman, D.M., Rozov, A., Whittington, M.A., Traub, R.D., Rawlins, J.N.P., et al. (2007). Recruitment of parvalbumin-positive interneurons determines hippocampal function and associated behavior. Neuron *53*, 591–604.

Fukazawa, Y., Saitoh, Y., Ozawa, F., Ohta, Y., Mizuno, K., and Inokuchi, K. (2003). Hippocampal LTP is accompanied by enhanced F-actin content within the dendritic spine that is essential for late LTP maintenance in vivo. Neuron *38*, 447–460.

Fuss, B., Mallon, B., Phan, T., Ohlemeyer, C., Kirchhoff, F., Nishiyama, A., and Macklin, W.B. (2000). Purification and analysis of in vivo-differentiated oligodendrocytes expressing the green fluorescent protein. Dev Biol *218*, 259–274.

Galanopoulou, A.S. (2008). GABA(A) receptors in normal development and seizures: friends or foes? Curr Neuropharmacol *6*, 1–20.

Gallo, G. (2011). The cytoskeletal and signaling mechanisms of axon collateral branching. Dev Neurobiol *71*, 201–220.

Galow, L.V., Schneider, J., Lewen, A., Ta, T.-T., Papageorgiou, I.E., and Kann, O. (2014). Energy substrates that fuel fast neuronal network oscillations. Front Neurosci *8*, 398.

García-Frigola, C., Carreres, M.I., Vegar, C., Mason, C., and Herrera, E. (2008). Zic2 promotes axonal divergence at the optic chiasm midline by EphB1-dependent and -independent mechanisms. Development *135*, 1833–1841.

Garcia-Junco-Clemente, P., Ikrar, T., Tring, E., Xu, X., Ringach, D.L., and Trachtenberg, J.T. (2017). An inhibitory pull-push circuit in frontal cortex. Nat Neurosci *20*, 389–392.

Gaspar, P., Cases, O., and Maroteaux, L. (2003). The developmental role of serotonin: news from mouse molecular genetics. Nat Rev Neurosci *4*, 1002–1012.

Gelman, D.M., and Marín, O. (2010). Generation of interneuron diversity in the mouse cerebral cortex. Eur J Neurosci *31*, 2136–2141.

Gentet, L.J., Kremer, Y., Taniguchi, H., Huang, Z.J., Staiger, J.F., and Petersen, C.C.H. (2012). Unique functional properties of somatostatin-expressing GABAergic neurons in mouse barrel cortex. Nat Neurosci *15*, 607–612.

Goebbels, S., Bormuth, I., Bode, U., Hermanson, O., Schwab, M.H., and Nave, K.-A. (2006). Genetic targeting of principal neurons in neocortex and hippocampus of NEX-Cre mice. Genesis *44*, 611–621.

Goetz, R., Dover, K., Laezza, F., Shtraizent, N., Huang, X., Tchetchik, D., Eliseenkova, A.V., Xu, C.-F., Neubert, T.A., Ornitz, D.M., et al. (2009). Crystal structure of a fibroblast growth factor homologous factor (FHF) defines a conserved surface on FHFs for binding and modulation of voltage-gated sodium channels. J Biol Chem *284*, 17883–17896.

Gogolla, N., Caroni, P., Lüthi, A., and Herry, C. (2009). Perineuronal nets protect fear memories from erasure. Science *325*, 1258–1261.

Goldberg, J.L. (2003). How does an axon grow? Genes Dev *17*, 941–958.

Goldberg, E.M., Clark, B.D., Zagha, E., Nahmani, M., Erisir, A., and Rudy, B. (2008). K+ channels at the axon initial segment dampen near-threshold excitability of neocortical fast-spiking GABAergic interneurons. Neuron *58*, 387–400.

Goldberg, E.M., Jeong, H.-Y., Kruglikov, I., Tremblay, R., Lazarenko, R.M., and Rudy, B. (2011). Rapid developmental maturation of neocortical FS cell intrinsic excitability. Cereb Cortex *21*, 666–682.

Goldfarb, M., Schoorlemmer, J., Williams, A., Diwakar, S., Wang, Q., Huang, X., Giza, J., Tchetchik, D., Kelley, K., Vega, A., et al. (2007). Fibroblast growth factor homologous factors control neuronal excitability through modulation of voltage-gated sodium channels. Neuron *55*, 449–463.

Golshani, P., Truong, H., and Jones, E.G. (1997). Developmental expression of GABAA receptor subunit and GAD genes in mouse somatosensory barrel cortex. Journal of Comparative Neurology.

Gouarné, C., Tardif, G., Tracz, J., Latyszenok, V., Michaud, M., Clemens, L.E., Yu-Taeger, L., Nguyen, H.P., Bordet, T., and Pruss, R.M. (2013). Early deficits in glycolysis are specific to striatal neurons from a rat model of huntington disease. PLoS ONE *8*, e81528.

Grabowski, P.J., and Black, D.L. (2001). Alternative RNA splicing in the nervous system. Prog Neurobiol *65*, 289–308.

Graf, E.R., Zhang, X., Jin, S.-X., Linhoff, M.W., and Craig, A.M. (2004). Neurexins induce differentiation of GABA and glutamate postsynaptic specializations via neuroligins. Cell *119*, 1013–1026.

Gray, L.R., Tompkins, S.C., and Taylor, E.B. (2014). Regulation of pyruvate metabolism and human disease. Cell Mol Life Sci *71*, 2577–2604.

Greig, L.C., Woodworth, M.B., Galazo, M.J., Padmanabhan, H., and Macklis, J.D. (2013). Molecular logic of neocortical projection neuron specification, development and diversity. Nat Rev Neurosci *14*, 755–769.

Grubb, M.S., and Burrone, J. (2010a). Building and maintaining the axon initial segment. Curr Opin Neurobiol *20*, 481–488.

Grubb, M.S., and Burrone, J. (2010b). Activity-dependent relocation of the axon initial segment fine-tunes neuronal excitability. Nature *465*, 1070–1074.

Grubb, M.S., Shu, Y., Kuba, H., Rasband, M.N., Wimmer, V.C., and Bender, K.J. (2011). Short- and long-term plasticity at the axon initial segment. J Neurosci *31*, 16049–16055.

Gu, S., Jin, L., Zhang, Y., Huang, Y., Zhang, F., Valdmanis, P.N., and Kay, M.A. (2012). The loop position of shRNAs and pre-miRNAs is critical for the accuracy of dicer processing in vivo. Cell *151*, 900–911.

Gulyás, a I., Megías, M., Emri, Z., and Freund, T.F. (1999). Total number and ratio of excitatory and inhibitory synapses converging onto single interneurons of different types in the CA1 area of the rat hippocampus. The Journal of Neuroscience the Official Journal of the Society for Neuroscience.

Gulyás, A.I., Buzsáki, G., Freund, T.F., and Hirase, H. (2006). Populations of hippocampal inhibitory neurons express different levels of cytochrome c. Eur J Neurosci *23*, 2581–2594.

Gundelfinger, E.D., and Fejtova, A. (2012). Molecular organization and plasticity of the cytomatrix at the active zone. Curr Opin Neurobiol *22*, 423–430.

Hall, B.J., and Ghosh, A. (2008). Regulation of AMPA receptor recruitment at developing synapses. Trends Neurosci *31*, 82–89.

Hall, A.C., Lucas, F.R., and Salinas, P.C. (2000). Axonal remodeling and synaptic differentiation in the cerebellum is regulated by WNT-7a signaling. Cell *100*, 525–535.

Hanse, E., Durand, G.M., Garaschuk, O., and Konnerth, A. (1997). Activity-dependent wiring of the developing hippocampal neuronal circuit. Semin Cell Dev Biol *8*, 35–42.

Hanse, E., Taira, T., Lauri, S., and Groc, L. (2009). Glutamate synapse in developing brain: an integrative perspective beyond the silent state. Trends Neurosci *32*, 532–537.

Hanse, E., Seth, H., and Riebe, I. (2013). AMPA-silent synapses in brain development and pathology. Nat Rev Neurosci *14*, 839–850.

Harbom, L.J., Chronister, W.D., and McConnell, M.J. (2016). Single neuron transcriptome analysis can reveal more than cell type classification: Does it matter if every neuron is unique? Bioessays *38*, 157–161.

Harris, K.D., and Mrsic-Flogel, T.D. (2013). Cortical connectivity and sensory coding. Nature *503*, 51–58.

Harris, K.D., and Shepherd, G.M.G. (2015). The neocortical circuit: themes and variations. Nat Neurosci *18*, 170–181.

Harris, J.J., Jolivet, R., and Attwell, D. (2012). Synaptic energy use and supply. Neuron *75*, 762–777.

Harwell, C.C., Parker, P.R.L., Gee, S.M., Okada, A., McConnell, S.K., Kreitzer, A.C., and Kriegstein, A.R. (2012). Sonic hedgehog expression in corticofugal projection neurons directs cortical microcircuit formation. Neuron *73*, 1116–1126.

Häusser, M., Spruston, N., and Stuart, G.J. (2000). Diversity and dynamics of dendritic signaling. Science *290*, 739–744.

Hayashi, S., and Takeichi, M. (2015). Emerging roles of protocadherins: from self-avoidance to enhancement of motility. J Cell Sci *128*, 1455–1464.

Hayashi, K., Kubo, K.-I., Kitazawa, A., and Nakajima, K. (2015). Cellular dynamics of neuronal migration in the hippocampus. Front Neurosci *9*, 135.

Hedstrom, K.L., Xu, X., Ogawa, Y., Frischknecht, R., Seidenbecher, C.I., Shrager, P., and Rasband, M.N. (2007). Neurofascin assembles a specialized extracellular matrix at the axon initial segment. J Cell Biol *178*, 875–886.

Henley, J.M., and Wilkinson, K.A. (2016). Synaptic AMPA receptor composition in development, plasticity and disease. Nat Rev Neurosci *17*, 337–350.

Hensch, T.K., and Fagiolini, M. (2005). Excitatory-inhibitory balance and critical period plasticity in developing visual cortex.

Hensch, T.K., Fagiolini, M., Mataga, N., Stryker, M.P., Baekkeskov, S., and Kash, S.F. (1998). Local GABA circuit control of experience-dependent plasticity in developing visual cortex. Science *282*, 1504–1508.

Herrera, E., Brown, L., Aruga, J., Rachel, R.A., Dolen, G., Mikoshiba, K., Brown, S., and Mason, C.A. (2003). Zic2 patterns binocular vision by specifying the uncrossed retinal projection. Cell *114*, 545–557.

Hippenmeyer, S., Vrieseling, E., Sigrist, M., Portmann, T., Laengle, C., Ladle, D.R., and Arber, S. (2005). A developmental switch in the response of DRG neurons to ETS transcription factor signaling. PLoS Biol *3*, e159.

Hirano, S., and Takeichi, M. (2012). Cadherins in brain morphogenesis and wiring. Physiol Rev *92*, 597–634.

Hlushchenko, I., Koskinen, M., and Hotulainen, P. (2016). Dendritic spine actin dynamics in neuronal maturation and synaptic plasticity. Cytoskeleton (Hoboken) *73*, 435–441.

Hobert, O. (2016). Terminal selectors of neuronal identity. Curr Top Dev Biol *116*, 455–475.

Hockfield, S., and McKay, R.D. (1983). A surface antigen expressed by a subset of neurons in the vertebrate central nervous system. Proc Natl Acad Sci U S A *80*, 5758–5761.

Hoogendoorn, E., Crosby, K.C., Leyton-Puig, D., Breedijk, R.M., Jalink, K., Gadella, T.W., and Postma,

M. (2014). The fidelity of stochastic single-molecule super-resolution reconstructions critically depends upon robust background estimation. Sci Rep *4*, 3854.

Howard, A., Tamas, G., and Soltesz, I. (2005). Lighting the chandelier: new vistas for axo-axonic cells. Trends Neurosci *28*, 310–316.

Hsu, F., Zhang, G., Raol, Y.S.H., Valentino, R.J., Coulter, D.A., and Brooks-kayal, A.R. (2003). Repeated neonatal handling with maternal separation permanently alters hippocampal GABA A receptors and behavioral stress responses.

Hu, H., Gan, J., and Jonas, P. (2014). Interneurons. Fast-spiking, parvalbumin^{+} GABAergic interneurons: from cellular design to microcircuit function. Science *345*, 1255263.

Huang, Z.J., and Scheiffele, P. (2008). GABA and neuroligin signaling: linking synaptic activity and adhesion in inhibitory synapse development. Curr Opin Neurobiol *18*, 77–83.

Huang, Z.J., Kirkwood, A., Pizzorusso, T., Porciatti, V., Morales, B., Bear, M.F., Maffei, L., and Tonegawa, S. (1999). BDNF regulates the maturation of inhibition and the critical period of plasticity in mouse visual cortex. Cell *98*, 739–755.

Huupponen, J., Molchanova, S.M., Lauri, S.E., and Taira, T. (2013). Ongoing intrinsic synchronous activity is required for the functional maturation of CA3-CA1 glutamatergic synapses. Cereb Cortex *23*, 2754–2764.

Imamura, F., Ayoub, A.E., Rakic, P., and Greer, C.A. (2011). Timing of neurogenesis is a determinant of olfactory circuitry. Nat Neurosci *14*, 331–337.

Inan, M., and Anderson, S.A. (2014). The chandelier cell, form and function. Curr Opin Neurobiol *26*, 142–148.

Inan, M., Blázquez-Llorca, L., Merchán-Pérez, A., Anderson, S.A., DeFelipe, J., and Yuste, R. (2013). Dense and overlapping innervation of pyramidal neurons by chandelier cells. J Neurosci *33*, 1907–1914.

Inan, M., Zhao, M., Manuszak, M., Karakaya, C., Rajadhyaksha, A.M., Pickel, V.M., Schwartz, T.H., Goldstein, P.A., and Manfredi, G. (2016). Energy deficit in parvalbumin neurons leads to circuit dysfunction, impaired sensory gating and social disability. Neurobiol Dis *93*, 35–46.

Inda, M.C., DeFelipe, J., and Muñoz, A. (2009). Morphology and distribution of chandelier cell axon terminals in the mouse cerebral cortex and claustroamygdaloid complex. Cereb Cortex *19*, 41–54.

Inoue, A., and Sanes, J.R. (1997). Lamina-specific connectivity in the brain: regulation by N-cadherin, neurotrophins, and glycoconjugates. Science *276*, 1428–1431.

Isaac, J.T., Nicoll, R.A., and Malenka, R.C. (1995). Evidence for silent synapses: implications for the expression of LTP. Neuron *15*, 427–434.

Isaacson, J.S., and Scanziani, M. (2011). How inhibition shapes cortical activity. Neuron *72*, 231–243.

Itami, C., Kimura, F., and Nakamura, S. (2007). Brain-derived neurotrophic factor regulates the maturation of layer 4 fast-spiking cells after the second postnatal week in the developing barrel cortex. J Neurosci *27*, 2241–2252.

Ivanova, A.V., Goparaju, C.M.V., Ivanov, S.V., Nonaka, D., Cruz, C., Beck, A., Lonardo, F., Wali, A., and Pass, H.I. (2009). Protumorigenic role of HAPLN1 and its IgV domain in malignant pleural mesothelioma. Clin Cancer Res *15*, 2602–2611.

Jackson, J., Ayzenshtat, I., Karnani, M.M., and Yuste, R. (2016). VIP+ interneurons control neocortical activity across brain states. J Neurophysiol *115*, 3008–3017.

Jackson, V.A., del Toro, D., Carrasquero, M., Roversi, P., Harlos, K., Klein, R., and Seiradake, E. (2015). Structural basis of latrophilin-FLRT interaction. Structure *23*, 774–781.

Jacobson, M. (1969). Development of specific neuronal connections. Science *163*, 543–547.

Jan, L.Y., and Jan, Y.N. (2012). Voltage-gated potassium channels and the diversity of electrical signalling. J Physiol (Lond) *590*, 2591–2599.

Jang, S., Nelson, J.C., Bend, E.G., Rodríguez-Laureano, L., Tueros, F.G., Cartagenova, L., Underwood, K., Jorgensen, E.M., and Colón-Ramos, D.A. (2016). Glycolytic Enzymes Localize to Synapses

under Energy Stress to Support Synaptic Function. Neuron *90*, 278–291.

Jiang, X., Shen, S., Cadwell, C.R., Berens, P., Sinz, F., Ecker, A.S., Patel, S., and Tolias, A.S. (2015). Principles of connectivity among morphologically defined cell types in adult neocortex. Science *350*, aac9462.

John, N., Krügel, H., Frischknecht, R., Smalla, K.-H., Schultz, C., Kreutz, M.R., Gundelfinger, E.D., and Seidenbecher, C.I. (2006). Brevican-containing perineuronal nets of extracellular matrix in dissociated hippocampal primary cultures. Mol Cell Neurosci *31*, 774–784.

Johnston, J., Forsythe, I.D., and Kopp-Scheinpflug, C. (2010). Going native: voltage-gated potassium channels controlling neuronal excitability. J Physiol (Lond) *588*, 3187–3200.

Kalashnikova, E., Lorca, R.A., Kaur, I., Barisone, G.A., Li, B., Ishimaru, T., Trimmer, J.S., Mohapatra, D.P., and Díaz, E. (2010). SynDIG1: an activity-regulated, AMPA- receptor-interacting transmembrane protein that regulates excitatory synapse development. Neuron *65*, 80–93.

Kalil, K., and Dent, E.W. (2014). Branch management: mechanisms of axon branching in the developing vertebrate CNS. Nat Rev Neurosci *15*, 7–18.

Kann, O., Huchzermeyer, C., Kovács, R., Wirtz, S., and Schuelke, M. (2011). Gamma oscillations in the hippocampus require high complex I gene expression and strong functional performance of mitochondria. Brain *134*, 345–358.

Kann, O., Papageorgiou, I.E., and Draguhn, A. (2014). Highly energized inhibitory interneurons are a central element for information processing in cortical networks. J Cereb Blood Flow Metab *34*, 1270–1282.

Kapfer, C., Glickfeld, L.L., Atallah, B.V., and Scanziani, M. (2007). Supralinear increase of recurrent inhibition during sparse activity in the somatosensory cortex. Nat Neurosci *10*, 743–753.

Karson, M.A., Tang, A.-H., Milner, T.A., and Alger, B.E. (2009). Synaptic cross talk between perisomatic-targeting interneuron classes expressing cholecystokinin and parvalbumin in hippocampus. J Neurosci *29*, 4140–4154.

Katona, I., Sperlágh, B., Sík, A., Käfalvi, A., Vizi, E.S., Mackie, K., and Freund, T.F. (1999). Presynaptically located CB1 cannabinoid receptors regulate GABA release from axon terminals of specific hippocampal interneurons. J Neurosci *19*, 4544–4558.

Katz, L.C., and Shatz, C.J. (1996). Synaptic activity and the construction of cortical circuits. Science *274*, 1133–1138.

Kawaguchi, Y. (1995). Physiological subgroups of nonpyramidal cells with specific morphological characteristics in layer II/III of rat frontal cortex. J Neurosci *15*, 2638–2655.

Kawaguchi, Y., and Kubota, Y. (1997). GABAergic cell subtypes and their synaptic connections in rat frontal cortex. Cereb Cortex *7*, 476–486.

Kepecs, A., and Fishell, G. (2014). Interneuron cell types are fit to function. Nature *505*, 318–326.

Kessaris, N., Fogarty, M., Iannarelli, P., Grist, M., Wegner, M., and Richardson, W.D. (2006). Competing waves of oligodendrocytes in the forebrain and postnatal elimination of an embryonic lineage. Nat Neurosci *9*, 173–179.

Kessels, H.W., and Malinow, R. (2009). Synaptic AMPA receptor plasticity and behavior. Neuron *61*, 340–350.

Kettenmann, H., Kirchhoff, F., and Verkhratsky, A. (2013). Microglia: new roles for the synaptic stripper. Neuron *77*, 10–18.

Kim, E., and Sheng, M. (2004). PDZ domain proteins of synapses. Nat Rev Neurosci *5*, 771–781.

Kim, D., Pertea, G., Trapnell, C., Pimentel, H., Kelley, R., and Salzberg, S.L. (2013). TopHat2: accurate alignment of transcriptomes in the presence of insertions, deletions and gene fusions. Genome Biol *14*, R36.

Kim, S., Burette, A., Chung, H.S., Kwon, S.-K., Woo, J., Lee, H.W., Kim, K., Kim, H., Weinberg, R.J., and Kim, E. (2006). NGL family PSD-95-interacting adhesion molecules regulate excitatory synapse formation. Nat Neurosci *9*, 1294–1301.

Kiss, J.Z., Wang, C., Olive, S., Rougon, G., Lang, J., Baetens, D., Harry, D., and Pralong, W.F. (1994). Activity-dependent mobilization of the adhesion molecule polysialic NCAM to the cell surface of neurons and endocrine cells. EMBO J *13*, 5284–5292.

Kitamura, T., Sun, C., Martin, J., Kitch, L.J., Schnitzer, M.J., and Tonegawa, S. (2015). Entorhinal Cortical Ocean Cells Encode Specific Contexts and Drive Context-Specific Fear Memory. Neuron *87*, 1317–1331.

Klassen, M.P., and Shen, K. (2007). Wnt signaling positions neuromuscular connectivity by inhibiting synapse formation in C. elegans. Cell *130*, 704–716.

Klausberger, T., and Somogyi, P. (2008). Neuronal diversity and temporal dynamics: the unity of hippocampal circuit operations. Science *321*, 53–57.

Klausberger, T., Magill, P.J., Márton, L.F., Roberts, J.D.B., Cobden, P.M., Buzsáki, G., and Somogyi, P. (2003). Brain-state- and cell-type-specific firing of hippocampal interneurons in vivo. Nature *421*, 844–848.

Kneussel, M., and Loebrich, S. (2007). Trafficking and synaptic anchoring of ionotropic inhibitory neurotransmitter receptors. Biol Cell *99*, 297–309.

Knight, A.L., Yan, X., Hamamichi, S., Ajjuri, R.R., Mazzulli, J.R., Zhang, M.W., Daigle, J.G., Zhang, S., Borom, A.R., Roberts, L.R., et al. (2014). The glycolytic enzyme, GPI, is a functionally conserved modifier of dopaminergic neurodegeneration in Parkinson's models. Cell Metab *20*, 145–157.

Ko, J., Kim, S., Chung, H.S., Kim, K., Han, K., Kim, H., Jun, H., Kaang, B.-K., and Kim, E. (2006). SALM synaptic cell adhesion-like molecules regulate the differentiation of excitatory synapses. Neuron *50*, 233–245.

Kochlamazashvili, G., Henneberger, C., Bukalo, O., Dvoretskova, E., Senkov, O., Lievens, P.M.-J., Westenbroek, R., Engel, A.K., Catterall, W.A., Rusakov, D.A., et al. (2010). The extracellular matrix molecule hyaluronic acid regulates hippocampal synaptic plasticity by modulating postsynaptic L-type Ca(2+) channels. Neuron *67*, 116–128.

Komiyama, T., Sweeney, L.B., Schuldiner, O., Garcia, K.C., and Luo, L. (2007). Graded expression of semaphorin-1a cell-autonomously directs dendritic targeting of olfactory projection neurons. Cell *128*, 399–410.

Kratsios, P., Pinan-Lucarré, B., Kerk, S.Y., Weinreb, A., Bessereau, J.-L., and Hobert, O. (2015). Transcriptional coordination of synaptogenesis and neurotransmitter signaling. Curr Biol *25*, 1282–1295.

Kuhlman, S.J., Olivas, N.D., Tring, E., Ikrar, T., Xu, X., and Trachtenberg, J.T. (2013). A disinhibitory microcircuit initiates critical-period plasticity in the visual cortex. Nature *501*, 543–546.

Kuo, M.-W., Wang, C.-H., Wu, H.-C., Chang, S.-J., and Chuang, Y.-J. (2011). Soluble THSD7A is an N-glycoprotein that promotes endothelial cell migration and tube formation in angiogenesis. PLoS ONE *6*, e29000.

Kuzirian, M.S., and Paradis, S. (2011). Emerging themes in GABAergic synapse development. Prog Neurobiol *95*, 68–87.

Laezza, F., Lampert, A., Kozel, M.A., Gerber, B.R., Rush, A.M., Nerbonne, J.M., Waxman, S.G., Dib-Hajj, S.D., and Ornitz, D.M. (2009). FGF14 N-terminal splice variants differentially modulate Nav1.2 and Nav1.6-encoded sodium channels. Mol Cell Neurosci *42*, 90–101.

Lagler, M., Ozdemir, A.T., Lagoun, S., Malagon-Vina, H., Borhegyi, Z., Hauer, R., Jelem, A., and Klausberger, T. (2016). Divisions of Identified Parvalbumin-Expressing Basket Cells during Working Memory-Guided Decision Making. Neuron *91*, 1390–1401.

Lander, C., Kind, P., Maleski, M., and Hockfield, S. (1997). A family of activity-dependent neuronal cell-surface chondroitin sulfate proteoglycans in cat visual cortex. J Neurosci *17*, 1928–1939.

Langley, J.N. (1895). Note on Regeneration of Prae-Ganglionic Fibres of the Sympathetic. J Physiol (Lond) *18*, 280–284.

Lauri, S.E., Palmer, M., Segerstrale, M., Vesikansa, A., Taira, T., and Collingridge, G.L. (2007). Presynaptic mechanisms involved in the expression of STP and LTP at CA1 synapses in the hippocampus. Neuropharmacology *52*, 1–11.

Ledda, F., Paratcha, G., Sandoval-Guzmán, T., and Ibáñez, C.F. (2007). GDNF and GFRalpha1 promote formation of neuronal synapses by ligand-induced cell adhesion. Nat Neurosci *10*, 293–300.

Lee, A.T., Gee, S.M., Vogt, D., Patel, T., Rubenstein, J.L., and Sohal, V.S. (2014a). Pyramidal neurons in prefrontal cortex receive subtype-specific forms of excitation and inhibition. Neuron *81*, 61–68.

Lee, H., Brott, B.K., Kirkby, L.A., Adelson, J.D., Cheng, S., Feller, M.B., Datwani, A., and Shatz, C.J. (2014b). Synapse elimination and learning rules co-regulated by MHC class I H2-Db. Nature *509*, 195–200.

Lee, S., Kruglikov, I., Huang, Z.J., Fishell, G., and Rudy, B. (2013). A disinhibitory circuit mediates motor integration in the somatosensory cortex. Nat Neurosci *16*, 1662–1670.

Lee, S.-H., Marchionni, I., Bezaire, M., Varga, C., Danielson, N., Lovett-Barron, M., Losonczy, A., and Soltesz, I. (2014c). Parvalbumin-positive basket cells differentiate among hippocampal pyramidal cells. Neuron *82*, 1129–1144.

Leinekugel, X., Medina, I., Khalilov, I., Ben-Ari, Y., and Khazipov, R. (1997). Ca2+ oscillations mediated by the synergistic excitatory actions of GABA(A) and NMDA receptors in the neonatal hippocampus. Neuron *18*, 243–255.

Letzkus, J.J., Wolff, S.B.E., Meyer, E.M.M., Tovote, P., Courtin, J., Herry, C., and Lüthi, A. (2011). A disinhibitory microcircuit for associative fear learning in the auditory cortex. Nature *480*, 331–335.

Levinson, J.N., and El-Husseini, A. (2005). Building excitatory and inhibitory synapses: balancing neuroligin partnerships. Neuron *48*, 171–174.

Lewis, T.L., Courchet, J., and Polleux, F. (2013). Cell biology in neuroscience: Cellular and molecular mechanisms underlying axon formation, growth, and branching. J Cell Biol *202*, 837–848.

Li, B., Woo, R.-S., Mei, L., and Malinow, R. (2007). The neuregulin-1 receptor erbB4 controls glutamatergic synapse maturation and plasticity. Neuron *54*, 583–597.

Liao, D., Hessler, N.A., and Malinow, R. (1995). Activation of postsynaptically silent synapses during pairing-induced LTP in CA1 region of hippocampal slice. Nature *375*, 400–404.

Lin, M.-Y., and Sheng, Z.-H. (2015). Regulation of mitochondrial transport in neurons. Exp Cell Res *334*, 35–44.

Lin, J.C., Ho, W.-H., Gurney, A., and Rosenthal, A. (2003). The netrin-G1 ligand NGL-1 promotes the outgrowth of thalamocortical axons. Nat Neurosci *6*, 1270–1276.

Lin, Y., Bloodgood, B.L., Hauser, J.L., Lapan, A.D., Koon, A.C., Kim, T.-K., Hu, L.S., Malik, A.N., and Greenberg, M.E. (2008). Activity-dependent regulation of inhibitory synapse development by Npas4. Nature *455*, 1198–1204.

Linhoff, M.W., Laurén, J., Cassidy, R.M., Dobie, F.A., Takahashi, H., Nygaard, H.B., Airaksinen, M.S., Strittmatter, S.M., and Craig, A.M. (2009). An unbiased expression screen for synaptogenic proteins identifies the LRRTM protein family as synaptic organizers. Neuron *61*, 734–749.

Lippi, G., Fernandes, C.C., Ewell, L.A., John, D., Romoli, B., Curia, G., Taylor, S.R., Frady, E.P., Jensen, A.B., Liu, J.C., et al. (2016). MicroRNA-101 Regulates Multiple Developmental Programs to Constrain Excitation in Adult Neural Networks. Neuron *92*, 1337–1351.

Lippmann, M., Bress, A., Nemeroff, C.B., Plotsky, P.M., and Monteggia, L.M. (2007). Long-term behavioural and molecular alterations associated with maternal separation in rats. Eur J Neurosci *25*, 3091–3098.

Lipscombe, D., Allen, S.E., and Toro, C.P. (2013a). Control of neuronal voltage-gated calcium ion channels from RNA to protein. Trends Neurosci *36*, 598–609.

Lipscombe, D., Andrade, A., and Allen, S.E. (2013b). Alternative splicing: functional diversity among voltage-gated calcium channels and behavioral consequences. Biochim Biophys Acta *1828*, 1522–1529.

Llinás, R.R. (2003). The contribution of Santiago Ramón y Cajal to functional neuroscience. Nat Rev Neurosci *4*, 77–80.

Lohmann, C., and Bonhoeffer, T. (2008). A role for local calcium signaling in rapid synaptic partner selection by dendritic filopodia. Neuron *59*, 253–260.

Lovero, K.L., Fukata, Y., Granger, A.J., Fukata, M., and Nicoll, R.A. (2015). The LGI1-ADAM22 protein complex directs synapse maturation through regulation of PSD-95 function. Proc Natl Acad Sci U S A *112*, E4129–E4137.

Lu, B., Wang, K.H., and Nose, A. (2009). Molecular mechanisms underlying neural circuit formation. Curr Opin Neurobiol *19*, 162–167.

Lu, J., Tucciarone, J., Padilla-Coreano, N., He, M., Gordon, J.A., and Huang, Z.J. (2017). Selective inhibitory control of pyramidal neuron ensembles and cortical subnetworks by chandelier cells. BioRxiv.

Lu, Y.C., Nazarko, O.V., Sando, R., Salzman, G.S., Südhof, T.C., and Araç, D. (2015). Structural Basis of Latrophilin-FLRT-UNC5 Interaction in Cell Adhesion. Structure *23*, 1678–1691.

Luscher, B., Fuchs, T., and Kilpatrick, C.L. (2011). GABAA receptor trafficking-mediated plasticity of inhibitory synapses. Neuron *70*, 385–409.

Madisen, L., Garner, A.R., Shimaoka, D., Chuong, A.S., Klapoetke, N.C., Li, L., van der Bourg, A., Niino, Y., Egolf, L., Monetti, C., et al. (2015). Transgenic mice for intersectional targeting of neural sensors and effectors with high specificity and performance. Neuron *85*, 942–958.

Le Magueresse, C., and Monyer, H. (2013). GABAergic interneurons shape the functional maturation of the cortex. Neuron *77*, 388–405.

Majdan, M., and Shatz, C.J. (2006). Effects of visual experience on activity-dependent gene regulation in cortex. Nat Neurosci *9*, 650–659.

Marder, E., and Taylor, A.L. (2011). Multiple models to capture the variability in biological neurons and networks. Nat Neurosci *14*, 133–138.

Marín, O. (2012). Interneuron dysfunction in psychiatric disorders. Nat Rev Neurosci *13*, 107–120.

Marín, O. (2016). Developmental timing and critical windows for the treatment of psychiatric disorders. Nat Med *22*, 1229–1238.

Marín, O., Valiente, M., Ge, X., and Tsai, L.-H. (2010). Guiding neuronal cell migrations. Cold Spring Harb Perspect Biol *2*, a001834.

Marko, M., Leichter, M., Patrinou-Georgoula, M., and Guialis, A. (2014). Selective interactions of hnRNP M isoforms with the TET proteins TAF15 and TLS/FUS. Mol Biol Rep *41*, 2687–2695.

Markram, H., Muller, E., Ramaswamy, S., Reimann, M.W., Abdellah, M., Sanchez, C.A., Ailamaki, A., Alonso-Nanclares, L., Antille, N., Arsever, S., et al. (2015). Reconstruction and simulation of neocortical microcircuitry. Cell *163*, 456–492.

Marques-Smith, A., Favuzzi, E., and Rico, B. (2016a). Shaping Early Networks to Rule Mature Circuits: Little MiRs Go a Long Way. Neuron *92*, 1154–1157.

Marques-Smith, A., Lyngholm, D., Kaufmann, A.-K., Stacey, J.A., Hoerder-Suabedissen, A., Becker, E.B.E., Wilson, M.C., Molnár, Z., and Butt, S.J.B. (2016b). A transient translaminar gabaergic interneuron circuit connects thalamocortical recipient layers in neonatal somatosensory cortex. Neuron *89*, 536–549.

Massi, L., Lagler, M., Hartwich, K., Borhegyi, Z., Somogyi, P., and Klausberger, T. (2012). Temporal dynamics of parvalbumin-expressing axo-axonic and basket cells in the rat medial prefrontal cortex in vivo. J Neurosci *32*, 16496–16502.

Mataga, N., Mizuguchi, Y., and Hensch, T.K. (2004). Experience-dependent pruning of dendritic spines in visual cortex by tissue plasminogen activator. Neuron *44*, 1031–1041.

Matsuda, K. (2017). Synapse organization and modulation via C1q family proteins and their receptors in the central nervous system. Neurosci Res *116*, 46–53.

Matsuda, K., and Yuzaki, M. (2011). Cbln family proteins promote synapse formation by regulating distinct neurexin signaling pathways in various brain regions. Eur J Neurosci *33*, 1447–1461.

Matsuda, K., Miura, E., Miyazaki, T., Kakegawa, W., Emi, K., Narumi, S., Fukazawa, Y., Ito-Ishida, A., Kondo, T., Shigemoto, R., et al. (2010). Cbln1 is a ligand for an orphan glutamate receptor delta2, a bidirectional synapse organizer. Science *328*, 363–368.

Matsuoka, R.L., Chivatakarn, O., Badea, T.C., Samuels, I.S., Cahill, H., Katayama, K.-I., Kumar, S.R., Suto, F., Chédotal, A., Peachey, N.S., et al. (2011a). Class 5 transmembrane semaphorins control selective Mammalian retinal lamination and function. Neuron *71*, 460–473.

Matsuoka, R.L., Nguyen-Ba-Charvet, K.T., Parray, A., Badea, T.C., Chédotal, A., and Kolodkin, A.L. (2011b). Transmembrane semaphorin signalling controls laminar stratification in the mammalian retina. Nature *470*, 259–263.

Matta, J.A., Pelkey, K.A., Craig, M.T., Chittajallu, R., Jeffries, B.W., and McBain, C.J. (2013). Developmental origin dictates interneuron AMPA and NMDA receptor subunit composition and plasticity. Nat Neurosci *16*, 1032–1041.

Mauney, S.A., Athanas, K.M., Pantazopoulos, H., Shaskan, N., Passeri, E., Berretta, S., and Woo, T.-U.W. (2013). Developmental pattern of perineuronal nets in the human prefrontal cortex and their deficit in schizophrenia. Biol Psychiatry *74*, 427–435.

McGarry, L.M., Packer, A.M., Fino, E., Nikolenko, V., Sippy, T., and Yuste, R. (2010). Quantitative classification of somatostatin-positive neocortical interneurons identifies three interneuron subtypes. Front Neural Circuits *4*, 12.

McMahon, S.A., and Díaz, E. (2011). Mechanisms of excitatory synapse maturation by trans-synaptic organizing complexes. Curr Opin Neurobiol *21*, 221–227.

Miles, R., Tóth, K., Gulyás, A.I., Hájos, N., and Freund, T.F. (1996). Differences between somatic and dendritic inhibition in the hippocampus. Neuron *16*, 815–823.

Millard, S.S., Lu, Z., Zipursky, S.L., and Meinertzhagen, I.A. (2010). Drosophila dscam proteins regulate postsynaptic specificity at multiple-contact synapses. Neuron *67*, 761–768.

Millstein, R.A., and Holmes, A. (2007). Effects of repeated maternal separation on anxiety- and depression-related phenotypes in different mouse strains. Neurosci Biobehav Rev *31*, 3–17.

Minocha, S., Valloton, D., Arsenijevic, Y., Cardinaux, J.-R., Guidi, R., Hornung, J.-P., and Lebrand, C. (2017). Nkx2.1 regulates the generation of telencephalic astrocytes during embryonic development. Sci Rep *7*, 43093.

Missaire, M., and Hindges, R. (2015). The role of cell adhesion molecules in visual circuit formation: from neurite outgrowth to maps and synaptic specificity. Dev Neurobiol *75*, 569–583.

Miura, S.K., Martins, A., Zhang, K.X., Graveley, B.R., and Zipursky, S.L. (2013). Probabilistic splicing of Dscam1 establishes identity at the level of single neurons. Cell *155*, 1166–1177.

Miyoshi, G., Butt, S.J.B., Takebayashi, H., and Fishell, G. (2007). Physiologically distinct temporal cohorts of cortical interneurons arise from telencephalic Olig2-expressing precursors. J Neurosci *27*, 7786–7798.

Mizumoto, K., and Shen, K. (2013). Interaxonal interaction defines tiled presynaptic innervation in C. elegans. Neuron *77*, 655–666.

Molyneaux, B.J., Arlotta, P., Menezes, J.R.L., and Macklis, J.D. (2007). Neuronal subtype specification in the cerebral cortex. Nat Rev Neurosci *8*, 427–437.

Molyneaux, B.J., Goff, L.A., Brettler, A.C., Chen, H.-H., Brown, J.R., Hrvatin, S., Rinn, J.L., and Arlotta, P. (2015). DeCoN: genome-wide analysis of in vivo transcriptional dynamics during pyramidal neuron fate selection in neocortex. Neuron *85*, 275–288.

Monroy, E., Hernández-Torres, E., and Flores, G. (2010). Maternal separation disrupts dendritic morphology of neurons in prefrontal cortex, hippocampus, and nucleus accumbens in male rat offspring. J Chem Neuroanat *40*, 93–101.

Morgan, J.R., Di Paolo, G., Werner, H., Shchedrina, V.A., Pypaert, M., Pieribone, V.A., and De Camilli, P. (2004). A role for talin in presynaptic function. J Cell Biol *167*, 43–50.

Morimura, N., Inoue, T., Katayama, K., and Aruga, J. (2006). Comparative analysis of structure, expression and PSD95-binding capacity of Lrfn, a novel family of neuronal transmembrane proteins. Gene *380*, 72–83.

Muller, D., Wang, C., Skibo, G., Toni, N., Cremer, H., Calaora, V., Rougon, G., and Kiss, J.Z. (1996). PSA-NCAM is required for activity-induced synaptic plasticity. Neuron *17*, 413–422.

Muñoz, W., Tremblay, R., Levenstein, D., and Rudy, B. (2017). Layer-specific modulation of neocortical dendritic inhibition during active wakefulness. Science *355*, 954–959.

Munoz-Sanjuan, I., Smallwood, P.M., and Nathans, J. (2000). Isoform diversity among fibroblast growth factor homologous factors is generated by alternative promoter usage and differential splicing. J Biol Chem *275*, 2589–2597.

Murayama, M., Pérez-Garci, E., Nevian, T., Bock, T., Senn, W., and Larkum, M.E. (2009). Dendritic encoding of sensory stimuli controlled by deep cortical interneurons. Nature *457*, 1137–1141.

Murray, A.J., Sauer, J.F., Riedel, G., McClure, C., Ansel, L., Cheyne, L., Bartos, M., Wisden, W., and Wulff, P. (2011). Parvalbumin-positive CA1 interneurons are required for spatial working but not for reference memory. Nat Neurosci *14*, 297–299.

Musa, H., Kline, C.F., Sturm, A.C., Murphy, N., Adelman, S., Wang, C., Yan, H., Johnson, B.L., Csepe, T.A., Kilic, A., et al. (2015). SCN5A variant that blocks fibroblast growth factor homologous factor regulation causes human arrhythmia. Proc Natl Acad Sci U S A *112*, 12528–12533.

Nabel, E.M., and Morishita, H. (2013). Regulating critical period plasticity: insight from the visual system to fear circuitry for therapeutic interventions. Frontiers in Psychiatry *4*, 146.

Nadarajah, B., and Parnavelas, J.G. (2002). Modes of neuronal migration in the developing cerebral cortex. Nat Rev Neurosci *3*, 423–432.

Navarro, A.I., and Rico, B. (2014). Focal adhesion kinase function in neuronal development. Curr Opin Neurobiol *27*, 89–95.

Nelson, S.B., and Valakh, V. (2015). Excitatory/inhibitory balance and circuit homeostasis in autism spectrum disorders. Neuron *87*, 684–698.

O'Brien, R.J., Kamboj, S., Ehlers, M.D., Rosen, K.R., Fischbach, G.D., and Huganir, R.L. (1998). Activity-dependent modulation of synaptic AMPA receptor accumulation. Neuron *21*, 1067–1078.

O'Brien, R.J., Xu, D., Petralia, R.S., Steward, O., Huganir, R.L., and Worley, P. (1999). Synaptic clustering of AMPA receptors by the extracellular immediate-early gene product Narp. Neuron *23*, 309–323.

O'Donnell, P., Do, K.Q., and Arango, C. (2014). Oxidative/Nitrosative stress in psychiatric disorders: are we there yet? Schizophr Bull *40*, 960–962.

Ohba, S., Ikeda, T., Ikegaya, Y., Nishiyama, N., Matsuki, N., and Yamada, M.K. (2005). BDNF locally potentiates GABAergic presynaptic machineries: target-selective circuit inhibition. Cereb Cortex *15*, 291–298.

Okabe, S., Kim, H.D., Miwa, A., Kuriu, T., and Okado, H. (1999). Continual remodeling of postsynaptic density and its regulation by synaptic activity. Nat Neurosci *2*, 804–811.

Okaty, B.W., Miller, M.N., Sugino, K., Hempel, C.M., and Nelson, S.B. (2009). Transcriptional and electrophysiological maturation of neocortical fast-spiking GABAergic interneurons. J Neurosci *29*, 7040–7052.

Oláh, S., Füle, M., Komlósi, G., Varga, C., Báldi, R., Barzó, P., and Tamás, G. (2009). Regulation of cortical microcircuits by unitary GABA-mediated volume transmission. Nature *461*, 1278–1281.

Oliva, A.A., Jiang, M., Lam, T., Smith, K.L., and Swann, J.W. (2000). Novel hippocampal interneuronal subtypes identified using transgenic mice that express green fluorescent protein in GABAergic interneurons. J Neurosci *20*, 3354–3368.

Olsen, S.K., Garbi, M., Zampieri, N., Eliseenkova, A.V., Ornitz, D.M., Goldfarb, M., and Mohammadi, M. (2003). Fibroblast growth factor (FGF) homologous factors share structural but not functional homology with FGFs. J Biol Chem *278*, 34226–34236.

Onwuli, D.O., and Beltran-Alvarez, P. (2016). An update on transcriptional and post-translational regulation of brain voltage-gated sodium channels. Amino Acids *48*, 641–651.

Ortinski, P.I., Lu, C., Takagaki, K., Fu, Z., and Vicini, S. (2004). Expression of distinct alpha subunits of GABAA receptor regulates inhibitory synaptic strength. J Neurophysiol *92*, 1718–1727.

O'Sullivan, M.L., de Wit, J., Savas, J.N., Comoletti, D., Otto-Hitt, S., Yates, J.R., and Ghosh, A. (2012). FLRT proteins are endogenous latrophilin ligands and regulate excitatory synapse development.

Neuron *73*, 903–910.

Overstreet-Wadiche, L., and McBain, C.J. (2015). Neurogliaform cells in cortical circuits. Nat Rev Neurosci *16*, 458–468.

Owens, D.F., and Kriegstein, A.R. (2002). Is there more to GABA than synaptic inhibition? Nat Rev Neurosci *3*, 715–727.

Pablo, J.L., Wang, C., Presby, M.M., and Pitt, G.S. (2016). Polarized localization of voltage-gated Na+ channels is regulated by concerted FGF13 and FGF14 action. Proc Natl Acad Sci U S A *113*, E2665–E2674.

Palmer, L., Murayama, M., and Larkum, M. (2012). Inhibitory Regulation of Dendritic Activity in vivo. Front Neural Circuits *6*, 26.

Pandya, D.N., Seltzer, B., Petrides, M., and Cipolloni, P.B. (2015). Cerebral cortex: Architecture, connections, and the dual origin concept (Oxford: Oxford University Press).

Pathak, D., Berthet, A., and Nakamura, K. (2013). Energy failure: does it contribute to neurodegeneration? Ann Neurol *74*, 506–516.

Paulick, M.G., and Bertozzi, C.R. (2008). The glycosylphosphatidylinositol anchor: a complex membrane-anchoring structure for proteins. Biochemistry *47*, 6991–7000.

Pawson, T., and Nash, P. (2000). Protein-protein interactions define specificity in signal transduction. Genes Dev *14*, 1027–1047.

Paz, J.T., and Huguenard, J.R. (2015). Microcircuits and their interactions in epilepsy: is the focus out of focus? Nat Neurosci *18*, 351–359.

Pecho-Vrieseling, E., Sigrist, M., Yoshida, Y., Jessell, T.M., and Arber, S. (2009). Specificity of sensory-motor connections encoded by Sema3e-Plxnd1 recognition. Nature *459*, 842–846.

Pelkey, K.A., and McBain, C.J. (2008). Target-cell-dependent plasticity within the mossy fibre-CA3 circuit reveals compartmentalized regulation of presynaptic function at divergent release sites. J Physiol (Lond) *586*, 1495–1502.

Pelkey, K.A., Barksdale, E., Craig, M.T., Yuan, X., Sukumaran, M., Vargish, G.A., Mitchell, R.M., Wyeth, M.S., Petralia, R.S., Chittajallu, R., et al. (2015). Pentraxins coordinate excitatory synapse maturation and circuit integration of parvalbumin interneurons. Neuron *85*, 1257–1272.

Petilla Interneuron Nomenclature Group, Ascoli, G.A., Alonso-Nanclares, L., Anderson, S.A., Barrionuevo, G., Benavides-Piccione, R., Burkhalter, A., Buzsáki, G., Cauli, B., Defelipe, J., et al. (2008). Petilla terminology: nomenclature of features of GABAergic interneurons of the cerebral cortex. Nat Rev Neurosci *9*, 557–568.

Petrovic, M., and Hummel, T. (2008). Temporal identity in axonal target layer recognition. Nature *456*, 800–803.

Pfeffer, C.K., Xue, M., He, M., Huang, Z.J., and Scanziani, M. (2013). Inhibition of inhibition in visual cortex: the logic of connections between molecularly distinct interneurons. Nat Neurosci *16*, 1068–1076.

Philpot, B.D., Sekhar, A.K., Shouval, H.Z., and Bear, M.F. (2001). Visual experience and deprivation bidirectionally modify the composition and function of NMDA receptors in visual cortex. Neuron *29*, 157–169.

Pi, H.-J., Hangya, B., Kvitsiani, D., Sanders, J.I., Huang, Z.J., and Kepecs, A. (2013). Cortical interneurons that specialize in disinhibitory control. Nature *503*, 521–524.

Del Pino, I., García-Frigola, C., Dehorter, N., Brotons-Mas, J.R., Alvarez-Salvado, E., Martínez de Lagrán, M., Ciceri, G., Gabaldón, M.V., Moratal, D., Dierssen, M., et al. (2013). Erbb4 deletion from fast-spiking interneurons causes schizophrenia-like phenotypes. Neuron *79*, 1152–1168.

Del Pino, I., Brotons-Mas, J.R., Marques-Smith, A., Marighetto, A., Frick, A., Marín, O., and Rico, B. (2017). Abnormal wiring of CCK(+) basket cells disrupts spatial information coding. Nat Neurosci.

Pizzorusso, T., Medini, P., Berardi, N., Chierzi, S., Fawcett, J.W., and Maffei, L. (2002). Reactivation of ocular dominance plasticity in the adult visual cortex. Science *298*, 1248–1251.

Platonova, E., Winterflood, C.M., and Ewers, H. (2015). A simple method for GFP- and RFP-based dual color single-molecule localization microscopy. ACS Chem Biol *10*, 1411–1416.

Pluta, S., Naka, A., Veit, J., Telian, G., Yao, L., Hakim, R., Taylor, D., and Adesnik, H. (2015). A direct translaminar inhibitory circuit tunes cortical output. Nat Neurosci *18*, 1631–1640.

Polleux, F., Ince-Dunn, G., and Ghosh, A. (2007). Transcriptional regulation of vertebrate axon guidance and synapse formation. Nat Rev Neurosci *8*, 331–340.

Poo, M.M. (2001). Neurotrophins as synaptic modulators. Nat Rev Neurosci *2*, 24–32.

Poon, V.Y., Klassen, M.P., and Shen, K. (2008). UNC-6/netrin and its receptor UNC-5 locally exclude presynaptic components from dendrites. Nature *455*, 669–673.

Portera-Cailliau, C., Weimer, R.M., De Paola, V., Caroni, P., and Svoboda, K. (2005). Diverse modes of axon elaboration in the developing neocortex. PLoS Biol *3*, e272.

Poskanzer, K., Needleman, L.A., Bozdagi, O., and Huntley, G.W. (2003). N-cadherin regulates ingrowth and laminar targeting of thalamocortical axons. J Neurosci *23*, 2294–2305.

Potschka, H., Pekcec, A., Weinhold, B., and Gerardy-Schahn, R. (2008). Deficiency of neural cell adhesion molecule or its polysialylation modulates pharmacological effects of the AMPA receptor antagonist NBQX. Neuroscience *152*, 1093–1098.

Pouille, F., and Scanziani, M. (2001). Enforcement of temporal fidelity in pyramidal cells by somatic feed-forward inhibition. Science *293*, 1159–1163.

Pouille, F., and Scanziani, M. (2004). Routing of spike series by dynamic circuits in the hippocampus. Nature *429*, 717–723.

Poulin, J.-F., Tasic, B., Hjerling-Leffler, J., Trimarchi, J.M., and Awatramani, R. (2016). Disentangling neural cell diversity using single-cell transcriptomics. Nat Neurosci *19*, 1131–1141.

Poulopoulos, A., Aramuni, G., Meyer, G., Soykan, T., Hoon, M., Papadopoulos, T., Zhang, M., Paarmann, I., Fuchs, C., Harvey, K., et al. (2009). Neuroligin 2 drives postsynaptic assembly at perisomatic inhibitory synapses through gephyrin and collybistin. Neuron *63*, 628–642.

Prange, O., Wong, T.P., Gerrow, K., Wang, Y.T., and El-Husseini, A. (2004). A balance between excitatory and inhibitory synapses is controlled by PSD-95 and neuroligin. Proc Natl Acad Sci U S A *101*, 13915–13920.

Pribiag, H., Peng, H., Shah, W.A., Stellwagen, D., and Carbonetto, S. (2014). Dystroglycan mediates homeostatic synaptic plasticity at GABAergic synapses. Proc Natl Acad Sci U S A *111*, 6810–6815.

Puranam, R.S., He, X.P., Yao, L., Le, T., Jang, W., Rehder, C.W., Lewis, D.V., and McNamara, J.O. (2015). Disruption of Fgf13 causes synaptic excitatory-inhibitory imbalance and genetic epilepsy and febrile seizures plus. J Neurosci *35*, 8866–8881.

Qureshi, G.A., and Parvez, H. (2007). Oxidative stress and neurodegenerative disorders (Amsterdam: Elsevier).

Rademacher, N., Schmerl, B., Lardong, J.A., Wahl, M.C., and Shoichet, S.A. (2016). MPP2 is a postsynaptic MAGUK scaffold protein that links SynCAM1 cell adhesion molecules to core components of the postsynaptic density. Sci Rep *6*, 35283.

Raj, B., and Blencowe, B.J. (2015). Alternative Splicing in the Mammalian Nervous System: Recent Insights into Mechanisms and Functional Roles. Neuron *87*, 14–27.

Rakic, P. (2009). Evolution of the neocortex: a perspective from developmental biology. Nat Rev Neurosci *10*, 724–735.

Rangaraju, V., Calloway, N., and Ryan, T.A. (2014). Activity-driven local ATP synthesis is required for synaptic function. Cell *156*, 825–835.

Rao, A., and Craig, A.M. (1997). Activity regulates the synaptic localization of the NMDA receptor in hippocampal neurons. Neuron *19*, 801–812.

Rapti, G., Richmond, J., and Bessereau, J.-L. (2011). A single immunoglobulin-domain protein required for clustering acetylcholine receptors in C. elegans. EMBO J *30*, 706–718.

Rebsam, A., and Mason, C.A. (2011). Cadherins as matchmakers. Neuron *71*, 566–568.

Reisel, D., Bannerman, D.M., Schmitt, W.B., Deacon, R.M.J., Flint, J., Borchardt, T., Seeburg, P.H., and Rawlins, J.N.P. (2002). Spatial memory dissociations in mice lacking GluR1. Nat Neurosci *5*, 868–873.

Romberg, C., Yang, S., Melani, R., Andrews, M.R., Horner, A.E., Spillantini, M.G., Bussey, T.J., Fawcett, J.W., Pizzorusso, T., and Saksida, L.M. (2013). Depletion of perineuronal nets enhances recognition memory and long-term depression in the perirhinal cortex. J Neurosci *33*, 7057–7065.

De Roo, M., Klauser, P., Mendez, P., Poglia, L., and Muller, D. (2008). Activity-dependent PSD formation and stabilization of newly formed spines in hippocampal slice cultures. Cereb Cortex *18*, 151–161.

Rudy, B., Fishell, G., Lee, S., and Hjerling-Leffler, J. (2011). Three groups of interneurons account for nearly 100% of neocortical GABAergic neurons. Dev Neurobiol *71*, 45–61.

Rush, A.M., Wittmack, E.K., Tyrrell, L., Black, J.A., Dib-Hajj, S.D., and Waxman, S.G. (2006). Differential modulation of sodium channel Na(v)1.6 by two members of the fibroblast growth factor homologous factor 2 subfamily. Eur J Neurosci *23*, 2551–2562.

Rust, M.J., Bates, M., and Zhuang, X. (2006). Sub-diffraction-limit imaging by stochastic optical reconstruction microscopy (STORM). Nat Methods *3*, 793–795.

Sala, C., Piëch, V., Wilson, N.R., Passafaro, M., Liu, G., and Sheng, M. (2001). Regulation of dendritic spine morphology and synaptic function by Shank and Homer. Neuron *31*, 115–130.

Sanderson, D.J., Gray, A., Simon, A., Taylor, A.M., Deacon, R.M.J., Seeburg, P.H., Sprengel, R., Good, M.A., Rawlins, J.N.P., and Bannerman, D.M. (2007). Deletion of glutamate receptor-A (GluR-A) AMPA receptor subunits impairs one-trial spatial memory. Behav Neurosci *121*, 559–569.

Sanderson, D.J., Good, M.A., Skelton, K., Sprengel, R., Seeburg, P.H., Rawlins, J.N.P., and Bannerman, D.M. (2009). Enhanced long-term and impaired short-term spatial memory in GluA1 AMPA receptor subunit knockout mice: evidence for a dual-process memory model. Learn Mem *16*, 379–386.

Sando, R., Bushong, E., Zhu, Y., Huang, M., Considine, C., Phan, S., Ju, S., Uytiepo, M., Ellisman, M., and Maximov, A. (2017). Assembly of excitatory synapses in the absence of glutamatergic neurotransmission. Neuron *94*, 312–321.e3.

Sanes, J.R., and Lichtman, J.W. (2001). Induction, assembly, maturation and maintenance of a postsynaptic apparatus. Nat Rev Neurosci *2*, 791–805.

Sanes, J.R., and Yamagata, M. (1999). Formation of lamina-specific synaptic connections. Curr Opin Neurobiol *9*, 79–87.

Sanes, J.R., and Yamagata, M. (2009). Many paths to synaptic specificity. Annu Rev Cell Dev Biol *25*, 161–195.

Santiago, C., and Bashaw, G.J. (2014). Transcription factors and effectors that regulate neuronal morphology. Development *141*, 4667–4680.

Sanz-Clemente, A., Nicoll, R.A., and Roche, K.W. (2013). Diversity in NMDA receptor composition: many regulators, many consequences. Neuroscientist *19*, 62–75.

Sassoè-Pognetto, M., Frola, E., Pregno, G., Briatore, F., and Patrizi, A. (2011). Understanding the molecular diversity of GABAergic synapses. Front Cell Neurosci *5*, 4.

Savas, J.N., De Wit, J., Comoletti, D., Zemla, R., Ghosh, A., and Yates, J.R. (2014). Ecto-Fc MS identifies ligand-receptor interactions through extracellular domain Fc fusion protein baits and shotgun proteomic analysis. Nat Protoc *9*, 2061–2074.

Schafer, D.P., and Stevens, B. (2010). Synapse elimination during development and disease: immune molecules take centre stage. Biochem Soc Trans *38*, 476–481.

Scheiffele, P. (2003). Cell-cell signaling during synapse formation in the CNS. Annu Rev Neurosci *26*, 485–508.

Scheiffele, P., Fan, J., Choih, J., Fetter, R., and Serafini, T. (2000). Neuroligin expressed in nonneuronal cells triggers presynaptic development in contacting axons. Cell *101*, 657–669.

Schmidt, N., Akaaboune, M., Gajendran, N., Martinez-Pena y Valenzuela, I., Wakefield, S., Thurnheer,

R., and Brenner, H.R. (2011). Neuregulin/ErbB regulate neuromuscular junction development by phosphorylation of α-dystrobrevin. J Cell Biol *195*, 1171–1184.

Schmieder, R., Lim, Y.W., and Edwards, R. (2012). Identification and removal of ribosomal RNA sequences from metatranscriptomes. Bioinformatics *28*, 433–435.

Schoch, S., and Gundelfinger, E.D. (2006). Molecular organization of the presynaptic active zone. Cell Tissue Res *326*, 379–391.

Schulte, U., Thumfart, J.-O., Klöcker, N., Sailer, C.A., Bildl, W., Biniossek, M., Dehn, D., Deller, T., Eble, S., Abbass, K., et al. (2006). The epilepsy-linked Lgi1 protein assembles into presynaptic Kv1 channels and inhibits inactivation by Kvbeta1. Neuron *49*, 697–706.

Schwarz, T.L. (2013). Mitochondrial trafficking in neurons. Cold Spring Harb Perspect Biol *5*.

Schweizer, M., Streit, W.J., and Müller, C.M. (1993). Postnatal development and localization of an N-acetylgalactosamine containing glycoconjugate associated with nonpyramidal neurons in cat visual cortex. J Comp Neurol *329*, 313–327.

Seidenbecher, C.I., Richter, K., Rauch, U., Fässler, R., Garner, C.C., and Gundelfinger, E.D. (1995). Brevican, a chondroitin sulfate proteoglycan of rat brain, occurs as secreted and cell surface glycosylphosphatidylinositol-anchored isoforms. J Biol Chem *270*, 27206–27212.

Seidenbecher, C.I., Smalla, K.H., Fischer, N., Gundelfinger, E.D., and Kreutz, M.R. (2002). Brevican isoforms associate with neural membranes. J Neurochem *83*, 738–746.

Senkov, O., Tikhobrazova, O., and Dityatev, A. (2012). PSA-NCAM: synaptic functions mediated by its interactions with proteoglycans and glutamate receptors. Int J Biochem Cell Biol *44*, 591–595.

Shapiro, E., Biezuner, T., and Linnarsson, S. (2013). Single-cell sequencing-based technologies will revolutionize whole-organism science. Nat Rev Genet *14*, 618–630.

Shapiro, L., Love, J., and Colman, D.R. (2007). Adhesion molecules in the nervous system: structural insights into function and diversity. Annu Rev Neurosci *30*, 451–474.

Shen, K., and Scheiffele, P. (2010). Genetics and cell biology of building specific synaptic connectivity. Annu Rev Neurosci *33*, 473–507.

Sheng, M., and Kim, E. (2011). The postsynaptic organization of synapses. Cold Spring Harb Perspect Biol *3*.

Siddiqui, T.J., and Craig, A.M. (2011). Synaptic organizing complexes. Curr Opin Neurobiol *21*, 132–143.

Siddiqui, T.J., Tari, P.K., Connor, S.A., Zhang, P., Dobie, F.A., She, K., Kawabe, H., Wang, Y.T., Brose, N., and Craig, A.M. (2013). An LRRTM4-HSPG complex mediates excitatory synapse development on dentate gyrus granule cells. Neuron *79*, 680–695.

Sigler, A., Oh, W.C., Imig, C., Altas, B., Kawabe, H., Cooper, B.H., Kwon, H.-B., Rhee, J.-S., and Brose, N. (2017). Formation and maintenance of functional spines in the absence of presynaptic glutamate release. Neuron *94*, 304–311.e4.

Smith, C.S., Joseph, N., Rieger, B., and Lidke, K.A. (2010). Fast, single-molecule localization that achieves theoretically minimum uncertainty. Nat Methods *7*, 373–375.

Sohal, V.S., Zhang, F., Yizhar, O., and Deisseroth, K. (2009). Parvalbumin neurons and gamma rhythms enhance cortical circuit performance. Nature *459*, 698–702.

Sommeijer, J.-P., and Levelt, C.N. (2012). Synaptotagmin-2 is a reliable marker for parvalbumin positive inhibitory boutons in the mouse visual cortex. PLoS ONE *7*, e35323.

Somogyi, P., and Klausberger, T. (2005). Defined types of cortical interneurone structure space and spike timing in the hippocampus. J Physiol (Lond) *562*, 9–26.

Speidel, C.C. (1942). Adjustments of nerve endings: harvey lecture, january 16, 1941. Bull N Y Acad Med *18*, 625–653.

Sperry, R.W. (1963). CHEMOAFFINITY IN THE ORDERLY GROWTH OF NERVE FIBER PATTERNS AND CONNECTIONS. Proc Natl Acad Sci U S A *50*, 703–710.

Spiegel, I., Mardinly, A.R., Gabel, H.W., Bazinet, J.E., Couch, C.H., Tzeng, C.P., Harmin, D.A., and

Greenberg, M.E. (2014). Npas4 regulates excitatory-inhibitory balance within neural circuits through cell-type-specific gene programs. Cell *157*, 1216–1229.

Spillane, M., and Gallo, G. (2014). Involvement of Rho-family GTPases in axon branching. Small Gtpases *5*, e27974.

Srinivasan, J., Schachner, M., and Catterall, W.A. (1998). Interaction of voltage-gated sodium channels with the extracellular matrix molecules tenascin-C and tenascin-R. Proc Natl Acad Sci U S A *95*, 15753–15757.

Star, E.N., Kwiatkowski, D.J., and Murthy, V.N. (2002). Rapid turnover of actin in dendritic spines and its regulation by activity. Nat Neurosci *5*, 239–246.

Stevens, B., Allen, N.J., Vazquez, L.E., Howell, G.R., Christopherson, K.S., Nouri, N., Micheva, K.D., Mehalow, A.K., Huberman, A.D., Stafford, B., et al. (2007). The classical complement cascade mediates CNS synapse elimination. Cell *131*, 1164–1178.

Stuart, G., and Häusser, M. (1994). Initiation and spread of sodium action potentials in cerebellar Purkinje cells. Neuron *13*, 703–712.

Südhof, T.C. (2006). Synaptogenesis: When Long-Distance Relations Become Intimate. In Molecular Mechanisms of Synaptogenesis, (New York, NY : Springer, c2006.: Springer), pp. 1–9.

Südhof, T.C. (2013). Neurotransmitter release: the last millisecond in the life of a synaptic vesicle. Neuron *80*, 675–690.

Sugino, K., Hempel, C.M., Miller, M.N., Hattox, A.M., Shapiro, P., Wu, C., Huang, Z.J., and Nelson, S.B. (2006). Molecular taxonomy of major neuronal classes in the adult mouse forebrain. Nat Neurosci *9*, 99–107.

Sun, X., and Lin, Y. (2016). Npas4: linking neuronal activity to memory. Trends Neurosci *39*, 264–275.

Sun, Y., Ikrar, T., Davis, M.F., Gong, N., Zheng, X., Luo, Z.D., Lai, C., Mei, L., Holmes, T.C., Gandhi, S.P., et al. (2016). Neuregulin-1/ErbB4 signaling regulates visual cortical plasticity. Neuron.

Sylwestrak, E.L., and Ghosh, A. (2012). Elfn1 regulates target-specific release probability at CA1-interneuron synapses. Science *338*, 536–540.

Sytnyk, V., Leshchyns'ka, I., Nikonenko, A.G., and Schachner, M. (2006). NCAM promotes assembly and activity-dependent remodeling of the postsynaptic signaling complex. J Cell Biol *174*, 1071–1085.

Sytnyk, V., Leshchyns'ka, I., and Schachner, M. (2017). Neural cell adhesion molecules of the immunoglobulin superfamily regulate synapse formation, maintenance, and function. Trends Neurosci.

Szabadics, J., Varga, C., Molnár, G., Oláh, S., Barzó, P., and Tamás, G. (2006). Excitatory effect of GABAergic axo-axonic cells in cortical microcircuits. Science *311*, 233–235.

Tai, Y., Janas, J.A., Wang, C.-L., and Van Aelst, L. (2014). Regulation of chandelier cell cartridge and bouton development via DOCK7-mediated ErbB4 activation. Cell Rep *6*, 254–263.

Takahashi, H., Katayama, K.-I., Sohya, K., Miyamoto, H., Prasad, T., Matsumoto, Y., Ota, M., Yasuda, H., Tsumoto, T., Aruga, J., et al. (2012). Selective control of inhibitory synapse development by Slitrk3-PTPδ trans-synaptic interaction. Nat Neurosci *15*, 389–398, S1.

Takahashi, T., Svoboda, K., and Malinow, R. (2003). Experience strengthening transmission by driving AMPA receptors into synapses. Science *299*, 1585–1588.

Takeichi, M. (2007). The cadherin superfamily in neuronal connections and interactions. Nat Rev Neurosci *8*, 11–20.

Takesian, A.E., and Hensch, T.K. (2013). Balancing plasticity/stability across brain development. Prog Brain Res *207*, 3–34.

Tamás, G., Somogyi, P., and Buhl, E.H. (1998). Differentially interconnected networks of GABAergic interneurons in the visual cortex of the cat. J Neurosci *18*, 4255–4270.

Taniguchi, H., He, M., Wu, P., Kim, S., Paik, R., Sugino, K., Kvitsiani, D., Fu, Y., Lu, J., Lin, Y., et al. (2011). A resource of Cre driver lines for genetic targeting of GABAergic neurons in cerebral cortex.

Neuron *71*, 995–1013.

Taniguchi, H., Lu, J., and Huang, Z.J. (2013). The spatial and temporal origin of chandelier cells in mouse neocortex. Science *339*, 70–74.

Tao, Y., Chen, Y.-J., Shen, C., Luo, Z., Bates, C.R., Lee, D., Marchetto, S., Gao, T.-M., Borg, J.-P., Xiong, W.-C., et al. (2013). Erbin interacts with TARP γ-2 for surface expression of AMPA receptors in cortical interneurons. Nat Neurosci *16*, 290–299.

Tarr, P. (2012). CSHL Scientists solve birth and migration mysteries of cortex's powerful inhibitors, "chandelier" cells.

Tasic, B., Menon, V., Nguyen, T.N., Kim, T.K., Jarsky, T., Yao, Z., Levi, B., Gray, L.T., Sorensen, S.A., Dolbeare, T., et al. (2016). Adult mouse cortical cell taxonomy revealed by single cell transcriptomics. Nat Neurosci *19*, 335–346.

Terauchi, A., Johnson-Venkatesh, E.M., Toth, A.B., Javed, D., Sutton, M.A., and Umemori, H. (2010). Distinct FGFs promote differentiation of excitatory and inhibitory synapses. Nature *465*, 783–787.

Tessier-Lavigne, M., and Goodman, C.S. (1996). The molecular biology of axon guidance. Science *274*, 1123–1133.

Ting, A.K., Chen, Y., Wen, L., Yin, D.-M., Shen, C., Tao, Y., Liu, X., Xiong, W.-C., and Mei, L. (2011). Neuregulin 1 promotes excitatory synapse development and function in GABAergic interneurons. J Neurosci *31*, 15–25.

Togashi, H., Sakisaka, T., and Takai, Y. (2009). Cell adhesion molecules in the central nervous system. Cell Adh Migr *3*, 29–35.

Toth, A.B., Terauchi, A., Zhang, L.Y., Johnson-Venkatesh, E.M., Larsen, D.J., Sutton, M.A., and Umemori, H. (2013). Synapse maturation by activity-dependent ectodomain shedding of SIRPα. Nat Neurosci *16*, 1417–1425.

Tran, T.S., Rubio, M.E., Clem, R.L., Johnson, D., Case, L., Tessier-Lavigne, M., Huganir, R.L., Ginty, D.D., and Kolodkin, A.L. (2009). Secreted semaphorins control spine distribution and morphogenesis in the postnatal CNS. Nature *462*, 1065–1069.

Trapnell, C., Roberts, A., Goff, L., Pertea, G., Kim, D., Kelley, D.R., Pimentel, H., Salzberg, S.L., Rinn, J.L., and Pachter, L. (2012). Differential gene and transcript expression analysis of RNA-seq experiments with TopHat and Cufflinks. Nat Protoc *7*, 562–578.

Trapnell, C., Hendrickson, D.G., Sauvageau, M., Goff, L., Rinn, J.L., and Pachter, L. (2013). Differential analysis of gene regulation at transcript resolution with RNA-seq. Nat Biotechnol *31*, 46–53.

Traunmüller, L., Gomez, A.M., Nguyen, T.-M., and Scheiffele, P. (2016). Control of neuronal synapse specification by a highly dedicated alternative splicing program. Science *352*, 982–986.

Tremblay, R., Lee, S., and Rudy, B. (2016). Gabaergic interneurons in the neocortex: from cellular properties to circuits. Neuron *91*, 260–292.

Tripodi, M., Stepien, A.E., and Arber, S. (2011). Motor antagonism exposed by spatial segregation and timing of neurogenesis. Nature *479*, 61–66.

Tsien, R.Y. (2013). Very long-term memories may be stored in the pattern of holes in the perineuronal net. Proc Natl Acad Sci U S A *110*, 12456–12461.

Tuncdemir, S.N., Wamsley, B., Stam, F.J., Osakada, F., Goulding, M., Callaway, E.M., Rudy, B., and Fishell, G. (2016). Early somatostatin interneuron connectivity mediates the maturation of deep layer cortical circuits. Neuron *89*, 521–535.

Turrigiano, G. (2012). Homeostatic synaptic plasticity: local and global mechanisms for stabilizing neuronal function. Cold Spring Harb Perspect Biol *4*, a005736.

Turrigiano, G.G., and Nelson, S.B. (2000). Hebb and homeostasis in neuronal plasticity. Curr Opin Neurobiol *10*, 358–364.

Tyagarajan, S.K., Ghosh, H., Yévenes, G.E., Nikonenko, I., Ebeling, C., Schwerdel, C., Sidler, C., Zeilhofer, H.U., Gerrits, B., Muller, D., et al. (2011). Regulation of GABAergic synapse formation and plasticity by GSK3beta-dependent phosphorylation of gephyrin. Proc Natl Acad Sci U S A *108*, 379–384.

Uemura, T., Lee, S.-J., Yasumura, M., Takeuchi, T., Yoshida, T., Ra, M., Taguchi, R., Sakimura, K., and Mishina, M. (2010). Trans-synaptic interaction of GluRdelta2 and Neurexin through Cbln1 mediates synapse formation in the cerebellum. Cell *141*, 1068–1079.

Ullrich, B., Ushkaryov, Y.A., and Südhof, T.C. (1995). Cartography of neurexins: more than 1000 isoforms generated by alternative splicing and expressed in distinct subsets of neurons. Neuron *14*, 497–507.

Umemori, H., Linhoff, M.W., Ornitz, D.M., and Sanes, J.R. (2004). FGF22 and its close relatives are presynaptic organizing molecules in the mammalian brain. Cell *118*, 257–270.

Underwood, E. (2015). NEUROSCIENCE. Lifelong memories may reside in nets around brain cells. Science *350*, 491–492.

Vaithianathan, T., Matthias, K., Bahr, B., Schachner, M., Suppiramaniam, V., Dityatev, A., and Steinhaüser, C. (2004). Neural cell adhesion molecule-associated polysialic acid potentiates alpha-amino-3-hydroxy-5-methylisoxazole-4-propionic acid receptor currents. J Biol Chem *279*, 47975–47984.

Valenzuela, J.C., Heise, C., Franken, G., Singh, J., Schweitzer, B., Seidenbecher, C.I., and Frischknecht, R. (2014). Hyaluronan-based extracellular matrix under conditions of homeostatic plasticity. Philos Trans R Soc Lond, B, Biol Sci *369*, 20130606.

Varga, C., Oijala, M., Lish, J., Szabo, G.G., Bezaire, M., Marchionni, I., Golshani, P., and Soltesz, I. (2014). Functional fission of parvalbumin interneuron classes during fast network events. Elife *3*.

Varoqueaux, F., Sigler, A., Rhee, J.-S., Brose, N., Enk, C., Reim, K., and Rosenmund, C. (2002). Total arrest of spontaneous and evoked synaptic transmission but normal synaptogenesis in the absence of Munc13-mediated vesicle priming. Proc Natl Acad Sci U S A *99*, 9037–9042.

Verhage, M., Maia, A.S., Plomp, J.J., Brussaard, A.B., Heeroma, J.H., Vermeer, H., Toonen, R.F., Hammer, R.E., van den Berg, T.K., Missler, M., et al. (2000). Synaptic assembly of the brain in the absence of neurotransmitter secretion. Science *287*, 864–869.

Verret, L., Mann, E.O., Hang, G.B., Barth, A.M.I., Cobos, I., Ho, K., Devidze, N., Masliah, E., Kreitzer, A.C., Mody, I., et al. (2012). Inhibitory interneuron deficit links altered network activity and cognitive dysfunction in Alzheimer model. Cell *149*, 708–721.

van Versendaal, D., Rajendran, R., Saiepour, M.H., Klooster, J., Smit-Rigter, L., Sommeijer, J.-P., De Zeeuw, C.I., Hofer, S.B., Heimel, J.A., and Levelt, C.N. (2012). Elimination of inhibitory synapses is a major component of adult ocular dominance plasticity. Neuron *74*, 374–383.

Vidal, G.S., Djurisic, M., Brown, K., Sapp, R.W., and Shatz, C.J. (2016). Cell-Autonomous Regulation of Dendritic Spine Density by PirB. eNeuro *3*.

Vogel, C., and Marcotte, E.M. (2012). Insights into the regulation of protein abundance from proteomic and transcriptomic analyses. Nat Rev Genet *13*, 227–232.

Vogels, T.P., and Abbott, L.F. (2009). Gating multiple signals through detailed balance of excitation and inhibition in spiking networks. Nat Neurosci *12*, 483–491.

Vrieseling, E., and Arber, S. (2006). Target-induced transcriptional control of dendritic patterning and connectivity in motor neurons by the ETS gene Pea3. Cell *127*, 1439–1452.

Waddington, C.H. (1959). Canalization of development and genetic assimilation of acquired characters. Nature *183*, 1654–1655.

Wamsley, B., and Fishell, G. (2017). Genetic and activity-dependent mechanisms underlying interneuron diversity. Nat Rev Neurosci *18*, 299–309.

Wang, H.-X., and Gao, W.-J. (2010). Development of calcium-permeable AMPA receptors and their correlation with NMDA receptors in fast-spiking interneurons of rat prefrontal cortex. J Physiol (Lond) *588*, 2823–2838.

Wang, Y., and Navin, N.E. (2015). Advances and applications of single-cell sequencing technologies. Mol Cell *58*, 598–609.

Wang, C.-H., Su, P.-T., Du, X.-Y., Kuo, M.-W., Lin, C.-Y., Yang, C.-C., Chan, H.-S., Chang, S.-J., Kuo, C., Seo, K., et al. (2010). Thrombospondin type I domain containing 7A (THSD7A) mediates

endothelial cell migration and tube formation. J Cell Physiol *222*, 685–694.

Wang, C.-Y., Chang, K., Petralia, R.S., Wang, Y.-X., Seabold, G.K., and Wenthold, R.J. (2006). A novel family of adhesion-like molecules that interacts with the NMDA receptor. J Neurosci *26*, 2174–2183.

Wang, P., Saraswati, S., Guan, Z., Watkins, C.J., Wurtman, R.J., and Littleton, J.T. (2004a). A Drosophila temperature-sensitive seizure mutant in phosphoglycerate kinase disrupts ATP generation and alters synaptic function. J Neurosci *24*, 4518–4529.

Wang, S., Ren, H., Xu, J., Yu, Y., Han, S., Qiao, H., Cheng, S., Xu, C., An, S., Ju, B., et al. (2015). Diminished serum repetin levels in patients with schizophrenia and bipolar disorder. Sci Rep *5*, 7977.

Wang, X., Tang, H., Wei, E.Q., Wang, Z., Yang, J., Yang, R., Wang, S., Zhang, Y., Pitt, G.S., Zhang, H., et al. (2017). Conditional knockout of Fgf13 in murine hearts increases arrhythmia susceptibility and reveals novel ion channel modulatory roles. J Mol Cell Cardiol.

Wang, X.J., Tegnér, J., Constantinidis, C., and Goldman-Rakic, P.S. (2004b). Division of labor among distinct subtypes of inhibitory neurons in a cortical microcircuit of working memory. Proc Natl Acad Sci U S A *101*, 1368–1373.

Wang, Y., Toledo-Rodriguez, M., Gupta, A., Wu, C., Silberberg, G., Luo, J., and Markram, H. (2004c). Anatomical, physiological and molecular properties of Martinotti cells in the somatosensory cortex of the juvenile rat. J Physiol (Lond) *561*, 65–90.

Wang, Y., Zhang, P., and Wyskiel, D.R. (2016). Chandelier Cells in Functional and Dysfunctional Neural Circuits. Front Neural Circuits *10*, 33.

Watabe-Uchida, M., John, K.A., Janas, J.A., Newey, S.E., and Van Aelst, L. (2006). The Rac activator DOCK7 regulates neuronal polarity through local phosphorylation of stathmin/Op18. Neuron *51*, 727–739.

Weber, R.J.M., Li, E., Bruty, J., He, S., and Viant, M.R. (2012). MaConDa: a publicly accessible mass spectrometry contaminants database. Bioinformatics *28*, 2856–2857.

Wefelmeyer, W., Cattaert, D., and Burrone, J. (2015). Activity-dependent mismatch between axo-axonic synapses and the axon initial segment controls neuronal output. Proc Natl Acad Sci U S A *112*, 9757–9762.

West, A.E., and Greenberg, M.E. (2011). Neuronal activity-regulated gene transcription in synapse development and cognitive function. Cold Spring Harb Perspect Biol *3*.

Williams, M.E., de Wit, J., and Ghosh, A. (2010). Molecular mechanisms of synaptic specificity in developing neural circuits. Neuron *68*, 9–18.

Williams, M.E., Wilke, S.A., Daggett, A., Davis, E., Otto, S., Ravi, D., Ripley, B., Bushong, E.A., Ellisman, M.H., Klein, G., et al. (2011). Cadherin-9 regulates synapse-specific differentiation in the developing hippocampus. Neuron *71*, 640–655.

Wilson, N.R., Runyan, C.A., Wang, F.L., and Sur, M. (2012). Division and subtraction by distinct cortical inhibitory networks in vivo. Nature *488*, 343–348.

Winterflood, C.M., Platonova, E., Albrecht, D., and Ewers, H. (2015). Dual-color 3D superresolution microscopy by combined spectral-demixing and biplane imaging. Biophys J *109*, 3–6.

de Wit, J., and Ghosh, A. (2014). Control of neural circuit formation by leucine-rich repeat proteins. Trends Neurosci *37*, 539–550.

de Wit, J., and Ghosh, A. (2016). Specification of synaptic connectivity by cell surface interactions. Nat Rev Neurosci *17*, 22–35.

de Wit, J., Sylwestrak, E., O'Sullivan, M.L., Otto, S., Tiglio, K., Savas, J.N., Yates, J.R., Comoletti, D., Taylor, P., and Ghosh, A. (2009). LRRTM2 interacts with Neurexin1 and regulates excitatory synapse formation. Neuron *64*, 799–806.

de Wit, J., Hong, W., Luo, L., and Ghosh, A. (2011). Role of leucine-rich repeat proteins in the development and function of neural circuits. Annu Rev Cell Dev Biol *27*, 697–729.

de Wit, J., O'Sullivan, M.L., Savas, J.N., Condomitti, G., Caccese, M.C., Vennekens, K.M., Yates, J.R., and Ghosh, A. (2013). Unbiased discovery of glypican as a receptor for LRRTM4 in regulating excitatory synapse development. Neuron *79*, 696–711.

Wittmack, E.K., Rush, A.M., Craner, M.J., Goldfarb, M., Waxman, S.G., and Dib-Hajj, S.D. (2004). Fibroblast growth factor homologous factor 2B: association with Nav1.6 and selective colocalization at nodes of Ranvier of dorsal root axons. J Neurosci *24*, 6765–6775.

Wonders, C.P., and Anderson, S.A. (2006). The origin and specification of cortical interneurons. Nat Rev Neurosci *7*, 687–696.

Woodruff, A., Xu, Q., Anderson, S.A., and Yuste, R. (2009). Depolarizing effect of neocortical chandelier neurons. Front Neural Circuits *3*, 15.

Woodruff, A.R., Anderson, S.A., and Yuste, R. (2010). The enigmatic function of chandelier cells. Front Neurosci *4*, 201.

Woodruff, A.R., McGarry, L.M., Vogels, T.P., Inan, M., Anderson, S.A., and Yuste, R. (2011). State-dependent function of neocortical chandelier cells. J Neurosci *31*, 17872–17886.

Wu, Q.-F., Yang, L., Li, S., Wang, Q., Yuan, X.-B., Gao, X., Bao, L., and Zhang, X. (2012a). Fibroblast growth factor 13 is a microtubule-stabilizing protein regulating neuronal polarization and migration. Cell *149*, 1549–1564.

Wu, X., Fu, Y., Knott, G., Lu, J., Di Cristo, G., and Huang, Z.J. (2012b). GABA signaling promotes synapse elimination and axon pruning in developing cortical inhibitory interneurons. J Neurosci *32*, 331–343.

Wurtz, R.H. (2009). Recounting the impact of Hubel and Wiesel. J Physiol (Lond) *587*, 2817–2823.

Xiao, T., Staub, W., Robles, E., Gosse, N.J., Cole, G.J., and Baier, H. (2011). Assembly of lamina-specific neuronal connections by slit bound to type IV collagen. Cell *146*, 164–176.

Xie, L., Korkmaz, K.S., Braun, K., and Bock, J. (2013). Early life stress-induced histone acetylations correlate with activation of the synaptic plasticity genes Arc and Egr1 in the mouse hippocampus. J Neurochem *125*, 457–464.

Xu, X., and Callaway, E.M. (2009). Laminar specificity of functional input to distinct types of inhibitory cortical neurons. J Neurosci *29*, 70–85.

Xu, H., Jeong, H.-Y., Tremblay, R., and Rudy, B. (2013). Neocortical somatostatin-expressing GABAergic interneurons disinhibit the thalamorecipient layer 4. Neuron *77*, 155–167.

Xu, Q., Tam, M., and Anderson, S.A. (2008). Fate mapping Nkx2.1-lineage cells in the mouse telencephalon. J Comp Neurol *506*, 16–29.

Xue, M., Atallah, B.V., and Scanziani, M. (2014). Equalizing excitation-inhibition ratios across visual cortical neurons. Nature *511*, 596–600.

Yamada, S., and Nelson, W.J. (2007). Synapses: sites of cell recognition, adhesion, and functional specification. Annu Rev Biochem *76*, 267–294.

Yamagata, M., and Sanes, J.R. (2005). Versican in the developing brain: lamina-specific expression in interneuronal subsets and role in presynaptic maturation. J Neurosci *25*, 8457–8467.

Yamagata, M., and Sanes, J.R. (2008). Dscam and Sidekick proteins direct lamina-specific synaptic connections in vertebrate retina. Nature *451*, 465–469.

Yamagata, M., Weiner, J.A., and Sanes, J.R. (2002). Sidekicks: synaptic adhesion molecules that promote lamina-specific connectivity in the retina. Cell *110*, 649–660.

Yamamoto, N., Kurotani, T., and Toyama, K. (1989). Neural connections between the lateral geniculate nucleus and visual cortex in vitro. Science *245*, 192–194.

Yang, J.-M., Zhang, J., Chen, X.-J., Geng, H.-Y., Ye, M., Spitzer, N.C., Luo, J.-H., Duan, S.-M., and Li, X.-M. (2013). Development of GABA circuitry of fast-spiking basket interneurons in the medial prefrontal cortex of erbb4-mutant mice. J Neurosci *33*, 19724–19733.

Yang, L., Dong, F., Yang, Q., Yang, P.-F., Wu, R., Wu, Q.-F., Wu, D., Li, C.-L., Zhong, Y.-Q., Lu, Y.-J., et al. (2017). FGF13 Selectively Regulates Heat Nociception by Interacting with Nav1.7. Neuron *93*, 806–821.e9.

Yazaki-Sugiyama, Y., Kang, S., Câteau, H., Fukai, T., and Hensch, T.K. (2009). Bidirectional plasticity in fast-spiking GABA circuits by visual experience. Nature *462*, 218–221.

Yogev, S., and Shen, K. (2014). Cellular and molecular mechanisms of synaptic specificity. Annu Rev Cell Dev Biol *30*, 417–437.

Yuan, B., Cheng, T.-L., Yang, K., Zhang, X., and Qiu, Z. (2017). Autism-related protein MeCP2 regulates FGF13 expression and emotional behaviors. J Genet Genomics *44*, 63–66.

Yuzaki, M. (2010). Synapse formation and maintenance by C1q family proteins: a new class of secreted synapse organizers. Eur J Neurosci *32*, 191–197.

Zeisel, A., Muñoz-Manchado, A.B., Codeluppi, S., Lönnerberg, P., La Manno, G., Juréus, A., Marques, S., Munguba, H., He, L., Betsholtz, C., et al. (2015). Brain structure. Cell types in the mouse cortex and hippocampus revealed by single-cell RNA-seq. Science *347*, 1138–1142.

Zheng, C.-Y., Seabold, G.K., Horak, M., and Petralia, R.S. (2011). MAGUKs, synaptic development, and synaptic plasticity. Neuroscientist *17*, 493–512.

Zhou, K. Evolution of the Cerebral Cortex Makes Us Human | Yale Scientific Magazine.

Zhu, Y., Stornetta, R.L., and Zhu, J.J. (2004). Chandelier cells control excessive cortical excitation: characteristics of whisker-evoked synaptic responses of layer 2/3 nonpyramidal and pyramidal neurons. J Neurosci *24*, 5101–5108.

UNIVERSITAS Miguel Hernández